

A correlation between the dark content of elliptical galaxies and their ellipticity.

A. Deur

University of Virginia, Charlottesville, VA 22904. USA

Abstract

Observations indicate that the baryonic matter of galaxies is surrounded by vast dark matter halos, which nature remains unknown. This document details the analysis of the results published in Ref. [32] reporting an empirical correlation between the ellipticity of elliptical galaxies and their dark matter content. Large and homogeneous samples of elliptical galaxies for which their dark matter content is inferred were selected using different methods. Possible methodological biases in the dark mass extraction are alleviated by the multiple methods employed. Effects from galaxy peculiarities are minimized by a homogeneity requirement and further suppressed statistically. After forming homogeneous samples (rejection of galaxies with signs of interaction or dependence on their environment, of peculiar elliptical galaxies and of S0-type galaxies) a clear correlation emerges. Such a correlation is either spurious –in which case it signals an ubiquitous systematic bias in elliptical galaxy observations or their analysis– or genuine –in which case it implies in particular that at equal luminosity, flattened medium-size elliptical galaxies are on average five times heavier than rounder ones, and that the non-baryonic matter content of medium-size round galaxies is small. It would also provides a new testing ground for models of dark matter and galaxy formation.

Contents

1	Scope of this document	3
2	Introduction	4
3	Choice of data set and method	4
3.1	General selection criteria	5
3.1.1	Local galaxies	5
3.1.2	Distant galaxies	6
3.2	Uncertainties	6
3.3	Systematic studies	6
4	Data sets using virial theorem	7
4.1	Bacon <i>et al.</i> (1985)	8
4.2	Bender <i>et al.</i> (1989)	10
4.3	Kelson <i>et al.</i> (2000)	10
4.4	Lauer (1985)	11
4.5	Leier (2009)	12
4.6	Prugniel & Simien (1996)	12
4.6.1	Main study	12
4.6.2	Systematic studies	13
4.7	Rettura <i>et al.</i> (2006)	14
4.8	van der Weet <i>et al.</i> (2006)	14
5	Data using light profile measurements and stellar orbit modeling	15
5.1	Cappellari <i>et al.</i> SAURON IV data set (2006)	15
5.2	Cappellari <i>et al.</i> ATLAS project (2013)	16
5.3	Kronawitter <i>et al.</i> (2000)	16
5.4	Magorrian <i>et al.</i> (1998)	17
5.5	Thomas <i>et al.</i> (2007, 2011) and Wegner <i>et al.</i> (2012)	18

5.6	van der Marel (1991)	21
5.7	van der Marel and van Dokkum (2007a)	21
5.8	van der Marel and van Dokkum (2007b)	23
6	Data sets using Planetary Nebulae and Globular Clusters	23
6.1	Capaccioli, Napolitano and Arnaboldi (1992)	24
6.2	Deason <i>et al.</i> (2012)	24
6.3	Magorrian and Ballantyne (2001)	25
6.4	Romanowsky <i>et al.</i> (2003)	26
7	Data sets using X-ray	26
7.1	Fukazawa <i>et al.</i> (2006)	27
7.2	Nagino and Matsushita (2009)	29
8	Data sets using warm or cold gas disk dynamics	29
8.1	Bertola <i>et al.</i> (1991 and 1993)	30
8.2	Pizzella <i>et al.</i> (1997)	30
9	Data sets using strong lensing	31
9.1	Auger <i>et al.</i> (2010)	32
9.1.1	Analysis on full sample of Elliptical galaxies	32
9.1.2	Luminosity and environment study	33
9.1.3	Conclusion	34
9.2	Barnabe <i>et al.</i> (2011)	34
9.3	Cardone <i>et al.</i> (2009)	35
9.4	Cardone <i>et al.</i> (2011)	37
9.5	Faure <i>et al.</i> (2011)	38
9.6	Ferreras, Saha and Williams (2005)	38
9.7	Ferreras, Saha and Burles (2008)	39
9.8	Grillo <i>et al.</i> (2009)	40
9.9	Jackson <i>et al.</i> (1998)	40
9.10	Jiang and Kochanek (2007)	41
9.11	Keeton, Kochanek and Falco (1997)	43
9.12	Koopmans <i>et al.</i> (2006)	43
9.13	Leier (2009)	44
9.14	Leier <i>et al.</i> (2011)	45
9.15	Ruff <i>et al.</i> (2011)	45
9.16	Treu and Koopmans (2004)	46
10	Ellipticity and projection corrections	48
10.1	Ellipticity corrections	48
10.2	Projection correction	48
11	Correlations	49
11.1	Measurement bias study	51
12	S0 contamination study	52
12.1	Independent S0 rejection criterion	52
12.2	Consequence of a S0 contamination for galaxy census	52
12.2.1	Analysis using virial data (Prugniel & Simien data set)	52
12.2.2	Analysis using lensing data (Auger <i>et al.</i> data set)	54
12.3	Case of the S0 contamination at small R_{min}/R_{max} only	54
12.4	Stellar M_*/L ratio vs ellipticity study	55
12.5	Correlation with distance moduli	55
12.6	Correlation with apparent magnitude	55
13	Global results	55
13.1	Results	57

14 Summary and conclusion	58
A Other data	63
B Correlation between stellar M_*/L and axis ratio	66
B.1 data sets	66
B.1.1 Capaccioli <i>et al.</i>	66
B.1.2 Cappellari <i>et al.</i> SAURON project (2006)	66
B.1.3 Cappellari <i>et al.</i> ATLAS project (2013).	66
B.1.4 Thomas <i>et al.</i> (2007, 2011) and Wegner <i>et al.</i> (2012)	67
B.1.5 Conroy and van Dokkum	67
B.1.6 Deason <i>et al.</i>	68
B.1.7 Auger <i>et al.</i>	68
B.1.8 Barnabe <i>et al.</i>	68
B.1.9 Cardone <i>et al.</i> (2009)	68
B.1.10 Grillo <i>et al.</i>	70
B.1.11 Jiang and Kochanek	70
B.1.12 Leier <i>et al.</i> (2011)	71
B.1.13 Treu and Koopman	71
B.2 Global results for M_*/L	72
C Summary table of the NGC, IC and UGC galaxies	73
D Summary table for the SLACS lensing galaxies	78
E Summary table for the COSMOS lensing galaxies	81
F Summary table for the CL 3C295, CL 0016+16 and CL 1601+42 cluster galaxies	82
G Summary table for SL2S lensing galaxies	83
H CDFS Summary table	84
I Cluster CL1358+62 elliptical galaxies summary table	86
J Summary table for other lensing galaxies	87
K Summary of the individual analyses	90
L Detailed analysis of the Bacon <i>et al.</i> data	92
L.1 Data quality and galaxy selection	92
L.2 Data analysis	94
L.3 Correlations	97
L.3.1 Expected correlations	98
L.3.2 Correlation study	99
L.3.3 Discussion	110
L.4 Corrections	113
L.4.1 Corrections for measurement biases	113
L.4.2 Surface brightness vs absolute blue magnitude	114
L.4.3 Hubble parameter correction	114
L.4.4 Projection correction	116
L.5 Final result	116

1 Scope of this document

This document is an archival article that details the analysis performed in Ref. [32] to investigate the relation between the amount of dark matter in elliptical galaxies and their shape. A significant correlation was found and reported in [32]. Here, we provide the details of the analysis method, the data used and the systematic studies conducted to understand the nature of the correlation and the influences of specific factors such as the

environment of the galaxies. We also provide a similar analysis as that performed in [32], but for the baryonic mass rather than the dark mass. No similar correlation is found.

2 Introduction

Dark matter is an essential ingredient of cosmology. It provides together with dark energy for a consistent description of many large-scale features of the universe [63]. However, at the galactic and semi-galactic scales, open questions remain [1, 80]. There, galaxies are depicted as constituted of a vast dark matter halo surrounding a smaller baryonic component. One method to advance our understanding at the galactic scale is to look for relationships between the dark matter content of a galaxy and its observed luminous matter. Useful empirical relations have been found, e.g. that of Tully-Fisher [101] for spiral galaxies which links the galactic rotation speed to the galaxy absolute luminosity. For elliptical galaxies, a prominent empirical correlation is the “Fundamental Plane” [37, 38] which combines the Kormendy [66] and the Faber-Jackson [41] relations and links the galactic effective radius R_{eff} , the surface brightness and the dispersion of stellar velocities σ . Intriguingly, none of these correlation directly involve dark matter. Equally puzzling is the observation that some elliptical galaxies harbor little dark matter [87]. We discuss here the correlation between the defining characteristic of elliptical galaxies –the ellipticity, on which e.g. their Hubble sequence is entirely founded– and their relative dark matter content, expressed as the total galactic mass (baryonic+dark) normalized to luminosity (M/L ratio).

The conventional Hubble classification groups galaxies into four broad morphological categories based on visual appearance: spiral, elliptical (with smooth featureless distribution), lenticular (with a bright central bulge and external disk but no spiral structure) and irregular (without well-defined structure). In this study, we focus on elliptical galaxies. Although those generally have tri-axial ellipsoidal structures and ellipticities depending on radii, to first approximation the geometric structure of elliptical galaxies can generally be simply modeled as oblate ellipsoids with constant ellipticities (ε). Those span a wide range, from $\varepsilon = 0$ (round galaxies) to $\varepsilon = 0.7$ (highly flattened ellipsoids). This essentially continuous variation of ε allows us to investigate how the general elliptical galaxy characteristics evolve with ε . A caveat, however, is that only the ellipticity projected on our observation plane (hereafter $\varepsilon_{apparent}$, the apparent ellipticity) is observed. The true ellipticity (henceforth ε_{true}) can be inferred only by detailed modeling of the galaxy. Furthermore M/L for elliptical galaxies are difficult to measure comparatively to disk galaxies [87]. These difficulties can be circumvented statistically: in a large and homogeneous samples of elliptical galaxies one can minimize the effects of galaxy peculiarities by a homogeneity requirement. The large number of galaxies further suppresses these effects statistically. Performing this analysis with M/L extracted using different methods allows to minimize possible systematic bias associated with a particular method. Finally, the projection problem can also be addressed statistically: it is straightforward to model its overall effect on the studied correlation and correcting for it.

The actual shape of the dark halo remains an open question. A correlation between the amount of dark matter and the ellipticity of galaxies offers an opportunity to experimentally address this question as well as the fundamental questions of the interaction of baryonic and dark matter, and the present tensions between the standard model of galaxy formation and the data.

Throughout this document, the M/L are expressed in solar unit M_{\odot}/L_{\odot} and to characterize the shape of a galaxy (assumed to be oblate) we use its axis ratio $R_{min}/R_{max} = 1 - \varepsilon$ where R_{min} is the minor radius and R_{max} the major radius. Finally, DM will stand for Distance Modulus, not dark matter.

3 Choice of data set and method

We used 42 separate publications that provide M/L or related ratios for at least several elliptical galaxies. We also considered 24 other articles, but without using their results for reasons given in Appendix A. Overall, after selecting appropriate galaxies, we obtained 255 different galaxies for a total of 685 data points. Tables listing the galaxies used are given in appendices C to J. The last appendix presents our most detailed analysis, including a study of the interrelation between the various variables characterizing the galaxies to check whether the M/L correlation with R_{min}/R_{max} that was eventually identified could be a consequence of other correlations. We grouped the publications according to the methods used to extract M/L (or related ratios such as M_{total}/M_{*} with M_{*} the part of the galactic mass from stars, or the dark matter fraction $DMf = 1 - M_{*}/M_{total}$). In the following sections we describe the methods, their advantages and caveats. In the subsections, we summarize our analysis for each data set and its specificities. We classified the results into reliability groups defined as:

- Group 1: reliable results.
- Group 2: somewhat reliable.

- Group 3 somewhat less reliable.
- Group 4: less reliable.

Authors whose work belong to groups 4 or 3 should not be offended: this grouping is pertinent solely in the context of the work relevance to our study, and not in any other sense: all the results are published in peer-reviewed journals (except for [16]) and thus should be reliable. This reliability criterion was used in Section 13 to weight the results when combining them. This procedure is coarse and might introduce some subjectivity but in practice, its effects turned out to be numerically small because lower reliability groups typically have lower statistics. After combining the results in Section 13, correcting them (Section 10.2) if necessary for the fact that the correlation was studied vs the projected axis ratio (apparent axis ratio $R_{min}/R_{max}|_{apparent}$) rather than the intrinsic one (true axis ratio $R_{min}/R_{max}|_{true}$), we present and discuss the global results in Section 13.

3.1 General selection criteria

For each publication, we chose of subset of the analyzed elliptical galaxies as homogeneous as possible. This was done for two reasons:

- 1) it reduces the noise coming from effects peculiar to given galaxies which would obscure a possible correlation with point-to-point uncorrelated variations;
- 2) it avoids biasing the studied correlation with systematic effects from a class of galaxies, e.g. giant elliptical galaxies (point-to-point correlated effect).

Our selection criteria are more strictly applied to sets of local galaxies and have to be relaxed for sets of distant galaxies because these are not characterized as accurately. (Typically, one can use only distant galaxies for strong lensing analyses or those using the Fundamental Plane time-evolution, see e.g. Ref. [61]).

The local and distant selection criteria are listed bellow, with galaxy characteristics obtained from either the NASA/IPAC Extragalactic Database (NED) [110] or from the publication that provided the M/L . It is important to take notice that the selection criteria have been decided before carrying out the analysis. Thus, the analysis is “blind” with minimal subjective bias.

3.1.1 Local galaxies

When possible, only medium size elliptical galaxies were selected. Those tend to be “disky” and to have almost isotropic random velocities. We also required the galaxies to be undisturbed because galaxy interactions often compromise the applicability of the formulae used to extract the dark matter content (e.g. strong lensing equations, virial theorem, hydrostatic equilibrium equations). We reject galaxies that are, according to the NASA/IPAC Extragalactic Database (NED) [110] or the article in which M/L is calculated:

- Lenticular galaxies (S0-type);
- Active Galactic Nucleus (AGN) galaxies because an AGN may signal a recent disturbance of the galaxy. Furthermore, AGNs emit at all wavelengths and can consequently bias our study by lowering the M/L ratios;
- LINERS galaxies (because they may be due to AGN), Seyfert (Sy) and BL Lacertae objects (BLLAC) active galaxies, for the same reasons as AGN;
- Peculiar galaxies, or any galaxy listed in the Arp catalogue [111] of peculiar galaxies;
- Giant elliptical galaxies (D), supergiant elliptical galaxies (cD), Brightest Cluster Galaxies (BrClG), EXG [112] and XE galaxies. These galaxies belong to different classes of elliptical galaxies, tend to be triaxial and moreover, the “boxy” giant galaxies are characterized by anisotropic random velocities. In addition, the determination of their amount of dark matter could be skewed by contribution from the cluster or group the galaxy belong to; Further reasons to reject large elliptical galaxies are provided in [17];
- Compact elliptical galaxies (cE);
- E? galaxies in the NED because the lack of definite morphology assignment may reflect poor measurements and may contaminate our galaxy set with non-elliptical galaxies;
- Transition-type (E+) and galaxies formerly described as elliptical but now identified as spiral galaxies;
- HII emission galaxies, because it may signal a recent disturbance. In any case, the presence of HII regions is unusual for elliptical galaxies, making those to fulfill the “peculiar galaxy” rejection criterion. HII emission might also bias the M/L determination because newly born blue stars increase significantly the luminosity L ;

- VCXG galaxies [112] since they show signs of disturbed hydrostatic equilibrium.
- NELG (narrow emission line galaxy) galaxies since it may signal a recently disturbed galaxy.

We keep LERG (low excitation radio galaxies) and WLRG (weak emission-line radio-galaxies) since we saw no obvious reason to exclude them.

3.1.2 Distant galaxies

Distant galaxies are usually not well enough characterized to apply the above criteria. Nevertheless, they are very useful to include in our study since typically only distant galaxies are available to apply the strong lensing method e.g. [2] or [59] or that of the Fundamental Plane time-evolution, e.g. [61] or [86]. The rejection criteria for distant galaxies are:

- Massive galaxies, with typically $M \gtrsim 5 \times 10^{11} M_{\odot}$. This criterion should minimize the amount of contamination of our sample by cD, D or BrClG galaxies. The choice for mass selection is based on the work of Ferreras *et al.* [46]: the authors noted that galaxies with $M_{tot} > 10^{12} M_{\odot}$ behave differently than those with $M_{tot} \ll 10^{12} M_{\odot}$;
- Galaxies with relatively low velocity dispersions, $\sigma \leq 225 \text{ km.s}^{-1}$, if S0 and elliptical galaxies are not separated but considered altogether in the publication, or if the classification may not be reliable enough. This should suppress possible S0 contamination: S0 tend to have $\sigma \leq 225 \text{ km.s}^{-1}$. We verified that, within a sample of well identified local elliptical galaxies, rejecting the genuine elliptical galaxies with $\sigma \leq 225 \text{ km.s}^{-1}$ does introduce a bias of the M/L vs R_{min}/R_{max} correlation, see Section 4.6.2. Hence, this criterion is adequate to reject S0 without biasing our study.

In addition, if some of the characteristics listed in Section 3.1.1 are available (such as AGN or known interaction with another galaxy), then these galaxies are also rejected.

3.2 Uncertainties

Since all the data sets will be eventually combined in a single overall determination of M/L vs. R_{min}/R_{max} , the uncertainties for M/L and R_{min}/R_{max} must be estimated consistently lest galaxy samples with optimistic determinations of their uncertainties will be given an unwarranted preponderance. In addition, some publications do not provide any uncertainties and these then need to be assessed without the detailed knowledge of the analyses carried in the publication. To obtain a consistent determination of the uncertainties, we employ the *unbiased estimate*, i.e, we re-scaled the uncertainties¹ so that, when a fit of M/L vs. R_{min}/R_{max} is performed, its χ^2/ndf is set to unity. This supposes a gaussian dispersion of the data of a given galaxy set. For the fit, we choose it to be linear for simplicity and to minimize the number of fit parameters. If the true dependence of M/L vs. R_{min}/R_{max} is not linear, then the χ^2/ndf would increase which in turn would increase the final uncertainties when χ^2/ndf is set to unity. Hence, the linearity assumption is accounted for in the final uncertainty.

A caveat of forcing χ^2/ndf to unity when fitting M/L vs *apparent* axis ratio comes from the fact that a large part of the data scatter is not due to the data gaussian dispersion. Rather, it is due to the random projection of the real 3D shape of the galaxy onto our 2D observation plan, see Section 10.2 and in particular Fig. 43 or 44. Still, we adopt the procedure of forcing $\chi^2/ndf = 1$ because 1) it is the simplest method to estimate uncertainties when data are provided without uncertainties; 2) we can apply the same procedure to all data sets for consistency; and 3) it was a conservative procedure, as discussed above.

Finally, conscious that some assumptions underlie the fit procedure and the unbiased estimate method, we independently assessed the degree of correlation using the Pearson correlation coefficient.

3.3 Systematic studies

In sections 4 to 9, we summarize the analyses made on each galaxy set for obtain M/L vs R_{min}/R_{max} . When possible, the systematic effect associated with a particular galaxy characteristic was also studied. This was done when the set contained a large enough number of galaxies and the galaxy characteristic was provided. We list below these auxiliary studies.

- Effect of galactic metallicity using the Lauer data [69] based on the virial theorem. (no effect) ;

¹If the uncertainties are not provided in the publication, we assume $\Delta M/L$ to be proportional to M/L , assume no uncertainty on R_{min}/R_{max} , and then apply the *unbiased estimate* method.

- Influence of the correlation between M/L_B and central luminosity density, using the Lauer data [69] based on the virial theorem. (Large effect);
- The effect of luminosity was also studied using the Auger *et al.* data [2] based on lensing. This also check the correlation with galaxy boxy/disk shape: more luminous galaxies tend to be boxy and less ones tend to be disk. No correlation between the DMf and the luminosity/boxy-disk galaxy character was observed.
- Effect rejecting bona-fide galaxies with low velocity dispersion, using the Prugniel & Simien data [84] based on the virial theorem. (No effect);
- Effects of LINERS, using the Prugniel & Simien data [84] based on the virial theorem. (No effect);
- Effect of ellipticity projection, using Bertola *et al.* [9] and Pizzella *et al.* [83], both based on analyzing embedded gas disks, and the Barnabe *et al.* [5] data based on lensing. (Large effect, except for the Barnabe *et al.* [5] data).
- The effect of environment was studied using the Auger *et al.* [2], Barnabe *et al.* [5] and Cardone *et al.* (2009, 2011) [21, 22] data sets based on lensing. Galaxies residing in clusters tend to show a smaller DMf vs axis ratio correlation (smaller slope) with more jitter (larger relative uncertainty). The lensing data set from Cardone *et al.* (2009) [21] shows, however, the opposite trend.
- The effect of choosing a particular initial mass function (IMF) to interpret the data can be checked with the Auger *et al.* [2] and Barnabe *et al.* [5] data sets based on lensing, and the Deason *et al.* [30] data employing PNe and GC. See also the Cappellari *et al.* [17] data based on using light profile measurements and stellar orbit modeling.

4 Data sets using virial theorem

Galactic mass-to-light ratio can be extracted using the virial theorem. Its simple form (scalar virial theorem) gives $M/L = c\sigma^2/Ir$ where σ is the stellar velocity dispersion, c a proportionality coefficient, r a given radius (e.g. the effective radius R_{eff} or the core radius) and I is the surface brightness. The value of c is in principle the same for galaxies of an homogeneous sample. The formula assumes spherical symmetry and a virialized system. The ellipticity of the galaxy can be accounted for using the tensor virial theorem, see [3] and references within. The data discussed in this section were obtained using ellipticity corrected virial formulae. When the published data did not account for ellipticity, we used the Bacon *et al.* [3] ellipticity corrections formula (simplified formula using central dispersion only and $R_{min}/R_{max}|_{true} = R_{min}/R_{max}|_{apparent}$). This correction, derived analytically, is important. It was independently verified by the results of van der Marel [104], see Section 5.6. In addition, without this correction, the averaged M/L would be too small compared to an expected value around $8 M_\odot/L_\odot$. We remark that the modification to the (spherical) Newton Shell Theorem to include ellipticity yields a similar figure, see Section 7.

Caveats for this method of extracting M/L are:

- Anisotropy effects are generally not accounted for;
- Only M/L for the galaxy inner part are obtained. This one tends to be rounder and dominated by baryonic matter, thereby biasing and diluting the effect we study;
- A constant M/L is assumed. Although it is now established that M/L varies significantly with the galaxy radius, see e.g. [67, 97, 104, 16, 74, 78, 79, 9], a constant M/L is a good assumption for $r < R_{eff}$.

Another potential caveat of this method is that unphysical correlations between M/L and R_{min}/R_{max} can be induced by anisotropic star motions. However, this should not be an issue because, as assessed in Ref. [3], the effect is small. Furthermore anisotropies have little effects on the slopes of Figs. 1a and 1b of [3] whilst affecting primarily the absolute values. Because we are investigating a dependence of M/L on R_{min}/R_{max} , the absolute scale of M/L is of secondary importance. Therefore, possible effects of the anisotropies are not critical. Furthermore, the absolute values of M/L will be normalized to the expected $M/L=8 M_\odot/L_\odot$ when all the data sets are combined, see Section 13. In addition, bright galaxies –which tend to display these anisotropies– are discarded from our samples by our selection criteria. Our assessment that anisotropies should be of small concern was *a posteriori* justified by checking that the results from [3] –which used a large set of galaxies and the virial method– displayed no significant M/L vs brightness correlation, see the correlation study in appendix L.

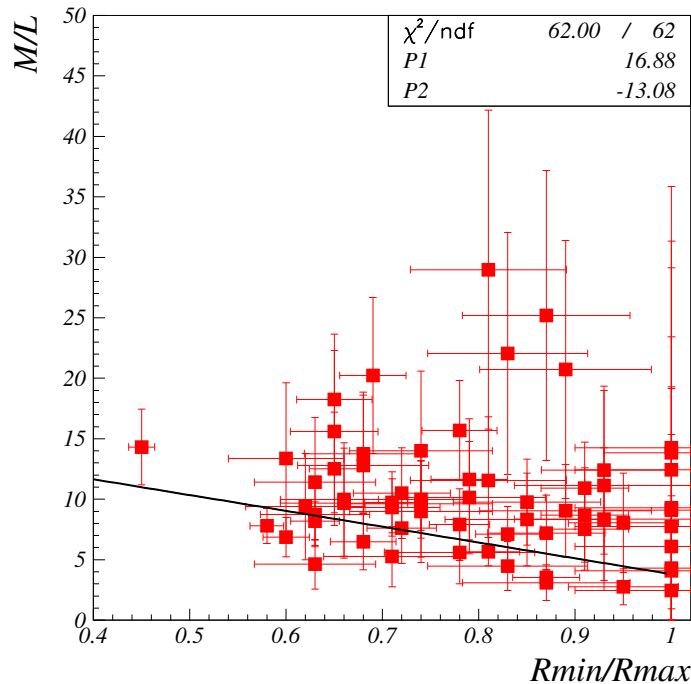


Figure 1: M/L_B vs apparent axis ratios from Bacon *et al.* [3] for Sample 1 (ellipticity corrections from the σ^2 isotropic method). In this figure and the 40 others that follow, the straight line shows the best linear fit to the data. The χ^2/ndf is given in the top right box together with the M/L -intercept at $R_{min}/R_{max} = 0$ ($P1$) and the slope ($P2$).

4.1 Bacon *et al.* (1985)

Bacon *et al.* [3] extracted M/L_B (M/L in the B-band) for 197 early-type galaxies. We analyzed these data thoroughly using additional selection criteria² and studying possible correlations between various galaxy characteristics that could have biased our study. The full analysis is presented in appendix L. Depending on data availability, ellipticity corrections formulae of various accuracies were used.

After applying the selection criteria, we were left with of 64 elliptical galaxies in our main sample (Sample 1). Better ellipticity corrections are available for 11 galaxies (Sample 2). The results of fits to these data using the Bacon *et al.* values for R_{min}/R_{max} and distance moduli are shown in Figs. 1, 2 and 3 and are:

$M/L_B = (-13.08 \pm 2.97) R_{min}/R_{max}|_{apparent} + (16.88 \pm 2.32)$ for Sample 1 (ellipticity corrections from σ^2 isotropic method).

$M/L_B = (-5.91 \pm 4.67) R_{min}/R_{max}|_{apparent} + (10.50 \pm 3.48)$ for Sample 2 (ellipticity corrections from μ^2 isotropic method, where μ^2 is the quadratic sum of the galaxy velocity and its central velocity dispersion σ , see [3]).

$M/L_B = (-6.19 \pm 3.59) R_{min}/R_{max}|_{apparent} + (9.18 \pm 2.64)$ for Sample 2 (ellipticity corrections from μ^2 anisotropic method).

The uncertainties on R_{min}/R_{max} were taken as the difference between the Bacon *et al.* and NED values. The M/L_B uncertainties are from Bacon *et al.*, rescaled so that $\chi^2/ndf = 1$ (*unbiased estimate*).

There are several advantages to this data set:

- The virial formula used to obtain the published M/L is corrected for galactic ellipticity;
- The large data set (197 galaxies) allowed strict criteria to be used to remove unsuitable or suspicious galaxies;
- Three methods were used to obtain M/L ;
- Triaxial galaxies were excluded from the original data set, as they are less suited for the virial method.

The analysis is dated (1985) but we have used only data consistent with the more recent NED numbers, so we do not consider this to be an important caveat. We assigned the results to group 2 reliability for Samples 1 and 2 with ellipticity corrections from the μ^2 isotropic method, and reliability group 1 for Sample 2 with ellipticity correction from the μ^2 anisotropic method.

²We required in addition to the selection criteria described in 3.1.1 that the galaxy characteristics listed in the 1985 Ref. [3] are compatible with the up-to-date (as of 2008, when the analysis was performed) characteristics provided in the NED [110].

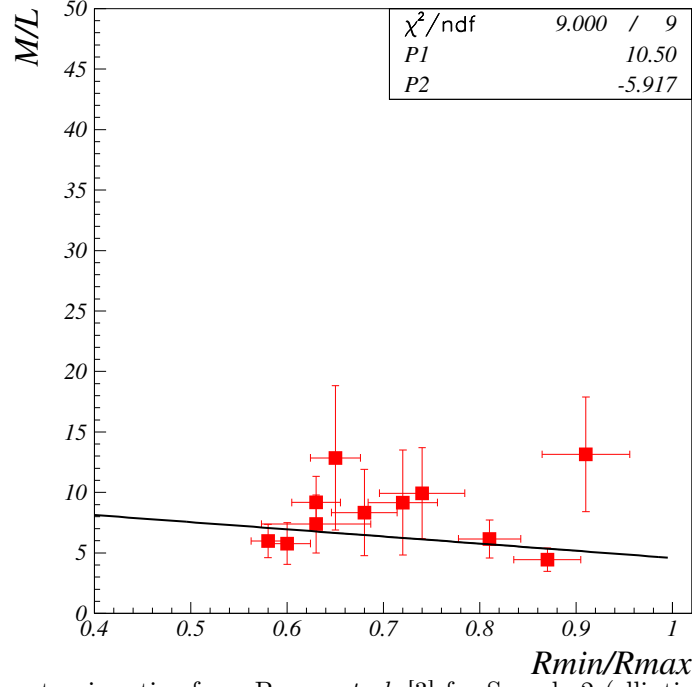


Figure 2: M/L_B vs apparent axis ratios from Bacon *et al.* [3] for Sample 2 (ellipticity corrections from the μ^2 isotropic method).

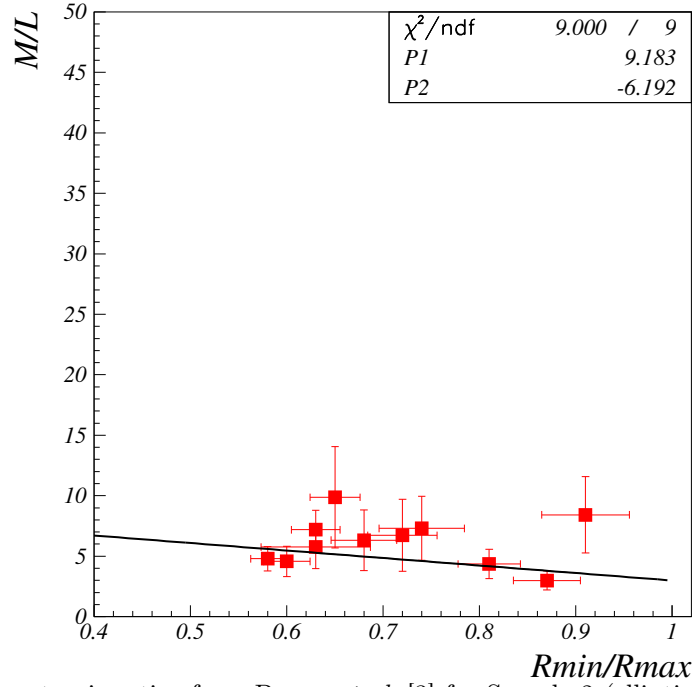


Figure 3: M/L_B vs apparent axis ratios from Bacon *et al.* [3] for Sample 2 (ellipticity corrections from the μ^2 anisotropic method).

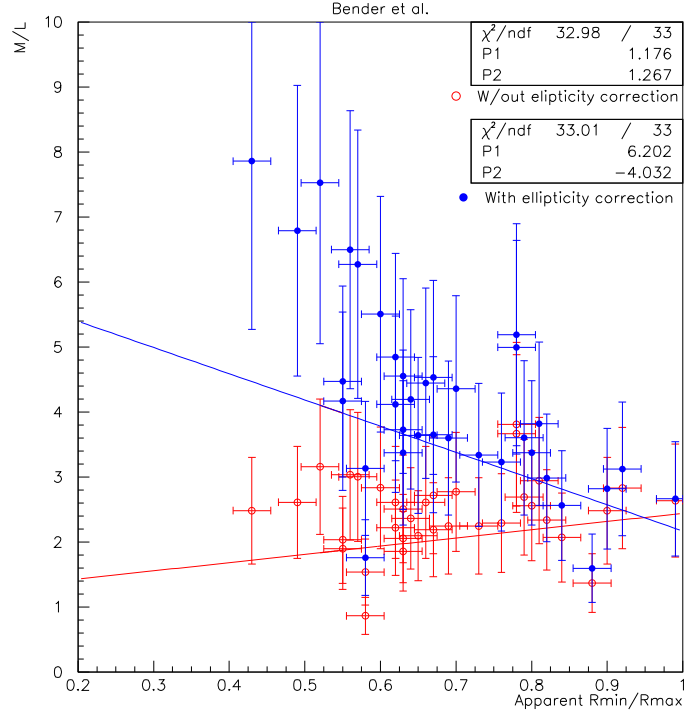


Figure 4: M/L_B vs apparent axis ratios from Bender *et al.* [6] before applying ellipticity corrections (empty red circles) and after (blue filled circles).

4.2 Bender *et al.* (1989)

Bender *et al.* [6] analysis assumed spherical symmetry. There was 109 galaxies in the original sample. After selection, we retained 35 galaxies. M/L_B vs apparent axis ratio is shown in Fig. 4. The fit result for the 35 selected galaxies (using NED values for R_{min}/R_{max} with a ± 0.025 uncertainty) is:

$$M/L_B = (-4.03 \pm 1.44) R_{min}/R_{max}|_{apparent} + (6.20 \pm 1.07).$$

The M/L_B uncertainty was assigned to be proportional to M/L_B with the overall scale factor adjusted so that $\chi^2/ndf = 1$.

Specific caveats of this analysis are: the analysis is dated; There were frequent large discrepancies between the values used in the original analysis and the NED values (e.g. redshift, ellipticity or luminosity values); No uncertainty was provided.

We remark that the M/L_B values without ellipticity corrections appear to be too low: in average, $\langle M/L_B \rangle = 2.05 \pm 0.08$. Using the more modern value for the Hubble constant $H_0 = 70$ km/s/Mpc rather than 50 km/s/Mpc as used by the authors, we obtained $\langle M/L_B \rangle = 1.46 \pm 0.06$. This is well below the expected (minimal) value of $\langle M/L_B \rangle \sim 4 M_\odot/L_\odot$ for an elliptical galaxy without dark matter contribution, and $\langle M/L_B \rangle \sim 8 M_\odot/L_\odot$ with dark matter contribution. This proves the necessity of the ellipticity corrections. We assigned the results to group 3 reliability.

4.3 Kelson *et al.* (2000)

Kelson *et al.* [61] determined the internal kinematics, length scale and surface brightness of 53 galaxies from cluster CL1358+62, 11 of them elliptical galaxies. The data were used to form M/L_B . Applying an absolute magnitude selection $M_B \leq -19.5$ to minimize the contamination from boxy galaxies would have left only one available galaxy. Relaxing the selection to $M_B \leq -20$ left 5 galaxies to study. We applied the ellipticity corrections from Bacon *et al.* [3]. The M/L_B vs apparent axis ratio is shown in Fig. 5. Uncertainties were slightly scaled to force $\chi^2/ndf = 1$. The best linear fit is:

$$M/L_B = (-15.53 \pm 7.21) R_{min}/R_{max}|_{apparent} + (20.52 \pm 5.95).$$

The specific caveats of this analysis are that the galaxies are not as well characterized (morphology, spectra) as local ones, and they belong to a dense cluster. Thus, they may not be in virial equilibrium, and we cannot apply the usual strict criteria that select galaxies likely to be in virial equilibrium. Consequently, we assigned these data to group 4 reliability.

For completeness, the fit before ellipticity corrections yields $M/L = (-2.29 \pm 4.79) R_{min}/R_{max}|_{apparent} + (7.78 \pm 3.79)$.

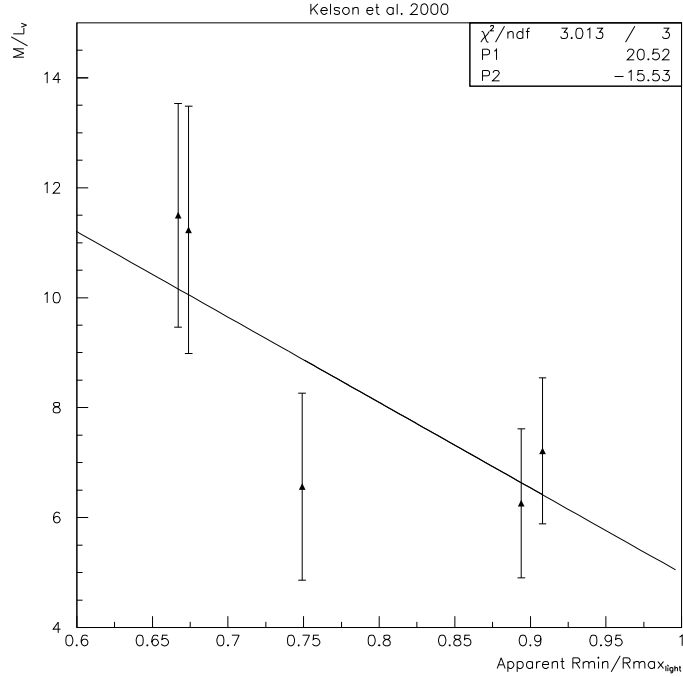


Figure 5: M/L_B vs apparent axis ratio from Kelson *et al.* [61] (after applying ellipticity corrections).

4.4 Lauer (1985)

The Lauer data set [69] contains 42 galaxies. M/L_B was extracted from the stellar velocity dispersion in the galaxy core, assuming a spherical star distribution. Thus, the M/L were determined for radii $r \lesssim 0.03R_{eff}$. The M/L_B ratios were given without uncertainty estimates. The uncertainty we assigned did not follow our standard procedure: we assigned a constant uncertainty of $\Delta(M/L) = 3.0$ rather than $\Delta(M/L) \propto M/L$ because of the low M/L outlier at $R_{min}/R_{max} = 0.58$, see Fig. 6. With the standard procedure, the outlier would have had a very small uncertainty and would have driven the fit. The value $\Delta(M/L) = 3.0$ is chosen so that $\chi^2/ndf = 1$. Lauer classified galaxies in 3 classes, depending on the quality of the core resolution. Class 1 is for well resolved cores, class 2 for partially resolved cores and class 3 for unresolved cores. In addition to M/L_B for the core, Lauer provided a secondary analysis that determined more globally $\langle M/L_B \rangle$ using effective radius rather than the core radius, which extends his analysis beyond the galaxy core. However, because his main analysis concerns galaxy cores, we will consider only M/L_B rather than $\langle M/L_B \rangle$. We applied our usual selection criteria with, as in Section 4.1, the added requirement that the galaxy characteristics listed in Lauer’s 1985 publication are compatible with the one in NED [110], with the exception of the axis ratio because it was not provided in [69]. We used the NED values for the axis ratios. The sample was reduced to 10 galaxies after selection. If we had restricted the sample to galaxies with resolved (class 1) or partially resolved (class 2) cores, only two galaxies would have remained (one in class 1: NGC 720 and one class 2: NGC 7619). Hence we did not apply this additional requirement and used galaxies from the 3 classes indiscriminately.

The M/L_B dependence with axis ratio is shown in Fig 6. The fit results gives:

$$M/L_B = (-10.94 \pm 10.18)R_{min}/R_{max}|_{apparent} + (23.83 \pm 7.80).$$

The data set has several specific caveats: it is dated and no ellipticity correction was originally done. The M/L_B ratios were computed for the galaxy cores and given without uncertainty estimates. The uncertainty was determined following a particular procedure rather than our standard one due to an outlier having a M/L value close to 0. Because of the above caveats, we assigned the results to group 4 reliability.

For information we note that:

- Before applying ellipticity corrections the fit was: $M/L_B = (+10.2 \pm 6.7)R_{min}/R_{max}|_{apparent} + (2.8 \pm 4.5)$.
- Results using the more recent NED distances [110] are: $M/L_B = (-5.35 \pm 10.16)R_{min}/R_{max}|_{apparent} + (21.17 \pm 7.78)$.
- Results for the global mass to light ratio $\langle M/L_B \rangle$ are: $\langle M/L_B \rangle = (+14.70 \pm 14.73)R_{min}/R_{max}|_{apparent} + (7.71 \pm 11.29)$. Using the more recent NED distances: $\langle M/L_B \rangle = (+24.56 \pm 17.67)R_{min}/R_{max}|_{apparent} + (2.51 \pm 13.53)$. The opposite correlation sign appears to be spurious and due to correlations between the luminosity density ρ_e and R_{min}/R_{max} on the one hand and ρ_e and $\langle M/L_B \rangle$ on the other. This is discussed next.

Correlations

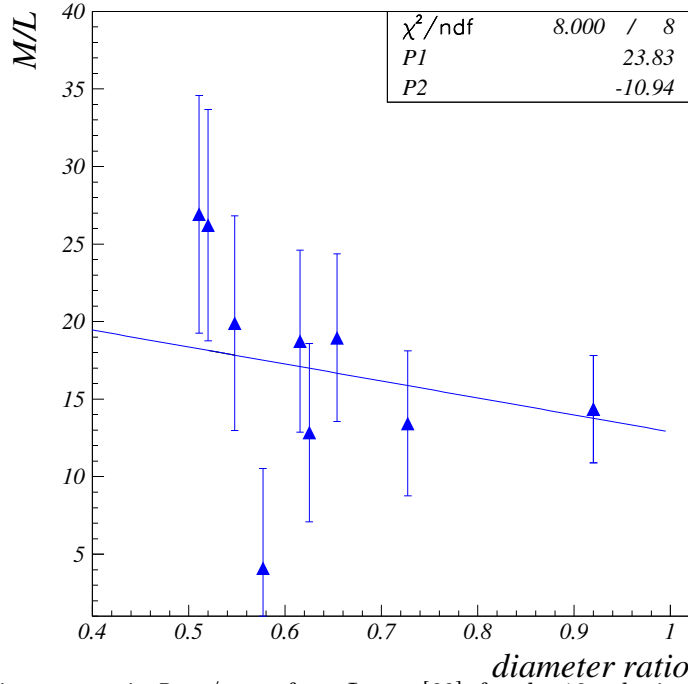


Figure 6: M/L_B ratio vs diameter ratio R_{\min}/R_{\max} , from Lauer [69], for the 10 galaxies of our sample. The original Lauer data is corrected for ellipticity and uncertainties are assigned so that $\chi^2/\text{ndf} = 1$.

Correlation with metallicity Lauer noticed a correlation between galaxy metallicity M_{g_2} and M/L . Indeed we found $M/L = (61.0 \pm 24.9)M_{g_2} - (6.4 \pm 7.6)$ and $\langle M/L \rangle = (55.2 \pm 24.3)M_{g_2} - (4.6 \pm 7.4)$. However, we found no clear correlation between M_{g_2} and R_{\min}/R_{\max} . Consequently, the relation between M_{g_2} and M/L should not induce the correlation observed between M/L and R_{\min}/R_{\max} .

Correlation with central luminosity density Lauer also signaled a correlation between the luminosity density ρ and M/L . We found $M/L = (-6.5 \pm 1.6)\rho_0 + (22.2 \pm 2.6)$ and $\langle M/L \rangle = (7.3 \pm 1.8)\rho_e - (3.0 \pm 4.4)$. Notice the opposite correlations between central and effective densities. There is no clear correlation between ρ_0 and R_{\min}/R_{\max} , whilst a correlation exists between ρ_e and R_{\min}/R_{\max} : $R_{\min}/R_{\max} = (0.14 \pm 0.04)\rho_e + (0.40 \pm 0.10)$. Thus, the correlation between $\langle M/L \rangle$ and R_{\min}/R_{\max} may be biased by, or even due to, the $(\rho_e, R_{\min}/R_{\max})$ and $(\langle M/L \rangle, \rho_e)$ correlations. This can explain the opposite (positive) sign of the $(R_{\min}/R_{\max}, \langle M/L \rangle)$ correlation compared to the (negative sign) $(R_{\min}/R_{\max}, M/L)$ correlation: subtracting the ρ_e correlation from $\langle M/L_B \rangle = (+14.70 \pm 14.73)R_{\min}/R_{\max}|_{\text{apparent}} + \text{cst}$, we get $\langle M/L \rangle = (-37.4 \pm 44.9)R_{\min}/R_{\max}|_{\text{apparent}} + \text{cst}$, consistent with the negative slope in $M/L_B = (-10.94 \pm 10.18)R_{\min}/R_{\max}|_{\text{apparent}} + (23.83 \pm 7.80)$ and the expectation that M/L below R_{eff} should not vary strongly. We will not use the $\langle M/L_B \rangle$ results in the global analysis of Section 13.

4.5 Leier (2009)

Leier [71] analyzed distant galaxies using both the strong lensing and the virial methods. These results are discussed in Section 9.13. The result based on the virial method were assigned to group 2 reliability.

4.6 Prugniel & Simien (1996)

4.6.1 Main study

Prugniel & Simien [84] compiled kinematics and photometric data for 371 early-type galaxies. They remarked that this set might be biased toward flat galaxies since those are preferably chosen for major axis kinematic measurements. This should be of no consequence in our context. We selected adequate elliptical galaxies following the usual morphology and emission criteria. We did not use the galaxies from the PCG catalog, although some seem to be good elliptical galaxies, since they all have low velocity dispersions. The set obtained contains 102 galaxies.

We formed $M/L_B \propto \sigma_0/L_B^{1/2}I_e^{1/2}$ from the virial theorem and corrected it for ellipticity using the virial tensor correction formula from Bacon *et al.* [3]. The galaxy type and characteristics, including axis ratio, were obtained

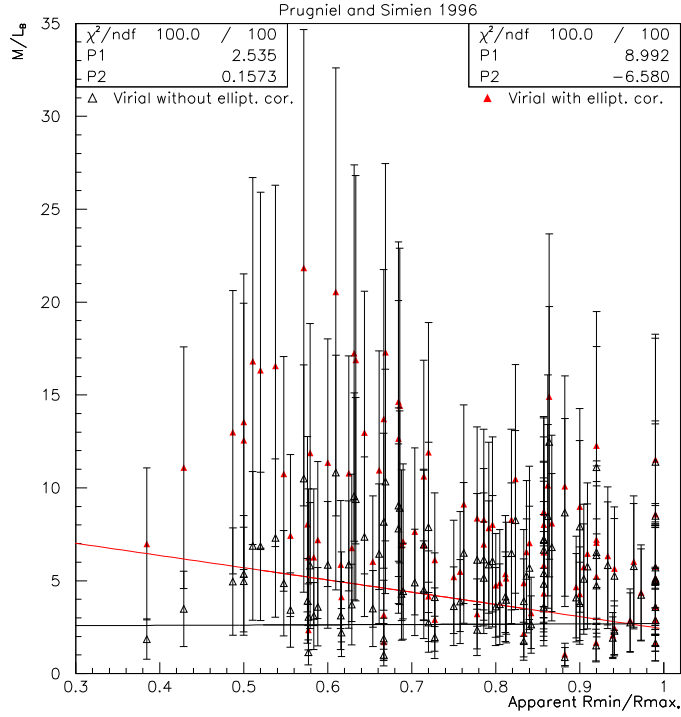


Figure 7: M/L_B vs apparent axis ratios from Prugniel & Simien [84] before applying ellipticity corrections (empty triangles) and after (red filled triangles).

from NED. The M/L uncertainties were assumed to be proportional to M/L and set so that $\chi^2/ndf = 1$. M/L_B vs apparent axis ratio is shown in Fig. 7. The best linear fit is:

$$M/L_B = (-6.58 \pm 1.98) R_{min}/R_{max}|_{apparent} + (8.99 \pm 1.68).$$

The advantage of this analysis is that the data are numerous and relatively recent compared to the other extractions of M/L that used the virial theorem. The only specific caveat of this analysis is that no uncertainties are provided. We assigned these results to group 2 reliability.

For information, the result before applying the ellipticity corrections is: $M/L_B = (+0.16 \pm 1.19) R_{min}/R_{max}|_{apparent} + (2.54 \pm 0.93)$.

4.6.2 Systematic studies

Effect of a velocity dispersion selection The large sample of well identified elliptical galaxies provided the opportunity to check the effect of removing from the sample good elliptical galaxies with low velocity dispersion ($\sigma < 225 \text{ km.s}^{-1}$). Such selection is applied in the analyses of distant galaxies that have less reliable type identification, in order to minimize possible S0 contamination. However, this selection may at the same time also remove genuine elliptical galaxies. Thus, it is important to check if a low velocity dispersion selection produces a bias. Once the $\sigma > 225 \text{ km.s}^{-1}$ criterion was applied, only 44 galaxies out of 112 remained. The mean value of M/L increased significantly because $M/L \propto \sigma$. However, normalizing the fit result to the same average $\langle M/L \rangle$ value as in the main study yielded a correlation similar to that of the main study:

$$M/L_B = (-7.10 \pm 1.05) R_{min}/R_{max}|_{apparent} + (9.57 \pm 0.89),$$

This indicates that no bias arises from the the $\sigma > 225 \text{ km.s}^{-1}$ criterion. This test is statistically significant because more than 50% of the 112 galaxies has been removed. (We performed the same study on data without ellipticity corrections and reached the same conclusion).

Effects of LINERs We added 17 LINER elliptical galaxies to the main sample. The best fit from this larger sample including LINERs agrees well with the main result given in previous section. However, this is not statistically significant because the sample size increased only by 13% (from 112 to 127 galaxies). We also checked the results of the linear fit using only LINERs and found it compatible with the main data (again with large statistical uncertainty). However, we notice that:

- The LINER distribution may be biased toward apparently rounder galaxies: $94 \pm 24\%$ of LINER have $R_{min}/R_{max}|_{apparent} > 0.65$, for only $76 \pm 8\%$ of our non-LINER sample. If true, this could bias the magnitude of the M/L and R_{min}/R_{max} correlation in the case of the LINER if that correlation is not linear (e.g. a weaker

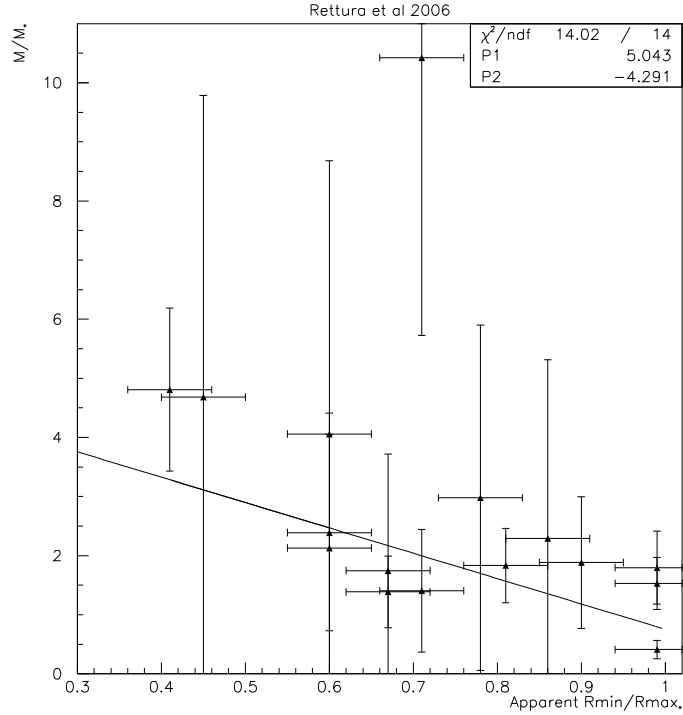


Figure 8: M_{dyn}/M_* vs apparent axis ratio from Rettura *et al.* [86] after applying ellipticity corrections. The uncertainties on M_{dyn}/M_* have been scaled so that $\chi^2/ndf \simeq 1$.

correlation at high R_{min}/R_{max} values would lower more the average M/L vs R_{min}/R_{max} slope in the case of LINERs).

- The shape of the M/L vs R_{min}/R_{max} distribution is similar for LINER and non-LINER. They are both flat before ellipticity corrections and thus similar after applying identical ellipticity corrections.

4.7 Rettura *et al.* (2006)

Rettura *et al.* [86] studied the relation between galaxy stellar masses M_* and dynamical masses M_{dyn} for a sample of 37 elliptical, 5 lenticular and 6 bulge-dominated spiral galaxies. M_* was obtained by matching the spectral energy distribution to composite stellar population model templates obtained from stellar population models in which a Kroupa Initial Mass Function -IMF- [68] was assumed. Several models were used but the results are not strongly model-dependent. M_* includes masses from stars and stars remnants (white dwarves, Black Holes,...) masses. M_{dyn} was computed assuming that galaxies are spheroidal non rotation-supported systems in virial equilibrium: $M_{dyn} \propto \sigma_0^2 R_{eff}$. From the 37 elliptical galaxies, we formed a sample excluding known AGN, two interacting giant galaxies belonging to the CL1252 cluster, O-II emission galaxies, E+A galaxies, and large X-ray emission galaxies. Furthermore, because the morphology of the galaxies is not as well known as for local galaxies, we excluded galaxies with velocity dispersion $\sigma_0 < 200 \text{ km.s}^{-1}$ to minimize possible S0 contamination (this selection could *a priori* bias our investigation because of the relation $M_{dyn} \propto \sigma_0^2$. However, our study in Section 4.6 indicated no such bias). Our final sample contains 16 galaxies. The axis ratios are obtained from [102], [40] or [55]. We assumed a ± 0.05 uncertainty on them. We applied the ellipticity corrections from Bacon *et al.* [3]. The M_{dyn}/M_* vs apparent axis ratio is shown in Fig. 8. The best linear fit is:

$$M_{dyn}/M_* = (-4.29 \pm 1.36)R_{min}/R_{max}|_{apparent} + (5.04 \pm 1.25).$$

Advantages of this analysis are that the stellar component was calculated differently from the other analyses and the data are relatively recent. A caveat is the additional model dependency (stellar population model, IMF choice) of the method. In addition, the galaxies are not as well characterized (morphology, spectra) as local ones. We assigned these data to group 3 reliability.

For completeness, the fit before ellipticity corrections yields $M_{dyn}/M_* = (-1.36 \pm 0.67)R_{min}/R_{max}|_{apparent} + (2.03 \pm 0.59)$.

4.8 van der Wel *et al.* (2006)

In Ref. [102], van der Wel *et al.* used a similar galaxy set as Rettura *et al.* [86]. The M/L_B vs apparent axis ratio is shown in Fig. 9. We apply the ellipticity corrections from Bacon *et al.* [3]. There are 13 galaxies in our sample.

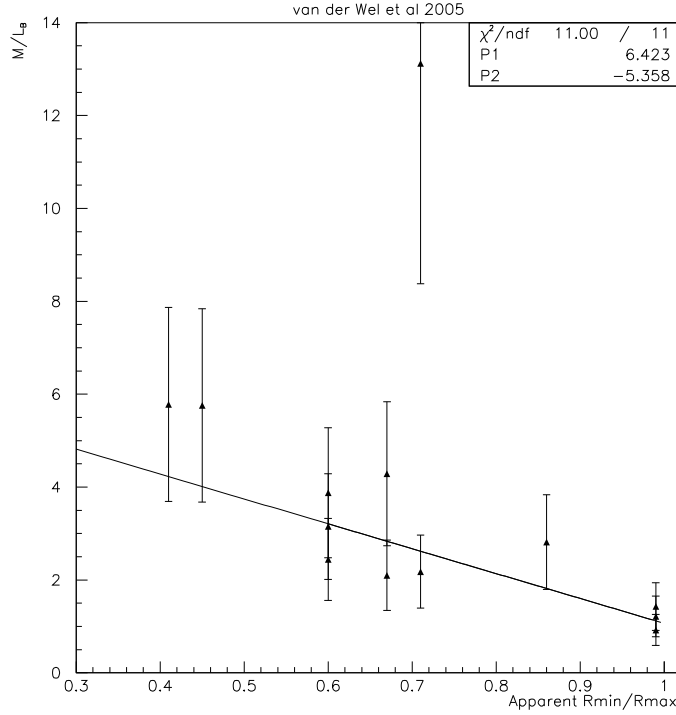


Figure 9: M_{dyn}/L_B vs apparent axis ratio from van der Wel *et al.* [102] after applying ellipticity corrections. The *unbiased estimate* method (forcing $\chi^2/ndf = 1$ by rescaling uncertainties has been applied).

The best linear fit is:

$$M/L_B = (-5.36 \pm 1.24) R_{min}/R_{max}|_{apparent} + (6.42 \pm 1.12).$$

As for Rettura *et al.* [86], we assign these data to group 3 reliability.

For completeness, the fit before ellipticity correction yields $M/L_B = (-1.12 \pm 0.75) R_{min}/R_{max}|_{apparent} + (2.28 \pm 0.57)$

5 Data using light profile measurements and stellar orbit modeling

This approach relies on modeling the stellar dynamics of galaxies using photometry data at different radii (light profile). Potentials for stellar and dark components are assumed and the light of the stars moving in the total potential is simulated. Parameters of the potentials are adjusted until the models match the data. We applied on the data sets the usual homogeneity selection criteria. However, when models did not rely on virial or isothermal equilibrium, we have relaxed the standard selection and include LINERS, AGN and Seyfert galaxies. An advantage of this method is that the true ellipticity of the galaxy can be inferred and accounted for in the determinations of M/L . A caveat is that the results are necessary model-dependent.

5.1 Cappellari *et al.* SAURON IV data set (2006)

Cappellari *et al.* [17] used stellar photometry data to provide M/L at $r = R_{eff}$ for 25 nearby bright elliptical galaxies. Careful extraction of M/L is argued, leading the authors to estimate a 6% error on M/L and 10% on stellar mass to light ratios, M_*/L . The true ellipticity was input in the calculations. It was obtained by modeling the photometry data. The authors chose to work with the velocity dispersion at R_{eff} , σ_e , rather than the central velocity dispersion σ_0 because σ_e is less sensitive to the aperture used for the observation device, and to details of orbitals. Out of an initial sample of 48 galaxies the authors selected 25 galaxies, requesting them to have accurate distance determination, a Hubble Space Telescope WFPC2 photometry and no strong evidence of a bar. After our selection we obtained a set of 6 galaxies. The authors provided two estimates of M/L . One is based on a 2-integral Jeans model (numerically accurate but less general) and one on a 3-integral Schwarzschild model [92] (numerically noisier but more general). The authors cautioned that large elliptical galaxies (more massive and slow rotators, redder and more metal rich) tend to be tri-axial, which may alter the M/L determination. The fits to the M/L vs ellipticity are shown in Fig. 10. The best fits, slightly corrected for the stellar M_*/L dependence with the intrinsic axis ratio $R_{min}/R_{max}|_{true}$ are:

$$M/L|_{Jeans} = (-1.47 \pm 1.56) R_{min}/R_{max}|_{true} + (3.84 \pm 1.10) \text{ and}$$

$$M/L|_{Schw} = (-1.09 \pm 1.68) R_{min}/R_{max}|_{true} + (3.48 \pm 1.17).$$

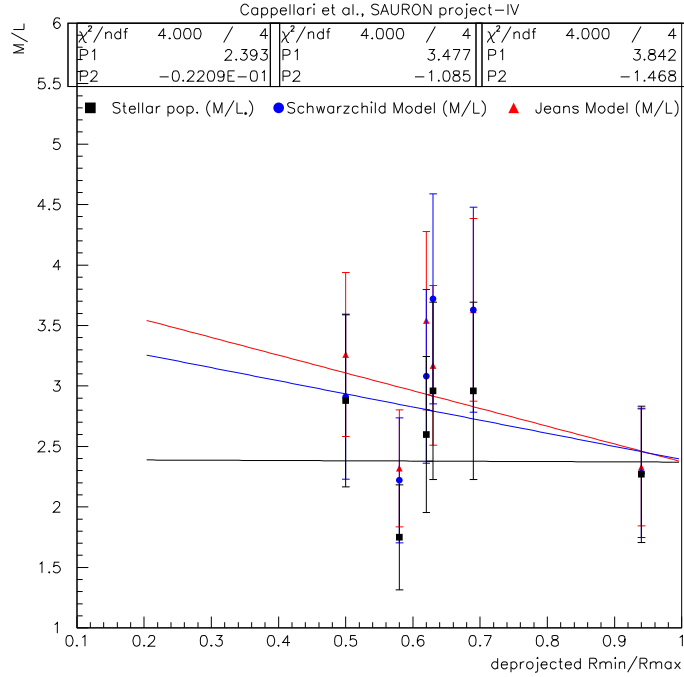


Figure 10: M/L vs intrinsic axis ratio $R_{min}/R_{max}|_{true}$ from M. Cappellari *et al.* [17]. The red triangles, blue circles and black squares are for $M/L|_{jeans}$, $M/L|_{schw}$ and M/L_* respectively.

The fit result for the stellar population is $M/L_* = (-0.02 \pm 1.72)R_{min}/R_{max}|_{true} + (2.39 \pm 1.16)$.

The analysis is based on a robust M/L extraction, with true ellipticity and projection effect accounted for. We assigned the results to group 1 reliability.

5.2 Cappellari *et al.* ATLAS project (2013)

The data used here come from two publications from Cappellari *et al.* [19, 20]. The authors analyzed a set of 32 elliptical galaxies using either the Salpeter IMF or the JAM model for modeling the light distribution. The authors also provide a quality factor for their extracted M/L and ellipticities, classifying each galaxy model from 0 (lower quality) to 3 (better quality). Thus, in addition to the full galaxy sample, we also considered two subsamples, the largest containing 23 galaxies with models of quality 1 to 3, and a smaller sample of 12 galaxies with models of quality 2 or 3. (The quality 3 model provides a sample of only 4 galaxies, a too small sample to be of use). The fits to the M/L vs axis ratio are shown for the full sample and subsamples in Fig. 11. The best fits for these samples are:

Quality 0-3, Salpeter IMF: $M/L| = (-4.72 \pm 2.19)R_{min}/R_{max}|_{true} + (8.04 \pm 1.69)$

Quality 0-3, JAM model: $M/L| = (-2.02 \pm 1.48)R_{min}/R_{max}|_{true} + (5.53 \pm 1.13)$

Quality 1-3, Salpeter IMF: $M/L| = (-0.10 \pm 0.97)R_{min}/R_{max}|_{true} + (5.83 \pm 0.30)$

Quality 1-3, JAM model: $M/L| = (-0.23 \pm 1.72)R_{min}/R_{max}|_{true} + (4.39 \pm 0.54)$

Quality 2-3, Salpeter IMF: $M/L| = (-0.97 \pm 1.07)R_{min}/R_{max}|_{true} + (6.64 \pm 1.07)$

Quality 2-3, JAM model: $M/L| = (-1.62 \pm 3.23)R_{min}/R_{max}|_{true} + (5.68 \pm 2.22)$

The M/L used in the analysis are robust and the true ellipticities are assessed consistently. Thus, we assigned the results to group 1 reliability.

As the four (sub)samples are not independent, we can use only one of them when combining all the data reported in this article to obtain an overall correlation. We used the results from the full sample (32 galaxies).

5.3 Kronawitter *et al.* (2000)

Kronawitter *et al.* [67] used non-parametric spherical models to map the gravitational fields of 21 round elliptical galaxies. From the maps, M/L_B in the inner (central M/L) and outer (outermost kinematic data point) parts of the galaxies were calculated. The technique used here did not rely on isothermal or virial equilibrium. We thus

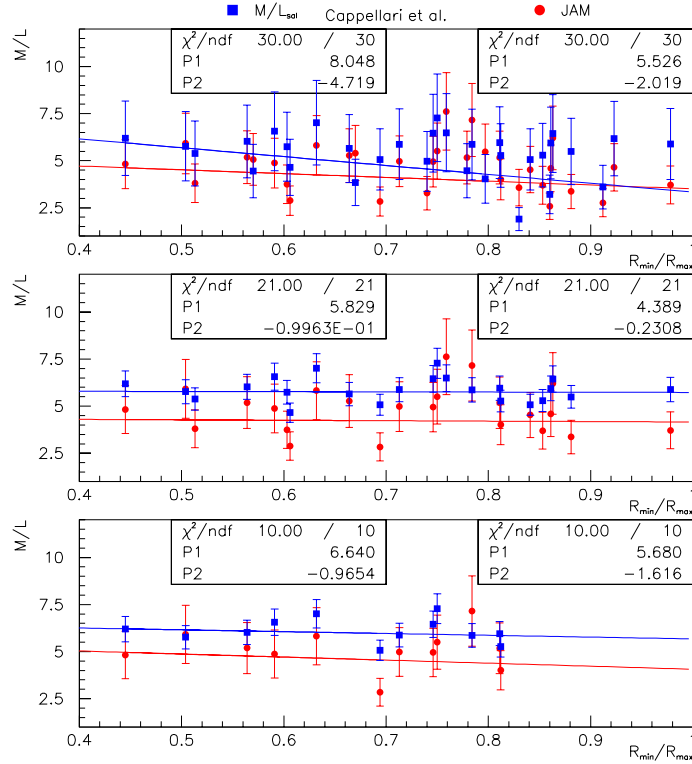


Figure 11: M/L vs intrinsic axis ratio from M. Cappellari *et al.* [19, 20]. The top panel shows the full sample, the middle panel a subsample with galaxy models of quality 1 to 3, and the bottom panel a subsample with model quality 2 or 3. The blue squares represent data obtained with a Salpeter IMF for modeling the light distribution, and the red circles were obtained with the JAM model. The best fit parameters are provided in the left boxes (Salpeter IMF) or right boxes (JAM model).

rejected only the cD, S0, peculiar, cE, SA0 and Arp galaxies present in the initial sample, keeping in particular LINERS, AGN and Seyfert galaxies. We remark that after standard selection, only three elliptical galaxies would have remained. This relaxed selection provided a sample of 10 galaxies. To estimate the model uncertainty, we took the difference between low and high M/L values provided in [67]. In addition, we added an uncertainty proportional to M/L_B to account for possible experimental uncertainties that would be common to the low and high estimates. The uncertainties were adjusted so that $\chi^2/ndf \simeq 1$ for the best fits. The authors estimated the effects of non-sphericity on their data and we corrected their M/L_B based on their numbers. Fig. 12 shows M/L_B vs apparent axis ratio. The best fits to the data are:

$$M/L_B|_{inner} = (-4.58 \pm 7.04) R_{min}/R_{max}|_{apparent} + (9.58 \pm 6.17).$$

$$M/L_B|_{outer} = (+6.53 \pm 14.48) R_{min}/R_{max}|_{apparent} + (1.25 \pm 12.48).$$

The $M/L_B|_{outer}$ ratio was originally determined at the outermost kinematic data point with r_{max} varying between $0.45R_{eff}$ and $2.95R_{eff}$, a domain where the dependence of M/L with radius becomes important. To obtain the M/L at the same radius value ($r = 1.25R_{eff}$, the average value for r_{max}), we interpolated or extrapolated the authors results.

The caveat of this data set is that the galaxies are chosen preferentially round. In the case of $M/L_B|_{outer}$, the smaller uncertainties on two galaxies (NGC3640 and NGC3379) drives the fit results. An advantage of the analysis is the correction for (apparent) ellipticity. We assigned the results to group 1 reliability.

5.4 Magorrian *et al.* (1998)

Magorrian *et al.* [73] modeled 32 galaxies to obtain M/L and central black hole mass M_{BH} (the main goal of [73]). The models assumed that galaxies are axisymmetric with an arbitrary inclination (not provided in the article), have a constant M/L , and have a central black hole. The models did not include anisotropies. The black hole, stellar and dark matter gravity fields were obtained respectively from a fit to Hubble Space Telescope (HST) photometry data, a given M_{BH} and assuming a given constant M/L . Jeans equations were used to obtain velocity and velocity dispersion profiles that were compared with ground based data. The ground based and HST data do not extend further than R_{eff} and are typically a few tenths of R_{eff} . After our standard selection, 7 galaxies

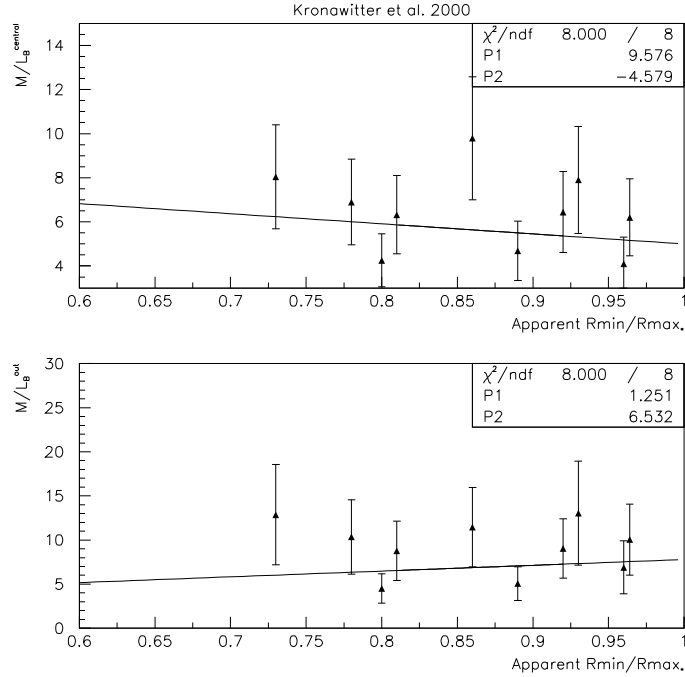


Figure 12: M/L_B vs apparent axis ratio from Kronawitter *et al.* [67]. The top (bottom) panel is for the inner (outer) M/L_B .

remained. We used axis ratios from NED. The M/L uncertainty was symmetrize and rescaled so that $\chi^2/ndf = 1$. M/L vs apparent axis ratio is shown in Fig. 13. The best fit is:

$$M/L = (+0.69 \pm 4.95) R_{min}/R_{max}|_{apparent} + (3.26 \pm 4.73).$$

A caveat is that the models do not include anisotropies. M/L is assumed to be constant, which is now known to be incorrect in general but is probably valid in the radial range addressed in this study. Advantages of the analysis are the corrections for ellipticity and inclination. We assigned the results to group 1 reliability.

5.5 Thomas *et al.* (2007, 2011) and Wegner *et al.* (2012)

Thomas *et al.* [97] studied 19 galaxies from the Coma cluster. Dark and luminous masses were obtained within R_{eff} using a dynamical model employing Schwarzschild orbit superposition techniques [92]. Galaxies were assumed to be axisymmetric and in dynamical equilibrium. The flattening of the galaxies was included in the model, although only 3 possible values for the galaxy inclinations were considered: 90° (assumes $R_{min}/R_{max}|_{true} = R_{min}/R_{max}|_{apparent}$), minimum inclination (assumes the galaxy is a E7) and intermediate inclination (assumes galaxy is a E5). A Log or a Navarro-Frenk-White (NFW) [81] profile was used for dark matter distribution and it was assumed that the baryonic mass profile is the same as the light emission profile (mass follows light assumption). Using these mass profiles, the potential was calculated and all possible orbits were determined. The light profiles obtained were compared to the data and the best fit determined the best model. The authors cautioned that, although this procedure should determine the most likely of the 3 possible inclinations, the selection procedure may be biased toward the 90° case. The uncertainty on M/L was calculated by accounting for all possible inclinations. We rescaled it so that our fit χ^2/ndf is 1. The authors computed the lens characteristics of their galaxies, although there is no known lensing observation from them, in order to compare their results to the SLACS strong lensing results, see sections 9.1 and 9.2. From this they provided, in the R_c -band, a dark matter fraction (DMf) within the Einstein radius R_{Ein} .

The same group that reported in [97] used the same methods and tools to analyze 8 early-type galaxies from the Abell 262 cluster (Wegner *et al.* [108]). We can thus add these data to the ones of [97]. Differences between the two works include:

- The Abell 262 cluster is less densely populated than the Coma cluster, so these galaxies are less liable to interaction with environment;
- The values of the Hubble constant is 69 in [97] and 70 in [108]. We have corrected the data from [108] to account for this difference.
- The galaxies discussed in [97] tend to be flat whilst the ones in [108] are selected to be round.

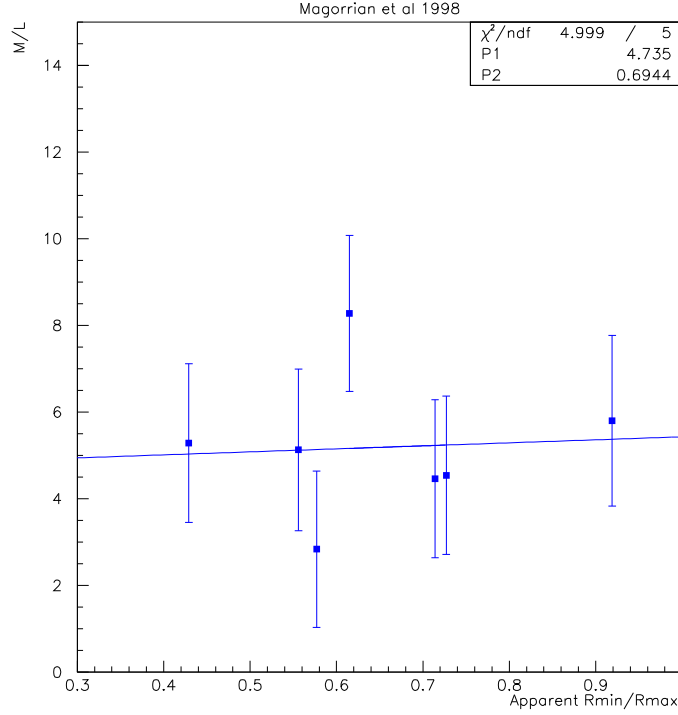


Figure 13: M/L vs apparent axis ratio from Magorrian *et al.* [73].

Four galaxies from [97] and three galaxies from [108] passed our selection criteria. The mass over light ratios and DMf within R_{eff} are shown in Fig. 14. M/L_{dyn} is obtained from the relation $M/L_{dyn} = \frac{M_*/L_{dyn}}{(1-DMf_{dyn})}$. The best fits are:

$$M/L_{R_{eff}, dyn} = (-9.43 \pm 9.74) R_{min}/R_{max}|_{apparent} + (14.05 \pm 8.43),$$

$$DMf_{R_{eff}, dyn} = (-0.36 \pm 0.54) R_{min}/R_{max}|_{apparent} + (0.62 \pm 0.25)$$

for the apparent axis ratio and:

$$M/L_{R_{eff}, dyn} = (-2.57 \pm 6.80) R_{min}/R_{max}|_{true} + (8.82 \pm 5.30),$$

$$DMf_{R_{eff}, dyn} = (-0.35 \pm 0.36) R_{min}/R_{max}|_{true} + (0.54 \pm 0.27)$$

for the true axis ratio.

The fit parameters obtained with apparent and true axis ratios are compatible, as expected since the uncertainties cover all 3 assumed inclinations.

The advantage of this analysis is that the effect of ellipticity was fully accounted for, although necessarily in a model dependent way and with only 3 possible values for the galaxy inclination. The caveat of this study is that the galaxies belong to a cluster. They thus may be subject to their environment. The results were assigned to group 1 reliability.

For information, we show other quantities in Fig. 14 : the $stellar M_*/L$ computed using a Kroupa or Salpeter IMF (available only from [97]); M/L_{sc} : this quantity assumes that the total mass follows light, i.e, M/L is independent of the galaxy radius. This assumption has been ruled out for $r > R_{eff}$ by many recent studies, including the one of Thomas *et al.*; Projected and deprojected $DMf(R_{Ein})$: these quantities are available only from [97]. They depend on the choice of linear relation between R_{Ein} and σ_{eff} , which is rather arbitrary. The procedure is adequate in the context of [97] but somewhat arbitrary for our purpose.

The best fits for these quantities are:

$$M_*/L_{Krou} = (+2.35 \pm 1.75) R_{min}/R_{max}|_{apparent} + (2.01 \pm 1.37),$$

$$M_*/L_{Sal} = (+2.87 \pm 3.82) R_{min}/R_{max}|_{apparent} + (3.69 \pm 2.92),$$

$$M/L_{sc} = (+1.47 \pm 9.88) R_{min}/R_{max}|_{apparent} + (5.92 \pm 8.14),$$

$$DMf_{proj}(R_{Ein}) = (+0.22 \pm 0.85) R_{min}/R_{max}|_{apparent} + (0.24 \pm 0.67),$$

$$DMf_{deproj}(R_{Ein}) = (-0.48 \pm 0.12) R_{min}/R_{max}|_{apparent} + (0.44 \pm 0.10)$$

for the apparent axis ratios and

$$M_*/L_{Krou} = (+0.94 \pm 1.48) R_{min}/R_{max}|_{true} + (3.09 \pm 1.05),$$

$$M_*/L_{Sal} = (+1.30 \pm 2.62) R_{min}/R_{max}|_{true} + (4.89 \pm 1.85),$$

$$M/L_{sc} = (+0.57 \pm 7.02) R_{min}/R_{max}|_{true} + (6.67 \pm 5.57). \text{ (We will use this result for our global analysis with a reliability factor 2)}$$

$$DMf_{proj}(R_{Ein}) = (+0.14 \pm 0.60) R_{min}/R_{max}|_{true} + (0.31 \pm 0.44),$$

$$DMf_{deproj}(R_{Ein}) = (-0.32 \pm 0.27) R_{min}/R_{max}|_{true} + (0.29 \pm 0.24)$$

for the true axis ratios.

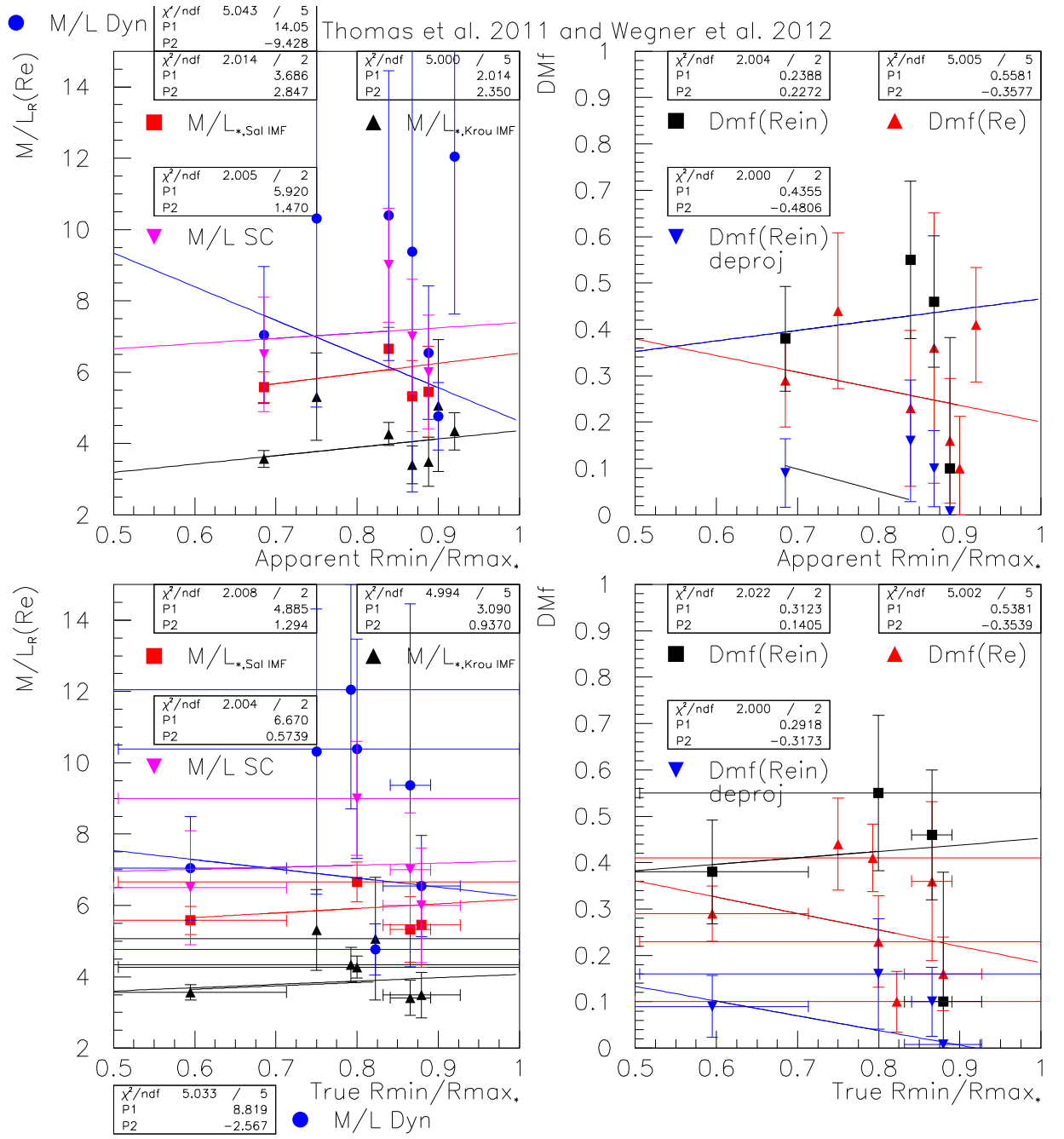


Figure 14: Mass over light ratios and DMf vs apparent and true axis ratios from Thomas *et al.* [97] and Wegner *et al.* [108]. The top left (resp. right) panel shows various M/L (resp. DMf) vs apparent axis ratio. Bottom row: same as top but for true axis ratio. The quantities of interest are M/L_{dyn} (blue filled circles) and $DMf(Re)$ (red filled triangles). Other quantities are shown for information.

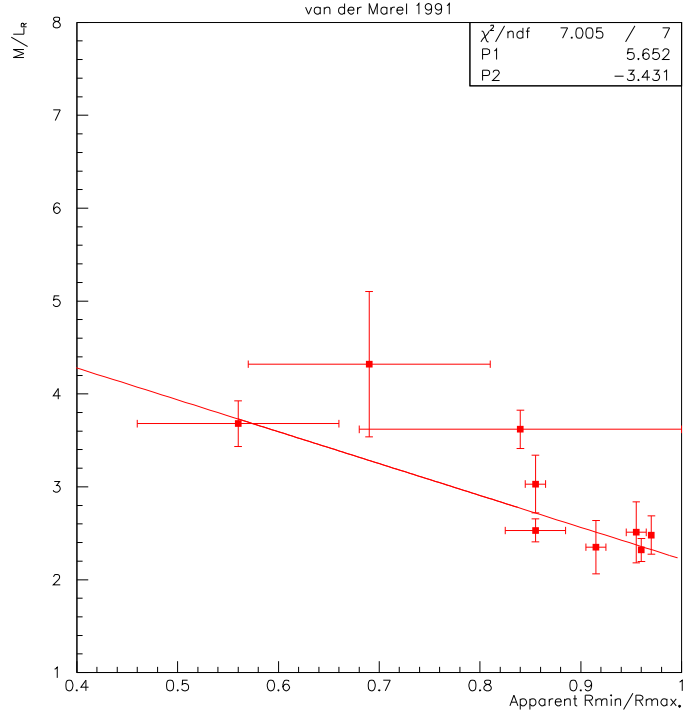


Figure 15: M/L_R vs axis ratio from van der Marel [104].

5.6 van der Marel (1991)

In [104] van der Marel constructed axisymmetric dynamical models for 37 local early-type galaxies selected for their high quality photometry. The models include anisotropy and rotation but kept M/L constant with radius. M/L was obtained by fitting the major and minor axis kinematics, which is more accurate than core fitting using the virial theorem. However, the author checked his work by also computing M/L using the virial tensor formula of Bacon *et al.* [3] which includes ellipticity but assumes M/L to be constant with radius. The two results, $M/L|_{\text{Virial tensor}}$ and $M/L|_{\text{axisy. dyn. model}}$ correlate well but the virial results are in average $2/3$ smaller. The good correlation confirms Bacon *et al.* [3] formula, which we used throughout Section 4 to correct results that did not account for the galaxy ellipticity. To form M/L , the mass density was obtained by deprojecting the luminosity profile and assuming $M/L = \text{constant}$. From that density, the gravitational potential was calculated by solving the Poisson equation. Finally, the Jeans equations, which assume hydrostatic equilibrium, were solved. M/L was calculated for two inclination angles: $i = 90^\circ$ and $i = 60^\circ$ but the difference is small: M/L is larger by about 10% for axis ratios of about 0.7 and, as expected, disappears for axis ratios near 1. The M/L used here are the average between the $i = 90^\circ$ and $i = 60^\circ$ results. The author computed the axis ratios using his models. We used the average of his result with the NED axis ratio, the difference being taken as uncertainty. The M/L_R ratios vs apparent axis ratios are shown in Fig. 15 for the 9 galaxies that passed selection. In addition to the standard selection criteria, we further rejected S0 candidates (NGC636, 3557, 4494 and IC0179) and S (NGC1370) galaxies, although they are listed as elliptical galaxies in NED. The best fit is:

$$M/L_R = (-3.43 \pm 0.92) R_{\min}/R_{\max}|_{\text{apparent}} + (5.65 \pm 0.84).$$

We rescaled the M/L uncertainties so that $\chi^2/ndf = 1$. The advantage of the analysis is that care has been taken in accounting and studying the effects of apparent ellipticities, inclination angles, anisotropies and rotations. The caveats are that the analysis is dated, but this is balanced by the author's galaxy selection based on the high quality of their photometry. The models assumed hydrostatic equilibrium, which we enforced by strict selection that removes about two thirds of the original galaxy sample. Finally a constant M/L is assumed. This is known to be incorrect at large radii, as the author and many other studies found, but this is reasonable at radius up to R_{eff} . We assigned the results to group 1 reliability.

5.7 van der Marel and van Dokkum (2007a)

In Ref. [105], van der Marel and van Dokkum studied 25 early-type galaxies using stellar rotation and velocity dispersion data. The galaxies belong to 3 clusters at redshift $z \simeq 0.5$ (except for one field galaxy. But we will ignore it as it is classified as a E/S0). The data were interpreted with oblate axisymmetric 2-integral dynamical models based on Jeans' equations of hydrostatic equilibrium. M/L_B was assumed to be constant

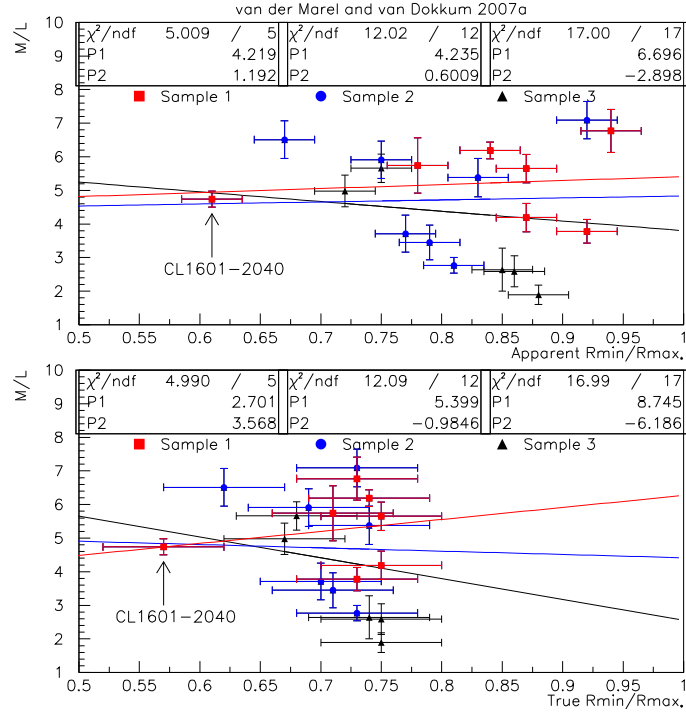


Figure 16: M/L vs apparent (top) and “true” (bottom) axis ratios from van der Marel and van Dokkum [105].

with radius. This assumption has been ruled out by many recent studies (e.g. [67, 97, 104, 16, 74, 78, 79, 9]), although it appears reasonable in the radius range considered here ($r < R_{eff}$). Using the inferred probability distribution of true axis ratio for elliptical galaxies, the authors computed for each galaxy a most-likely true axis ratio. This one was calculated by taking the average over all possible values of the true axis ratio for a galaxy ($0.3 \leq R_{min}/R_{max}|_{true} \leq R_{min}/R_{max}|_{apparent}$) weighted by the true axis ratio probability distribution. The resulting “true” axis ratio may not be the actual one but is a reasonable guess that follows the expected gaussian distribution of true axis ratios. The galaxies in [105] were identified only by visual inspection. To address the possibility of S0 contaminating the galaxy set, we estimated the probability to be a S0 using the expected characteristics of S0 (σ tends to be lower, high rotational support and strong ellipticity dependence with radius. We did not consider the additional fact that ellipticities of S0 are large to not bias our study). Based upon this criteria, of the 25 galaxies 7 were unlikely to be S0 (none of those are listed as S0 in [105]), 12 were possibly S0 (4 listed as S0 or E/S0 in [105]) and 6 were likely to be S0 (1 of those is a known S0/Sb). Assuming that about half of the 12 possible S0 are indeed S0, the 25 early-type sample contained about 13 E and 12 S0, agreeing with the known repartition of the local E and S0 galaxies. Removing the 5 galaxies listed in [105] as visually identified as S0, E/S0 or S0/Sb, we obtained Sample 3 of 19 galaxies. Removing from it 5 galaxies that are likely to be S0 based on our criteria, we obtained Sample 2 (15 galaxies). Finally considering only the galaxies unlikely to be S0, we obtained Sample 1 (7 galaxies). The M/L_B ratios vs apparent and true axis ratios are shown in Fig. 16. We can see that the S0 rejection criteria removed the low M/L points, possibly biasing our study. To address this, we did not use this criteria for the determination of the slopes but only to estimate the uncertainty due to possible S0 contamination. The best fits are:

$$\begin{aligned}
 M/L_B &= (+1.19 \pm 3.31)^{R_{min}/R_{max}|_{apparent}} + (4.22 \pm 2.65) \text{ for Sample 1,} \\
 M/L_B &= (+3.57 \pm 5.12)^{R_{min}/R_{max}|_{true}} + (2.70 \pm 3.55) \text{ for Sample 1,} \\
 M/L_B &= (+0.60 \pm 3.83)^{R_{min}/R_{max}|_{apparent}} + (4.24 \pm 3.06) \text{ for Sample 2,} \\
 M/L_B &= (-0.98 \pm 6.04)^{R_{min}/R_{max}|_{true}} + (5.40 \pm 4.24) \text{ Sample 2,} \\
 M/L_B &= (-2.90 \pm 3.84)^{R_{min}/R_{max}|_{apparent}} + (6.70 \pm 3.10) \text{ for Sample 3,} \\
 M/L_B &= (-6.19 \pm 5.99)^{R_{min}/R_{max}|_{true}} + (8.75 \pm 4.23) \text{ for Sample 3.}
 \end{aligned}$$

All in all using the samples 1 and 2 to estimate the S0 contamination to the main sample (sample 3), we obtain:

$$\begin{aligned}
 M/L_B &= (-2.90 \pm 5.60)^{R_{min}/R_{max}|_{apparent}} + (6.70 \pm 3.97), \\
 M/L_B &= (-6.19 \pm 11.45)^{R_{min}/R_{max}|_{true}} + (8.75 \pm 7.38).
 \end{aligned}$$

The uncertainties from [105] were rescaled so that $\chi^2/\text{ndf} = 1$. Advantages of this study are that ellipticity was mostly accounted for in the calculations, and a true ellipticity was tentatively given. Caveats of this analysis are the lack of good galaxy identification (S0 contamination) and of features revealing possible disturbance, whereas the M/L extraction assumes hydrostatic equilibrium. Thus, we could not implement our standard selection of

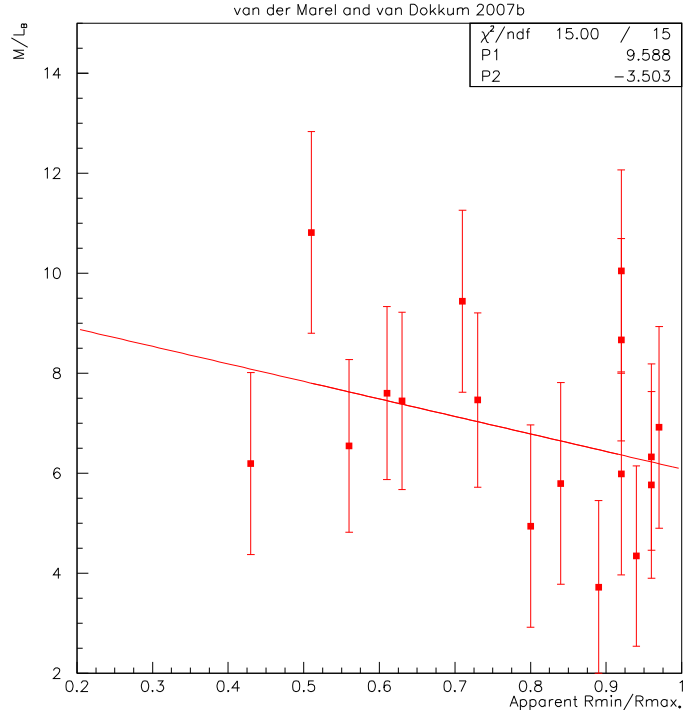


Figure 17: M/L vs apparent axis ratio from van der Marel and van Dokkum [106].

undisturbed galaxies. An uncertainty for the S0 contamination was assessed using tight selection. Other caveats are the redshift $z \simeq 0.5$ may cause systematic differences between the sample and local galaxies, and that M/L was assumed to be constant. Finally, the positive fit slopes are driven by a single galaxy of large ellipticity and small uncertainty: CL1601-2040. As can be seen in Fig. 16, all slopes would be negative without CL1601-2040. However, we had no reason to exclude it from the study. The *unbias estimate* method partly accounted for this outlier. Since the S0 and outlier issues are reflected in the final uncertainty, the results are still assigned to group 2 reliability rather than a lower reliability group.

5.8 van der Marel and van Dokkum (2007b)

In order to compare the $z \simeq 0.5$ results of the previous section with results from local galaxies, van der Marel and van Dokkum compiled from the literature a homogenized M/L_B for 60 early-type galaxies [106]. The M/L_B were corrected using a consistent distance determination and, if needed to be, re-expressed in the B-band. The redshift of the galaxies forming the set is $z \simeq 0.005$. All the literature sources compiled in [106] were also used in the our present study: van der Marel: Section 5.6, Magorrian *et al.*: Section 5.4, Gebhardt *et al.*: Section A, Kronawitter *et al.*: Section 5.3 and Cappellari *et al.*: Section 5.1. However, it is still interesting to consider the compilation of [106] because results have been homogenized. Applying our standard selection to the initial 60 galaxies, we obtained a sample of 17 galaxies. The sources contribute with similar statistics (van der Marel: 8 galaxies, Magorrian *et al.*: 5 galaxies, Kronawitter *et al.*: 4 galaxies, Gebhardt *et al.*: 6 galaxies, Cappellari *et al.*: 6 galaxies). Hence, our final sample is a representative average rather than being strongly bias toward a particular work. The M/L_B ratio vs apparent axis ratio is shown in Fig. 17. The best fit gives:

$$M/L_B = (-3.50 \pm 2.62) R_{min}/R_{max}|_{apparent} + (9.59 \pm 2.08).$$

The advantages and caveats of these data are already discussed in the sections 5.6 (group 1 reliability), 5.4 (group 1 reliability), A (data unused, due to low statistics and correlations), 5.3 (group 1 reliability) and 5.1 (group 1 reliability). Most of these data were already used for our analysis, although they have been homogenized and averaged when a particular galaxy was available from several of the literature sources. The results are assigned to group 1 reliability but partly weighted out when we consider the global results incorporating all M/L vs axis ratio, see Section 13.

6 Data sets using Planetary Nebulae and Globular Clusters

Planetary Nebulae (PNe) and Globular Clusters (GC) provide well resolved tracers extending to large radii. They offer the possibility to examine individual stars (PNe) or compact stellar assemblies (GC) to robustly assess

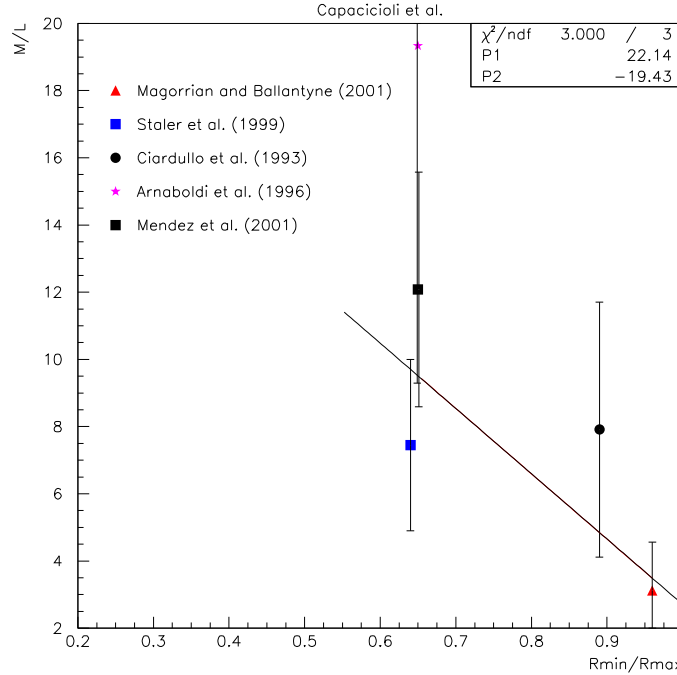


Figure 18: $M/L_B(R_{eff})$ ratio vs apparent axis ratio R_{min}/R_{max} for the compilation of Capaccioli, Napolitano and Arnaboldi [16]. The various symbols refer to the original authors of the M/L extraction, see references in [16].

the gravitational potential over a large radial range. Caveats of this method in our context is that the ellipticity determined from photometry might not match the ellipticity at large radii, and that the tracers at large radii may be influenced by the cluster or group hosting the galaxy. A general concern with GC is that they may be decoupled from the evolution their host galaxy: they are good tracers of the overall gravity field but may have a different rotational structure and whilst PNe tend to follow the light distribution, GC tend to be more extended. However, this is unimportant in the context of our study. Furthermore, since GC tend to belong to heavier galaxies which typically do not fulfill the selection criteria, the role of GC in our study is minimal.

All the literature sources used below assumed spherical symmetry. To account for ellipticity, we noted that the ellipticity corrections to the virial method (Section 4) and the X-ray method (Section 7) are close, as can be seen by comparing our Fig. 22 to the figures 1a and 1b of Bacon *et al.* [3]. We assumed the same correction to the M/L extracted from PNe and GC data.

6.1 Capaccioli, Napolitano and Arnaboldi (1992)

Capaccioli, Napolitano and Arnaboldi [16] provided a compilation from the literature on M/L_B . The mass to light ratio for 14 galaxies was obtained from PNe tracers (no GC) at two different radii (inner and outer M/L_B), so that the M/L_B gradient could be calculated. The radii at which the M/L_B were given differ from galaxy to galaxy so we interpolated linearly between the inner and outer M/L_B to obtain a value at R_{eff} for all the galaxies. Following the authors, we used uncertainties of 10% and 30% for the inner and outer M/L_B respectively, and propagated them to R_{eff} . None of the galaxies in [16] passed our selection criteria. Relaxing the selection to include all galaxies except the disrupted ones, galaxies showing possible interactions and clear non-elliptical galaxies, we obtained a set of 5 galaxies: NGC 1379 (maybe a spiral), 1700 (EXG), 3379 (LINER, VCXG), 4406 (SO(3)/E3) and 4697 (LLAGN). The fit to the M/L_B vs axis ratio is shown in Fig. 18. The best fit is:

$$M/L_B(R_{eff}) = (-19.43 \pm 7.85) R_{min}/R_{max}|_{apparent} + (22.14 \pm 6.82).$$

Caveats are that the data were obtained from difference sources (which may result in author-to-author bias) and include galaxies of unsure type, cD, LINERS and LLAGN. We assigned the results to group 3 reliability.

For information, the best fit before ellipticity corrections is:

$$M/L_B(R_{eff}) = (-9.62 \pm 5.87) R_{min}/R_{max}|_{apparent} + (12.59 \pm 5.10).$$

6.2 Deason *et al.* (2012)

Deason *et al.* [30] employed PNe and GC as kinematic tracers to provide M/L and DMf integrated up to a radius of $5R_{eff}$. The DMf was extracted model dependently using either a Chabrier/Kroupa [25]/[68] or a Salpeter [89] Initial Mass Function (IMF). The authors studied 15 galaxies using a spherically symmetric model.

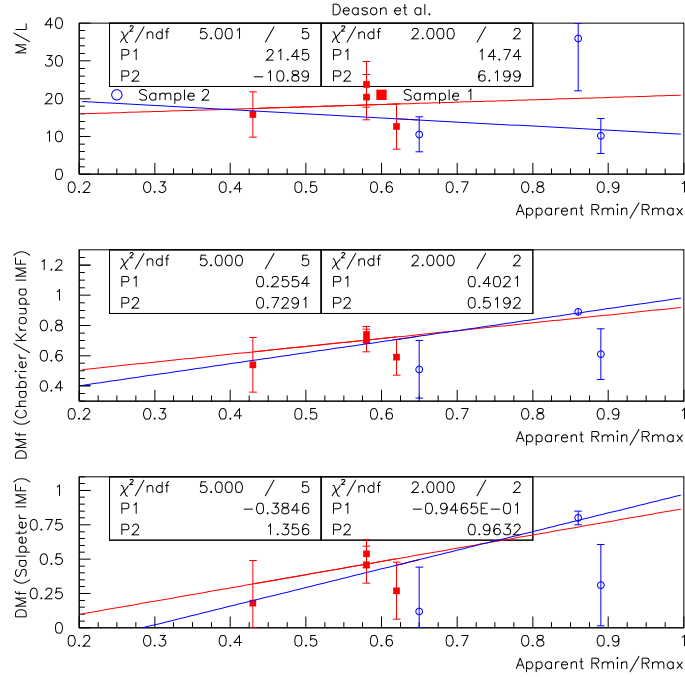


Figure 19: M/L and DMf vs diameter ratio R_{min}/R_{max} for the Deason *et al.* analysis [30]. The red and blue lines represent the best fits to the data of Sample 1 and 2 respectively. The DMf values on the middle and bottom panels were obtained with different IMF models.

The model allowed to form line of sight velocity distributions that were matched to the measured ones using a maximum likelihood method. It was assumed that the tracers' orbit are dominated by random motion rather than systematic motion. Furthermore, any possible galaxy rotation was ignored and simple power-law profiles for tracer density and potential were assumed. Velocity anisotropies were accounted for. The potentials and anisotropy parameters were determined by the best fit to the measurements of the tracer line of sight velocity distribution. From this, the mass was extracted. The usual galaxy selection yielded a first sample (Sample 1) of 4 good elliptical galaxies (NGC 821, 1344, 3377 and 4564). For this analysis, we can relax the selection to include LINERS, Sy, VCXG and LLAGN galaxies. We obtained then Sample 2 with 3 additional galaxies NGC 3379, 4374 and 4697. DMf vs R_{min}/R_{max} is shown on Fig. 19. The fits yield:

$$M/L = (+6.20 \pm 41.49) R_{min}/R_{max}|_{apparent} + (14.74 \pm 23.12) \text{ for sample 1 and}$$

$$M/L = (-10.89 \pm 17.71) R_{min}/R_{max}|_{apparent} + (21.45 \pm 12.73) \text{ for sample 2.}$$

We assigned the M/L result to group 1 reliability and used Sample 2 when combining all the publication together into one global result in Section 13.

For information, the best fits before ellipticity corrections are:

for sample 1:

$$M/L = (+18.86 \pm 24.59) R_{min}/R_{max}|_{apparent} + (-0.17 \pm 13.70),$$

$$DMf = (+0.52 \pm 1.12) R_{min}/R_{max}|_{apparent} + (0.40 \pm 0.65(\text{fit}) \pm 0.49 \text{ for the Chabrier/Kroupa IMF and}$$

$$DMf = (+0.96 \pm 1.91) R_{min}/R_{max}|_{apparent} + (-0.08 \pm 1.10 \text{ for the Salpeter IMF.}$$

For Sample 2:

$$M/L = (+5.88 \pm 13.72) R_{min}/R_{max}|_{apparent} + (5.41 \pm 9.86),$$

$$DMf = (+0.73 \pm 0.30) R_{min}/R_{max}|_{apparent} + (0.26 \pm 0.25 \text{ for the Chabrier/Kroupa IMF and}$$

$$DMf = (+1.37 \pm 0.59) R_{min}/R_{max}|_{apparent} + (-0.38 \pm 0.50 \text{ for the Salpeter IMF.}$$

6.3 Magorrian and Ballantyne (2001)

Magorrian and Ballantyne [74] used PNe data to compute $M/L(r)$ for 18 round early-type galaxies. The following method was employed: the velocity dispersion $\sigma(r)$ was calculated assuming a $M/L(r)$ form and using Jeans equations and the luminosity density. This one was obtained from the measured surface brightness deprojected assuming a spherically symmetric galaxy. The obtained $\sigma(r)$ was fit to measured stellar or PNe velocity dispersions. The best fit determined the free parameters of the assumed $M/L(r)$ form.

After we applied our standard selection, 6 elliptical galaxies remained. We used values of $M/L(r)$ integrated up to R_{eff} . The M/L vs stellar axis ratios are shown in Fig. 20. The best fit yields:

$$M/L = (-2.45 \pm 8.60) R_{min}/R_{max}|_{apparent} + (9.18 \pm 7.57).$$

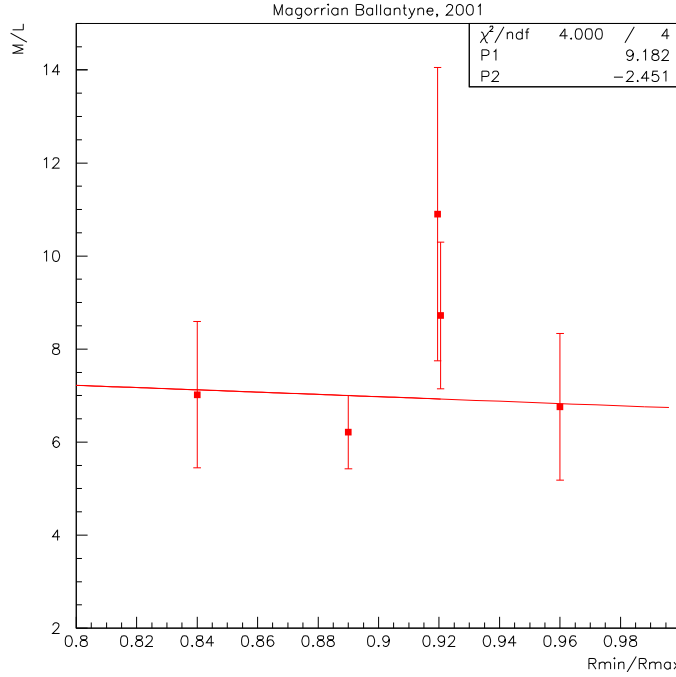


Figure 20: M/L vs apparent axis ratio from the data analyzed by Magorrian and Ballantyne [74].

Advantages of this analysis are that the authors provided a detailed study of the effect of anisotropy and spherical asymmetry assumptions. They concluded that anisotropies have a small effect on M/L whilst the spherical symmetry is a critical assumption with large effects on M/L . The difficulty is that the effects of anisotropies or flattening are not distinguishable on the observed velocity dispersion data whilst, as just said, the magnitude of their influence on the M/L value is different. According to [74] their spherically symmetric model underestimates M/L . We assigned the result to reliability group 1.

For information, the best fit before ellipticity corrections is:

$$M/L = (+4.38 \pm 7.99) R_{min}/R_{max}|_{apparent} + (2.34 \pm 7.03).$$

6.4 Romanowsky *et al.* (2003)

Romanowsky *et al.* [87] used kinematics of PNe to extract the rotation curves of three elliptical galaxies, each of them possessing about a hundred of observable PNe. The possible effect of anisotropies was studied with a spherical Jeans model in which an anisotropy parameter spans its full possible range. From the model, $M/L_B(r = 5R_{eff})$ were obtained. Furthermore, a different method was used with NGC3379 to investigate the effect of velocity anisotropy variation with radius. The true axis ratios of the galaxies investigated in [87] had been inferred in [17], [48] and [95]. The M/L_B vs axis ratios are shown in Fig. 21. The best fits are:

$$M/L_B(r = 5R_{eff}) = (-58.20 \pm 4.40) R_{min}/R_{max}|_{apparent} + (59.47 \pm 3.48),$$

$$M/L_B(r = 5R_{eff}) = (-142.47 \pm 63.47) R_{min}/R_{max}|_{true} + (111.50 \pm 42.86),$$

where we rescaled the uncertainties on both M/L and R_{min}/R_{max} so that the fit $\chi^2/ndf = 1$. An advantage of this work is the detailed study of the effect of anisotropies using two different techniques. We assigned the results to group 1 reliability.

For information, the best fits before ellipticity corrections are:

$$M/L_B(r = 5R_{eff}) = (-28.99 \pm 4.42) R_{min}/R_{max}|_{apparent} + (32.30 \pm 3.56),$$

$$M/L_B(r = 5R_{eff}) = (-68.78 \pm 33.08) R_{min}/R_{max}|_{true} + (56.83 \pm 22.38).$$

7 Data sets using X-ray

The extraction of a galaxy mass $M(r)$ from X-ray emitting interstellar medium (ISM) data assumes that 1) the hot gas is in hydrostatic equilibrium under the galaxy gravitational potential: $dP/dr = -GM(r)\rho(r)/r^2$, and 2) that the gas follows the perfect gas law: $Pm = \rho kT(r)$. Here, P is the ISM gas pressure, ρ its density, T its temperature, m the gas molecule average mass ($m \simeq 582$ MeV) and k is the Boltzmann constant. $M(r)$ can be extracted by combining the two previous equations: $M(r) = -\frac{kTr}{Gm} \frac{d\ln(\rho) + d\ln(T)}{d\ln(r)}$.

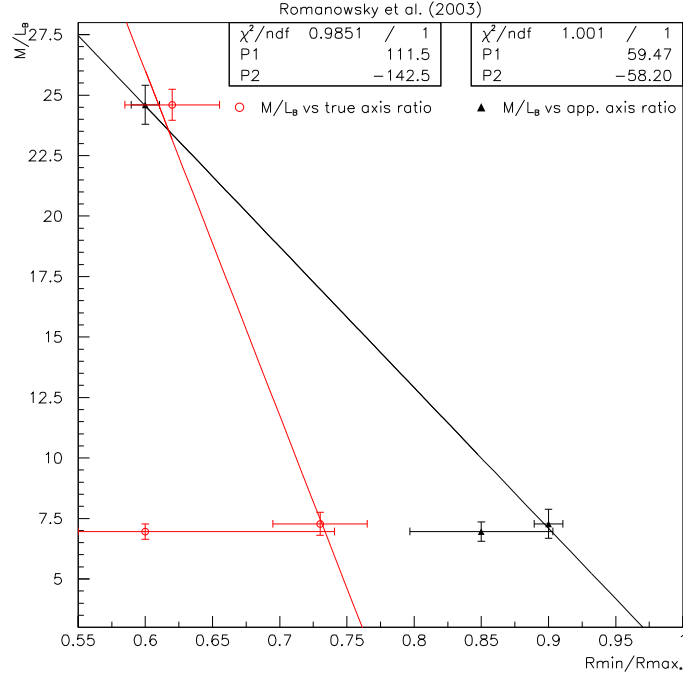


Figure 21: M/L from Romanowsky *et al.* [87] vs apparent axis ratio (full black triangles) and inferred true axis ratio (open red circles).

In the context of our study, this method has caveats. X-ray emission occurs mostly in giant galaxies, usually the one dominating its group or cluster (cD galaxies). Hot gas is highly collisional and can be heated by inner processes (electromagnetic emissions) or outer influences (galaxy interacting with its environment) and hence may be off equilibrium. In fact, results may correlate with the galaxy environment, as found in Das *et al.* [29].

All publications used here assumed spherical symmetry. We can partly account for ellipticity effects by replacing Newton's shell theorem used to derive $dP/dr = -GM(r)\rho(r)/r^2$ by a relation accounting for the ellipticity. In Fig. 22, we show the gravitational force in function of the axis ratio of an oblate spheroid of constant density, normalized to the force one would obtain if it were computed from Newton's shell theorem. We set the mass of the spheroid to be independent of the axis ratio. Thus the density increases with ellipticity. This is relevant for a galaxy of known mass (luminosity) and unknown density³. Although this simple correction is only accounting for part of the ellipticity effects, we have used the median case in Fig. 22 to correct the X-ray data.

7.1 Fukazawa *et al.* (2006)

X-ray data from Chandra X-ray Observatory satellite were used by Fukazawa *et al.* [49] to extract the temperature profiles of 53 elliptical galaxies. Each luminosity profile was obtained assuming a de Vaucouleur law [39]. Values for M/L were provided at R_{eff} . After standard selection, our final sample contains 7 adequate elliptical galaxies. M/L vs axis ratio (from NED) is shown in Fig. 23. No uncertainties were provided in [49], so we assumed them to be proportional to their corresponding M/L , and adjusted them so that the best fit has $\chi^2/ndf = 1$. The best fit to the data yields:

$$M/L_B(R_{eff}) = (-0.55 \pm 15.44)R_{min}/R_{max}|_{apparent} + (5.29 \pm 11.74).$$

The caveats of these results are as follow. Our correction for ellipticity is basic (see Section 7). There is no correction for the asymmetry of the gas distribution (due e.g. to AGN jets), although this particular caveat is alleviated by our selection requirement. No uncertainties were provided. Because of the simplicity of the ellipticity corrections, the possible gas asymmetry effects and the absence of provided uncertainties, we assigned the results to group 2 reliability.

For information, the fit before ellipticity correction is:

$$M/L_B(R_{eff}) = (+0.38 \pm 11.45)R_{min}/R_{max}|_{apparent} + (3.54 \pm 8.52).$$

³To obtain similar results at constant density (relevant to galaxies of known density but unknown luminosity), one should take the results of Fig. 22 and multiply them by the axis ratio R_{min}/R_{max} , because an oblate spheroid volume is $(4/3)\pi r_{min}^2 r_{max}$. However, this case is irrelevant to us.

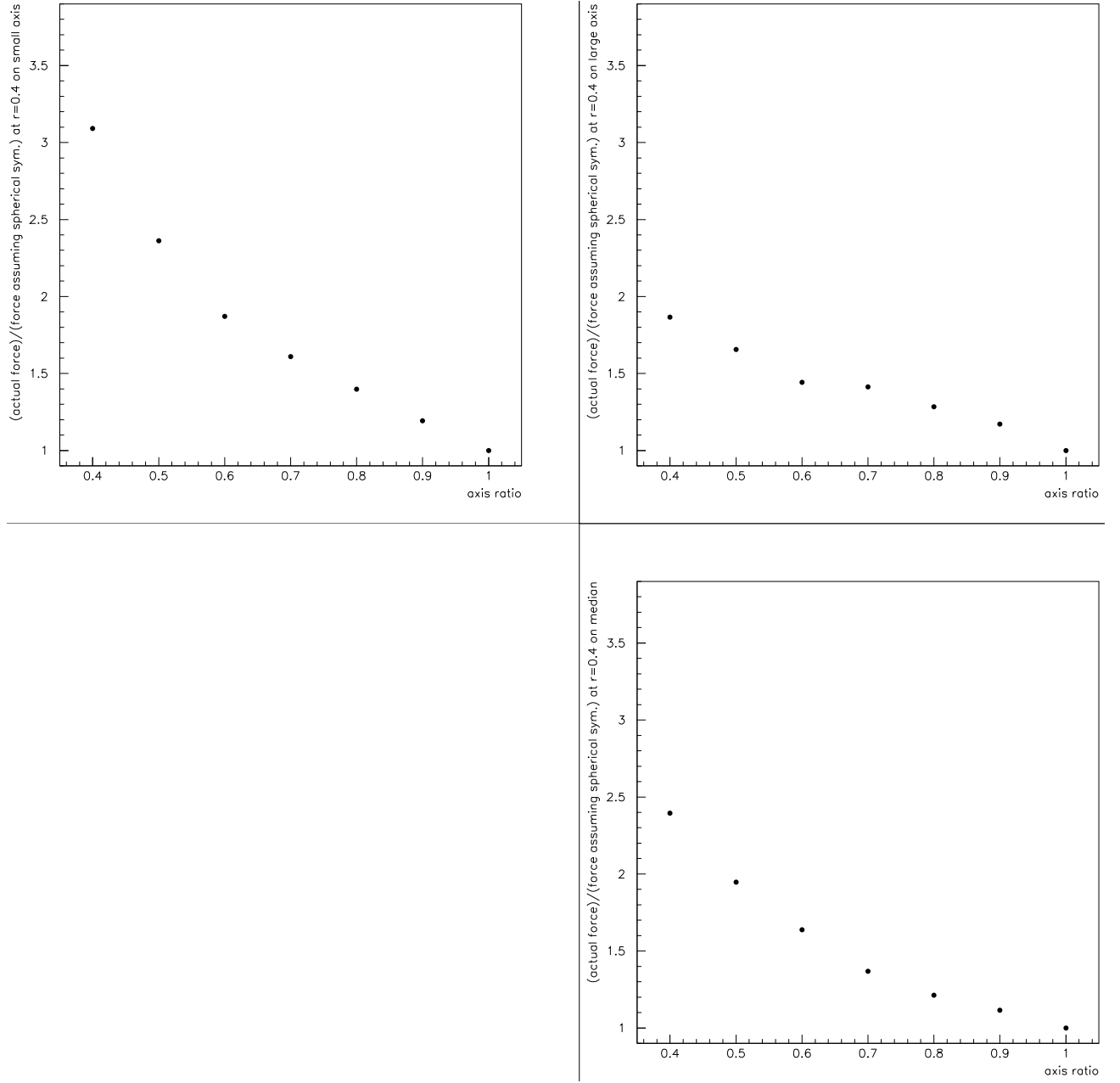


Figure 22: Gravitational force in function of the axis ratio for an oblate spheroid of constant density, normalized to the force one would (erroneously) obtain assuming Newton's shell theorem. Top left plot: the force is computed at point on a small axis at a radius $r=0.4R_{max}$. Top right plot: same as left but the force is computed at a $r=0.4R_{max}$ point on a large axis. Bottom plot: same as top plots but for the force on a point on the median between a small and a large axis ($r=0.4R_{max}$).

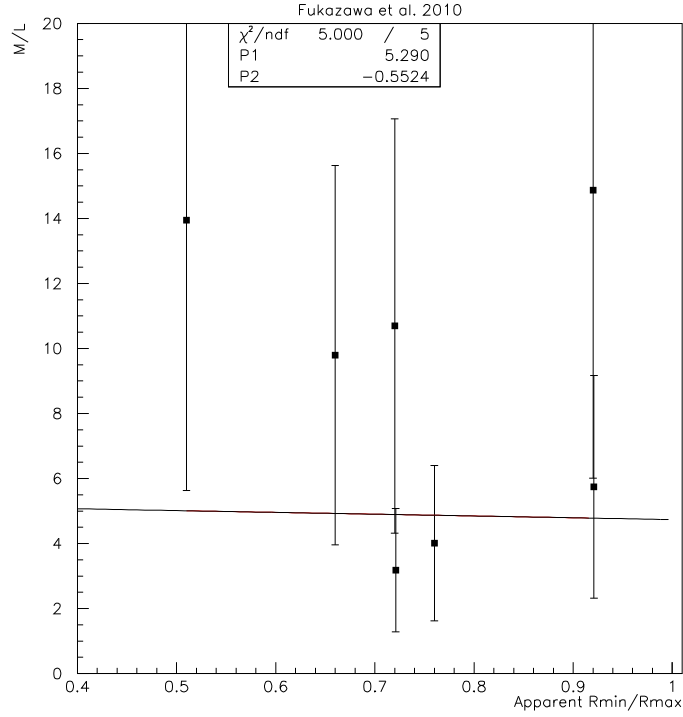


Figure 23: M/L vs apparent axis ratio for Fukazawa *et al.* [49].

7.2 Nagino and Matsushita (2009)

Nagino and Matsushita [78] used X-ray data from the XMM-Newton and Chandra satellites to extract M/L integrated up to 3 different radii ($0.5R_{eff}$, $3R_{eff}$ and $6R_{eff}$) for 22 early-type galaxies. To obtain $M(r)$, the temperature and density profiles were deprojected assuming the ISM to be spherically symmetric. Likewise, the luminosity was deprojected to obtain the stellar mass profile assuming spherical symmetry and a de Vaucouleur profile [39]. After standard selection, 4 galaxies remain. M/L was extracted both in the B-band and K-band. We assumed the uncertainties to be proportional to the corresponding M/L values, with $\chi^2/ndf = 1$. However, only two points are available for $6R_{eff}$ so χ^2/ndf is undefined. In that case, we used the average of the uncertainties from $0.5R_{eff}$ and $3R_{eff}$. The axis ratios are from NED. The best fits (shown in Fig. 24) are:

$$\begin{aligned} M/L_B(< 0.5R_{eff}) &= (-12.24 \pm 8.41)R_{min}/R_{max}|_{apparent} + (20.94 \pm 6.01), \\ M/L_K(< 0.5R_{eff}) &= (-1.76 \pm 3.26)R_{min}/R_{max}|_{apparent} + (3.21 \pm 2.32), \\ M/L_B(< 3R_{eff}) &= (-20.85 \pm 33.35)R_{min}/R_{max}|_{apparent} + (38.32 \pm 23.74), \\ M/L_K(< 3R_{eff}) &= (-1.21 \pm 10.36)R_{min}/R_{max}|_{apparent} + (4.39 \pm 7.31). \end{aligned}$$

The lines going through the 2 data points at $6R_{eff}$ are:

$$\begin{aligned} M/L_B(< 6R_{eff}) &= (-232.0 \pm 94.0)R_{min}/R_{max}|_{apparent} + (182.5 \pm 59.9), \\ M/L_K(< 6R_{eff}) &= (-60.35 \pm 34.68)R_{min}/R_{max}|_{apparent} + (43.58 \pm 22.52). \end{aligned}$$

As for the results from Section 7.1, we assigned these results to reliability group 2.

For information, the fit results before ellipticity correction are:

$$\begin{aligned} M/L_B(< 0.5R_{eff}) &= (3.43 \pm 3.79)R_{min}/R_{max}|_{apparent} + (6.38 \pm 2.58), \\ M/L_K(< 0.5R_{eff}) &= (0.36 \pm 1.94)R_{min}/R_{max}|_{apparent} + (1.18 \pm 1.33), \\ M/L_B(< 3R_{eff}) &= (5.02 \pm 19.22)R_{min}/R_{max}|_{apparent} + (13.55 \pm 13.14), \\ M/L_K(< 3R_{eff}) &= (1.05 \pm 6.91)R_{min}/R_{max}|_{apparent} + (1.833 \pm 4.73). \end{aligned}$$

The lines going through the 2 data points at $6R_{eff}$ are:

$$\begin{aligned} M/L_B(< 6R_{eff}) &= (-88.00 \pm 44.54)R_{min}/R_{max}|_{apparent} + (78.48 \pm 27.76), \\ M/L_K(< 6R_{eff}) &= (-27.33 \pm 17.25)R_{min}/R_{max}|_{apparent} + (20.64 \pm 11.08). \end{aligned}$$

8 Data sets using warm or cold gas disk dynamics

Cold hydrogen gas (HI) can be found in some elliptical galaxies. It extends to large distances ($r > 10R_{eff}$). M/L is determined using ionized gas disks embedded in the galaxies as kinematical tracers. Ionized warm gas can also be used but warm gas disks are less extended and thus can be determined only in the inner regions. The M/L are obtained the same way as for spiral galaxies, i.e, using a model with visible and dark component potentials to match the disk rotation curve. Thus virial or hydrostatic equilibrium is not assumed and our usual selection criteria can be relaxed. A caveat for our study with this method of M/L determination is that extended

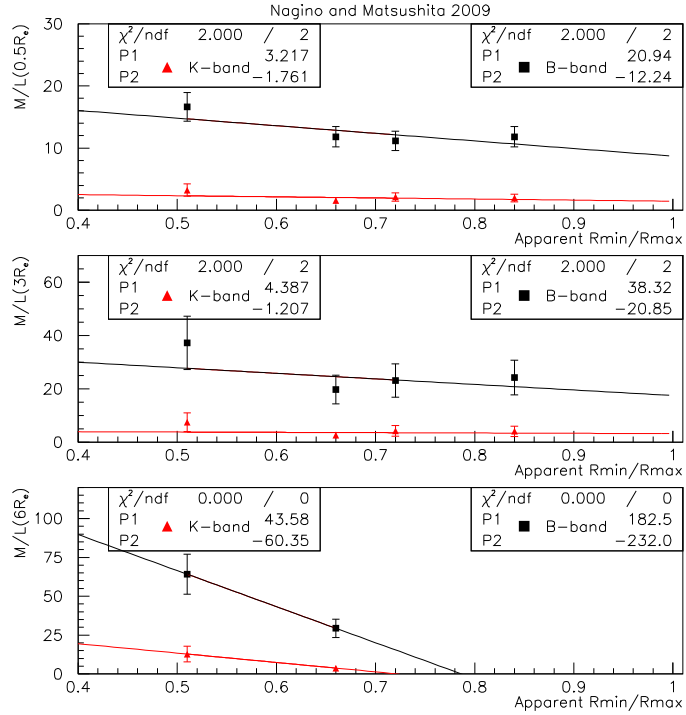


Figure 24: M/L vs apparent axis ratio for Nagino and Matsushita [78]. The top panel is for M/L integrated up to $0.5R_{eff}$. The black (red) symbols and fits are for M/L determined in the B-band (K-band). The middle and bottom panels are for M/L integrated up to $3R_{eff}$ and $6R_{eff}$ respectively. There are only 2 data points for $\frac{M}{L}(\leq 6R_{eff})$ (no data for NGC4349).

HI rings are located mostly in S0 galaxies. In most cases elliptical galaxies with HI disks are gas rich, and thus are unusual among elliptical galaxies.

8.1 Bertola *et al.* (1991 and 1993)

Bertola *et al.* [9] provided M/L_B for inner regions ($0.3R_{eff} < r < 0.9R_{eff}$) of 5 elliptical and 2 S_0 galaxies using ionized gas disks. They also determined values for the outer regions of 4 elliptical galaxies using HI disks ($3.3R_{eff} < r < 10R_{eff}$). They had already used the same technique to obtain the inner $\frac{M}{L_B}(r = 1.3R_{eff})$ for NGC5077, see [8], which we added to the sample. All galaxies are LINERS and/or Sy type. Their true ellipticities were obtained by fitting data with a tri-axial model for four of the elliptical galaxies and one of the lenticular galaxies. The best fit for the 4 elliptical galaxies is (see Fig. 25):

$$M/L_B = (-4.21 \pm 3.55)^{bc/a^2} + (5.83 \pm 2.09) \text{ for the 4 elliptical galaxies,}$$

where a, b and c are the radii of the triaxial shape model for the elliptical galaxy. Uncertainties were not given. We assumed that $\Delta(M/L) \propto M/L$, with the proportionality constant such as $\chi^2/ndf = 1$ in the fit. We assigned a ± 0.05 uncertainty on the intrinsic “axis ratio” bc/a^2 . We did not include the S_0 galaxy in the fit reported above. Including it changes little the results, except that the correlation is more marked. Using the 5 elliptical galaxies for which M/L are provided and determining the correlation with the *apparent* axis ratio R_{min}/R_{max} , we found:

$$M/L_B = (+1.14 \pm 4.64)^{R_{min}/R_{max}|_{apparent}} + (2.67 \pm 3.42).$$

This illustrates the importance of the galaxy projection effect.

The data analysis accounted for the true shapes of the galaxies, so that there was no need of projection correction. The analysis used special galaxies (presence of a gas disks, Sy2, LINERS) and no uncertainty was given. On the other hand, the method is robust (similar to M/L determination for spiral galaxies). We assigned the result to group 1 reliability.

8.2 Pizzella *et al.* (1997)

Pizzella *et al.* [83] used the velocity field measurements on ionized warm gas disks embedded in 4 elliptical galaxies to obtain their gravitational potentials. For each galaxy, an intrinsic triaxial galactic shape was obtained, which was argued by the authors to not be strongly model-dependent. The galactic mass integrated up to the maximum available radius was obtained from the velocity field. The modeling worked well for 3 galaxies but not as well for

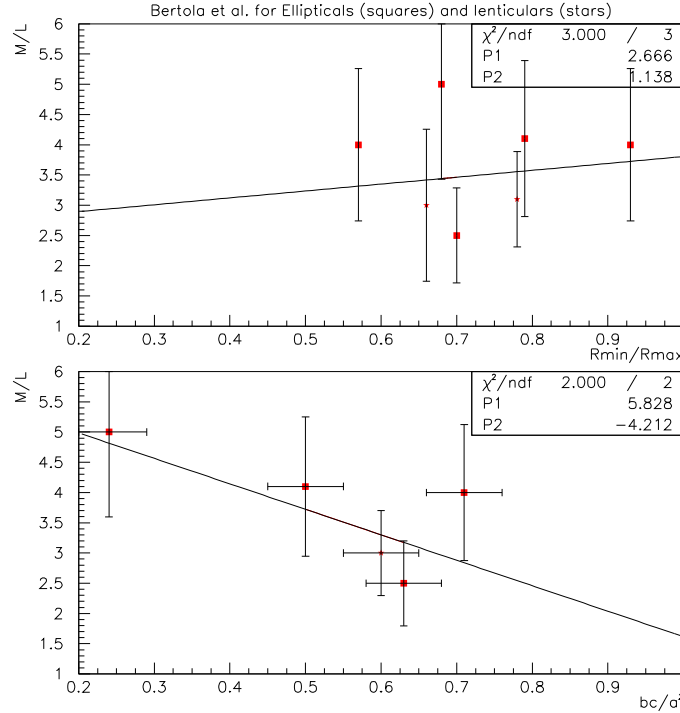


Figure 25: M/L vs apparent (top plot) and intrinsic axis ratios, defined as bc/a^2 , with a, b and c the radii of the elliptical galaxy triaxial shape model. Data are from, Bertola *et al.* [9], [8]. The square symbols represent elliptical galaxies. The S_0 galaxies are indicated (star symbols), but not included in the fits.

NGC7097 (which has a counter-rotating core). All galaxies are LINERS and two (NGC2974 and 5077) are Sy galaxies. We kept NGC7097 because its results are published nonetheless and its intrinsic ellipticity ($1 - q_0 p_0$, where q_0 and p_0 are the intrinsic axis ratios of the triaxial galaxy) is close to the one given by Bertola *et al.* [9]. M/L_T was obtained from the potential and the light density profile. M/L_T vs apparent and intrinsic axis ratios are shown in Fig. 26.

The best fits are:

$$M/L_T(R_{eff}/2) = (+13.30 \pm 9.58) R_{min}/R_{max}|_{apparent} + (-4.48 \pm 6.27),$$

$$M/L_T(R_{eff}/2) = (-1.39 \pm 13.13) q_0 p_0 + (4.83 \pm 6.80).$$

The uncertainties on M/L_T were scaled so that $\chi^2/ndf = 1$, and a ± 0.05 uncertainty was assumed for the intrinsic axis ratio. The bias for using apparent rather than intrinsic axis ratios is clear (the effect of using the true shape rather than the projected one to get M/L is already accounted for). We assigned the results to reliability group 1.

9 Data sets using strong lensing

Strong lensing has become a standard technique to extract M/L . Its advantage is that the determination of $M(R_{Ein})$, the total mass within the Einstein radius R_{Ein} , is in principle model independent. Obtaining M/L at other radii necessitates assuming a mass profile. Since strong lensing galaxies are distant, a light profile must be assumed too. Nevertheless, the method is the least model dependent way to obtain a galactic total mass. Virial or hydrostatic equilibria are not assumed, so our tight selection can be relaxed, keeping in mind that evidence of starburst or H-II emission can bias M/L by affecting the luminosity. Selection enforcing a homogeneous galaxy sample (i.e, discarding cD, S0, cE galaxies...) is still necessary. Although equilibrium is not required, internal or external shears due to interaction with nearby neighbors can bias the determination of the mass. They are usually corrected for by the authors, although such correction is not unambiguous. Lensing galaxies are often found in clusters or groups. Our systematic study of the effects of environment shows that the galaxies in groups or clusters display more dispersion around their M/L vs R_{min}/R_{max} correlation, see Sections 9.1, 9.2 and 9.4 (we found the opposite in Section 9.3 but it may be a statistical fluctuation). This is expected if unaccounted galaxy-galaxy interactions cause a data jitter. In addition, the correlation slope seems larger for isolated galaxies.

A general caveat of this technique is that the probability of observing lensing from a galaxy is low so the known ones are distant. Consequently, their detailed characteristics are not known. In addition, distant galaxies may be at different evolution stages compared to the local ones. Furthermore, lensing equations bias samples

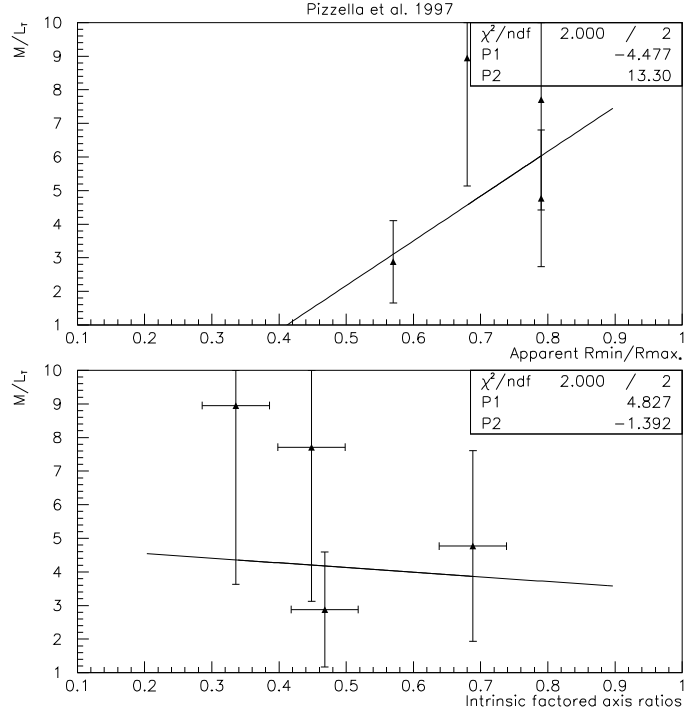


Figure 26: M/L_T from Pizzella *et al.* [83] vs apparent (top panel) and intrinsic (bottom panel) axis ratios.

toward heavier elliptical galaxies on the one hand, and higher ellipticity on the other hand. whilst the galaxies are at large redshifts z , we chose to not correct for a possible $M/L-z$ correlation because it is unclear whether it comes from structure evolution (as investigated e.g. in [60]), or from structure and sample bias (lensing sample biased toward flatter galaxies, with flatness correlating with M/L).

9.1 Auger *et al.* (2010)

Auger *et al.* [2] modeled the light and mass of 73 early-type galaxies based on photometric and strong lensing data from the Sloan Lens ACS (SLACS) survey [12]. The galaxies are located at $0.06 < z < 0.51$ redshifts. The data are interpreted with a de Vaucouleur profile [39] for photometry and a SIE (Singular Isothermal Ellipsoid) for the mass profile. The interpretation includes the effects of (apparent) ellipticity. From this, DMf was estimated at $R_{eff}/2$. S0 galaxies were identified so we did not apply the standard $\sigma \geq 225 \text{ km.s}^{-1}$ criterion for this analysis (and all other analyses using SLACS data).

9.1.1 Analysis on full sample of Elliptical galaxies

We kept 34 elliptical galaxies, rejecting S0 galaxies (we relied on the identification from [1]) and minimizing the contamination of giant galaxies by requesting $M < 10^{12} M_\odot$ (the masses were taken from [53]). Mass axis ratios $R_{min}/R_{max}|_{mass}$,⁴ apparent axis ratios $R_{min}/R_{max}|_*$ and luminosities are from [12]. If none were provided for a given galaxy, it was rejected. In addition, we rejected the galaxies signaled by the authors as significant fit outliers in the size- σ - M_* correlation space. The DMf vs axis is shown in Fig. 27. The best fits give, for the results derived with a SIE model using a Chabrier IMF [25]:

$$DMf = (-0.62 \pm 0.17) R_{min}/R_{max}|_{mass} + (1.08 \pm 0.13)$$

and, for results derived with a Salpeter IMF [89]:

$$DMf = (-1.05 \pm 0.28) R_{min}/R_{max}|_{mass} + (1.11 \pm 0.22).$$

For the mass ratio, we have:

$$M_{tot}/M_* = (-3.38 \pm 0.79) R_{min}/R_{max}|_{mass} + (4.92 \pm 0.66) \text{ (Chabrier)},$$

$$M_{tot}/M_* = (-1.86 \pm 0.46) R_{min}/R_{max}|_{mass} + (2.76 \pm 0.38) \text{ (Salpeter)}.$$

Using apparent axis ratio rather than mass, we obtain for the Chabrier IMF:

$$DMf = (-0.12 \pm 0.17) R_{min}/R_{max}|_{apparent} + (0.69 \pm 0.12)$$

and, for the Salpeter IMF:

$$DMf = (-0.22 \pm 0.27) R_{min}/R_{max}|_{apparent} + (0.46 \pm 0.21),$$

⁴ $R_{min}/R_{max}|_{mass}$ is the axis ratio of the modeled mass system.

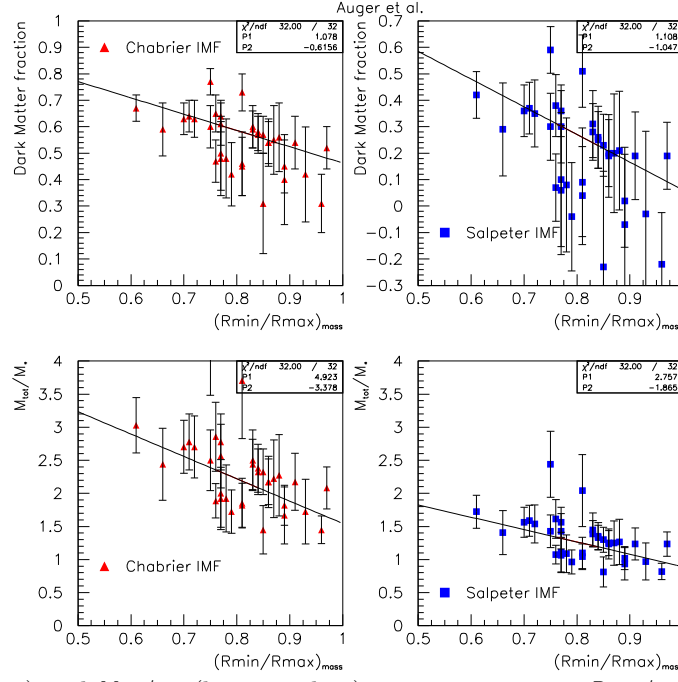


Figure 27: DMf (top plots) and M_{tot}/M_* (bottom plots) vs mass axis ratio R_{min}/R_{max} for the Auger *et al.* data set [2]. The left plots are for mass SIE models using a Chabrier IMF and the right ones are for a Salpeter IMF. The lines are the best linear fits to the data.

$$M_{tot}/M_* = (-1.47 \pm 0.70)R_{min}/R_{max}|_{apparent} + (3.30 \pm 0.57) \text{ Chabrier),}$$

$$M_{tot}/M_* = (-0.79 \pm 0.40)R_{min}/R_{max}|_{apparent} + (1.84 \pm 0.32) \text{ (Salpeter).}$$

The published uncertainties were rescaled slightly so that $\chi^2/ndf = 1$. We assigned the results using a Chabrier IMF to reliability group 1.

9.1.2 Luminosity and environment study

Subsamples of galaxies allowed us to study the effect of luminosity (correlating with the boxy/disk galaxy shape) and environment on these results:

1. Subsample 1 contains elliptical galaxies not found in clusters according to Treu *et al.* [99] (17 elliptical galaxies);
2. Subsample 2 contains elliptical galaxies found in clusters (17 elliptical galaxies);
3. Subsample 3 contains elliptical galaxies with magnitude $M_B \gtrsim -19.5$. This selects less massive disk galaxies (25 elliptical galaxies);
4. Subsample 4 contains elliptical galaxies with magnitude $M_B \lesssim -19.5$ and no generic selection $M > 10^{12} M_\odot$ on the total mass. This selects more massive boxy galaxies (17 elliptical galaxies);
5. Subsample 5 contains elliptical galaxies with magnitude $M_B \gtrsim -19.5$ and not found in clusters (13 elliptical galaxies).

Subsample 1 results The best fit to the data obtained using a Chabrier IMF and mass axis ratio is:

$$DMf = (-0.81 \pm 0.20)R_{min}/R_{max}|_{mass} + (1.22 \pm 0.16)$$

and, for the Salpeter IMF and mass axis ratio:

$$DMf = (-1.43 \pm 0.34)R_{min}/R_{max}|_{mass} + (1.40 \pm 0.27).$$

Using apparent axis ratio, we obtain for the Chabrier IMF:

$$DMf = (-0.68 \pm 0.26)R_{min}/R_{max}|_{apparent} + (1.10 \pm 0.20)$$

and, for the Salpeter IMF:

$$DMf = (-1.13 \pm 0.45)R_{min}/R_{max}|_{apparent} + (1.13 \pm 0.35).$$

Subsample 2 results The best fit to the data obtained using a Chabrier IMF and mass axis ratio is:

$$DMf = (-0.45 \pm 0.25)^{R_{min}/R_{max}}|_{mass} + (0.97 \pm 0.20)$$

and, for the Salpeter IMF and mass axis ratio:

$$DMf = (-0.79 \pm 0.43)^{R_{min}/R_{max}}|_{mass} + (0.79 \pm 0.34).$$

Using apparent axis ratio, we obtain for the Chabrier IMF:

$$DMf = (+0.02 \pm 0.20)^{R_{min}/R_{max}}|_{apparent} + (0.60 \pm 0.15)$$

and, for the Salpeter IMF:

$$DMf = (+0.02 \pm 0.34)^{R_{min}/R_{max}}|_{apparent} + (0.30 \pm 0.26).$$

Subsample 3 results The best fit to the data obtained with a Chabrier IMF and mass axis ratio is:

$$DMf = (-0.41 \pm 0.23)^{R_{min}/R_{max}}|_{mass} + (0.89 \pm 0.19)$$

and, for the Salpeter IMF and mass axis ratio:

$$DMf = (-0.66 \pm 0.38)^{R_{min}/R_{max}}|_{mass} + (0.76 \pm 0.31).$$

Using apparent axis ratio, we obtain for the Chabrier IMF:

$$DMf = (+0.08 \pm 0.14)^{R_{min}/R_{max}}|_{apparent} + (0.50 \pm 0.12)$$

and, for the Salpeter IMF:

$$DMf = (+0.10 \pm 0.24)^{R_{min}/R_{max}}|_{apparent} + (0.16 \pm 0.19).$$

Subsample 4 results The best fit to the data obtained using a Chabrier IMF and mass axis ratio is:

$$DMf = (-0.41 \pm 0.19)^{R_{min}/R_{max}}|_{mass} + (0.94 \pm 0.14)$$

and, for the Salpeter IMF and mass axis ratio:

$$DMf = (-0.73 \pm 0.34)^{R_{min}/R_{max}}|_{mass} + (0.89 \pm 0.25).$$

Using apparent axis ratio, we obtain for the Chabrier IMF:

$$DMf = (-0.22 \pm 0.28)^{R_{min}/R_{max}}|_{apparent} + (0.80 \pm 0.21)$$

and, for the Salpeter IMF:

$$DMf = (-0.35 \pm 0.48)^{R_{min}/R_{max}}|_{apparent} + (0.62 \pm 0.36).$$

Subsample 5 results The best fit to the data derived with Chabrier IMF and mass axis ratio is:

$$DMf = (-0.62 \pm 0.25)^{R_{min}/R_{max}}|_{mass} + (1.06 \pm 0.20)$$

and, for results derived with Salpeter IMF and mass axis ratio:

$$DMf = (-1.13 \pm 0.43)^{R_{min}/R_{max}}|_{mass} + (1.14 \pm 0.35).$$

Using apparent axis ratio, we obtain for the Chabrier IMF:

$$DMf = (-0.15 \pm 0.36)^{R_{min}/R_{max}}|_{apparent} + (0.68 \pm 0.29)$$

and, for the Salpeter IMF:

$$DMf = (-0.23 \pm 0.63)^{R_{min}/R_{max}}|_{apparent} + (0.41 \pm 0.50).$$

9.1.3 Conclusion

The subsample results are generally compatible with the full sample ones. There is no clear difference between samples of luminous/boxy and of fainter/disk galaxies. Selecting field galaxies increased the DMf slope whilst the ones in groups/cluster appeared to have a smaller slope. The correlation for field galaxies is also clearer (smaller relative uncertainty for the slope)

The caveats of the analysis are that apparent axis ratios R_{min}/R_{max} were used. However, from the results of Barnabe *et al.* [5], considering intrinsic axis ratios rather than apparent ones has a small effect: the change in slope is compatible with 0: $(-18 \pm 59)\%$ for the Chabrier results and $(-33 \pm 70)\%$ for the Salpeter IMF. The results and the mass axis ratios are model dependent. The IMF dependency can be estimated by comparing the Salpeter and Chabrier IMF results.

9.2 Barnabe *et al.* (2011)

Barnabe *et al.* [5] modeled the dark matter and stellar contents within about $0.5R_{eff}$ for 16 E and S0 galaxies from the SLACS survey. In addition, they used spectroscopic observations from other sources than SLACS to further constrain their models. The stellar content was obtained with a Stellar Population Synthesis model using a Chabrier or a Salpeter IMF. Independently, they obtained a lower limit on DMf by using a “maximum bulge hypothesis”. The models provide intrinsic mass axis ratios and luminous axis ratios. We selected 10 elliptical galaxies, the rest being S0 galaxies or E for which $M > 10^{12}M_{\odot}$ (masses from [53]). Among the 10 elliptical galaxies, 2 are fast rotators and 8 are slow rotators, 4 belong to clusters and 6 are more isolated. We formed M/L using DMf and M_*/L . The best fits yield for the M/L correlation with intrinsic luminous axis ratio (see Fig. 28):

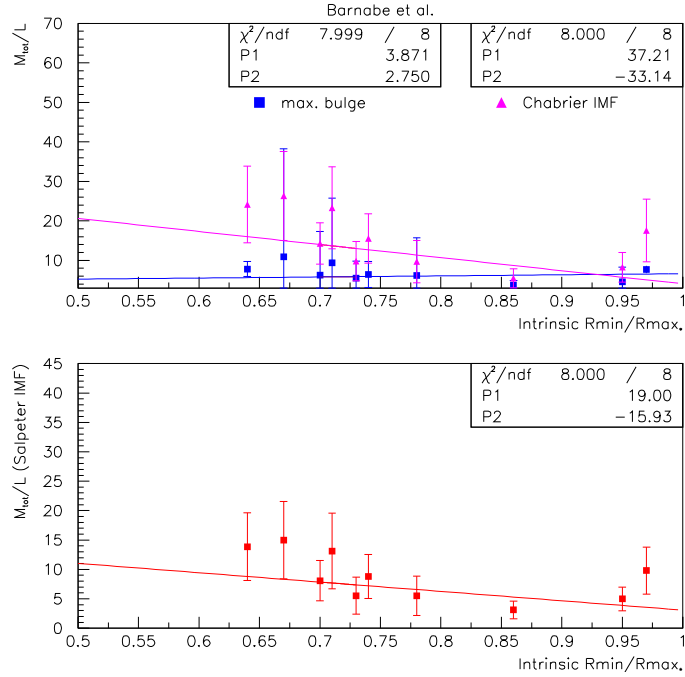


Figure 28: M/L vs true luminous axis ratio $R_{\min}/R_{\max}|_{\text{true}}$ from Barnabe *et al.* [5]. The top (bottom) plot is for the stellar population synthesis model using a Chabrier (Salpeter) IMF. The lines give the best fits to the data.

$$M/L = (-33.1 \pm 16.7) R_{\min}/R_{\max}|_{\text{true}(\text{light})} + (37.2 \pm 13.9) \text{ for the data computed with a Chabrier IMF,}$$

$$M/L = (-15.9 \pm 9.8) R_{\min}/R_{\max}|_{\text{true}(\text{light})} + (19.0 \pm 8.2) \text{ for the data computed with a Salpeter IMF.}$$

By fitting samples containing only isolated galaxies or galaxies belonging to clusters we check the effects of the environment on these results. The best fits yield for the galaxies not found in clusters:

$$M/L = (-59.2 \pm 16.4) R_{\min}/R_{\max}|_{\text{true}(\text{light})} + (56.24 \pm 13.2) \text{ for the data obtained with a Chabrier IMF,}$$

$$M/L = (-33.6 \pm 9.4) R_{\min}/R_{\max}|_{\text{true}(\text{light})} + (32.0 \pm 7.5) \text{ with a Salpeter IMF,}$$

and for the galaxies found in clusters:

$$M/L = (-47.9 \pm 22.9) R_{\min}/R_{\max}|_{\text{true}(\text{light})} + (55.8 \pm 20.8) \text{ for the data computed with a Chabrier IMF,}$$

$$M/L = (-26.3 \pm 13.4) R_{\min}/R_{\max}|_{\text{true}(\text{light})} + (31.1 \pm 12.3) \text{ with a Salpeter IMF.}$$

The isolated galaxies have a clearer, and possibly stronger, correlation as seen already in Section 9.1.

Finally, we checked the effect of the viewing angle projection on our analysis by repeating the analysis done on sample 1 but using the apparent light axis ratios rather than the intrinsic one:

$$M/L = (-39.0 \pm 11.9) R_{\min}/R_{\max}|_{\text{apparent}(\text{light})} + (44.8 \pm 10.7) \text{ for the data computed with a Chabrier IMF,}$$

$$M/L = (-21.1 \pm 7.18) R_{\min}/R_{\max}|_{\text{apparent}(\text{light})} + (24.7 \pm 6.5) \text{ with a Salpeter IMF.}$$

The projection effect is small and the fit values of the intrinsic and apparent cases are largely compatible. When the intrinsic axis ratio is used rather than the apparent one, the M/L vs axis ratio slope decreases by about $(18 \pm 59)\%$ for the Chabrier result and by about $(33 \pm 70)\%$ for the Salpeter result. (The uncertainties determination assumes that the Chabrier and Salpeter data are uncorrelated, which is not true. Hence, the 59% and 70% uncertainties are overestimated.)

Advantages of this analysis are that it was done in term of real axis ratio and it used additional spectroscopic data. We assigned the results to group 1 reliability.

9.3 Cardone *et al.* (2009)

Cardone *et al.* [21] examined 21 early-type galaxies from the SLACS survey. Among them, 18 are elliptical galaxies (identification from [1]). The strong-lensing/photometry method was used to extract the DMf up to the effective and Einstein radii, with a flexible M/L ansatz that interpolated between several types of halo models. The preferred halo was selected by χ^2 minimization. This reduces the model dependence of the DMf determination compared to other strong-lensing/photometry results. Spherical symmetry was assumed, the ellipticity of the galaxies being accounted for only in the deprojection procedure to obtain luminosity profiles. The stellar M_*/L was obtained from a Stellar Population Model using a Chabrier IMF. We formed M/L from M_*/L and DMf . The apparent and mass axis ratios were taken from [12]. We compared the luminosities reported by the authors with those in [12] and rejected galaxies disagreeing by more than $\sim 20\%$, and galaxies for which luminosities were

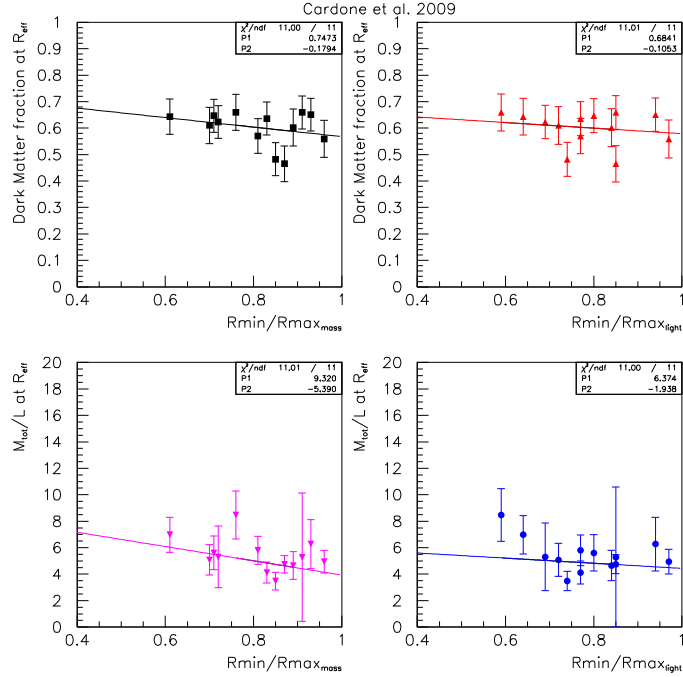


Figure 29: Dark matter content vs axis ratio for Cardone *et al.* [21]. Top plots: DMf vs mass axis ratio (left) and apparent R_{min}/R_{max} (right); bottom plots, M/L vs mass R_{min}/R_{max} (left) and apparent R_{min}/R_{max} (right).

not given in [12]. We also rejected 3 giant galaxies ($M > 10^{12}M_{\odot}$, masses from [53]). All in all, we kept 13 galaxies (Main Sample). We split the Main Sample in two subsamples containing field galaxies (subsample 1, with 9 elliptical galaxies) and galaxies found in clusters (subsample 2, with 4 elliptical galaxies) [99]. The fits to DMf or M/L vs R_{min}/R_{max} , shown in Fig 29, yield, for the quantities obtained at R_{eff} (uncertainties are from the 95% CL values of [21] scaled so that $\chi^2/ndf = 1$): $DMf = (-0.18 \pm 0.18)R_{min}/R_{max}|_{mass} + (0.75 \pm 0.15)$,

$$DMf = (-0.11 \pm 0.18)R_{min}/R_{max}|_{apparent} + (0.68 \pm 0.14),$$

$$M/L = (-5.39 \pm 3.40)R_{min}/R_{max}|_{mass} + (9.32 \pm 2.85),$$

$$M/L = (-1.94 \pm 3.52)R_{min}/R_{max}|_{apparent} + (6.37 \pm 2.82).$$

For the isolated galaxies (subsample 1), the best fits are:

$$DMf = (-0.08 \pm 0.30)R_{min}/R_{max}|_{mass} + (0.66 \pm 0.25),$$

$$DMf = (0.20 \pm 0.31)R_{min}/R_{max}|_{apparent} + (0.42 \pm 0.26),$$

$$M/L = (-1.68 \pm 3.97)R_{min}/R_{max}|_{mass} + (6.13 \pm 3.40),$$

$$M/L = (+3.91 \pm 3.21)R_{min}/R_{max}|_{apparent} + (1.48 \pm 2.65).$$

For the galaxies found in clusters, the best fits are:

$$DMf = (0.00 \pm 0.14)R_{min}/R_{max}|_{mass} + (0.64 \pm 0.10),$$

$$DMf = (-0.13 \pm 0.10)R_{min}/R_{max}|_{apparent} + (0.73 \pm 0.07),$$

$$M/L = (-13.25 \pm 8.83)R_{min}/R_{max}|_{mass} + (15.47 \pm 6.82),$$

$$M/L = (-22.93 \pm 6.10)R_{min}/R_{max}|_{apparent} + (21.73 \pm 4.39).$$

The trend is that, contrarily to the results in sections 9.1, 9.2 and 9.4, isolated galaxies have a weaker correlation than clustered ones. The low statistics may be the cause of this disagreement with the other studies.

Results obtained at the Einstein radius R_{Ein} yield similar slopes (R_{Ein} and R_{eff} results are correlated). However, they should be less model dependent⁵ than the results at R_{eff} . In average for our sample, $R_{Ein} = 0.6R_{eff}$. The best fits are:

$$DMf = (-0.11 \pm 0.15)R_{min}/R_{max}|_{mass} + (0.67 \pm 0.12),$$

$$DMf = (-0.07 \pm 0.14)R_{min}/R_{max}|_{apparent} + (0.64 \pm 0.11),$$

$$M/L = (-4.57 \pm 2.79)R_{min}/R_{max}|_{mass} + (8.39 \pm 2.32),$$

$$M/L = (-2.50 \pm 3.00)R_{min}/R_{max}|_{apparent} + (6.59 \pm 2.40).$$

For the isolated galaxies:

$$DMf = (-0.05 \pm 0.24)R_{min}/R_{max}|_{mass} + (0.62 \pm 0.21),$$

$$DMf = (0.15 \pm 0.27)R_{min}/R_{max}|_{apparent} + (0.45 \pm 0.23),$$

$$M/L = (-1.32 \pm 2.95)R_{min}/R_{max}|_{mass} + (5.65 \pm 2.51),$$

$$M/L = (+2.54 \pm 2.83)R_{min}/R_{max}|_{apparent} + (2.42 \pm 2.35).$$

⁵The DMf and M/L have still some model dependence because of the assumed luminosity and star mass profiles.

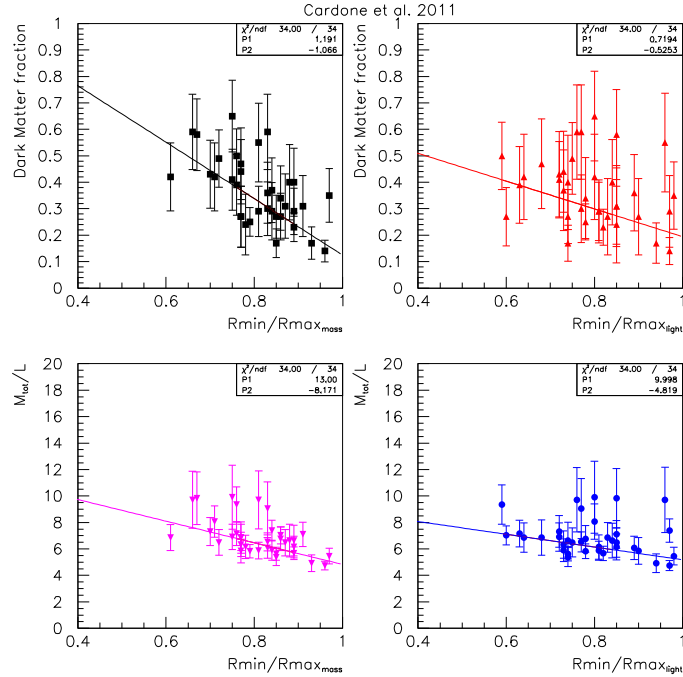


Figure 30: Dark matter content vs axis ratio for Cardone *et al.* (2011) [22]. Top plots: DMf vs mass R_{min}/R_{max} (left) and apparent R_{min}/R_{max} (right). Bottom plots: same as top plots but for M/L .

For the galaxies found in clusters, the best fits are:

$$\begin{aligned} DMf &= (0.00 \pm 0.08) R_{min}/R_{max}|_{mass} + (0.62 \pm 0.06), \\ DMf &= (-0.10 \pm 0.66) R_{min}/R_{max}|_{apparent} + (0.68 \pm 0.45), \\ M/L &= (-12.08 \pm 7.70) R_{min}/R_{max}|_{mass} + (14.12 \pm 5.98), \\ M/L &= (-20.74 \pm 1.34) R_{min}/R_{max}|_{apparent} + (19.74 \pm 0.97). \end{aligned}$$

An advantage of this analysis is the lesser model dependence claimed by the authors. A caveat is that the model assumes spherical symmetry. We assigned the results to group 1 reliability.

9.4 Cardone *et al.* (2011)

Cardone *et al.* [22] studied 59 early-type galaxies from the SLACS survey using a Secondary Infall Model which describes the collapse and virialization of a spherical halo. This theoretically sound model was for the first time employed to describe light and dark matter profiles. This allowed us, by comparing to other dark matter extractions, to investigate their model dependence. The study provided the total masses within $\sim R_{eff}/2$. The DMf was extracted using the stellar M_*/L results from Auger *et al.* (with Salpeter IMF) [2]. We formed the M/L using the luminosities given in [22]. Comparing them with the luminosities from [12], we found a 10% shift between the two results. We retained galaxies for which, apart for this 10% shift, luminosities from [22] and [12] agree within 15%. We also rejected 3 E/So galaxies, galaxies for which axis ratios were not available from [12] and giant galaxies ($M > 10^{12} M_\odot$, masses from [53]). All in all, we obtained a sample of 36 galaxies. Using either mass or apparent axis ratios, the best fits are (see Fig 30):

$$\begin{aligned} DMf &= (-1.07 \pm 0.19) R_{min}/R_{max}|_{mass} + (1.19 \pm 0.16), \\ DMf &= (-0.52 \pm 0.18) R_{min}/R_{max}|_{apparent} + (0.72 \pm 0.15), \\ M/L &= (-8.17 \pm 1.60) R_{min}/R_{max}|_{mass} + (13.00 \pm 1.37), \\ M/L &= (-4.82 \pm 1.32) R_{min}/R_{max}|_{apparent} + (10.00 \pm 1.09). \end{aligned}$$

We checked the influence of environment by analyzing 2 subsamples in which galaxies that are isolated (20 galaxies) or belong to clusters (16 galaxies), according to [99]. For the isolated galaxies, the best fits are:

$$\begin{aligned} DMf &= (-1.12 \pm 0.28) R_{min}/R_{max}|_{mass} + (1.12 \pm 0.28), \\ DMf &= (-0.46 \pm 0.33) R_{min}/R_{max}|_{apparent} + (0.65 \pm 0.27), \\ M/L &= (-6.47 \pm 2.51) R_{min}/R_{max}|_{mass} + (11.61 \pm 2.15), \\ M/L &= (-1.46 \pm 2.56) R_{min}/R_{max}|_{apparent} + (7.24 \pm 2.05). \end{aligned}$$

For the galaxies found in clusters, the best fits are:

$$\begin{aligned} DMf &= (-0.43 \pm 0.27) R_{min}/R_{max}|_{mass} + (0.67 \pm 0.22), \\ DMf &= (-0.23 \pm 0.25) R_{min}/R_{max}|_{apparent} + (0.50 \pm 0.19), \end{aligned}$$

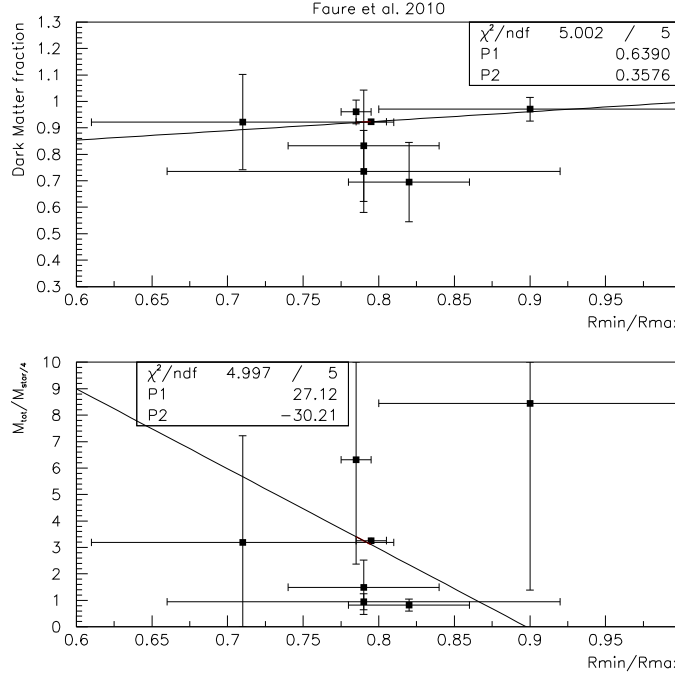


Figure 31: Results based on Faure *et al.* [44]. Top plot: DMf vs R_{min}/R_{max} . Bottom plot: M_{tot}/M_* vs R_{min}/R_{max} .

$$M/L = (-2.97 \pm 2.02) R_{min}/R_{max}|_{mass} + (8.74 \pm 1.64),$$

$$M/L = (-4.40 \pm 1.52) R_{min}/R_{max}|_{apparent} + (9.73 \pm 1.18).$$

Isolated galaxies display a stronger and clearer correlation than clustered ones, as already seen in sections 9.1 and 9.2.

This analysis is useful because it employed an original and physically founded model. Its caveats are its assumed spherical symmetry and usage of the old Salpeter IMF. We assigned the results to group 2 reliability.

9.5 Faure *et al.* (2011)

Faure *et al.* [44] examined 20 strong-lensing candidates from the COSMOS survey [109] and provided DMf within effective and Einstein Radii for 12 of them. The lens candidates were tentatively identified as elliptical and S0 galaxies. The galaxies are distant (redshift $0.34 \leq z \leq 1.13$). Standard strong-lensing and photometry methods to extract DMf were used, with a Synthesis Model to infer the stellar mass and a SIE model for the total mass. The authors assumed that mass follows light: a Sersic profile [93] was used for both the mass and light distributions. Consequently, mass axis ratio and apparent axis ratios are equal. Effect of the environment was accounted for in the model. We formed M_{tot}/M_* from the authors' M_{tot} and M_* . Out of the 12 galaxies, we rejected two for which, according to [44], the model does not fit well the data (0047-5023 and 0050+4901) and one (5914-1219) for which the mass suggests that it is a giant. Furthermore, we rejected a galaxy (5921+0638) for which the ellipticity from [44] disagrees with [43] because of less reliable modeling. In addition, its low mass and low velocity dispersion suggest that it is a S0. Finally, we rejected a galaxy (0038+4133) with an unphysical $DMf < 0$ and for which the low mass and velocity dispersion suggests again that it is a S0. The final sample contains 7 galaxies. The fits to DMf or M/M_* vs R_{min}/R_{max} yield,⁶ see Fig. 31:

$$DMf = (+0.36 \pm 0.10) R_{min}/R_{max} + (0.63 \pm 0.08),$$

$$M_{tot}/M_* = (-30.21 \pm 6.13) R_{min}/R_{max} + (27.12 \pm 4.88).$$

To compare with other works providing M/L_B we can use $1/4 M_{tot}/M_* \simeq M/L_B$ because for elliptical galaxies, $M_*/L_B \simeq 4$ typically. The specific caveats of this analysis are the “mass follows light” assumption (i.e., M/L constant with r), which is believed to be invalid for $r > R_{eff}$, and that the model assumed spherical symmetry. We assigned the results to group 1 reliability.

9.6 Ferreras, Saha and Williams (2005)

Ferreras, Saha and Williams [46] compared the Einstein masses M_{Ein} of 18 strong-lensing early-type galaxies to their visible masses M_* obtained from photometry. The stellar model used had its parameters varied over a large

⁶We recall that it is assumed that $R_{min}/R_{max}|_{mass} = R_{min}/R_{max}|_{apparent}$.

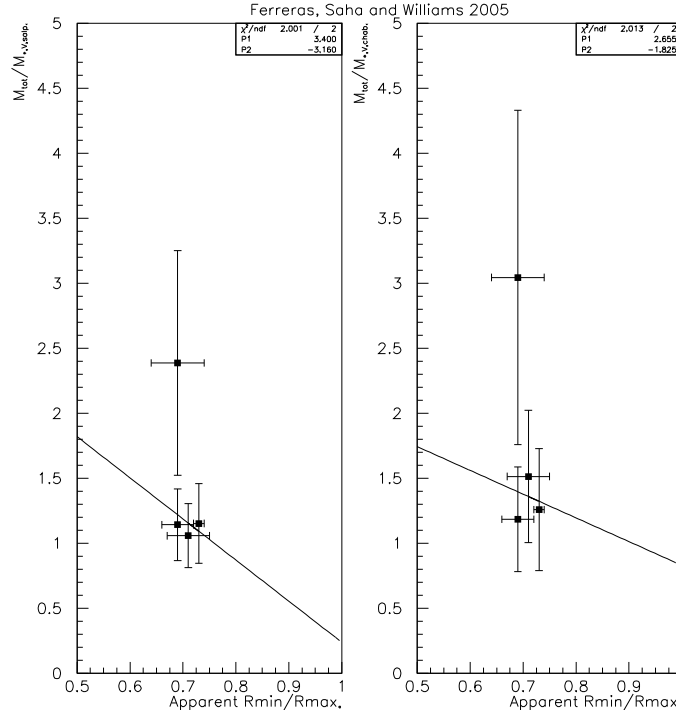


Figure 32: M_{tot}/M_* vs apparent and mass axis ratios from Ferreras *et al.* [46]. The right panel is with M_* determined with a Chabrier IMF and the left panel with a Salpeter IMF.

volume of the parameter space, which should make the M_* estimates robust [46]. M_* is given in the V-band and depends on the choice of IMF. The authors determined M_* with a Chabrier IMF but also provided it with a Salpeter IMF to assess the uncertainty attached to the choice of IMF. The masses given are contained within r_{lens} , which is a few R_{eff} : for our 4-galaxies sample $1.6R_{eff} \leq r_{lens} \leq 3.3R_{eff}$, with in average $r_{lens} = 1.8R_{eff}$. To select our sample, we rejected a galaxy known to be a spiral or S0 galaxy (B2237). To further suppress possible S0 contamination, we selected galaxies with $\sigma \geq 220 \text{ km.s}^{-1}$ (the σ are from [103], we slightly relaxed the usual $\sigma \geq 225 \text{ km.s}^{-1}$ otherwise only 2 galaxies would remain in the final sample). This rejected J0951, B0952, B1009, J1017, J1411, B1422 and B2149. We excluded galaxies with $M_{tot} > 10^{12} M_{\odot}$ (B1104 and J1417). We rejected B0818 since it may be interacting with its environment and had no axis ratio available from literature. We rejected B1030 and B1608 because of interaction with environment. Finally B1115 was excluded as a peculiar galaxy. There are only 4 galaxies remaining after this selection (B0047, B0142, J0414 and B1520). We plot M_{tot}/M_* vs axis ratio in Fig. 32. The uncertainty is assigned so that $\chi^2/ndf=1$. The best fits to the data yield:

$$M_{tot}/M_{*,V} = (-1.83 \pm 5.78)R_{min}/R_{max}|_{apparent} + (2.67 \pm 4.09) \text{ for the Chabrier IMF,}$$

$$M_{tot}/M_{*,V} = (-3.16 \pm 3.69)R_{min}/R_{max}|_{apparent} + (2.61 \pm 3.40) \text{ for the Salpeter IMF.}$$

The results were assigned to group 1 reliability.

9.7 Ferreras, Saha and Burles (2008)

Ferreras, Saha and Burles [47] fit photometric and strong lensing data from the SLACS survey [12] to extract M_{tot}/M_* for 9 E and S0 galaxies. The fit functions are based on models (de Vaucouleur profile for photometry and a SIE model for the mass profile). We kept 4 galaxies, rejecting 2 S0 galaxies (identifications from [1]), one galaxy for which $M_{tot} > 10^{12} M_{\odot}$ and 2 galaxies for which the integrated M_{tot}/M_* was determined at significantly larger radius ($1.66R_{eff}$ and $2.01R_{eff}$). The other M_{tot}/M_* were determined at $(\sim 1 \pm 0.2)R_{eff}$. Ellipticities from [47] differ from the mass and apparent ellipticities from the SLACS survey article [12]. We assign an uncertainty on R_{min}/R_{max} equals to the difference between the [12] and [47] values. The redshift correction to M_{tot}/M_* is small: there is at most a redshift difference of $\Delta z = 0.17$ among the galaxies of the sample. From Keeton *et al.* [60], this implies a modification of M_{tot}/M_* of 5%, therefore we neglected it. The M_{tot}/M_* dependence with apparent and mass R_{min}/R_{max} are shown in Fig. 33. The best fit results are:

$$M_{tot}/M_* = (+0.47 \pm 2.63)R_{min}/R_{max}|_{apparent} + (0.61 \pm 2.16) \text{ and}$$

$$M_{tot}/M_* = (+5.55 \pm 3.22)R_{min}/R_{max}|_{mass} + (-3.00 \pm 2.30).$$

We assigned the results to group 1 reliability.

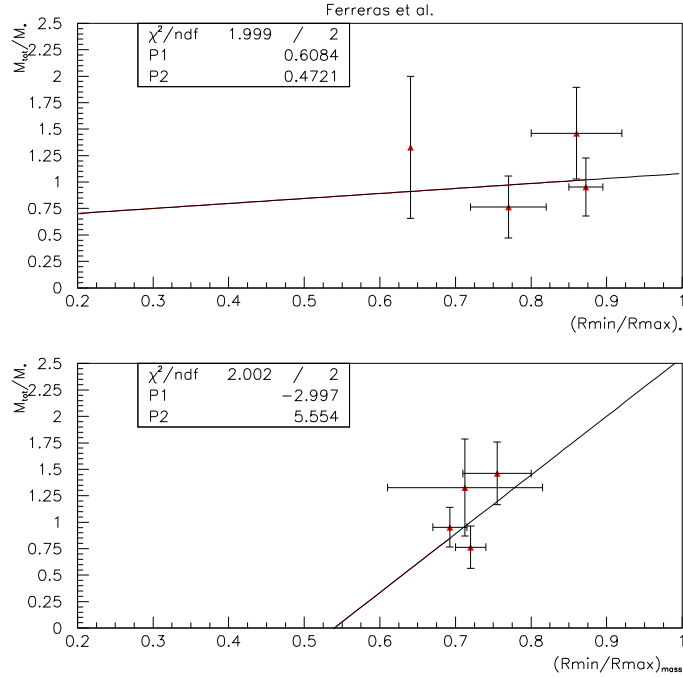


Figure 33: M_{tot}/M_* vs apparent (top panel) and mass (bottom panel) axis ratios for Ferreras, Saha and Burles [47].

9.8 Grillo *et al.* (2009)

Grillo *et al.* [53] studied the stellar and dark matter content of 57 early-type galaxies from the SLACS survey. A Stellar Composite Model was used to obtain the stellar mass M_* using two different sets of metallicity template and three different IMF (Salpeter [89], Kroupa [68], Chabrier [25]). The best choice was selected by the best fit to the galactic spectral energy density measurements. The total magnitude for each galaxy was obtained using a spherically symmetric de Vaucouleur profile. The total mass within R_{Ein} was calculated *via* a SIE model, although the authors noted that with their choice of normalization, the mass should not depend on the ellipticity. After our standard SLACS selection, we retained 40 galaxies. The values of axis ratios used are from [12]. All uncertainties were symmetrized and scaled so that for our fits, $\chi^2/ndf = 1$. The fits, shown in Fig. 34, yield:

$M_{tot}(< R_{Ein})/L_B = (-1.65 \pm 0.97) R_{min}/R_{max}|_{apparent} + (3.30 \pm 0.78)$ for the luminous model using a Salpeter IMF and a Maraston solar metallicity template (SMT) [75]. The corresponding DMf is:

$$DMf(< R_{Ein}) = (+0.72 \pm 0.20) R_{min}/R_{max}|_{apparent} + (-0.15 \pm 0.17).$$

$M_{tot}(< R_{Ein})/L_B = (-1.52 \pm 1.18) R_{min}/R_{max}|_{apparent} + (3.27 \pm 0.94)$ for a Salpeter IMF and a Bruzual & Charlot SMT [14]. The corresponding DMf is:

$$DMf(< R_{Ein}) = (+0.64 \pm 0.23) R_{min}/R_{max}|_{apparent} + (-0.16 \pm 0.19).$$

$M_{tot}(< R_{Ein})/L_B = (-1.12 \pm 1.10) R_{min}/R_{max}|_{apparent} + (2.95 \pm 0.87)$ for a Kroupa IMF and a Maraston SMT [75]. The corresponding DMf is:

$$DMf(< R_{Ein}) = (+0.52 \pm 0.14) R_{min}/R_{max}|_{apparent} + (0.21 \pm 0.11).$$

$M_{tot}(< R_{Ein})/L_B = (-1.75 \pm 1.06) R_{min}/R_{max}|_{apparent} + (3.42 \pm 0.85)$ for a Chabrier IMF and a Bruzual & Charlot SMT. The corresponding DMf is:

$$DMf(< R_{Ein}) = (+0.35 \pm 0.13) R_{min}/R_{max}|_{apparent} + (0.35 \pm 0.11).$$

The analysis assumes spherical symmetry but the authors argued this to be of minimal importance. We assigned the results to group 1 reliability.

9.9 Jackson *et al.* (1998)

Jackson *et al.* [58] studied 12 lensing systems in the context of a “dark galaxy” search. M/L within R_{Ein} were inferred using a Singular Isothermal Sphere model for the mass distribution. We kept 4 galaxies out of the original 14 (2 lensing systems are double-lenses). We rejected B2114+022 G1 as a E+A galaxy that has in addition unreliable M/L due to dust [26]. B1608+656, B1600+434, B1933+507 and B0218+357 are spiral galaxies. B2045+265 may be a Sa. Galaxies B1030+074 and B1127+385 show signs of interaction. The two lenses of B1127+385 seem to be late types galaxies [64], had no redshift values (they could be close and interacting) and their M/L were not given in the H-band. All these galaxies were rejected. Our sample comprised 4 galaxies:

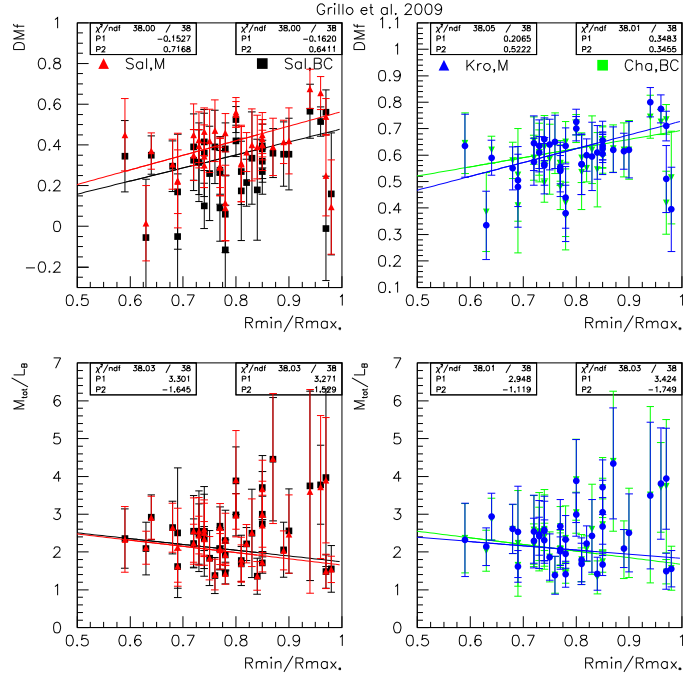


Figure 34: DMf (top plots) and M/L_B (bottom plots) vs apparent axis ratio from Grillo *et al.* [53]. The red triangles are for luminous models using a Salpeter IMF and a Maraston color metallicity template (SMT). The black squares are for a Salpeter IMF and a Bruzual & Charlot SMT. The blue circles are for a Kroupa IMF and a Maraston SMT. The inverted green triangles are for a Chabrier IMF and a Bruzual & Charlot SMT.

B2114+022 G2 (ellipticity from [26]), MG0414+054, B0712+472 (both ellipticities are from [60]) and B1938+666 (ellipticity from [62]). The M/L_H vs R_{min}/R_{max} fit is shown in Fig. 35 and yields:

$$M_{tot}(< R_{Ein})/L_H = (-0.80 \pm 1.67) R_{min}/R_{max}|_{apparent} + (1.61 \pm 1.31).$$

The caveats of this analysis are that the characteristics of the galaxies are poorly known and the M/L , which were not the main focus of [58], were computed in a simple way without accounting e.g. for environment interaction. The results were assigned to group 3 reliability.

One may question the inclusion of B2114+022 G2 in our sample because it belongs to a complicated 2-lenses system. G1 and G2 have different redshifts so they are not interacting with each other. However, the modeling is more delicate. In any case, not including G2 does not essentially change the results. The best fit gives: $M_{tot}(< R_{Ein})/L_B = (-0.58 \pm 2.36) R_{min}/R_{max} + (1.39 \pm 1.89)$.

9.10 Jiang and Kochanek (2007)

Jiang and Kochanek [59] used strong lensing data and stellar velocity dispersion measurements to model the total and stellar mass profiles $M_{tot}(r)$ and $M_*(r)$ for 22 early-type galaxies. It is the same galaxy sample as analyzed by Koopmans *et al.*, see Section 9.12, but the authors argued that they employed a more physical model for the profiles (Hernquist profile [54] for light and NFW [81] profile for dark matter). The analysis is otherwise similar to that of Section 9.12, with spherical symmetry assumed for the profiles and solving the spherical Jeans equations to obtain them. We rejected 4 S0 galaxies (according to [2]), 2 galaxies with $M_{tot} > 10^{12} M_\odot$ (using M_{tot} from [53]) and 3 galaxies for which Jiang and Kochanek did not reproduce well the measurements (“fit outliers” in [59]). Finally, we removed PG1115+080 as it was stated that it seems peculiar (“low probability to belong to an homogeneous sample” [59]). All the remaining galaxies are from the SLACS survey. We used axis ratios from Bolton *et al.* [12]. We used the M_{Ein} and L_B given in [59] to form M/L . However, M_{Ein} is the mass within R_{Ein} , with typically $R_{Ein} \sim 0.5 R_{eff}$, whilst L_B is the total luminosity. Hence, we underestimate the M/L_B and they may be subject to systematic variation from galaxy to galaxy. We still present these data for completeness but instead, we focus on M_E/M_* and DMf . Two classes of results were reported in [59]: one with adiabatic compression and another without. The authors concluded that the model including it is strongly favored. No uncertainties were given on DMf . We assumed them to be proportional to DMf with a proportionality constant so that $\chi^2/ndf = 1$. The fits are shown in Fig. 36 and yield for sample 1:

$$\begin{aligned} M_{tot}/M_*(R_{Ein}) &= (-1.24 \pm 0.92) R_{min}/R_{max}|_{apparent} + (2.73 \pm 0.72) \text{ (with adiabatic compression),} \\ M_{tot}/M_*(R_{Ein}) &= (-0.14 \pm 0.68) R_{min}/R_{max}|_{mass} + (1.87 \pm 0.50) \text{ (with adiabatic compression),} \\ M_{tot}/M_*(R_{Ein}) &= (-0.88 \pm 0.58) R_{min}/R_{max}|_{apparent} + (1.99 \pm 0.45) \text{ (without adiabatic compression),} \\ M_{tot}/M_*(R_{Ein}) &= (-0.10 \pm 0.45) R_{min}/R_{max}|_{mass} + (1.38 \pm 0.34) \text{ (without adiabatic compression),} \end{aligned}$$

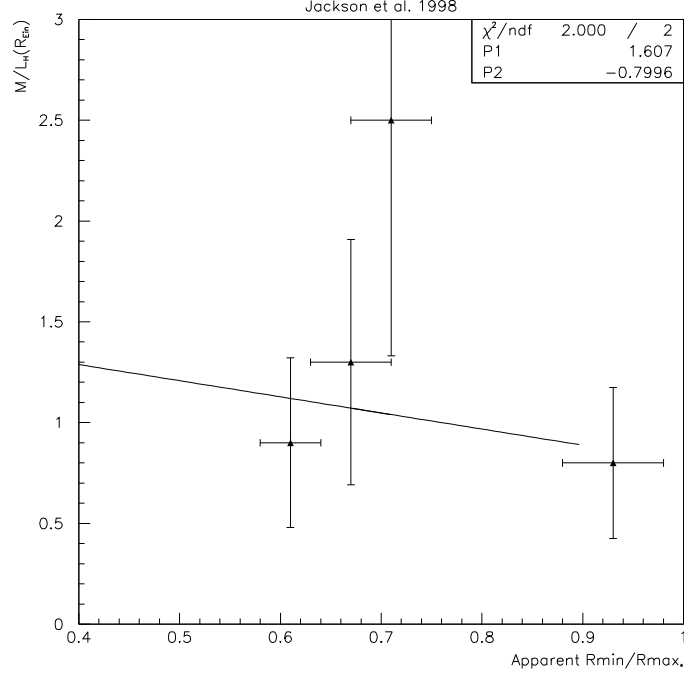


Figure 35: M/L_H vs axis ratio from Jackson *et al.* [58].

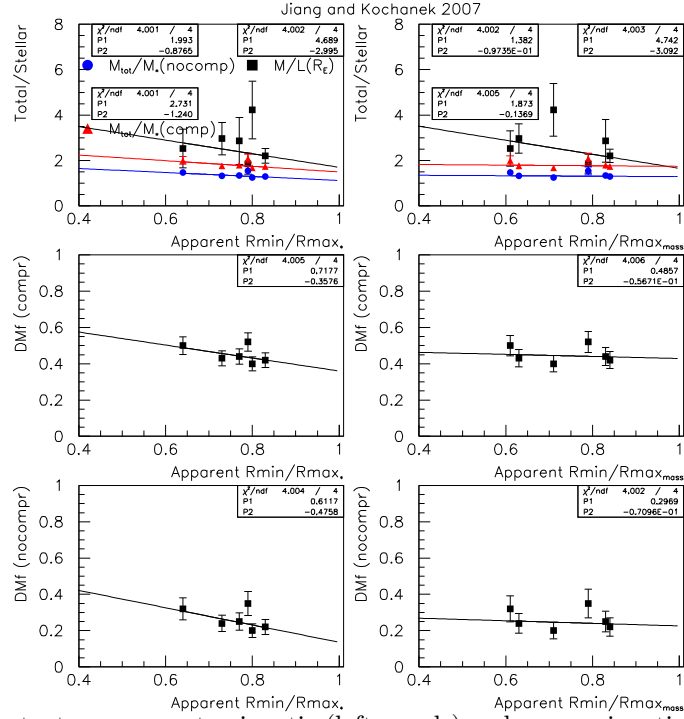


Figure 36: Dark matter content vs apparent axis ratio (left panels) and mass axis ratio (right panels) for Jiang and Kochanek [59]. The top panels display M_{tot}/M_* at $R_{E\text{in}}$ with adiabatic compression (red triangles) and without (blue filled circles), and M/L_B (black squares). The middle row displays the dark matter fractions including adiabatic compression and the bottom row is for the DMf s without compression.

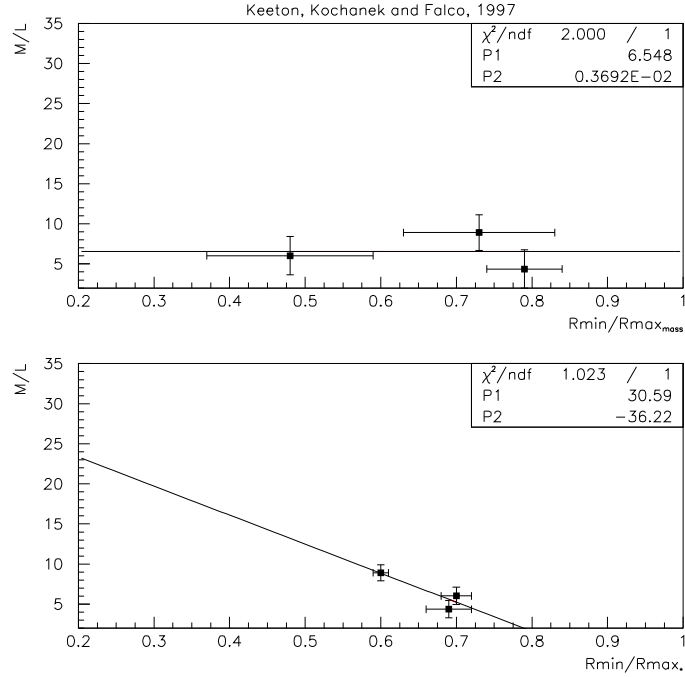


Figure 37: M/L vs mass axis ratio (top panel) and apparent axis ratio (bottom panel) for Keeton *et al.* [60].

$$\begin{aligned}
DMf(R_{Ein}) &= (-0.36 \pm 0.30) R_{min}/R_{max}|_{apparent} + (0.72 \pm 0.23) \text{ (with adiabatic compression)}, \\
DMf(R_{Ein}) &= (-0.06 \pm 0.23) R_{min}/R_{max}|_{mass} + (0.49 \pm 0.17) \text{ (with adiabatic compression)}, \\
DMf(R_{Ein}) &= (-0.48 \pm 0.35) R_{min}/R_{max}|_{apparent} + (0.61 \pm 0.27) \text{ (without adiabatic compression)}, \\
DMf(R_{Ein}) &= (-0.07 \pm 0.26) R_{min}/R_{max}|_{mass} + (0.30 \pm 0.20) \text{ (without adiabatic compression)}.
\end{aligned}$$

The analysis assumes spherical symmetry and no uncertainties were provided. For our global analysis, we used the M_{tot}/M_* and DMf results with compression (favored in [59]) and we assigned them to group 2 reliability.

For information:

$$\begin{aligned}
M_{tot}(R_{Ein})/L_B &= (-3.00 \pm 4.32) R_{min}/R_{max}|_{apparent} + (4.69 \pm 3.43), \\
M_{tot}(R_{Ein})/L_B &= (-3.09 \pm 2.57) R_{min}/R_{max}|_{mass} + (2.03 \pm 1.33).
\end{aligned}$$

9.11 Keeton, Kochanek and Falco (1997)

In [60] Keeton, Kochanek and Falco analyzed 17 strong lensing candidates. The total mass was obtained by using either a SIE model or a Singular Isothermal Sphere with tidal correction (SIS+Shear) model. The SIE model used to model the 2D mass profiles accounts for ellipticity. This implies a correlation between mass profile and ellipticity, with steeper profile galaxies having larger ellipticity. The luminosity profiles were assumed to follow a de Vaucouleur law. The luminosity uncertainty dominates that of M/L . From the 17 galaxies considered in [60], we excluded 2 spiral galaxies (B0218+357 and B1933+503), 3 for which M/L was not given (MG0414+0534, HST12531-2914 and BRI0952-0115), 4 that are clearly influenced by their environments (MG0751+2716, Q0957+561, B1422+231 and MG1131+0456) and 1 that was poorly understood in [60] (B1600+434). We removed galaxies B0712+472 and MG1549+304 that have a velocity dispersion $\sigma < 200 \text{ km.s}^{-1}$ (σ are from [103]). We relaxed our selection compared to our standard $\sigma < 225 \text{ km.s}^{-1}$, otherwise only Q0142-100 would have passed selection. We rejected PG1115+080 as it may be peculiar [59] and B1608+656 because it may have a companion. In all, 3 galaxies remained: Q0142-100, HST14176+5226 and MG1654+1346. We used the M/L values computed in the $\Omega_0 = 0.2$, $\lambda_0 = 0.8$ cosmological model. The M/L vs apparent and mass axis ratios are shown in Fig. 37. The best fits yield:

$$\begin{aligned}
M/L_B &= (-36.22 \pm 15.14) R_{min}/R_{max}|_{mass} + (30.59 \pm 9.89), \\
M/L_B &= (0.00 \pm 10.27) R_{min}/R_{max}|_{apparent} + (6.55 \pm 7.01).
\end{aligned}$$

The advantage of the analysis is that ellipticity is accounted for. The specific caveats are that the analysis is dated (for a strong lensing analysis) and due to the small number of galaxies we had to relax our standard criteria minimizing S0 and giant elliptical contaminations. For these reasons, results were assigned to group 3 reliability.

9.12 Koopmans *et al.* (2006)

Koopmans *et al.* [65] analyzed strong lensing and photometry data from 15 early-type field galaxies from the SLACS survey. The strong lensing data allowed them to determine the total mass M_{tot} within R_{Ein} . The

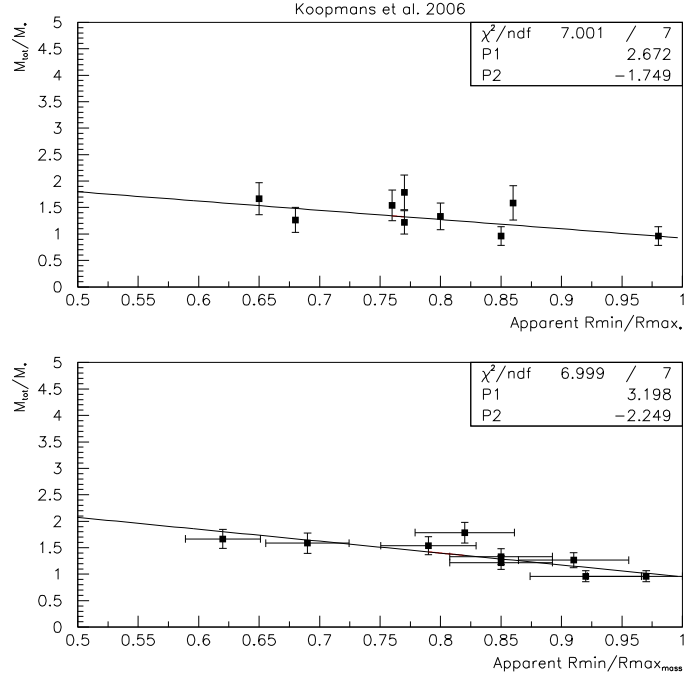


Figure 38: M_{tot}/M_* vs apparent and mass axis ratios (top and bottom, respectively) from Koopmans *et al.* [65].

photometry data was used to determine the total density profile $\rho(r)$ by solving the spherical Jeans equations with an assumed form $\rho(r) \propto r^{-\gamma'}$ and a Hernquist profile for the stellar density. Calculations were repeated with a Jaffe profile for stellar density in order to assess the model dependence on the choice of stellar profile. For mass deprojection, a SIE model was used and the mass axis ratio was deduced with precision better than 10%. A systematic study of uncertainties was carried out. There are 4 main sources of uncertainty. The unknown stellar velocity anisotropy has small effects, as does the influence of neighboring galaxies. The choice of model for the stellar and mass densities produced an uncertainty acceptable within the accuracy level of the data. The authors argued that the effect of the halo ellipticity on their study (dark matter fraction variation with radius) is small. We rejected 3 lenses identified as S0 in [2], excluded 2 galaxies with $M_{tot} > 10^{12} M_\odot$ and one with $\sigma < 225 \text{ km.s}^{-1}$. In all, our final sample comprises 9 galaxies. The M_{tot}/M_* vs axis ratio, is shown in Fig. 38. We rescaled the uncertainty provided by the authors so that $\chi^2/\text{ndf} \simeq 1$ for the best fits. they yield:

$$M_{tot}/M_* = (-1.75 \pm 0.77) R_{min}/R_{max}|_{\text{apparent}} + (2.67 \pm 0.64),$$

$$M_{tot}/M_* = (-2.25 \pm 0.57) R_{min}/R_{max}|_{\text{mass}} + (3.20 \pm 0.49).$$

Specific caveats are some model dependence, in particular in the choice of density profile which was argued to be unphysical in [46] and spherical symmetry was assumed (except for mass deprojection). The analysis has the advantages that systematic uncertainties and model dependence were studied and argued to be under control. Furthermore, care was taken in choosing and verifying that the galaxies are isolated. We assigned the results to group 1 reliability.

9.13 Leier (2009)

In [71], Leier analyzed 19 strong lenses with available photometry from the SLACS and CASTLE surveys. The lensing data were used to assess the projected total mass M_{lens} . From it and luminosity data, M_{lens}/L_I at $r = R_{lens}$ was extracted (R_{lens} is of the same order as R_{eff} for most lenses). M_{lens} was used with the virial theorem to form a velocity dispersion σ_{len} . It agrees generally well with the observed one, σ_{obs} , indicating that these galaxies are virialized. We rejected two galaxies for which data are not available (CFRS03.1077, HST14176), one known spiral (Q2237+656)⁷, two galaxies identified as S0 in [2], one with significant interaction and classified as peculiar in [59] (PG1115+080, which has $\sigma_{obs}/\sigma_{len} = 1.47$ and so may not be well virialized), one with significant contribution from its cluster (Q0957) and one with a close companion and unreliable axis ratio (B1608+656). In addition, we applied our standard selection to minimize contamination from giant elliptical galaxies and S0, rejecting one high mass galaxy (J0956+510). In all, 8 galaxies constitute our final sample. For all of them σ_{obs} and σ_{len} agree within 20%. Uncertainties on M/L were not provided. We estimated them using the uncertainties given for M_{lens}

⁷It has also one of the two worst $\sigma_{obs}/\sigma_{len}$ ratio, $\sigma_{obs}/\sigma_{len} = 1.47$, indicating it may not be well virialized.

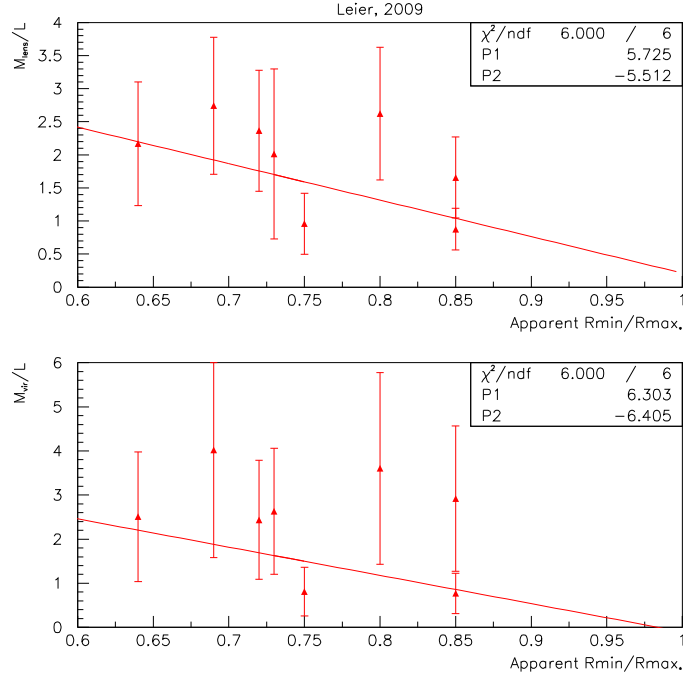


Figure 39: M_{tot}/L vs apparent axis ratio from Leier (2009) [71]. Top: $M_{tot} = M_{lens}$. Bottom: $M_{tot} = M_{vir}$.

and M_{vir} and assuming a 20% uncertainty on the luminosity. The resulting M/L_I uncertainties were then scaled so that $\chi^2/ndf = 1$. The $M/L(R_{lens})$ vs apparent axis ratio, shown in Fig. 39, have best fits:

$$M_{lens}/L_I(R_{lense}) = (-5.51 \pm 3.27) R_{min}/R_{max}|_{apparent} + (5.72 \pm 2.62),$$

$$M_{vir}/L_I(R_{lense}) = (-6.41 \pm 4.97) R_{min}/R_{max}|_{apparent} + (6.30 \pm 3.95).$$

The two fits agree well, indicating that the virial and strong lensing methods are consistent and that the galaxies are virialized. A limitation of this analysis is that spherical symmetry was assumed. The analysis has the advantage that care was taken in choosing virialized galaxies. We assigned the results to group 1 reliability.

9.14 Leier *et al.* (2011)

In [72], Leier *et al.* computed the baryon fraction profile for 19 strong lensing galaxies from the CASTLE survey. Lensing and photometry were used to recover the total mass and the mass and light profiles. A Sersic profile was used for stars and the apparent axis ratio was accounted for in the stellar mass calculation. M/L_B were extracted via a Stellar Population Synthesis model. Various IMF were used with results agreeing within 10%. Ignoring the spiral bulge Q2237, the giant MG2016 and RXJ0911 that is believed to not be a true lens, and applying our standard $M_{tot} < 10^{12} M_\odot$ and $\sigma_{obs} \geq 225 \text{ km.s}^{-1}$ criteria, we rejected 13 of the 19 galaxies (σ_{obs} are from [103]). 3 others had to be rejected because of notable interactions with environment, leaving only 3 galaxies (Q0142, Q0047 and MG1104). Slightly relaxing our selection to $\sigma_{obs} \geq 215 \text{ km.s}^{-1}$ or $\sigma_{lens} \geq 215 \text{ km.s}^{-1}$ provides a sample of 6 galaxies. The $M/L(R_{lens})$ vs apparent axis ratio is shown in Fig. 40. The best fit is:

$$M_{lens}/L_V = (+37.2 \pm 36.6) R_{min}/R_{max}|_{apparent} + (-13.2 \pm 26.3).$$

The uncertainties were scaled so that the $\chi^2/ndf = 1$. The caveats are that in order to get a reasonably sized sample, we relaxed our selection. Also, like in the other CASTLE lens survey analyses, the sample is more inhomogeneous, as noted e.g. in [71]. Finally, the axis ratios came from different authors thus possibly adding point-to-point fluctuations, although this was accounted for by forcing $\chi^2/ndf = 1$ for the fit. We assigned the results to group 2 reliability.

9.15 Ruff *et al.* (2011)

Ruff *et al.* [88] analyzed 11 early-type strong-lensing galaxies from the SL2S survey. The lenses have an average redshift of $\langle z \rangle = 0.5$. A SIE model was used to obtain the total mass M_{Ein} within R_{Ein} . Photometric data were used to compute both the stellar mass M_* , using either a Chabrier or a Salpeter IMF, and the size of the galaxy. An elliptical de Vaucouleur profile was used to obtain the surface brightness. The DM_f was calculated at $R_{eff}/2$ by solving the spherical Jeans equations. No galaxy type identification is given in the article. The requirements that $M_{tot} < 5 \times 10^{11} M_\odot$ and $\sigma \geq 225 \text{ km.s}^{-1}$ were used to remove possible S0 and giants. 7 galaxies passed the

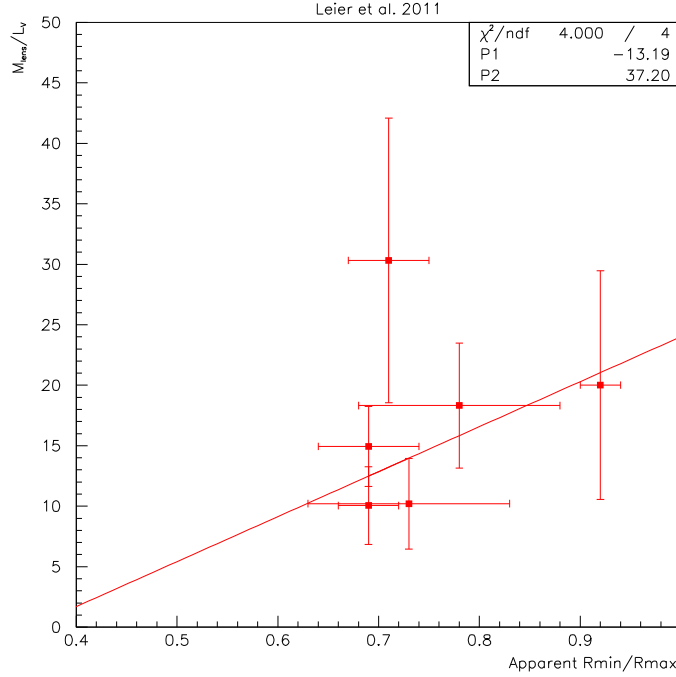


Figure 40: M_{lens}/L_V vs apparent axis ratio from Leier *et al.* (2011) [72]. The line is the best fit to the data.

selection. Mass ratios vs apparent and mass axis ratios are shown in Fig. 41. The best fits are:

$$\begin{aligned}
 M_{Ein}/M_* &= (+0.49 \pm 2.90) R_{min}/R_{max}|_{apparent} + (0.22 \pm 2.17), \\
 M_{Ein}/M_* &= (+0.53 \pm 2.47) R_{min}/R_{max}|_{mass} + (0.18 \pm 1.88), \\
 M_{tot}/M_*|_{Sal} &= (+3.62 \pm 8.81) R_{min}/R_{max}|_{apparent} + (0.50 \pm 6.33), \\
 M_{tot}/M_*|_{Sal} &= (-4.66 \pm 1.43) R_{min}/R_{max}|_{mass} + (5.84 \pm 0.85), \\
 M_{tot}/M_*|_{Chab} &= (-6.17 \pm 14.65) R_{min}/R_{max}|_{apparent} + (9.62 \pm 10.70), \\
 M_{tot}/M_*|_{Chab} &= (-9.89 \pm 4.85) R_{min}/R_{max}|_{mass} + (11.65 \pm 3.25), \\
 DMf|_{Sal} &= (-0.59 \pm 1.11) R_{min}/R_{max}|_{apparent} + (0.98 \pm 0.80), \\
 DMf|_{Sal} &= (-0.80 \pm 0.37) R_{min}/R_{max}|_{mass} + (1.09 \pm 0.26), \\
 DMf|_{Chab} &= (-0.65 \pm 0.52) R_{min}/R_{max}|_{apparent} + (1.20 \pm 0.39), \\
 DMf|_{Chab} &= (-0.48 \pm 0.29) R_{min}/R_{max}|_{mass} + (1.06 \pm 0.21),
 \end{aligned}$$

The mass ratio uncertainties were scaled so that $\chi^2/ndf = 1$.

The difference between M_{Ein}/M_* and M_{tot}/M_* is that M_{Ein}/M_* stands at $r = R_{Ein}$ and the models account for the apparent ellipticity and do not need IMF input. M_{tot}/M_* stands at $r = R_{eff}/2$, used models accounting for ellipticity but was obtained solving the spherical Jeans equations with an assumed IMF. For our sample, we have $0.73 < R_{Ein}/R_{eff} < 2.06$, but with $R_{Ein} \simeq R_{eff}$ in most cases.

A caveat here is that only a few tentative type identifications are available from [88] so we required $\sigma \geq 225 \text{ km.s}^{-1}$ and $M_{tot} < 5 \times 10^{11} M_\odot$ to exclude possible of S0 and giant galaxies. Little indication on the environment influence is given in [88]. Advantages are that ellipticities were accounted for in the mass calculations and the model dependence upon the IMF can be estimated. For these reasons, the M_{Ein}/M_* results are assigned to group 2 reliability and the M_{tot}/M_* and DMf using a Chabrier IMF are assigned to group 3 reliability.

9.16 Treu and Koopmans (2004)

Treu and Koopmans [98] analyzed 5 strong lenses to obtain the distributions of luminous and dark matter within R_{Ein} . The galaxies have redshifts $0.5 < z < 1$. A SIE model was used to provide a robust estimate of the total mass whilst the luminous mass profile was deduced from stellar dynamics data. Dark and luminous profiles were assumed to be spherical. The dark matter was assumed to follow a NFW profile and the luminous one a Hernquist profile. The lenses were chosen relatively isolated. The authors studied the effects of stellar anisotropy and of neglecting ellipticity and concluded that these effects are small. Applying standard $\sigma \geq 225 \text{ km.s}^{-1}$ and $M_{tot} < 10^{12} M_\odot$ would have selected only 2 galaxies (0047 and C0302). We slightly relaxed the selection to accept H1417 ($\sigma = 224 \text{ km.s}^{-1}$). We note that C0302 may belong to a small galaxy group and so subject to environment interaction. The 2 other available galaxies were rejected because one is a giant (MG2016) and the other most probably a S0 (H1543). The best fits to M_{tot}/L_B and DMf vs apparent axis ratio, shown in Fig. 42, are

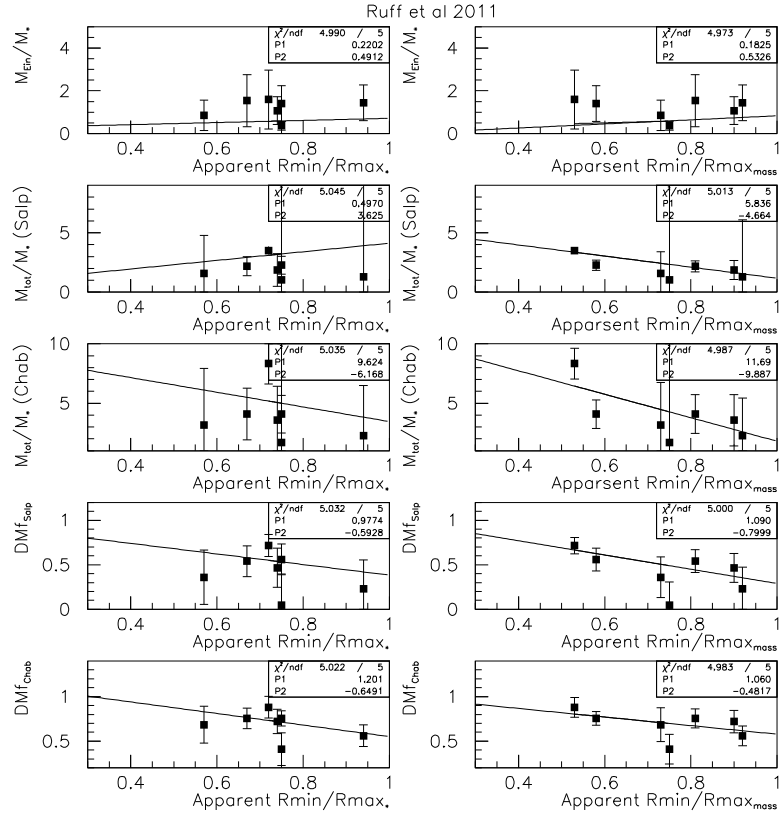


Figure 41: Mass ratios vs apparent (left column) and mass (right column) axis ratios from Ruff *et al.* [88]. The top row is for M_{Ein}/M_* . The 2nd and 3rd rows are for M_{tot}/M_* extracted using the DMf assuming either a Chabrier or a Salpeter IMF. The last two rows show the corresponding DMf .

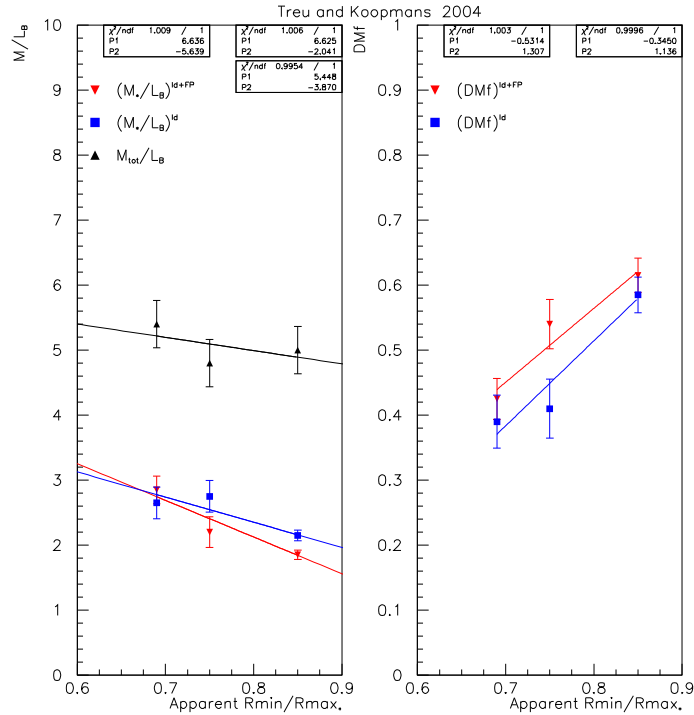


Figure 42: M_{tot}/L_B vs apparent axis ratio from Treu and Koopmans [98] (left column). The black up triangles are for the total mass over B-band luminosity. The stellar mass to apparent ratios are also given for information. Also shown is the corresponding DMf (right column) vs axis ratio. The reason why M_{tot}/L_B has a negative slope and the DMf have a positive one is because M_*/L drops faster with axis ratio than M_{tot}/L .

$M_{tot}/L_B = (-2.04 \pm 3.20)^{R_{min}/R_{max}|_{apparent}} + (6.63 \pm 2.45),$
 $DMf = (+1.31 \pm 0.30)^{R_{min}/R_{max}|_{apparent}} + (-0.53 \pm 0.24)$ and
 $DMf^{+FP} = (+1.14 \pm 0.24)^{R_{min}/R_{max}|_{apparent}} + (-0.35 \pm 0.19)$ for which Fundamental Plan assumptions were made to further constrain the data.

The uncertainties from [98] were symmetrized and scaled so that $\chi^2/ndf = 1$. The reason why M_{tot}/L_B has a negative slope and the DMf have a positive one is because M_*/L drops faster with axis ratio than M_{tot}/L .

The data were analyzed assuming spherical symmetry but the authors argued that accounting for ellipticities produced little difference. Likewise, the effect of stellar ellipticity was studied and found unimportant. We assigned the M_{tot}/L_B result to group 1 reliability.

10 Ellipticity and projection corrections

There are two types of ellipticity corrections. The first one is due to the ellipticity affecting the computation of quantities relevant to our analysis. We call this the “ellipticity corrections” proper and discuss it in the next Section. The second type is correcting for the fact that often only the apparent ellipticity of a galaxy is known, which strongly reduces the correlation we study in this article. We address this correction in Section 10.2.

10.1 Ellipticity corrections

The exact formula to compute M/L depends on ellipticity. Generally, assuming spherical symmetry underestimates M/L . Sensitivity to ellipticity differs for different methods. It is important e.g. for the virial method but less so for the strong lensing method when the total mass is extracted at the Einstein radius and the luminosity is obtained from deprojected data. Except for the strong lensing data for which the correction is expected to be small, the data discussed here at least approximately or partially corrected to account for ellipticity. The caveat is that the correction may be approximate and often uses apparent axis ratio rather than the true intrinsic axis ratio. Hence, it may still not correct fully the M/L .

10.2 Projection correction

This correction is independent of the technique used to extract M/L , as long as the axis ratio distribution of the galaxy sample is also independent of the technique, e.g. a technique does not preferentially choose galaxies with large or small apparent axis ratios. We assume that this is the case and apply the projection correction, unless it was already done in the original publication as e.g. in sections 5.1, 8.1 or 9.2. We use our results from Section 4.1 (Bacon *et al.* [3]) to estimate this correction since it is the second largest sample of galaxies (the largest sample is that of Prugniel & Simien [84]. However, the authors remarked it could be slightly biased).

For an oblate spheroid viewed at an angle θ , its real axis ratio $R_{min}/R_{max}|_{true}$ relates to its projected apparent axis ratio $R_{min}/R_{max}|_{apparent}$ as [94]:

$$R_{min}/R_{max}|_{apparent} = \sqrt{(R_{min}/R_{max}|_{true})^2 \sin^2 \theta + \cos^2 \theta} \quad (1)$$

We can safely assume that the galaxies in our study are oblate and none are prolate. We assume the $R_{min}/R_{max}|_{true}$ distribution to be gaussian, see top left plot of Fig. 43. The characteristics of the gaussian are determined by matching the simulated distribution of apparent axis ratios to the actual distribution of our data sample (bottom left plot). This results in a gaussian centered at 0.55 and with a full width of 0.07. The top right plot shows the assumed correlation between M/L and real axis ratio. The simplest choice is a linear relation. However, it could lead to unphysical (negative) M/L . To circumvent this problem, we can choose a function that is linear for most of the $R_{min}/R_{max}|_{true}$ values but flattens near the $R_{min}/R_{max}|_{true} = 0$ and $R_{min}/R_{max}|_{true} = 1$ limits, e.g. a Fermi-Dirac function. We do the projection correction for both linear (Fig. 43) and Fermi-Dirac functions (Fig. 44) cases in order to estimate the dependence upon the choice of function. The linear function fitting best the observed M/L vs R_{min}/R_{max} (bottom right plot) is $(\alpha x + \beta)$ with $\alpha = -49$ and $\beta = 38$. The best fit using a Fermi-Dirac function $(\frac{a}{e^x - b/c + 1} + d)$ is for $a = 45$, $b = 0.5$, $c = 0.1$ and $d = 0$. The bottom left panel shows the observed (red) and simulated (black) distributions of the apparent axis ratio. To obtain the simulated one, the gaussian distribution is transformed using Eq. 1 with the viewing angle θ randomly chosen between 0 and $\pi/2$. A random shift toward larger $R_{min}/R_{max}|_{apparent}$ values is added to reproduce the rounding effect of the resolution of the detector. (If, due to this shift, $R_{min}/R_{max}|_{apparent} > 1$, we either set it to 1 or redraw a random value for the original $R_{min}/R_{max}|_{true}$). The bottom right panel displays M/L vs apparent axis ratio. We use 10^4 events for the fit but for clarity, only the error bars of the first 100 events are shown. The distribution reproduces well the observed one (shown by red symbols). This supports that the M/L dispersion is not only gaussian but mostly

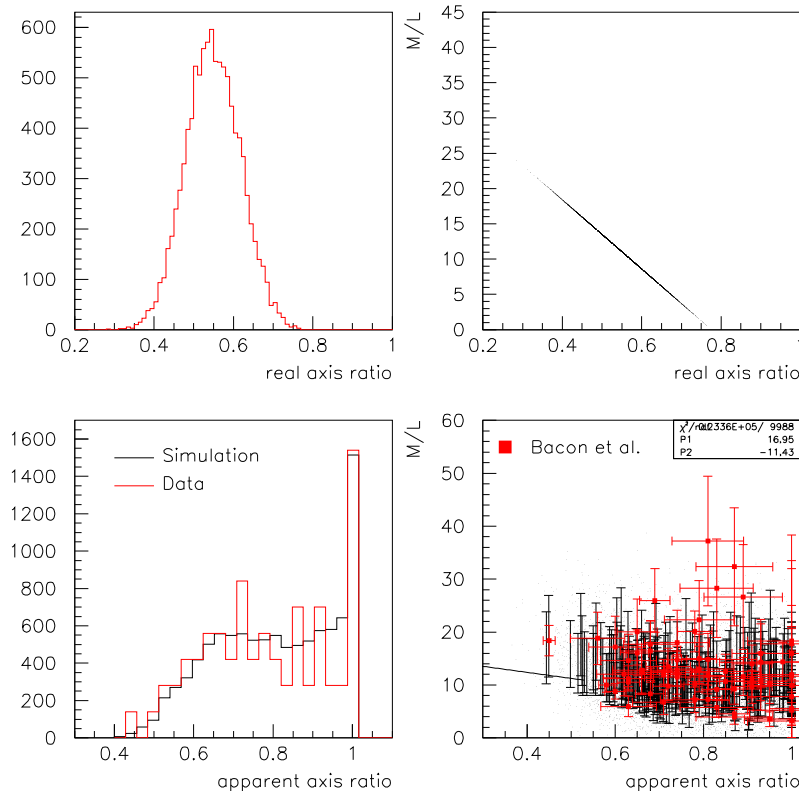


Figure 43: Effect of projecting the 3-dimensional elliptical galaxies in our 2-dimensional observation plan. Top left plot: simulated distribution of the real axis ratio. Top right panel: hypothesized linear relation between M/L and real axis ratio. Bottom left panel: projected axis ratio (black: simulation, red: data). Bottom right plot: M/L vs apparent axis ratio (Black: simulation, red observed data).

comes from the galaxies' random projections. As done with the observational data, we fit this distribution with a linear form $M/L = P_2(R_{min}/R_{max}|_{apparent}) + P_1$. In the simulation, the M/L uncertainties are proportional to M/L , as for the data. Using a gaussian distribution, we randomly offset the central values of the simulated points on the bottom right figure within their error bars.

The correction has some model dependence due to the following assumptions:

- No prolate galaxies in our sample;
- gaussian distribution of the real axis ratios;
- The assumed form for the relation between the real axis ratio and M/L ;
- The modeling of the detector resolution effect.

Furthermore, it is unclear how to apply the correction because the real axis ratios for the observed data are unknown and the correction is determined on statistical basis. Given the distribution of the real axis ratio (top left panel), it is sufficient to only consider the range $0.35 < R_{min}/R_{max}|_{true} < 0.65$. There, the Fermi-Dirac form is approximately linear. Averaging the results derived with both forms, the simulation of the projection effect gives a correction of about 5 ± 1 for the slope M/L vs axis ratio correlation.

11 Correlations

Many of the quantities describing galaxies are interrelated. Therefore they may indirectly generate correlations with R_{min}/R_{max} or M/L , some of them spurious: a measurement or observation bias unrelated to R_{min}/R_{max} and M/L may propagate to one or both of them due to interrelations. We systematically studied this possibility using mostly the galaxy sample from Ref. [3]. We summarize our findings in this section. The detailed analysis can be found in Appendix L. Using the galaxy sample from [3] is convenient due to its large statistics and the relatively large number of galactic characteristics provided. They are:

- The M/L ratios obtained from three different virial estimates.
- The apparent effective radius, Re (given in arcsec).

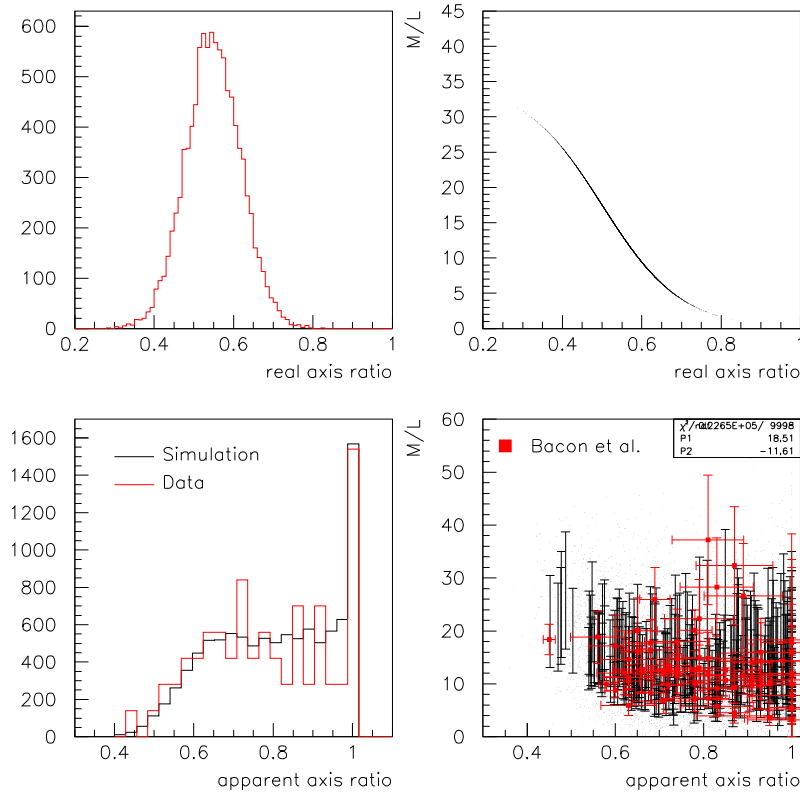


Figure 44: Same as Fig. 43 but with a Fermi-Dirac relation assumed between M/L ratio and real axis ratio.

- The absolute effective radius, Re (given in Kpc).
- The apparent axis ratio, R_{min}/R_{max} .
- The galactic surface brightness, I_e .
- The central velocity dispersion, σ_0 .
- The distance modulus, DM , for each galaxy.
- The galactic absolute blue magnitude, M_b .
- The galactic integrated apparent blue magnitude, B_t .

Furthermore, we also used galaxy samples other than that of Ref. [3] to check correlations with galactic characteristics other than those just listed.

That Ref [3]’s data are dated is not an issue because the selection criteria keeps only galaxies with characteristics agreeing with the NED ones, which are current. Furthermore, older data are presumably more contaminated with measurement or observation biases, and therefore, they are better suited to study spurious correlations and provide a useful upper limit for these biases. In other words, while the older data may be less sensitive to an actual M/L vs R_{min}/R_{max} correlation because it would be diluted by jitters and worst resolutions, they are more sensitive to spurious correlations and if an upper limit for those is determined to not be large, the genuine origin of the M/L vs R_{min}/R_{max} correlation can be validated.

Three types of interrelations are possible:

- I) Relations of well-understood origin, e.g. that between M/L and σ originating from the virial theorem, or the reduction of apparent sizes and luminosities as the distances from the galaxies to Earth increase.
- II) Relations known Phenomenologically, e.g. the Kormendy [66] and Faber-Jackson [41] relations.
- III) Unknown relations.

We looked for correlations for all the combinations between pairs of characteristics by linearly fitting them, a non-zero fit slope indicating a correlation. We directly used the uncertainties given in Ref. [3] (no rescaling according to the *unbiased estimate*). We clearly confirmed all known relations (types I and II above) except for the surface brightness I_e vs absolute blue magnitude M_b relation, which was reported in [10]. The correlation is seen, yet not as strongly as for the other known relations. We found several other relations. They are weaker

by a factor of 1.6 ± 0.81 . However, since this relies on linearly extrapolating over 31 DM units using a fit just done over 4.5 units, we decided to not correct $\frac{d(M/L)}{dR_{min}/R_{max}}$. Supporting this conservative choice are the facts that:

- I) It is unclear if the bias is real, the fit slope being just 1.6σ from zero;
- II) the errors on the extrapolation are large;
- III) This bias cannot be at the origin of the correlation we are studying since the correction would decrease it.

12 S0 contamination study

It is often delicate to distinguish between S0 galaxies and elliptical galaxies with large axis ratios. Such R_{min}/R_{max} -dependent contamination could cause the decrease of M/L with R_{min}/R_{max} reported in Section 13 because M/L tends to be smaller for S0 than for elliptical galaxies. If so, the correlation's origin would not be physical but a systematic bias in galaxy classification. The strict generic rejection criteria described in section 3.1.1 suppress that contamination because they systematically exclude galaxies of unclear/transitional morphologies, namely E/S0, E+ or E? types (E+ are “late elliptical galaxies”, a transition stage between E and S0) since those may be more prone to misclassification. Furthermore, effects of a S0 contamination would emerge in the systematic studies, specifically varying the strictness of the S0 rejection criteria cf. Section 12.1, the study of how the M/L vs M/L with R_{min}/R_{max} depends on DM cf. Section 12.5 and apparent magnitude cf. Section 12.6, and investigating a possible M_*/L vs R_{min}/R_{max} correlation (cf. Section 12.4 and appendix B).

We discuss here these specifics tests. They indicate that S0 being at the origin of the correlation is unlikely.

12.1 Independent S0 rejection criterion

A standard method to check the efficiency the main rejection criterion and the consequence of a possible contamination is to add an independent rejection criterion and varies its strictness. To do this, to the primary criterion (based on the NED classification) we added a second one consisting of rejecting low velocity dispersion galaxies, as S0 tend to have lower velocity dispersion values. These two rejection criteria are independent in the sense that any rejection inefficiency of one criterion is unrelated to the inefficiency of the other criterion.

Applying the second rejection criterion results in a correlation agreeing with the nominal analysis. This test is done on the largest sample of galaxies (112 galaxies, of which 44 pass the second criterion) so it is statistically significant. A possible issue is that the second criterion might bias the correlation e.g. because of the proportionality between M/L and velocity dispersion. The average value of M/L is in fact smaller once the second criterion is applied. To compensated for this, we increased uniformly those M/L so that their average matches that of the nominal analysis. If S0 contamination was biasing the nominal analysis, an agreement between the nominal and second analyses could still occur if:

- 1) a new effect emerged from introducing the second criterion, and
- 2) that effect mimics the (now suppressed) S0 contamination effect.

Such coincidence being unlikely, this check attests the reliability of the nominal rejection criterion. Another such misleading agreement between the nominal and second analyses could also occur if S0 and E display similar M/L vs R_{min}/R_{max} correlations⁸. If so, our check would not be able to assess the S0 contamination. However, this one would then have no influence on our final result.

12.2 Consequence of a S0 contamination for galaxy census

In this section, we assume that the M/L vs R_{min}/R_{max} correlation reported in this document stems S0 contamination, and we investigate the consequence on galaxy type census. To reduce possible systematic bias, we conducted the analysis on large samples of data determined either with the virial theorem [84] or from lensing [2]. Our analyses (described next) conclude that assuming that the correlation is due to S0 contamination would lead to a proportion of E and S0 galaxies clearly conflicting with the observed census.

12.2.1 Analysis using virial data (Prugniel & Simien data set)

We use here data from Prugniel & Simien [84]. From those, $M/L = (-6.58 \pm 1.98)R_{min}/R_{max}|_{apparent} + (8.99 \pm 1.68)$ (see table of Section K). At small values of R_{min}/R_{max} , S0 contamination is suppressed since S0 are highly flattened. Thus, the value of M/L at $R_{min}/R_{max}|_{apparent} \simeq 0.3$ offers a clean value of M/L_E . Our work hypothesis here being that for elliptical galaxies M/L is independent of R_{min}/R_{max} , we have under this hypothesis $M/L_E \geq$

⁸Such possibility appears to be ruled out by other checks performed in this manuscript.

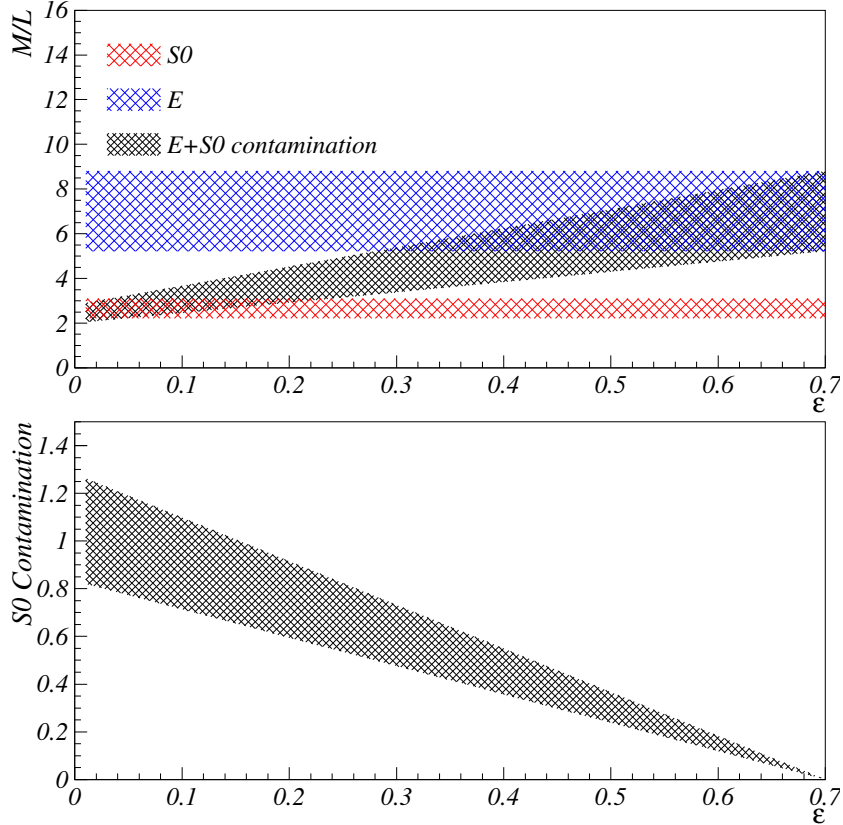


Figure 46: Top: observed M/L vs $\varepsilon \equiv 1 - R_{min}/R_{max}$ correlation for the Prugniel & Simien data [84] (black band). Hypothesized constant M/L for elliptical galaxies (blue band), and for S0 (red band) for the same data. Bottom: the putative S0 contamination to the elliptical galaxy set needed to explain the correlation seen in the top plot.

7.02 ± 1.80 .⁹ We have a lower bound for M/L_E because, to be consistent with the assumption that S0 contamination produces the correlation seen over the full span of R_{min}/R_{max} , there must be some remaining S0 contamination at $R_{min}/R_{max}|_{apparent} \simeq 0.3$.

To determine the mass-to-light ratio for S0, M/L_{S0} , we apply a similar procedure as that for elliptical galaxies. We keep only good S0, rejecting dwarf or peculiar S0, S0 listed in the Arp catalog, E/S0, S0?, SB0 (because a visible bar would surely identify a S0, even if it is face-on, which then would be rejected and unable to contaminate the elliptical galaxy sample), BrClg, etc. We obtain a set of 24 S0 with an average $M/L_{S0} = -2.86 \pm 0.38$. Using a subset of S0 with $R_{min}/R_{max} < 0.5$ to avoid possible E contamination, the average becomes $M/L_{S0} = -2.66 \pm 0.44$.

Supposing that M/L_E and M/L_{S0} are independent of R_{min}/R_{max} , and that a S0 contamination causes a $M/L = a[R_{min}/R_{max}|_{apparent}] + b$ correlation, imply a contamination $\mathcal{C}(R_{min}/R_{max}|_{apparent}) = a[R_{min}/R_{max}|_{apparent} - R_{min}/R_{max}|_0] / [M/L_{S0} - a(R_{min}/R_{max}|_0) - b]$, where $R_{min}/R_{max}|_0 = 0.3$ is the value of $R_{min}/R_{max}|_{apparent}$ at which the S0 contamination is supposed to become negligible, and $\mathcal{C}(R_{min}/R_{max}|_{apparent})$ is the ratio of misidentified S0 over the total amount of assumed elliptical galaxies. Results vs $\varepsilon \equiv 1 - R_{min}/R_{max}$ are displayed in Fig. 46. Clearly, the putative contamination would have to be implausibly large to account for the observed M/L vs R_{min}/R_{max} correlation. For instance, it would imply that all round ($\varepsilon \equiv 1 - R_{min}/R_{max}|_{apparent} = 0$) elliptical galaxies that we used in this analysis are in fact S0 misclassified as ellipticals. Even the rather conservative 2σ lower bound of the error band in the bottom panel of Fig. 46 implies a large $M(0.9 < R_{min}/R_{max}|_{apparent} < 1) = 0.54$, signifying that over half of the apparently round elliptical galaxies are misidentified and in fact are S0. Considering that $\sim 5\%$ of a set of disks oriented randomly would have $R_{min}/R_{max}|_{apparent} \gtrsim 0.95$, together with the fact that in the observed $R_{min}/R_{max}|_{apparent}$ distribution of ellipticals, $\sim 30\%$ of the galaxies identified as ellipticals have $R_{min}/R_{max} = 0.95 \pm 0.05$ (see e.g. Fig. 43), then the ratio of S0 to elliptical galaxies should be 7-to-1. Although estimated conservatively, this still disagrees with the censuses that indicate a similar number of elliptical and S0 galaxies [15]. We conclude that a S0 contamination cannot be the origin of the M/L vs R_{min}/R_{max} correlation.

⁹This is the value prior to the projection correction discussed in Section 10.2. This correction should in principle be implemented but, since it is proportionate to the *physical* correlation assumed here to not be present, the correction has no effect.

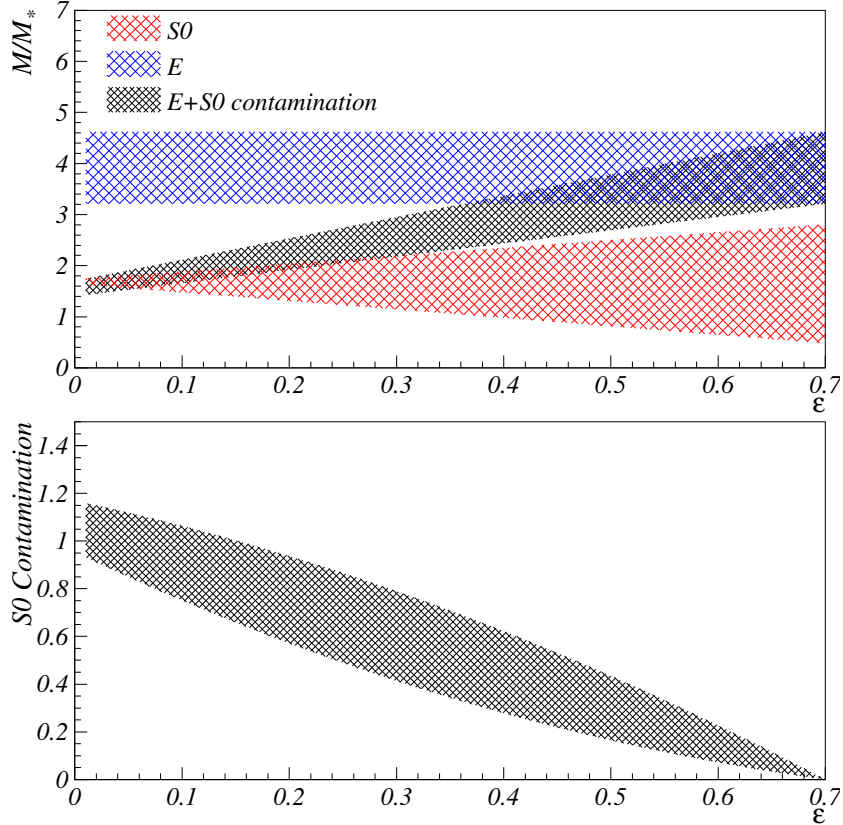


Figure 47: Same as Fig. 46 but for the lensing data from Auger *et al* [2].

12.2.2 Analysis using lensing data (Auger *et al.* data set)

The Prugniel & Simien data [84] are obtained using the virial theorem. We repeat here the analysis with the Auger *et al.* data [2], obtained using gravitational lensing for which the mass estimate procedure is generic to both E and S0. From these data, $M_{tot}/M_* = (-3.38 \pm 0.79)R_{min}/R_{max}|_{mass} + (4.92 \pm 0.66)$. We conservatively use the largest correlation ($R_{min}/R_{max} = R_{min}/R_{max}|_{mass}$, and M/M_* extracted using a Chabrier IMF), $M/M_*(R_{min}/R_{max} = 0.3) = 3.92 \pm 0.70$. Selecting S0 from the set [2], we obtain a subset of 5 S0 (we rejected 2 E/S0). From this sample, we obtain a M/L vs R_{min}/R_{max} correlation slope of $+0.06 \pm 1.60$. The deduced putative contamination is shown in Fig. 47. It is similar to the one obtained from virial data and so the same conclusion applies.

12.3 Case of the S0 contamination at small R_{min}/R_{max} only

In sections 12.2.1 and 12.2.2, the S0 contamination was chosen to dependent linearly with R_{min}/R_{max} in order to reproduce the linear dependence of M/L with R_{min}/R_{max} . However, this linear dependence stems from our choice of the fit function, which we chose to be linear as it is the simplest assumption, see Section 3.2. If S0 contamination were in fact at the origin of the M/L vs R_{min}/R_{max} correlation, it could be due e.g. to a large S0 contamination presents solely about $R_{min}/R_{max}|_{apparent} \sim 1$. If so, higher order polynomials would fit the data better. whilst this is not the case we nevertheless, for completeness, investigate here this possibility.

If a $R_{min}/R_{max}|_{apparent} \sim 1$ (i.e. face-on S0) S0 contamination were significant, removing these galaxies from the analysis should significantly decrease $d(M/L)/d(R_{min}/R_{max}|_{apparent})$. This prediction was investigated with the highest statistics data set of Prugniel & Simien [84]. Excluding galaxies with $R_{min}/R_{max}|_{apparent} > 0.9$ decreases the sample from 102 to 76 galaxies and yields $d(M/L)/d(R_{min}/R_{max}|_{apparent}) = -10.32 \pm 2.89$. This is compatible with the nominal value of -6.58 ± 1.98 and is, if anything, steeper than the nominal value in contrast to what we would have expected from face-on S0 contamination.

It is also immediately evident from any high statistics correlation plots, e.g. Fig. 1, that excluding galaxies with high $R_{min}/R_{max}|_{apparent}$ would not modify significantly $d(M/L)/dR_{min}/R_{max}|_{apparent}$.

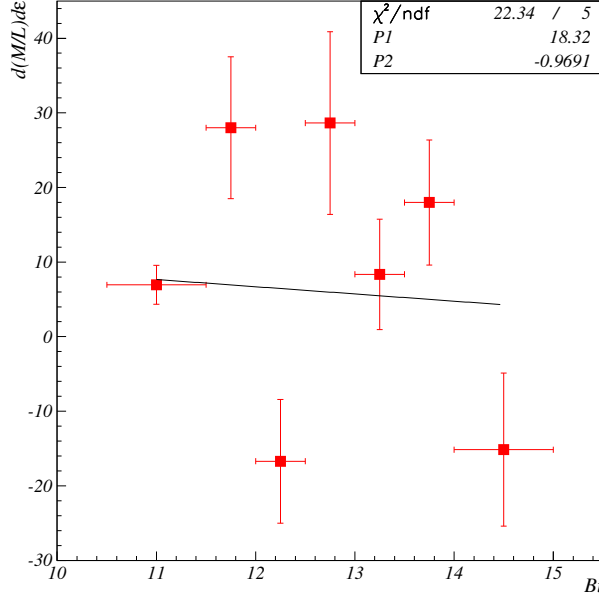


Figure 48: $d(M/L)/d\varepsilon$ vs apparent integrated blue magnitude. The Bacon *et al.* data set was used.

12.4 Stellar M_*/L ratio vs ellipticity study

We investigate in appendix B the possibility of a M_*/L vs ellipticity correlation. No such correlation was found. However, just like for M/L , the stellar M_*/L ratios tend to be smaller for S0: Ref [19], reports that low velocity dispersion σ early-type galaxies, i.e, galaxies more likely to be S0, have M_*/L of about $2 M_\odot/L_\odot$. High σ early-type galaxies, i.e, those more likely to be ellipticals, have M_*/L of about $4 M_\odot/L_\odot$.¹⁰ Consequently, if S0 contamination were at the origin of the M/L vs ellipticity correlation, it would also produce a M_*/L vs ellipticity correlation, which is not seen. This further rules out the possibility that S0 contamination is at the origin of the M/L correlation.

12.5 Correlation with distance moduli

If the M/L vs R_{min}/R_{max} correlation were due to contamination from S0, then its slope $d(M/L)/d(R_{min}/R_{max})$ should be steeper for distant galaxies because they are harder to classify. However, Fig. 49 shows that this is not the case: the M/L obtained using the strong lensing method pertain to distant galaxies, yet their $d(M/L)/d(R_{min}/R_{max})$ are similar (in fact slightly lower in average) to that obtained with the virial theorem, typically applied to local galaxies. Furthermore, a contamination from S0 would cause an increase of $d(M/L)/d(R_{min}/R_{max})$ with distance modulus, yet there is no evidence of such increase, see page 106.

12.6 Correlation with apparent magnitude

Following the same argument as in the previous section, a contamination from S0 would cause $d(M/L)/d(R_{min}/R_{max})$ to be inversely dependent on apparent magnitude because fainter galaxies are harder to identify. The apparent magnitude being strongly correlated with distance modulus, the conclusion of section 12.5 should directly apply. Nevertheless, we investigate explicitly here the possible correlation between $d(M/L)/d(R_{min}/R_{max})$ (or equivalently $d(M/L)/d\varepsilon$) and apparent magnitude. We grouped the M/L in seven equidistant bins of B_t , the integrated apparent blue magnitude, and then extracted for each bin the slope $d(M/L)/d\varepsilon$. The result is shown in Fig. 48. There is no increase of $d(M/L)/d\varepsilon$ with B_t . The best linear fit to the data yields $d(M/L)/d\varepsilon = (-0.97 \pm 1.97)B_t + 18.32 \pm 23.12$. As expected from the strong correlation between B_t and distance modulus, there is a hint of effect opposite to what should have been expected from a S0 contamination, i.e, a possibly negative slope $d^2(M/L)/(d\varepsilon dB_t) = -0.97 \pm 1.97$.

13 Global results

The results of sections 4 to 9 can be combined to extract $\left\langle \frac{d(M/L)}{d(R_{min}/R_{max})} \right\rangle$, the average slope of M/L vs axis ratio. Several points require caution:

¹⁰Similarly, in [17], it is shown that fast rotators have a smaller M_*/L (about 1.5 to 3 M_\odot/L_\odot) than slow rotators (about 2.5 to 3.5 M_\odot/L_\odot). If fast rotators tend to be S0, then S0 tend to have smaller M_*/L than elliptical galaxies.

- whilst M/L are most often estimated in the B-band, not all of them are. Another scaling factor occurs between M/L using different Hubble parameter values. Lastly, some results are expressed as M_{tot}/M_* instead of M/L . We assume here that $M_{tot}/M_* \propto M/L$. To address these points, we impose $M/L(R_{min}/R_{max} = 0.7) = M_{tot}/M_*(R_{min}/R_{max} = 0.7) = 8$. We choose to normalize to 8 as it is a typical value for M/L of elliptical galaxies. The choice $R_{min}/R_{max} = 0.7$ corresponds to where the distribution of elliptical galaxies peaks, which makes extrapolations unnecessary, in contrast to choosing other values such as e.g. $R_{min}/R_{max} = 1$.
- Some results use similar methods to obtain M/L and share a number of the same galaxies in their sample. Thus, these results can be highly correlated, biasing the average. Furthermore, some results are, in the context of our study, less reliable than others. This is addressed by applying the following procedure:
 - The uncertainty is scaled by the reliability factor from 1 (most reliable) to 4 (least reliable).
 - For extractions using a similar method, grouped in Sections 4 to 9, we identify the number of shared galaxies and increase each uncertainty assuming that the uncertainty is statistically dominated. This procedure accounts also for the difference in reliability factors between analyses because results are weighted by them when combined. Uncertainties on results using shared galaxies are multiplied by 1.3 to 6.1 for the virial methods, by 1.2 to 2.0 for the stellar modeling method, by 1.1 to 2.1 for the PNe and CG method, by 1.2 for the X-ray and disk methods and 1.2 to 6.2 for the strong lensing method (except for [60] which is fully weighted out as it employs only galaxies used by more reliable analysis). For this procedure, one must assume that analyses employing the same method and the same galaxies are exactly correlated. This is not true as a particular analysis uses different assumptions, IMF, profiles, etc... Particular analyses also vary in their details and the quality of the data differs since the results have been published over a 30 years range. Hence, our correction is conservative, yielding overestimated uncertainties. This is partly alleviated by fitting $d(M/L)/d(R_{min}/R_{max})$ vs radius with a constant and scaling the uncertainties so that $\chi^2/ndf = 1$.

We note that, whilst important, this procedure happens to numerically have a small influence.

- When the results of an analysis are provided for different IMF, we choose the result using a Chabrier IMF because, with the Salpeter one, it is the most commonly used IMF whilst being more recent than Salpeter's.
- With the strong lensing method, $d(M/L)/d(R_{min}/R_{max})$ can be extracted using apparent or mass axis ratios. We preferred using the apparent axis ratio rather than the mass one for several reasons:
 - The mass axis ratio is more model dependent.
 - It is not systematically calculated in the articles, although it can be obtained from other works using the same galaxies. However, its is desirable for consistency to use mass axis ratio obtained using the same model and assumptions as used for the M/L extraction. We remark that, apart for Grillo *et al.* [53], the M/L vs axis ratio correlation is always stronger for mass axis ratio, i.e., $\left| \frac{d(M/L)}{d(R_{min}/R_{max})|_{apparent}} \right| < \left| \frac{d(M/L)}{d(R_{min}/R_{max})|_{mass}} \right|$. It may be because $R_{min}/R_{max}|_{apparent}$ reflects better the intrinsic axis ratio, or it could be a systematic effect of the lensing method since this one does not fully account for ellipticity effects.
- We globally rescale the uncertainties so that for $d(M/L)/d(R_{min}/R_{max})$ vs radius, $\chi^2/ndf = 1$. (We use a one-parameter fit, viz $d(M/L)/d(R_{min}/R_{max})$ is assumed to be independent of radius.) Forcing $\chi^2/ndf = 1$ is justified since many different methods were used to obtain the M/L with either uncorrelated systematic uncertainties, or, for M/L using the same extraction method, we accounted for the correlation of the results.

Fig. 49 displays the slopes $d(M/L)/d(R_{min}/R_{max})$. For clarity, they are shown vs the approximate average value of the radius at which a M/L is extracted. The average slope $d(M/L)/d(R_{min}/R_{max})$ before the projection correction describe in Section 10.2 is:

$$\begin{aligned} \langle d(M/L)/d(R_{min}/R_{max}) \rangle &= -9.16 \pm 1.75, \text{ and} \\ \langle d(M/L)/d(R_{min}/R_{max}) \rangle &= -17.42 \pm 4.30 \text{ after correction}^{11}. \end{aligned}$$

Note: accounting for the reliability of the methods and for correlations between the various results is methodologically important but this happens to not change significantly the results. Without it, $\langle d(M/L)/d(R_{min}/R_{max}) \rangle = -8.52 \pm 0.84$ before projection correction, to be compared to -9.16 ± 1.75 with it.

¹¹The result is not approximately 5 \pm 1 times larger, as was obtained in Section 10.2, since the additional uncertainty from the projection correction is proportional to the slope. Thus, the contribution to points near $\langle d(M/L)/d(R_{min}/R_{max}) \rangle \sim 0$ is smaller and their relative weight in the averaging procedure increases.

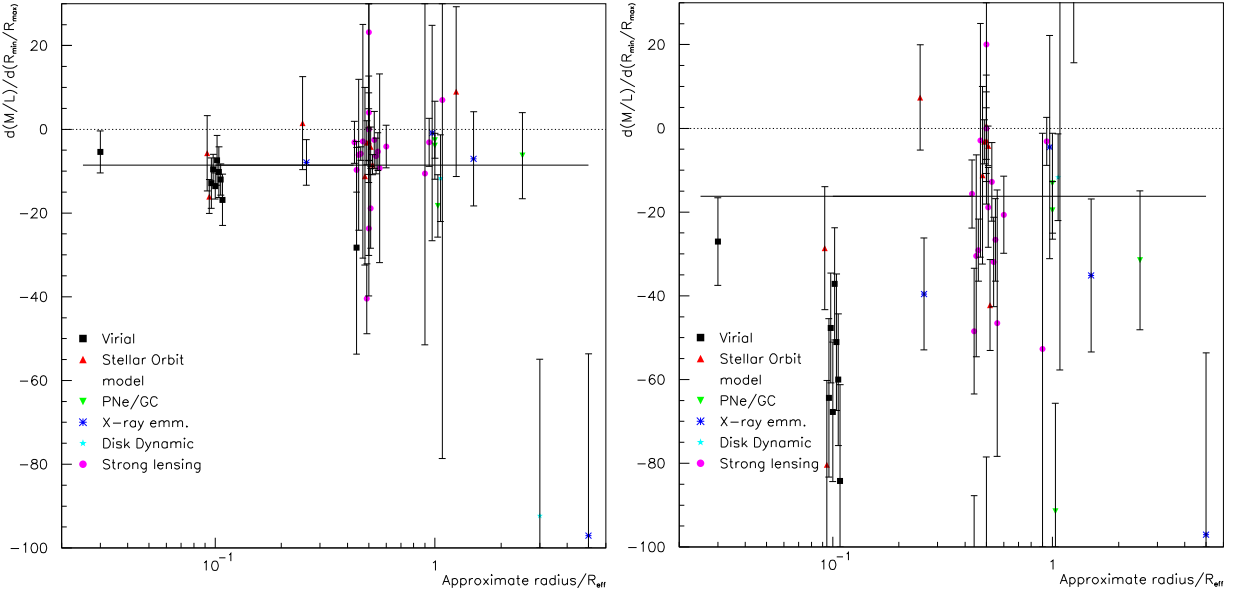


Figure 49: The $d(M/L)/d(R_{min}/R_{max})$ slopes vs the approximate radius values (normalized by their R_{eff}) where the M/L are obtained. Different symbols are for the different methods used to extract the M/L . The plain line shows the average value of $d(M/L)/d(R_{min}/R_{max})$ after accounting for the reliability of each M/L extraction and the shared statistics (the error bars shown do not account for this. They are the values quoted in sections 4 to 9). The left plot is before applying projection correction (see Section 10.2) unless it is directly provided in the original publication. The right plot is after projection correction, plotted on the same scale (consequently, some of the points are now off the graph). We added small offsets on the radius to enhance visual clarity.

These results assume that M/L is constant with radius r .

Fig. 49 reveals that combined results from different methods have systematic shifts, especially between the virial and the strong lensing combined results. This could come from the fact that different methods estimate M/L at typically different radius values: in fact, it has been reported that at smaller radii, the baryonic mass dominates over the dark one [9, 16, 67, 74, 78, 79, 97, 104]. In other words, the M/L values increase with radius. In our analysis however, all values $M/L(R_{min}/R_{max} = 0.7)$ are normalized to $8M_{\odot}/L_{\odot}$, which effectively removes the dependence on which particular radius value is used to obtain M/L . However, this introduces an artificial radius dependence of $d(M/L)/d(R_{min}/R_{max})$ since this one scales with the factor used to normalize M/L to $8M_{\odot}/L_{\odot}$, that factor itself depending by definition on the value of the extraction radius. This artificial dependence is opposite to the actual dependence of M/L with radius, i.e. $d(M/L)/d(R_{min}/R_{max})$ decreases with r , see Fig. 49. To fix this issue, we use a normalization derived from the results of Ref. [16],

$$M/L(R_{min}/R_{max,app} = 0.6) = (6 + 1.7r/R_{eff})M_{\odot}/L_{\odot}, \quad (2)$$

to include the r -dependence of M/L . Fig. 50 displays $d(M/L)/d(R_{min}/R_{max})$ obtained with Eq. (2) normalization. Compared to Figs. 49, the r -dependence of $d(M/L)/d(R_{min}/R_{max})$ in Fig. 50 has decreased. To completely cancel it, a factor of 3 to 4 (rather than 1.7 in Eq. 2) would be needed. As this larger factor remains compatible with the dependence derived from Ref. [16]’s data, the r -dependence seen in Fig. 49 may originate fully from the r -dependence of M/L . Nevertheless, other effects could contribute to the systematic differences noticed in Fig. 49. For example, the less stringent selection applied to the distant galaxies used with the strong lensing method could result in a contamination that reduces the correlation. Furthermore, the M/L extracted with the strong lensing method have no ellipticity correction since the method is less sensitive to R_{min}/R_{max} . Actually, we remark that if $d(M/L)/d(R_{min}/R_{max, mass})$ is used instead of $d(M/L)/d(R_{min}/R_{max, app})$, the ellipticity-corrected virial results and the strong lensing one would agree.

13.1 Results

Fig. 50 shows that the averaged $\frac{d(M/L)}{d(R_{min}/R_{max})}$ obtained using the six different methods are all negative and average to $\left\langle \frac{d(M/L)}{d(R_{min}/R_{max})} \right\rangle = (-14.53 \pm 3.79)M_{\odot}/L_{\odot}$. The uncertainty stemming from the r -dependence of the normalization is conservatively estimated from the difference between the two results obtained with the

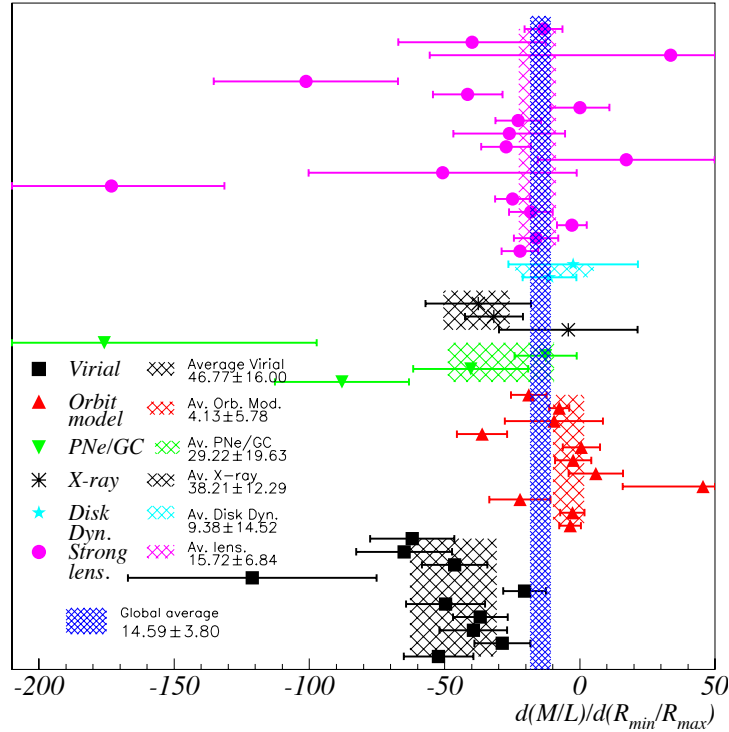


Figure 50: Same as Fig. 49, but with the radius dependence of M/L corrected using Eq. (2)

r -dependent normalization and with the constant one. With this additional uncertainty accounted for, the final result of the analysis is

$$\left\langle \frac{d(M/L)}{d(R_{min}/R_{max})} \right\rangle = (-14.53 \pm 4.77) M_{\odot}/L_{\odot}. \quad (3)$$

This signals a statistically meaningful correlation between M/L and R_{min}/R_{max} . The slope (3) is proportional to the normalization $M/L(r = R_{eff}, R_{min}/R_{max} = 0.7) = 7.7 M_{\odot}/L_{\odot}$, see Eq. 2. The slope (3) is large compared to $7.7 M_{\odot}/L_{\odot}$. We remark that if the galaxy selection criteria had not been applied, the correlation would vanish, diluted by large fluctuations. This may account for the fact that the correlation had not been identified earlier. The analyses of Ref [19, 20] e.g. did not find evidence of this correlation. However, whilst they analyzed a large galaxy sample (260 galaxies), only $\sim 10\%$ of those galaxies are bona-fide elliptical galaxies, and $\sim 80\%$ are lenticular or spiral galaxies. Similarly, we checked using the data [3] that when selection is not applied, the correlation vanishes.

14 Summary and conclusion

We investigated the possibility of a correlation between the dark matter content of elliptical galaxies and their ellipticity. Elliptical galaxies can differ importantly from each other, and peculiarities might bias the estimation of the dark mass, causing systematic and random variations. Therefore, it was important to select a large and homogeneous sample of galaxies. Effects of the peculiarities are then minimized by the homogeneity and suppressed statistically. Furthermore, since the value of M/L depends on the galactic radius r at which the ratio is extracted, as well as on the wavelength at which the galaxy luminosity L is calculated (typically the B-band, but not always), it was necessary to normalize the M/L at a given r to a unique value. We chose $r = 0.7 R_{eff}$ and there, used the typical value $8 M_{\odot}/L_{\odot} = M/L(0.7 R_{eff})$. With this normalization, we found a clear correlation: $\langle d(M/L)/d(R_{min}/R_{max}) \rangle = -14.53 \pm 4.77 M_{\odot}/L_{\odot}$. The dark matter information is obtained from six different approaches (virial theorem, stellar orbit modeling, orbits of planetary nebulae and globular clusters, embedded disk dynamics, hydrostatic equilibrium, and strong lensing) to minimize methodological bias. Possible effects of measurement or observation biases were studied thoroughly. Furthermore, we repeated the same analysis on the stellar M_*/L , see appendix B, and no significant correlation with ellipticity was found, as it should be. This suggests that our procedure is free of significant biases. Possible conclusions are either that:

1. There is a surprisingly strong influence of the dark matter halo on a galaxy shape, possibly from the halo shape as suggested by the stronger correlation generally seen when investigated with mass axis ratio rather

than apparent (project luminous) axis ratio. This would allow us to experimentally address the question of the shape of the dark halo and be critical to understand galaxy formation.

2. The dynamical evidences from which the dark matter content of galaxy is inferred are misinterpreted. In fact, the impulse for the present study originated from a prediction from Ref. [31] (see also Refs. [33, 36]). In this framework, if a homogenous system is locally dense enough so that in that location, the non-linearity of General Relativity are non negligible, this system should display a correlation between its dynamical total mass analyzed using Newton's law of gravity (in our case, the galaxy dark mass) and its asymmetry (in our case, the galaxy ellipticity). Beside the present correlation, this effect also explains [35] the correlation between dynamical and baryonic matter accelerations observed in Ref. [76]. Finally, it provides an explanation for the origin of dark energy: it emerges from the Universe inhomogeneities and anisotropies [34].
3. There is a significant bias in the data and/or methods, in which case they cannot be trusted to estimate accurately the dark matter content of elliptical galaxies. However, our thorough investigation of the various inter-dependences of the variables characterizing an elliptical galaxy reasonably suggests that this correlation is physical rather than a methodological, observational or measurement bias.

Finally, a practical use of the correlation is that once the total galactic mass is known the true ellipticity of the galaxy can be directly deduced.

Acknowledgment This research has made use of the NASA/IPAC Extragalactic Database (NED) which is operated by the Jet Propulsion Laboratory, California Institute of Technology, under contract with the National Aeronautics and Space Administration.

References

- [1] M. W. Auger *et al.* ApJ 705 1099 (2009)
- [2] M. W. Auger *et al.* ApJ 724 511 (2010)
- [3] R. Bacon, G. Monnet and F. Simien, A A 152 315 (1985)
- [4] M. Barnabe *et al.* MNRAS 399 21 (2009)
- [5] M. Barnabe *et al.* MNRAS 415 2215 (2011)
- [6] R. Bender *et al.* AA 217 35 (1989)
- [7] G. Bertin *et al.* AA 292 381 (1994); R. P. Saglia *et al.* ApJ 403 567 (1993)
- [8] F. Bertola *et al.* ApJ 373 369 (1991)
- [9] F. Bertola, A. Pizzella, M. Persic and P. Salucci. ApJ 416 45 (1993)
- [10] B. Binggeli, Proc. ESO/OHP Workshop on Dwarf Galaxies, ed. G. Meylan, & Ph. Prugniel, 13 (1994)
- [11] See. e.g. J. Binney and S. Tremaine, Galactic Dynamics. Princeton University Press; (2008)
- [12] A. S Bolton *et al.* ApJ. 682 964 (2008)
- [13] F. Brighenti, W. Mathews ApJ 486 L83 (1997)
- [14] G. Bruzual and S. Charlot MNRAS 344, 1000 (2003)
- [15] Calvi R., Poggianti B. M, Fasano G., Vulcani B., MNRAS 419, L14 (2012)
- [16] M. Capaccioli, N. R. Napolitano and M. Arnaboldi, astro-ph/0211323 (1992)
- [17] M. Cappellari *et al.* MNRAS 366 1126 (2006)
- [18] M. Cappellari *et al.* ApJ 704 L34 (2009)
- [19] M. Cappellari *et al.*, MNRAS, 432, 1709 (2013)

- [20] M. Cappellari et al., MNRAS, 432, 1862 (2013)
- [21] V. F. Cardone, C. Tortora, R. Molinaro and V. Salzano AA 504 769 (2009)
- [22] V. F. Cardone, A. Del Popolo, C. Tortora, and N.R. Napolitano MNRAS 416 1822 (2011)
- [23] C. M. Carollo and I. J. Danziger MNRAS 270 523 (1994); MNRAS 270 743 (1994)
- [24] C. M. Carollo *et al.* ApJ 441 25 (1995)
- [25] G. Chabrier PASP 115 763 (2003)
- [26] K. H. Chae, S. Mao and P. Augusto MNRAS 326 1012 (2001)
- [27] L. Coccato *et al.* MNRAS 394 1249 (2009)
- [28] C. Conroy and P. G. van Dokkum ApJ 760 71 (2012)
- [29] P. Das *et al.* MNRAS 402 1362 (2010)
- [30] A. J. Deason *et al.*, ApJ 748 2 (2012)
- [31] A. Deur, Phys. Lett. B **676**, 21 (2009)
- [32] A. Deur, MNRAS **438**, 2, 1535 (2014)
- [33] A. Deur A, Eur. Phys. J. C **77**, 412 (2017)
- [34] A. Deur, Eur. Phys. J. C **79**, 883 (2019)
- [35] A. Deur, C. Sargent and B. Terzic, ApJ 896, 2 94 (2020)
- [36] A. Deur, [arXiv:2004.05905 [astro-ph.GA]].
- [37] S. Djorgovski and M. Davis, ApJ 313 59 (1987)
- [38] A. Dressler, *et al.* ApJ 313 43 (1987)
- [39] G. de Vaucouleur, Annales d’Astrophysique 11 247 (1948)
- [40] S. di Serego Alighieri *et al.* AA 442, 125 (2005)
- [41] S. M. Faber and R. E. Jackson, ApJ 204 668 (1976)
- [42] C. D. Fassnacht and J.G. Cohen, ApJ 115 377 (1998)
- [43] C. Faure *et al.* ApJ 176 19 (2008)
- [44] C. Faure *et al.* AA 529 A72 (2011)
- [45] H. C. Ferguson *et al.* ApJ 600 L107 (2004); I. Trujillo *et al.* ApJ 604 521 (2004); A. W. Zirm *et al.* ApJ 656 66 (2007); A. Cimatti AA 482 21 (2008); I. Damjanov *et al.* Ap.J 695 101 (2009).
- [46] I. Ferreras, P. Saha and L. R. Williams ApJ 623 5 (2005)
- [47] I. Ferreras, P. Saha and S. Burles MNRAS 383 857 (2008)
- [48] C. Foster *et al.* NMRAS 415 3393 (2011)
- [49] Y. Fukazawa *et al.* ApJ 636 698 (2006)
- [50] R. Gavazzi *et al.* arXiv:1202.3852 (2012)
- [51] K. Gebhardt *et al.* ApJ 583 92 (2003)
- [52] C. Grillo *et al.* AA 477 25 (2008)
- [53] C. Grillo *et al.* AA 501 461 (2009)
- [54] L. Hernquist, ApJ 356 359 (1990)

- [55] B. P. Holden *et al.* ApJ, 620 83 (2005)
- [56] P. J. Humphrey *et al.* Proceedings of “The X-ray universe 2005”, A. Wilson Ed. (2005)
- [57] P. J. Humphrey *et al.* ApJ 646 899 (2006)
- [58] N. Jackson *et al.* AA 334 33 (1998)
- [59] G. Jiang and C. S. Kochanek ApJ 671 1568 (2007)
- [60] C. R. Keeton, C. S. Kochanek and E. E. Falco ApJ 509 561 (1998)
- [61] D. D. Kelson *et al.* ApJ 531 184 (2000)
- [62] L. J. King *et al.* MNRAS 295 41 (1998)
- [63] E. Komatsu *et al.*, Astrophys. J. Suppl. **192** 18 (2011)
- [64] L. V. E. Koopmans *et al.* MNRAS 303 727 (1999)
- [65] L. V. E. Koopmans *et al.* ApJ 649 599 (2006)
- [66] J. Kormendy, ApJ 218 333 (1977)
- [67] A. Kronawitter *et al.* AA 144 53 (2000)
- [68] P. Kroupa, C. A. Tout and G. Gilmore MNRAS 262 545 (1993)
- [69] T. R. Lauer ApJ **292** 104 (1985)
- [70] J. Lehar *et al.* ApJ 536 584 (2000)
- [71] D. Leier MNRAS 400 875 (2009)
- [72] D. Leier *et al.* ApJ 740 97 (2011)
- [73] J. Magorrian *et al.* ApJ 115 2285 (1998)
- [74] J. Magorrian and D. Ballantyne MNRAS 322 702 (2001)
- [75] C. Maraston MNRAS 362 799 (2005)
- [76] S. S. McGaugh, F. Lelli, and J. M. Schombert, Phys. Rev. Lett., 117, 201101 (2016)
- [77] A. More *et al.* ApJ 734 69 (2011)
- [78] R. Nagino and K. Matsushita AA 501 157 (2009)
- [79] N. R. Napolitano *et al.* MNRAS 357 691 (2005)
- [80] N. R. Napolitano *et al.* MNRAS **393** 329 (2009)
- [81] J. F. Navarro, C. S. Frenk and S. D. M. White ApJ 463 563 (1996)
- [82] E. O’sullivan, A. J. R. Sanderson and T. J. Ponman MNRAS 380 4 1409 (2007)
- [83] A. Pizzella *et al.* AA 323 349 (1997)
- [84] Ph. Prugniel and F. Simien AA 309 749 (1996)
- [85] R. N. Proctor *et al.* MNRAS 398 91 (2009)
- [86] A. Rettura *et al.* AA 458, 717 (2006)
- [87] A. J. Romanowsky *et al.* Science 301 1696 (2003)
- [88] A. Ruff *et al.* ApJ 727 96 (2011)
- [89] E. E. Salpeter ApJ 121 161 (1955)
- [90] R. P. Saglia, G Bertin and M. Stiavelli ApJ 384 433 (1992)

- [91] R. P. Saglia *et al.* ApJ 403 567 (1993)
- [92] M. Schwarzschild ApJ 232 236 (1979)
- [93] J. L. Sersic BAAA 6 41 (1963)
- [94] See. e.g. L. S. Sparke & J. S. Gallagher, Galaxies in the Universe. Cambridge University Press (2007)
- [95] T. S. Statler *et al.* AA 121 244 (2001)
- [96] S. H. Suyu *et al.* ApJ 750 10 (2012)
- [97] J. Thomas *et al.* MNRAS 282 657 (2007); MNRAS 415 545 (2011)
- [98] T. Treu and L.V.E. Koopmans, ApJ 611 739 (2004)
- [99] T. Treu *et al.* ApJ 690 670 (2009)
- [100] G. Trinchieri, G. Fabbiano, D.-W Kim AA 318 361 (1997)
- [101] R. B. Tully and J. R. Fisher AA 54 661 (1977)
- [102] A. van der Wel *et al.* ApJ 631 145 (2005)
- [103] G. van de Ven, P. G. van Dokkum and M. Franx MNRAS 344 924 (2003)
- [104] R. P. van der Marel MNRAS 253 710 (1991)
- [105] R. P. van der Marel and P. G. van Dokkum ApJ 668 738 (2007)
- [106] R. P. van der Marel and P. G. van Dokkum ApJ 668 756 (2007)
- [107] P. G. van Dokkum and S. A. Stanford ApJ 585 78 (2003)
- [108] G. A. Wegner *et al.* ApJ 144 3 (2012)
- [109] COSMOS ApJ Supplement Series 172 (2007)
- [110] <http://nedwww.ipac.caltech.edu/>
- [111] http://nedwww.ipac.caltech.edu/level5/Arp/Arp_contents.html
- [112] In Fukazawa *et al.* [49] galaxies are grouped into 3 classes: EXG (bright X-ray) CXG (faint X-ray) and VCXG (very faint X-ray) galaxies. VCXG galaxies show signs of disturbed hydrostatic equilibrium and the hot EXG gas property merges with the extragalactic gas of the group/cluster, indicating influence from the environment. Likewise, the galaxies in Nagino and Matsushita [78] are classified in two groups: one consisting of galaxies with their ISM temperature profile constant or decreasing with growing radius (XC group), and the other group made of galaxies of increasing temperature profile (XE group). They surmise that the ISM of the XE galaxies is influenced by the group/cluster hot gas. (Similar conclusions are obtained in by Fukazawa *et al.* [49].) The second group corresponds to the large massive EXG galaxies in [49] (although there is no perfect 1 to 1 correspondence). For the same reason as for cD or BrClG galaxies, we exclude EXG and XE galaxies from our analysis.
- [113] Without such selection criteria, the best linear fit of the [3] data, as discussed in Fig. 67, to the full data set has no significant slope: 1.9 ± 1.4 . This is understood as coming from the additional jitter caused by the wider characteristics of the galaxies and by systematic biases. For example, a systematic bias stems from galaxies now known to be disc galaxies. The M/L of those mis-identified galaxies is wrong because the virial method does not apply. Their M/L is generally very small, e.g. 3.6 for the SA0 galaxy NGC6909, but their apparent R_{min}/R_{max} is likely to be small e.g. 0.5 for NGC6909. Thus, these disc galaxies introduce an unphysical bias to the correlation and should be excluded.

A Other data

Other works studying the dark matter content for several elliptical galaxies can be found in the literature. We list them here, in alphabetical order, for completeness and state why they were not used in the present analysis:

- Bertin *et al.* (1994) and Saglia *et al.* (1993). The two articles are from the same group and use the same method. We may thus combine the two data sets without introducing a systematic bias. The authors estimate M/L using two models to fit stellar dynamics (model 2C: 2 components method and model QP: quadratic programming method) for 9 elliptical and lenticular galaxies. Applying our usual selection criteria and relying on NED for the galaxy type and R_{min}/R_{max} , only 2 suitable elliptical galaxies remain after rejecting E+/cD, S0, SA0 galaxies and NGC7144 since no realistic modeling for this galaxy was achieved. The two remaining galaxies are E0, with too little lever arm to obtain a meaningful M/L vs ellipticity relation. If we keep in addition the 3 cD galaxies, the fits to the M/L vs ellipticity indicate a correlation, see Fig. 51. The best fit result for the 2C method gives $M/L = (-12.6 \pm 10.2)R_{min}/R_{max} + (16.0 \pm 9.0)$. The best fit result for the QP method gives $M/L = (-23.7 \pm 12.1)R_{min}/R_{max} + (25.1 \pm 10.8)$. The respective χ^2/ndf are 1.5 and 4.6. This data set has a number of caveats: the data are dated (1994). The M/L are not estimated at the same relative radius (they are estimated at R around R_{eff} , with $0.8R_{eff} < R < 2.1R_{eff}$). No uncertainties are provided. We assumed 25% point-to-point uncertainty as this seems to be typical for such study. This leads to 2C and QP results that are compatible with each others, which indicate that 25% is reasonable. The R_{min}/R_{max} span is small ($0.8 < R_{min}/R_{max} < 0.96$), making the slope extracted from the fits less accurate. Finally, the statistics are limited (5 galaxies), the models assume spherical symmetry -which introduces a M/L vs R_{min}/R_{max} bias- and they also assume no galaxy rotation. The main drawback is that we have cD galaxies in the sample. It explains the strong correlation found: cD galaxies tend to have higher M/L than standard elliptical galaxies and, for this particular sample, the cD galaxies have higher ellipticity. For these reasons, we do not consider these results.

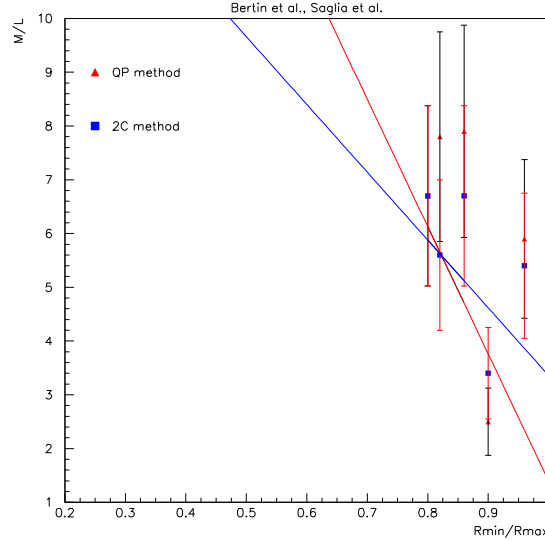


Figure 51: M/L vs R_{min}/R_{max} for the Bertin *et al.* and Saglia *et al.* data sets. The different symbols correspond to the two methods used to model stellar dynamics. The corresponding linear fits are the lines of matching colors.

- Barnabe *et al.* study 6 strong lensing early-type galaxies from the SLACS survey in [4]. This work is superseded by [5] and hence we do not use these results. However, we summarize them briefly: out of the 6 galaxies, we reject one potential giant that has $M_{Ein} > 10^{12}M_{\odot}$ (J0216-0813) and one E/S0 (J0912+0029). The fit to the 4 remaining elliptical galaxies yields $M_{tot}/M_{*} = (-1.12 \pm 0.85)R_{min}/R_{max}|_{true} + (1.14 \pm 0.62)$ and $M_{tot}/M_{*} = (0.11 \pm 0.52)R_{min}/R_{max}|_{mass} + (0.23 \pm 0.41)$.
- Brighenti and Mathews [13] determine the M/L for 3 early-type galaxies. However, only one is an elliptical. The two others are lenticular galaxies and belong to the Arp catalogue.
- Cappellari *et al.* [18] provide M/L ratios for 9 early-type galaxies at large redshift $z \simeq 2$. No detailed information on the early-type structure is available. With our standard $\sigma \geq 225 \text{ km.s}^{-1}$ to minimize S0, we can retain only one galaxy.

- Carollo *et al.* [24] study the dark matter content of 4 elliptical galaxies but provide only the velocity dispersion profile, without giving the total mass or M/L .
- Carollo and Danziger study 5 elliptical galaxies in [23]. Among them, 3 are SAB, one a SA0 or SApec and one is a cD, leaving only one suitable galaxy.
- Coccato *et al.* [27] study PNe as tracers for 6 galaxies and add 10 others from the literature. However, only their rotation curves are provided, without total mass or M/L .
- Conroy and van Dokkum [28] construct M/L for 38 early type galaxies. However just a few galaxies pass our selection criteria. Furthermore, only the stellar M/L is provided.
- Das *et al.* [29] extract mass distributions, circular velocity curves and DMf from the deprojected density and temperature profiles of the hot gas surrounding 6 X-ray bright elliptical galaxies. These extracted quantities are given from the galaxy center to a few R_{eff} ($2.5 R_{eff}$ for NGC4472 to $9 R_{eff}$ for NGC 1407). The DMf is extracted using the stellar M_*/L ratio from various references. However, no galaxy passes our standard selection and we thus cannot use these data.
- Fassnacht and Cohen [42] analyze 3 strong lenses from the CLASS survey (B0712+472, B1030+074 and B1600+434). However, the lens velocity dispersions are below our standard $\sigma < 225 \text{ km.s}^{-1}$ criterion, two of them well below. Furthermore B1600+434 is significantly affected by its environment. Hence, the 3 galaxies are not suitable for our study
- Gebhardt *et al.* [51] provide M/L for 12 early-type galaxies. M/L is obtained for the central region ($r < 1/4 R_{eff}$) where stars and central black holes dominate the gravitational potential. Consequently, the model used to infer M/L does not include a dark matter halo and assume instead that the total mass follows light, i.e, M/L is independent of the galaxy radius. This assumption, ruled out by many recent studies, remains reasonable in the radius range studied in [51]. After removing the S0, LINERS, AGN, galaxies for which M/L correlates with the central black hole mass, and Arp galaxies, we are left with only 2 adequate galaxies. Given all these limitations, we did not analyze these data.
- The data from Grillo *et al.* [52] are not used for two reasons: 1) Grillo *et al.* model only stellar masses and use the lensing masses from [65]. Since the stellar masses from [52] and [65] agree well, the M_{tot}/M_* will be similar to those obtained in [65]. 2) The same group has done a more recent study (Grillo *et al.* [53]) in which they consider more galaxies and compute both the lensing and stellar masses. This latter work supersedes the earlier results [52].
- Holden *et al.* [55] study 4 strong lenses. They belong to a cluster and may be subject to interaction with their environment. In addition two of the lenses are giant elliptical galaxies and a third one has a velocity dispersion of 130 km.s^{-1} , below our standard $\sigma < 225 \text{ km.s}^{-1}$ criterion. We are then left with only one suitable galaxy.
- The two studies from Humphrey *et al.* [56], [57] employ the same set of 7 early-type galaxies with X-ray data from *Chandra*. After rejecting galaxies that are peculiar, belonging to the Arp catalog, or being S0/Sy, LINER/Sy, 3 galaxies remain, one of them a LINER. The sample is then too small for a useful study.
- In the work of More *et al.* [77], 5 strong lensing candidates are analyzed. Out of the 5, one has a S0-like morphology, one is a spiral lens candidate, one might not be a true lens and one yielded inconsistent results, leaving only one potential elliptical candidate.
- Napolitano *et al.* [79] compile values of M/L for 21 early-type galaxies in order to study the M/L dependence with radius. At small and large radii (typically $R_{in} \sim R_{eff}/2$ and several R_{eff} , respectively), M/L is determined using PNe or GC kinematics. M/L is obtained either by fitting modeled orbital distributions to the line of sight velocity distribution or by fitting the velocity distribution profiles using Jeans or similar models. After standard selection insuring undisturbed galaxies we retain only 2 galaxies: NGC821 and 2434. This, with the fact that the data is a compilation of the literature (implying inhomogeneities in the M/L extraction) already used in this article, makes us to not use the results reported in [79].
- Proctor *et al.* [85] analyze data for 5 galaxies. However, only 2 are adequate elliptical galaxies (E0 and E1-2), with an additional E6?. The authors provide rotation curves but no M/L ratios.
- O’Sullivan, Sanderson and Ponman [82] determine M/L for 3 early-type galaxies. However, only one is an elliptical galaxy, the two others being E+ and S0 galaxies.

- Saglia, Bertin and Stiavelli [90] interpret with their model the photometry and kinematic profiles of 10 galaxies to extract M/L . However, after removing the NELG, cD, E+, peculiar, Seyfert, LERG, NLRG, S0 galaxies and the ones belonging to the Arp catalogue, we are left with only two galaxies, one of them a LINER. This sample is too small for a meaningful study.
- Saglia *et al.* [91] investigate the presence of dark matter for 3 galaxies. One of them is a RLG, BrClG and LINER and another a E2/S0, Sy2 LINER galaxy appearing in the Arp catalogue. We are then left with only one suitable galaxy.
- di Serego Alighieri *et al.* [40] compute M/L_B for 20 early-type galaxies from the K20 survey at large redshift $0.88 < z < 1.3$. However, no details are given on the galaxies. We inferred the axis ratios visually and, to minimize S0 and giants contamination, applied our standard $\sigma \geq 225 \text{ km.s}^{-1}$ and $M_{tot} > 5 \times 10^{11} M_\odot$ criteria. Only 3 galaxies pass this selection, one of them for which we could not determine the axis ratio. M/L_B is computed using simply the dynamical mass $M = 5\sigma^2 R_{eff}/G$. Such estimate can be easily done for many local galaxies with well established type and characteristics and there is no value *in our context* to consider an additional few galaxies of uncertain characteristics.
- Trinchieri, Fabbiano and Kim [100] use X-ray data to extract the temperature distribution of the hot gas in 5 early-type galaxies. From it they obtain their M/L . However, after removing the cD, peculiar, S0 galaxies and one belonging to the Arp catalogue, we are left with only one suitable galaxy.
- van Dokkum and Stanford [107] compute M/L for 3 early-type galaxies at large redshift $z = 1.27$. They belong to the RDCS J0848+4453 cluster. However, the galaxies' characteristics are unknown but may be giants, unsuitable in our context. M/L_B is simply computed as $M \propto \sigma^2 R_{eff}$. Such estimate can be easily done for many local galaxies with well established type and characteristics. Considering an additional few galaxies with uncertain characteristics would not add to our study.

B Correlation between stellar M_*/L and axis ratio

Since no strong correlation between the stellar M_*/L ratio and the axis ratio is expected, studying M_*/L vs R_{min}/R_{max} should provide a stringent test of our procedure. Among all the data sets considered in this article, 13 of them provide M_*/L . Here, we describe these sets and the M_*/L vs R_{min}/R_{max} correlations derived from them.

B.1 data sets

For all the analyses below except that of Section B.1.3, the uncertainty were taken to be proportional to the M_*/L values and scaled according to the *unbiased estimate*. Since the determination of M_*/L depends on modeling the stellar populations rather than being based on dynamical arguments as for M/L , we do not apply ellipticity corrections to the data (this concerns only the 2 PNe/GC data sets, the other sets had no corrections in the first place). We also do not correct for a possible radius dependence of M_*/L (see Section 13) because the radius at which the M_*/L are extracted is usually unspecified (if so we assign a value of $r \sim R_{eff}$, for plotting purpose only). Finally, since the object of the selection criteria is to insure the reliability of the dynamical determination of M/L , these criteria become irrelevant to for M_*/L . However, since the goal of the M_*/L vs R_{min}/R_{max} analysis is to test our primary M/L analysis, we use the same analysis procedure, including applying the selection criteria.

B.1.1 Capaccioli *et al.*

The data set is described in Section 6.1. M_*/L vs $R_{min}/R_{max}|_{light,true}$ is shown in Fig. 52. The best fit yields: $M_*/L = (-14.80 \pm 9.99)R_{min}/R_{max}|_{light,true} + (17.83 \pm 8.4)$

As discussed in Section 6.1, the data were assigned to the reliability group 3. In addition, the M_*/L is obtained

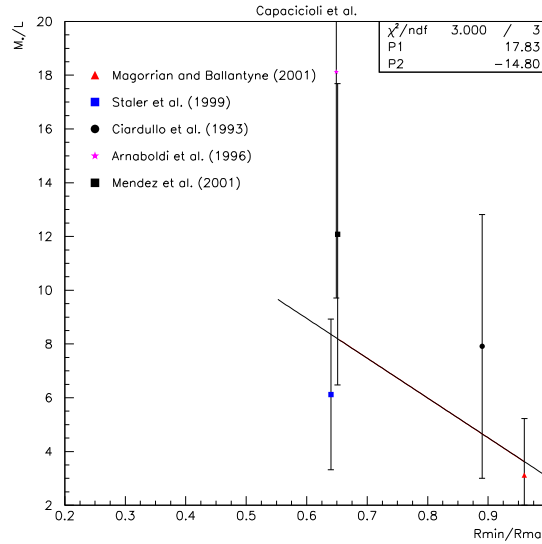


Figure 52: Stellar M_*/L vs the luminous axis ratio R_{min}/R_{max} for the Capaccioli *et al.* data set [16].

by assuming it to be equal to the calculated central M/L . Consequently, we assign the result to group 4 reliability.

B.1.2 Cappellari *et al.* SAURON project (2006)

The data and the M_*/L vs axis ratio analysis are described in Section 5.1. The fit for the stellar population yields $M_*/L = (-0.02 \pm 1.72)R_{min}/R_{max}|_{true} + (2.39 \pm 1.16)$.

The analysis is assigned to group 1 reliability.

B.1.3 Cappellari *et al.* ATLAS project (2013).

The data are described in Section 5.2. The M_*/L data are from [19]. The best fit for the stellar population yields $M/L_* = (-7.17 \pm 1.79)R_{min}/R_{max}|_{true} + (8.30 \pm 1.45)$.

The large slope is mostly driven by one single point (NGC 4489), with especially low M_*/L , which implies a low uncertainty $\Delta M_*/L$. Removing NGC4489 would yield a much smaller slope: $M/L_* = (-3.21 \pm 2.21)R_{min}/R_{max}|_{true} + (5.71 \pm 1.69)$, but we see no reason to remove it. To avoid the fit to be driven by the low $\Delta M_*/L$ of NGC 4489, we set the uncertainties to be constant rather than proportional to M_*/L . The resulting fit gives:

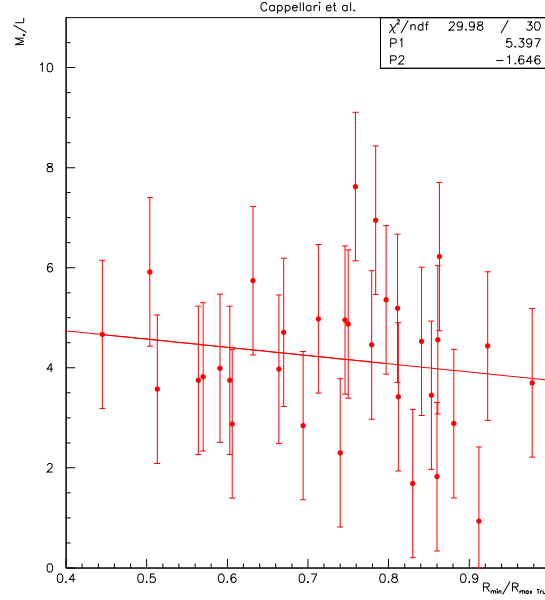


Figure 53: Stellar M_*/L vs true axis ratio R_{min}/R_{max} for the Cappellari *et al.* 2013 data set [19].

$M_*/L_* = (-1.65 \pm 1.96)R_{min}/R_{max}|_{true} + (5.40 \pm 1.47)$,
see Fig. 53. The analysis is assigned to group 1 reliability.

B.1.4 Thomas *et al.* (2007, 2011) and Wegner *et al.* (2012)

The data are discussed in Section 5.5, including the stellar M_*/L ratios. It was found that:

$$M_*/L_{Krou} = (+2.35 \pm 1.75)R_{min}/R_{max}|_{apparent} + (2.01 \pm 1.37),$$

$$M_*/L_{Sal} = (+2.87 \pm 3.82)R_{min}/R_{max}|_{apparent} + (3.69 \pm 2.92).$$

The Kroupa IMF results will be used for the global analysis. We assign the result to group 1 reliability.

B.1.5 Conroy and van Dokkum

These data, discussed in Section A, were not used in the main analysis because only stellar M_*/L are provided. We show M_*/L for different bands in Fig. 54. The best fits for the different data are:

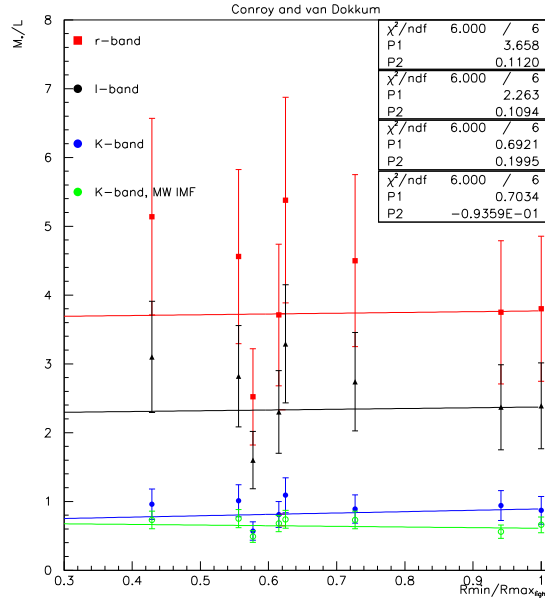


Figure 54: Stellar M_*/L vs axis ratio R_{min}/R_{max} for the Conroy and van Dokkum data set [28]. The different symbols correspond to different bands or IMF.

$$M_*/L_* = (+0.11 \pm 2.12)R_{min}/R_{max}|_{true} + (3.66 \pm 1.50) \text{ for the r-band (with varying IMF).}$$

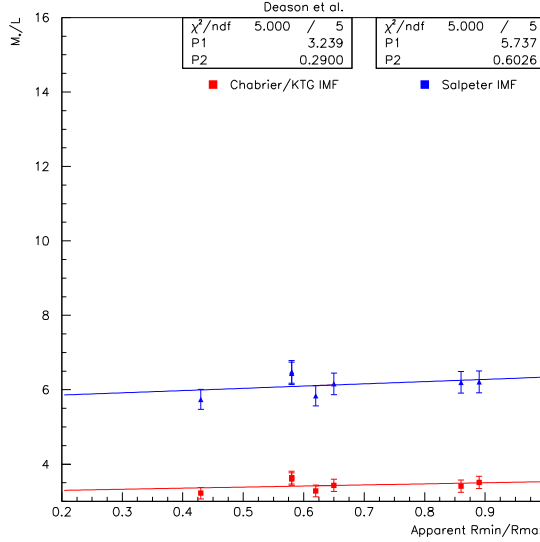


Figure 55: Stellar M_*/L vs apparent axis ratio R_{min}/R_{max} for the Deason *et al.* data set [30].

$M/L_* = (+0.11 \pm 1.24) R_{min}/R_{max}|_{true} + (2.26 \pm 0.88)$ for the I-band (with varying IMF).

$M/L_* = (+0.20 \pm 0.40) R_{min}/R_{max}|_{true} + (0.69 \pm 0.28)$ for the K-band (with varying IMF).

$M/L_* = (-0.09 \pm 0.22) R_{min}/R_{max}|_{true} + (0.70 \pm 0.15)$ for the K-band (with a Milky Way (Kroupa 2001) IMF).

All the fits indicate no ellipticity dependence. We will use the I-band results when combining with the other publications data. The analysis is assigned to group 1 reliability.

B.1.6 Deason *et al.*

The data set is described in Section 6.2. We form $M_*/L = M/L \times (1 - f_{dm})$. its correlation with $R_{min}/R_{max}|_{light}$ is shown in Fig. 55. The best fit for the results derived with a Chabrier IMF yields:

$$M_*/L = (+0.29 \pm 0.41) R_{min}/R_{max}|_{apparent} + (3.24 \pm 0.28)$$

and, for results derived with a Salpeter IMF:

$$M_*/L = (+0.60 \pm 0.71) R_{min}/R_{max}|_{apparent} + (5.74 \pm 0.48).$$

When forming the global result, we will use Chabrier result and assign it to group 1 reliability.

B.1.7 Auger *et al.*

The data are described in Section 9.1. The stellar mass M_* is given in [2]. The luminosity L is from [12]. Forming M_*/L , we obtain the correlation with $R_{min}/R_{max}|_{light}$ shown in Fig. 56. The best fit yields, for the results derived with a SIE model using a Chabrier IMF:

$$M_*/L = (+0.79 \pm 0.93) R_{min}/R_{max}|_{apparent} + (4.17 \pm 0.73)$$

and, for results derived with a Salpeter IMF:

$$M_*/L = (+0.54 \pm 0.49) R_{min}/R_{max}|_{apparent} + (2.31 \pm 0.39).$$

We assign the Chabrier result, to be used in the global result, to group 1 reliability.

B.1.8 Barnabe *et al.*

The data set is described in Section 9.2. M_*/L vs $R_{min}/R_{max}|_{light,true}$ is shown in Fig. 57. The best fit yields:

$$M_*/L = (-6.56 \pm 4.08) R_{min}/R_{max}|_{light,true} + (10.28 \pm 3.30).$$

We assign the result to group 1 reliability.

B.1.9 Cardone *et al.* (2009)

The Cardone *et al.* (2009) data are described in section 9.3. (We do not use the M_*/L from the Cardone *et al.* (2011) data discussed in Section 9.3 since they are from Auger *et al.*, which are already analyzed.) The M_*/L vs $R_{min}/R_{max}|_{light,true}$ are shown in Fig. 58. The best fit yields:

$$M_*/L = (-0.90 \pm 1.14) R_{min}/R_{max} + (2.85 \pm 0.89).$$

We assign the result to group 1 reliability.

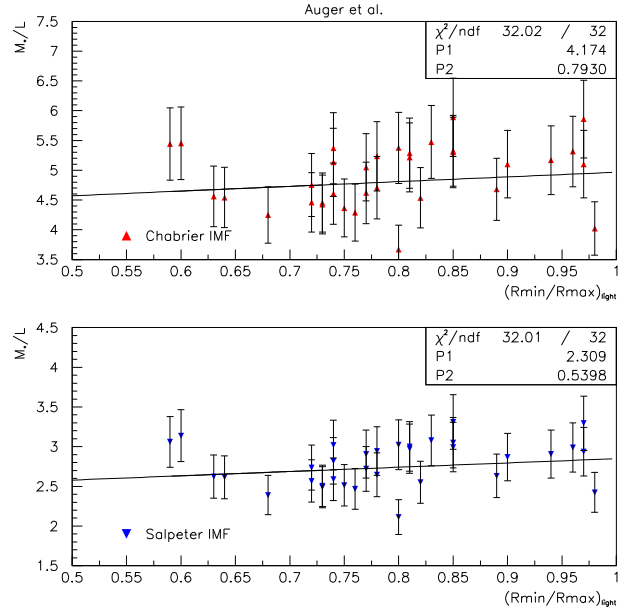


Figure 56: Stellar M_*/L vs apparent axis ratio R_{min}/R_{max} for the Auger *et al.* data set [2]. The top panel is for the mass SIE model using a Chabrier IMF, and the bottom panel is for a Salpeter IMF.

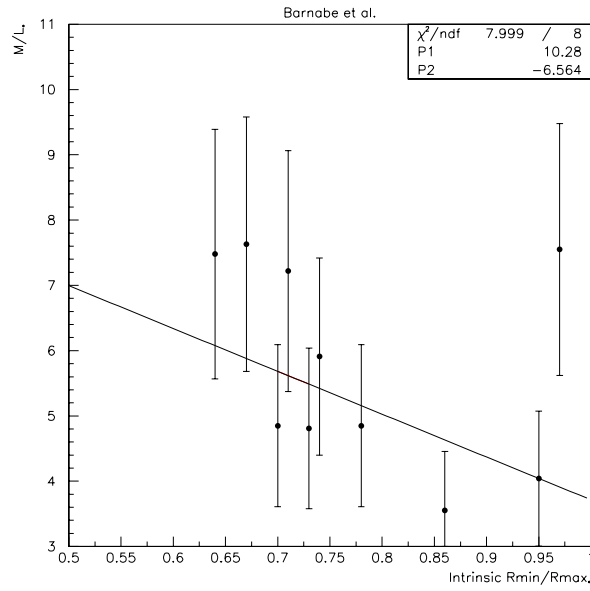


Figure 57: Stellar M_*/L vs the apparent axis ratio R_{min}/R_{max} for the Barnabe *et al.* data set [5].

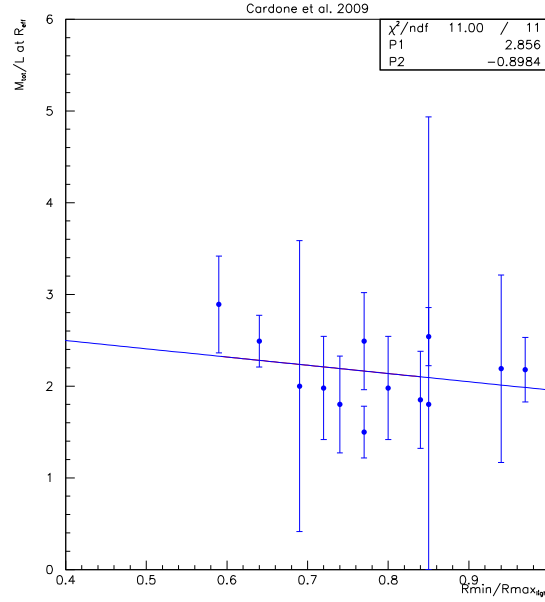


Figure 58: Stellar M_*/L vs the apparent axis ratio R_{min}/R_{max} for the Cardone *et al.* data set [21].

B.1.10 Grillo *et al.*

The Grillo *et al.* data set is described in Section 9.8. The M_*/L vs $R_{min}/R_{max}|_{light}$ are shown in Fig. 59 for various IMF and SMT. The best fit yields:

$M_*/L = (-2.43 \pm 1.55)R_{min}/R_{max}|_{light} + (6.75 \pm 1.25)$ for results using a Salpeter IMF and a Bruzual-Charlot SMT,

$M_*/L = (-2.22 \pm 1.63)R_{min}/R_{max}|_{light} + (5.70 \pm 1.31)$ for results using a Salpeter IMF and a Maraston SMT,

$M_*/L = (-1.77 \pm 0.86)R_{min}/R_{max}|_{light} + (4.12 \pm 0.69)$ for results using a Chabrier IMF and a Bruzual-Charlot SMT,

$M_*/L = (-1.20 \pm 1.13)R_{min}/R_{max}|_{light} + (3.42 \pm 0.90)$ for results using a Kroupa IMF and a Maraston SMT.

As in the main global analysis, we will use the results derived with a Chabrier IMF and a Bruzual-Charlot

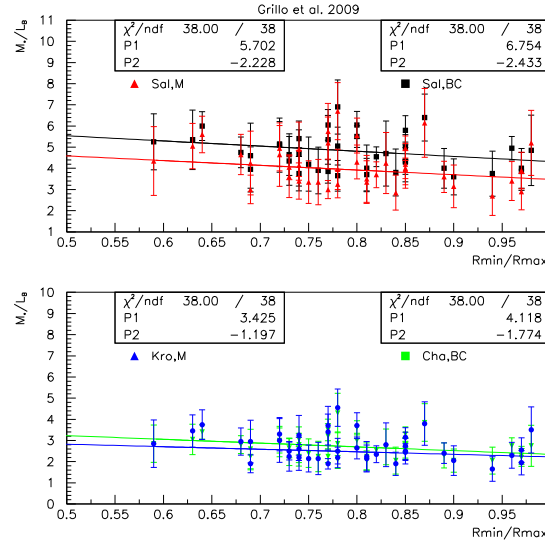


Figure 59: Stellar M_*/L vs the apparent axis ratio R_{min}/R_{max} for the Grillo *et al.* data set [53].

SMT. We assign the result to group 1 reliability.

B.1.11 Jiang and Kochanek

The Jiang and Kochanek data are described in Section 9.10. The M_*/L vs $R_{min}/R_{max}|_{light}$ are shown in Fig. 60. The best fit yields:

$M_*/L = (-0.63 \pm 3.06)R_{min}/R_{max} + (1.74 \pm 2.34)$.

We assign the result to group 3 reliability.

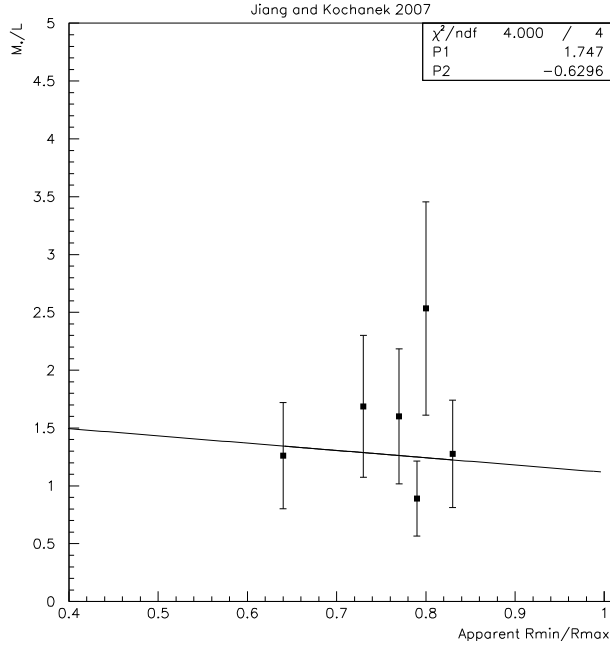


Figure 60: Stellar M_*/L vs the apparent axis ratio R_{min}/R_{max} for the Jiang and Kochanek data set [59].

B.1.12 Leier *et al.* (2011)

The Leier *et al.* data are described in Section 9.14. M_*/L vs $R_{min}/R_{max}|_{light}$ is shown in Fig. 61. The best fit yields: $M_*/L = (-7.02 \pm 4.37)R_{min}/R_{max} + (8.75 \pm 3.42)$.

We assign the result to group 2 reliability.

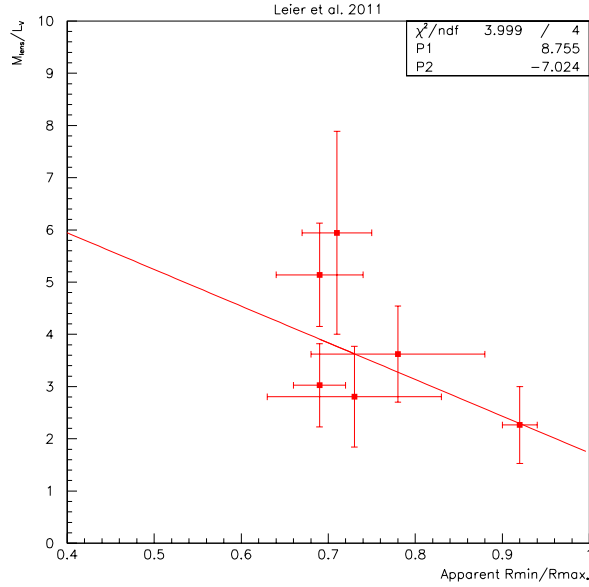


Figure 61: Stellar M_*/L vs the apparent axis ratio R_{min}/R_{max} for the Leier *et al.* (2011) data set [72].

B.1.13 Treu and Koopman

The data are discussed in Section 9.16. It was found that:

$$M_*/L = (-3.87 \pm 1.44)R_{min}/R_{max}|_{apparent} + (5.45 \pm 1.19), \text{ and}$$

$$M_*/L_{FP} = (-5.64 \pm 1.27)R_{min}/R_{max}|_{apparent} + (6.63 \pm 1.05),$$

for which Fundamental Plan assumptions were made to further constrain the data. The results without Fundamental Plan assumptions will be used for the global analysis. We assign the result to group 1 reliability.

B.2 Global results for M_*/L

To combine the individual M_*/L results, we follow the same procedure as for the main analysis (see Section 13, we choose to normalize the average M_*/L to 4) and correct for projection (see Section 10.2, the same correction factor 5 ± 1 , determined with the total M/L from [3]). The slopes $d(M_*/L)/d(R_{min}/R_{max})$ for the individual results are shown in Fig. 62. For clarity, they are plotted vs the approximate average radius value at which the M_*/L

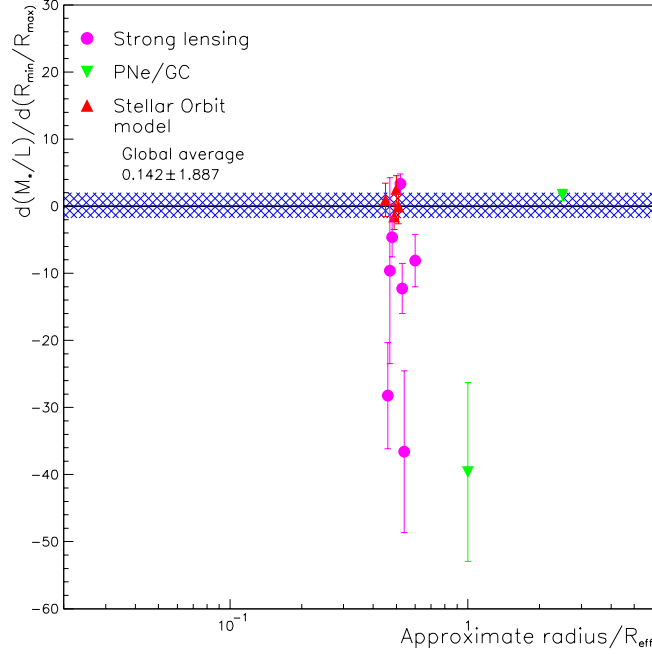


Figure 62: Slopes $d(M_*/L)/d(R_{min}/R_{max})$ vs the approximate radii (in R_{eff} unit) at which the M_*/L are obtained. The various symbols indicate the method used to obtain M_*/L . The band shows the average value of $d(M_*/L)/d(R_{min}/R_{max})$ after accounting for the reliability of each M_*/L extraction and the shared statistics (the uncertainties shown do not account for this. They are the values quoted in Section B). The plain line indicates 0, for reference.

are extracted. The average slope is

$$d(M_*/L)/d(R_{min}/R_{max}) = 0.14 \pm 1.19,$$

a value well compatible with zero. We can compare it to the results of the main analysis by normalizing the average mass over light ratios to a same value. Then, the slope for M_*/L is 50 times smaller than that for M/L .

We note that excluding the PNe/GC data sets, in case not applying the ellipticity corrections is questioned -a difference between the M_*/L and M/L analyses-, we obtain $d(M_*/L)/d(R_{min}/R_{max}) = -3.47 \pm 3.19$, which is still compatible with zero. Normalizing the average mass over light ratios to a same value, then the slope for M_*/L is twice smaller than that for M/L , and they are compatible within uncertainty. The inconclusive results, in the case of excluding the PNe/GC data sets, underline the limitation of this test due to its limited number of data sets and M/L extraction methods.

C Summary table of the NGC, IC and UGC galaxies

Key: x: used. (x): used in lower reliability group. The true $R_t = R_{min}/R_{max}$ is indicated when available. EXC and VCXG refer to [49], see Section 7.1. XE has a similar meaning as EXG and refers to [78]. The symbol - means the galaxy is available but does not pass the selection criteria. NM refers to an adequate elliptical galaxy, but unused because of mismatch between the NED numbers and the ones listed in [3].

name	Bac	Ben	Bert	Capa	Dea	Fuk	Kro	Lau	Mag01	Mag98	Nag	Piz	Pru	Rom	SAUR	Thomas	v.d. Mar 91	v.d. Mar 07b	comment
57	x												x						
83	x																		
97	x																		
194													x						
430	x																		
547	-							-											Arp
564													x						
584	x	x						x					x						
636	-	-						-					-				-	-	S0? [104]
720	x					x		x			x		x				x	x	CXG,XC
741	-					-		-					-						EXG
759																$R_t =$ 0.79			
821	x	x			x			x		x				x	$R_t =$ 0.62			x	
855													x						
990	NM												x						
1008	x																		
1016	x												x						
1052	-		$R_t =$ 0.63					NM											LINER/Sy2
1199	x	x											x						
1209	-												(x)						LINER
1282													x						
1283													x						
1293													x						
1344					x								x						
1374													x						
1379				x					-				-				-	-	spiral?
1395	NM					-		-			-		-				-	-	CXG, XE
1407	NM	-			-	-		NM					-				-	-	EXG
1426	x							x					x						
1439	x							x					x				x	x	
1453								(x)				$p_0 =$ 0.85 $q_0 =$ 0.81	(x)						LINER
1521	x																		
1549											x		x				x	x	XC
1573	x												x						
1600	NM	-				-		-		-			-				-		EXG
1700	NM	-		x		-		-					-				-	-	EXG, kin. distinct core.
2314	NM												x						
2320													x						
2325													x						
2340													x						
2434						x	x		x				x					x	CXG

name	Bac	Ben	Bert ola	Capa	Dea	Fuk	Kro	Lau	Mag 01	Mag 98	Nag	Piz	Pru	Rom	SAUR- ON4	Thomas	v.d. Mar 91	v.d. Mar 07b	comment
2513													x						
2663													x						
2675	x																		
2693	x	x											x						
2694													x						
2749	NM												(x)				-		LINER
2778	x									x			x					x	
2800	x																		
2810	x																		
2865						x							x						
2954	NM																		
2974												$p_0 =$ 0.78 $q_0 =$ 0.60							LINER, Sy2.
3070	x												x						
3078													x						
3091													x				x		
3121	NM																		
3136	NM																		
3158	NM												x						
3250													x						
3258													x						
3268													(x)						LINER
3305													x						
3309													x						
3348	NM	x																	
3377	NM	x			x	-				x			x		$R_t =$ 0.58			x	VCXG
3379	-			x	x	-		(x)	x	-			(x)	x			-	-	LINER, VCXG $R_t = 0.73$ [95]
3557	NM												(x)				-	-	LINER, S0 [104]
3562	x																		
3605	NM	x											x						
3608	-									-			(x)				-	-	LINER
3613		x											x						
3640	x	x					x						x					x	
3710	x																		
3731	NM																		
3812	x																		
3818	x	x											x						
3837	x												x						
3853	x												x						
3862	NM																		LERG
3872	NM	x																	
3873													x						
3904	x	x											x						
3923	NM	x				x					x		x						CXG,XC
3940	x												x						
3962	-												(x)						LINER
4070	x																		
4168							x												AGN:Sy1.9
4187	x																		

name	Bac	Ben	Bert ola	Capa	Dea	Fuk	Kro	Lau	Mag 01	Mag 98	Nag	Piz	Pru	Rom	SAUR- ON4	Thomas	v.d. Mar91	v.d. Mar 07b	comment
4213	x																		
4239	x												x						
4278	-		$R_t = 0.71$				x												Sy2, LINER
4283	NM												x						
4365	-					x					x		-						CXG, XC kinematically distinct core.
4374	-				x	-	x	-											AGN, LERG, LINER, Sy2, CXG
4387	NM	x						-					x						
4406	-			x															S0(3)/E3
4458	NM												x		$R_t = 0.94$			x	
4464				-					-										S?/Sab/S03
4467	NM								x	x			x						
4472	-					-					-								Arp E2/S0, EXG, XE
4473	x	x								x			x		$R_t = 0.50$			x	
4478	x	x							x				x						
4489	x	x											x						
4494	-				-	-	x		x				-	x			-	-	LINER, VCXG $R_t = 0.6 \pm 0.2$ [48] Possibly S0. Kinematically distinct core.
4510	NM																		
4551	x	x											x						
4555						-													EXG
4564	x	x			x					x			x					x	
4589	-						x						(x)					-	LINER, kinematically distinct core.
4621	NM	-				-		-		-			-		$(R_t = 0.69)$			-	VCXG
4648	x	x											x						
4649	-				-	-					-								Arp, EXG, XE
4660	x	x								x			x		$R_t = 0.71$			x	
4673													x						
4697	NM	x		x	x	-													LLAGN, CXG
4742	NM	x						x					x						
4860	x												x			$R_t = 0.80$			
4864	NM												x						
4867													x						
4869	x												x			$R_t = 0.88$			
4876													x						
4886	NM												x						
4906													x						
4915													x						
4926													x			$R_t = 0.87$			
4946																			cD, E+(?)

name	Bac	Ben	Bert ola	Capa	Dea	Fuk	Kro	Lau	Mag 01	Mag 98	Nag	Piz	Pru	Rom	SAUR- ON4	Thomas	v.d. Mar 91)	v.d. Mar 07b	comment
4952																$R_t = 0.59$			
5018						x							x						
5029	x																		
5044						-					-		(x)						EXG, XE, LINER
5061													x						
5077			$r_t = 0.50$									$p_0 = 0.58$ $q_0 = 0.75$							LINER, Seyfert1.9
5129	NM												x						
5198													x				x		
5223	x																		
5266			$(R_t = 0.6)$																SA0
5322	-										-		(x)						LINER,XC
5329	x																		
5490	NM	x											x						
5546	x																		
5557		x											x						
5576	NM	x											x						
5638	NM	x											x						
5642	x																		
5710	x																		
5791	NM												x						
5796	NM												x						
5812		x											x						
5813	-												(x)					-	LINER
5845	x	x						x							$R_t = 0.63$			x	
5846	-				-	-		-	-		-								LINER, HII,cE,EXG,XE
5898													x						
5903		x											x						
5966	x																		
5982	-												(x)						LINER
6020	x																		
6137	x												x						
6411	x	x											x						
6487	x																		
6623	-	-																	Galaxy pair
6702								(x)					(x)						LINER
6721																			cD, E+
6851													x						
6868						-							(x)						EXG, LINER
7052		x																	
7097			$R_t = 0.24$									$p_0 = 0.61$ $q_0 = 0.56$	(x)						LINER, counter rotating core.
7144													x				x	x	
7145							x						x				x	x	
7147																			low σ

name	Bac	Ben	Bert ola	Capa	Dea	Fuk	Kro	Lau	Mag 01	Mag 98	Nag	Piz	Pru	Rom	SAUR- ON4	Thomas	v.d. Mar91	v.d. Mar 07b	comment
7391	NM												x						
7454	x							x					x						
7458	x												x						
7507	x						x		x				x				x	x	
7618						-													EXG
7619	x	x				x		x					x				x	x	CXG
7660	x												x						
7778	x												x						
7785	x	x						x					x						
7796									-							($R_t = 0.75$)			cD, E+
IC171	-															x			E?/S0
IC179	-												-						Likely a S0
IC948	x																		
IC1152	x																		
IC1211	x																		
IC1459						-					-		(x)				-	-	LINER
IC3959													x						
IC4011													x						
IC4012													x						
IC4051	NM												x						
UGC 1308																$R_t = 0.82$			

D Summary table for the SLACS lensing galaxies

x=used, (x)=used but in lower reliability group, -=available but not used (if for reasons other than standard selection, we state the reasons. No symbol=not available. Masses -from [53]- indicating that the galaxy maybe a giant are highlighted in red). Values are given without uncertainties because only the central values are used for selection. The integration range for M_{tot} varies from authors to authors.

name	Ferr1	Aug	Bar	Card09	Card11	J&K	Koop	Lei09	Gril	Rotator	M_{tot} ($10^{10} M_{\odot}$)	σ (km/s)	type/ comment
J0008-0004					-				-		912[22], ~ 105 [53]	193[2]	E[1]
J0029-0055		- fit out- lier		x	x				x		1622[22], ~ 36[53]	231[2], 229[21]	E[1]
J0037-0942	- $R_M=1.7$	x	x		x	x	x	x	x	S[5]	52.3 [47], 4677[22], 27.3[59], 40[71] ~ 69[53]	265[47], 282[2], 265[59], , 230[71]	E[1]
J0044+0113		x			x				x		16596[22], ~ 27[53]	267[2]	E[1]
J0109+1500									x		~ 39[53]	251[2]	E[1]
J0157+0056				x	- lumi mism.				x		1288[22], ~ 78[53]	295[2], 295[21]	E[1]
J0216-0813		-	-	-	-	-	-		-	S[5]	7943[22], 48.2[59], ~ 147 [53]	334[2], 333[21], 332[59]	E[1]
J0252+0039		x		x	x				x		91[22], ~ 54[53]	170[2], 164[21]	E[1]
J0330-0020		x		x	- lumi mism.				x		891[22], ~ 75[53]	220[2], 212[21]	E[1]
J0405-0455									x		~ 3[53]	160[1]	E[1]
J0728+3835		x		x	x				x		155[22], ~ 60[53]	219[2], 214[21]	E[1]
J0737+3216	x	- fit out- lier			x	- Fit outlier	x	x	x		38.3 [47], 8511[22], 31.2[59] , 59[71], ~ 87[53]	310[47], 338[2], 310[59], , 313[71]	E[1]
J0808+4703				-								236[2]	E[1] No Axis ratio
J0819+4534		-	-		-						6166[22]	227[2], 236[21]	E[1] . No Axis ratio
J0822+2652		x			x				x		3548[22], ~ 72[53]	263[2]	E[1]
J0903+4116				-	-				-		676[22], ~ 135 [53]	223[2], 223[21]	E[1]
J0912+0029	-	-		-	-	-	-	-	-		71.2[47], 11220[22], 39[59], 80[71], ~ 120 [53]	313[47], 322[2], 326[21], , 313[59], 276[71]	E/S0[1]
J0935-0003		- (fit out- lier)	-		-				-	S[5]	34674[22], ~ 123 [53]	391[2]	E[1]
J0936+0913		x			x				x		851[22], ~ 45[53]	246[2]	E[1]
J0946+1006		x			x				x		8128[22], ~ 87[53]	265[2]	E[1]
J0956+5100	-	-			-	-		-	-		66.4[47], 12303[22], 37[59], 67[71], ~ 111 [53]	299[47], 338[2], 299[59], 299[71]	E[1]
J0959+0410		x	x	- lumi mism.	x	x	x		x	F[5]	2692[22] 7.7[59], ~ 27[53]	203[2], 197[21], 212[59]	E[1]
J1250+4901					-							256[2]	E[1]
J1250+0523		x	x	x	x	- Fit outlier	x		x	S[5]	1862[22], 18.9[59], ~ 54[53]	252[2], 252[21], 254[59]	E[1]
J0959+4416		-									~ 18[53]	248[2]	S0[1]
J1016+3859		x			x				x		2754[22], ~ 45[53]	254[2]	E[1]

name	Ferr.1	Aug.	Bar.	Card09	Card11	J&K	Koop.	Leier09	Grillo	Rotator	M_{tot} ($10^{10} M_{\odot}$)	σ (km/s)	type/ comment
J1020+1122		-			-				-		1318[22], ~ 102 [53]	290[2]	E[1]
J1023+4230		x		x	x				x		2951[22], ~ 69[53]	247[2], 242[21]	E[1]
J1029+0420		-							-			215[2]	S0[1]
J1100+5329					-				-		851[22], ~ 141 [53]	187[1]	E[1]
J1103+5322				-								196[2], 196[21]	S0/SA[1]
J1106+5228		x			x				x		~ 27[53]	266[2]	E[1]
J1112+0826		-			-				-		10000[22], ~ 135 [53]	328[2]	E[1]
J1134+6027		x			x				x		2089[22], ~ 39[53]	243[2]	E[1]
J1142+1001		x			x				x		2344[22], ~ 51[53]	225[2]	E[1]
J1143-0144		x			x				x		14125[22], ~ 57[53]	263[2]	E[1]
J1153+4612		x			x				x		2512[22], ~ 33[53]	233[2]	E[1]
J1204+0358		x	x		x				x	S[5]	4677[22], ~ 51[53]	274[2]	E[1]
J1205+4910	x	x		x	x			x	x		38.6[47], 5754[22], 45[71], ~ 75[53]	235[47], 282[2], 281[21], 235[71]	E[1]
J1213+6708		- fit out- lier			x				x		15849[22], ~ 42[53]	292[2]	E[1]
J1218+0830		x			x				x		2455[22], ~ 48[53]	218[2]	E[1]
J1251+0208			-									233[2]	S[1]
J1306+0600		-			-						8318[22]	241[2]	E[1] Axis ratio not avail.
J1313+4615		-			-						5623[22]	266[2]	E[1] Axis ratio not avail.
J1318-0313		-			-						2951[22]	211[2]	E[1] Axis ratio not avail.
J1330-0148	-	-	-		-	-	-	-			4.9[47], 3.2[59], 2.8[71]	178[47], 194[2], 178[59], 178[71]	S0[1]
J1402+6321		x		x	x	x	x		x		2400[22], 30.3[59], ~ 29[53]	268[2], 267[21], 275[59]	E[1]
J1403+0006		x			x				x		1259[22], ~ 30[53]	218[2]	E[1]
J1416+5136		-			-				-		1698[22], ~ 111 [53]	248[2]	E[1]
J1420+6019		-		-		-	-		-		3.9[59], ~ 12[53]	208[2], 205[21], 194[59]	S0[1]
J1430+4105		-			-				-		7244[22], ~ 162 [53]	325[2]	E[1]
J1436-0000		x			x				x		1950[22], ~ 69[53]	226[2]	E[1]
J1443+0304		-	-						-		~ 18[53]	218[2]	S0[1]
J1451-0239		x	x		x				x	S[5]	2754[22], ~ 24[53]	224[2]	E[1]
J1525+3327		-			-				-		1950[22], ~ 144 [53]	265[2]	E[1]
J1531-0105		x			x				x		6918[22], ~ 81[53]	280[2]	E[1]
J1538+5817		x			x				x		776[22], ~ 27[53]	194[2]	E[1]
J1614+4522		-			-						457[22]	183[2]	E[1] Axis ratio not avail.
J1621+3931		x			x				x		3388[22], ~ 87[53]	239[2]	E[1]
J1627-0053		x	x	x	x	- Fit outlier	x		x	S[5]	4266[22], 22[59], ~ 69[53]	295[2], 290[21], 275[59]	E[1]
J1630+4520		-		-	-	-	-		-		1202[22], 50.8[59], ~ 147 [53]	281[2], 276[21], 260[59]	E[1]

name	Ferr1	Aug	Bar	Card09	Card11	J&K	Koop	Lei09	Gril	Rotator	M_{tot} ($10^{10} M_{\odot}$)	σ (km/s)	type/ comment
J1636+4707	- $R_M=2.0$	x			x		-		x		52.9[47],490[22], 31[71], \sim 54[53]	221[47],237[2],221[71]	E[1]
J1644+2625					-						3236[22]	229[1]	E[1] Mass axis ratio not avail.
J1719+2939		-			-						11220[22]	295[2]	S0[1]
J2238-0754		x	x		x				x	F[5]	871[22], \sim 39[53]	200[2]	E[1]
J2300+0022	x	x	x	x	x	x	x	x	x	S[5]	40.9[47],7079,30.4[59] ,39[71], \sim 90[53]	283[47],284[2],279[21] ,283[59],283[71]	E[1]
J2303+1422	x	x	x	x	x	x	x	x	x	S[5]	49.8[47],4571,27.5[59] ,51[71], \sim 81[53]	260[47],253[2],255[21] ,260[59],260[71]	E[1]
J2321-0939		x	x		x	x	x		x	S[5]	3388[22],11.7[59], \sim 36[53]	246[2],236[59]	E[1]
J2341+0000		x		x	x				x		1778[22], \sim 66[53]	206[2],207[21]	E[1]
J2347-0005					- lumi mism.						10000[22]	404[1]	E[1]

E Summary table for the COSMOS lensing galaxies

x=used, -=available but not used.

name	Faure	M_{tot} ($10^{10} M_{\odot}$)	σ (km/s)
COSMOS 0012+2015	- No DMf		215[43]
COSMOS 0013+2249	- No DMf		
COSMOS 0018+3845	x	62[44]	289[44],303[43]
COSMOS 0038+4133	- $DMf < 0$, low σ	14[44]	207[44],225[43]
COSMOS 0047-5023	- High χ^2/ndf	145[44]	383[44],313[43]
COSMOS 049+5128	x	73[44]	313[44],380[43]
COSMOS 0050+4901	- High χ^2/ndf , M_{tot} $> 10^{12} M_{\odot}$	119[44]	386[44],342[43]
COSMOS 0056+1226	- No DMf		337[43]
COSMOS 0124+5121	x	36[44]	267[44],245[43]
COSMOS 0211+1139	-		466[43]
COSMOS 0216+2955	- No DMf		349[43]
COSMOS 0227+0451	- No DMf		428[43]
COSMOS 0254+1430	- No DMf		
COSMOS 5857+5949	- No DMf		398[43]
COSMOS 5914+1219	- M_{tot} $> 10^{12} M_{\odot}$	120[44]	358[44],338[43]
COSMOS 5921+0638	- (Rmin/Rmax mismatch), low σ	11[44]	189[44],221[43]
COSMOS 5941+3628	x	68[44]	315[44],285[43]
COSMOS 5947+4753	x	86[44]	326[44],370[43]
J100140+020040	x	30[44]	259[44]
J095930+023427	x	29[44]	255[44]

F Summary table for the CL 3C295, CL 0016+16 and CL 1601+42 cluster galaxies

x=used, -=available but not used (if for a reason other than the standard selection criteria, we state the reason).

name	van der Marel	Type
3C295-834	- shows extra structures S0 criteria: possibly S0	E[105]
3C295-968	- S0 criteria: possibly S0	E[105]
0016-438	x S0 criteria: unlikely to be S0	E[105]
0016-461	- S0 criteria: possibly S0	E[105]
0016-531	- S0 criteria: possibly S0	E[105]
0016-611	- S0 criteria: likely to be S0	E[105]
0016-612	x S0 criteria: unlikely to be S0	E[105]
0016-659	x S0 criteria: unlikely to be S0	E[105]
0016-724	x S0 criteria: unlikely to be S0	E[105]
0016-725	- S0 criteria: possibly S0	E[105]
0016-745	- S0 criteria: likely to be S0	E[105]
0016-2050	- S0 criteria: likely to be S0	E[105]
1601-292	- S0 criteria: possibly S0	E[105]
1601-524	x S0 criteria: unlikely to be S0	E[105]
1601-619	- S0 criteria: likely to be S0	E[105]
1601-753	x S0 criteria: unlikely to be S0	E[105]
1601-814	- S0 criteria: likely to be S0	E[105]
1601-2040	x S0 criteria: unlikely to be S0	E[105]
1601-2043	- S0 criteria: possibly S0	E[105]
1601-2060	- S0 criteria: likely to be S0	E[105]

G Summary table for SL2S lensing galaxies

x=used, -=available but not used (if for a reason other than the standard selection criteria, we state the reason).

name	Ruff	M_{tot} ($10^{10} M_{\odot}$)	σ (km/s)	type/comment
J02141-0405	- (no data)			Has a companion galaxy [50]
J02173-0513	-	54[88]	257[88]	Influenced by nearby group [50]
J02190-0829	x	19[88]	305[88]	
J02205-0639	x	28[88]	242[88]	
J02251-0454	x	40[88]	241[88]	
J02261-0420	x	40[88]	266[88]	
J02264-0406	- (no data)			S0? [50]
J02264-0904	-	65.2[88]	301[88]	
J02325-0408	x	23[88]	264[88]	
J14061-5202	- (no data)			Influenced by nearby galaxy? [50]
J14061-5202	- (no data)			
J14113-5651	x	15[88]	228[88]	
J22062-0057	- (no data)			Small companion [50]
J22132-0009	-	22[88]	183[88]	Edge-on disk galaxy [50]
J22140-1807	-	5.7[88]	167[88]	Probably a S0 from mass and σ [50]
J22160-1751	- (no data)		282[88]	Not a true lens. [50]
J221929-0017	x	9[88]	263[88]	

H CDFS Summary table

x=used, (x)=used but in lower reliability group, -=available but not used, no symbol=not available. Values are given without uncertainties because only the central values are used for selection.

Name	Rettura	van der Wel	M_{tot} ($10^{10} M_{\odot}$)	σ (km/s)	type/comment
CDFS-1	-	-	20.4[86], 22.4[102]	231[86],[102]	AGN
CDFS-2	x	x	20.0[86], 14.8[102]	200[86],[102]	
CDFS-3	x	x	12.6[86], 12.6[102]	300[86],[102]	
CDFS-4	-(Giant)	-(Giant)	97.7[86], 104.5[102]	336[86],[102]	Large X-ray emm.
CDFS-5	-(low σ)	-(low σ)	9.8[86], 11.5[102]	194[86],[102]	
CDFS-6	x	x	8.3[86], 5.4[102]	208[86],[102]	
CDFS-7	x	x	15.1[86], 38.9[102]	232[86],[102]	
CDFS-8	x	x	13.8[86], 12.0[102]	253[86],[102]	
CDFS-9	x	x	10.0[86], 9.3[102]	215[86],[102]	
CDFS-10	-	-	6.6[86], 6.6[102]	275[86],[102]	O-II
CDFS-11	-	-	9.8[86], 9.5[102]	208[86],[102]	O-II
CDFS-12	x	x	11.0[86], 9.3[102]	262[86],[102]	
CDFS-13	x	x	14.8[86], 17.0[102]	247[86],[102]	
CDFS-14	-(low σ)	-(low σ)	17.0 [86], 14.1[102]	197[86],[102]	
CDFS-15	x	x	33.9[86], 25.1[102]	317[86],[102]	
CDFS-16	-	-	18.2[86], 18.6[102]	262[86],[102]	AGN
CDFS-17	-	-	58.9[86], 70.8[102]	305[86],[102]	Spiral
CDFS-18		-(Giant)	51.3[102]	324[102]	
CDFS-19		-	16.6[102]	229[102]	O-II
CDFS-20	-(low σ)	-(low σ)	13.5[86], 12.6[102]	199[86],[102]	
CDFS-21	-(low σ)	-(low σ)	2.6[86], 1.4[102]	149[86],[102]	
CDFS-22	-	-	26.3[86], 28.8[102]	225[86],[102]	AGN, Large X-ray emm.
CDFS-23	-(low σ)	-(low σ)	1.51[86], 1.9[102]	70[86],[102]	
CDFS-24	-	-	63.1[86], 79.4[102]	210[86],[102]	Spiral

Name	Rettura	van der Wel	M_{tot} ($10^{10}M_{\odot}$)	σ (km/s)	type/comment
CDFS-25	x	x	9.1[86], 7.9[102]	258[86],[102]	
CDFS-26	-	-	72.4[86], 67.60[102]	249[86],[102]	Spiral
CDFS-27	- (low σ)	- (low σ)	10.5[86], 11.7[102]	135[86],[102]	
CDFS-28	-	-	74.1[86], 147.9[102]	445[86],[102]	Spiral
CDFS-29	x	x	11.7[86], 10.0[102]	221[86],[102]	
CDFS-354	- (low σ)		3.6[86]	99[86]	
CDFS-369	- (low σ)		2.0[86]	119[86]	
CDFS-467	- (low σ)		4.0[86]	140[86]	
CDFS-532	x		15.1[86]	260[86]	
CDFS-547	-		8.51[86]	256[86]	E+A
CDFS-571	-		20.0[86]	182[86]	Sa
CDFS-590	- (low σ)		5.4[86]	119[86]	
CDFS-633	x		41.7[86]	260[86]	
CL1252-1	-	-	19.1[86], 21.9[102]	219[86],[102]	AGN
CL1252-2	x	x	7.2[86], 8.3[102]	216[86],[102]	
CL1252-3	-	-	21.9[86], 24.5[102]	166[86],[102]	Spiral
CL1252-4	-	-	26.3[86], 34.7[102]	202[86],[102]	Spiral
CL1252-5	-	-	28.2[86], 20.4[102]	251[86],[102]	AGN
CL1252-6	x	x	9.1[86], 8.9[102]	211[86],[102]	
CL1252-7	-	-	13.2[86], 12.9[102]	213[86],[102]	AGN
CL1252-8	- (low σ)	- (low σ)	1.0[86], 1.0[102]	63[86],[102]	
CL1252-9	- (low σ)	- (low σ)	1.8[86], 2.2[102]	102[86],[102]	
CL1252-6106	x		30.2[86]	294[86]	
CL1252-9077	- (low σ)		7.9[86]	130[86]	
CL1252-4419	- (Giant)		141.3[86]	302[86]	Interacting
CL1252-4420	- (Giant)		97.7[86]	232[86]	Interacting

I Cluster CL1358+62 elliptical galaxies summary table

x=used -=available but not used.

ID	Kelson	type/comment
212	x	
242	-	$M_R > -20.0$
256	-	$M_R > -20.0$
303	-	$M_R > -20.0$
360	x	
375	-	$M_R > -20.0$
409	x	
412	x	
531	-	$M_R > -20.0$
534	x	
536	-	$M_R > -20.0$

J Summary table for other lensing galaxies

x=used, (x)=used but in lower reliability group, -=available but not used (if for a reason other than standard selection criteria, we stated the reason), no symbol=not available. Values are given without uncertainties because the central values only are used for selection. The integration value for M_{tot} varies from authors to authors.

Name	Kee	Jack	J&K	Lei 09	Lei 11	Fer 05	Treu 04	M_{tot} ($10^{10}M_{\odot}$)	σ (km/s)	type/comment
0047-28108			-	x	x	x	x	58[59], 21[71], 33[72], 34[46], 41[98]	250[59], 229[71], 254[103]	
Q0142-100	x				x	x		46[72], 25[46]	224[103]	E[60]
B0218+357	-	-						2[58]		S[60],[70],[58]
CFRS-3.1077				- (no data)						
C0302+006			-				x	67[59], 67[98]	256[59], 251[98]	Part of small group?[98]
MG0414+0534	- (no z values)	x			x	x		103[72], 83[46], 24[58]	303[103]	E[60]
B0712+472	-	x			-			16[72], 9[58]	181[103]	E[60]
MG0751+2716	- (interac- ting)									E[60]
HST0818					- (interac- ? No axis ratio)	- (interac- ? No axis ratio)		37[72], 67[46]	251[103]	
RXJ0911					- (not true lens?)			73[72]	260[103]	
FB0951+263						-		5[46]	128[103]	(probably S0 from mass and σ)
BRI0952- 0115	- (no z values)				-	-		15[72], 5[46]	117[103]	E[60] (probably S0 from mass and σ)
Q0957+561	- (interac- ting)			- (interac- ting)	- (interac- ting)			305[71], 151[72]	431[103], 288[71]	E[60]
LBQS1009					x	-		65[72], 18[46]	198[103]	
Q1017-207						-		5[46]	151[103]	(probably S0 from mass and σ)
FSC10214+4724									241[103]	
B1030+071		-			- (interac- ting)	-		55[72], 16[46], 22[58]	218[103]	
HE1104-1085					x	-		73[72], 122[46]	316[103]	E
PG1115+080	-		-	-	-	-		17[59], 8.2[71], 17[72], 28[46]	210[103], 281[59], 191[71]	E[60],peculiar? [59],interacting

Name	Kee	Jack	J&K	Lei 09	Lei 11	Fer 05	Treu 04	M_{tot} ($10^{10} M_{\odot}$)	σ (km/s)	type/comment
B1127+385 G1		-						2.7[58]		Late type? [64]
B1127+385 G2		-						1.1[58]		Late type? [64]
MG1131+0456	- (interacting)									
B1152					- (interacting)			30[72]		
HST12531-2914	- (no z values)								NA	E
HST14113+5211						-		34[46]	190[103]	
HST14176+5226	x		-	x		-	x	71[59], 34.3[71], 118[46], 71[98]	292[103], 212[59], 245, 224[98]	E[60]
B1422+231	- (interacting)	-			- (interacting)			5.7[72], 16[46], 12[58]	160[103]	E[60] (probably S0 from mass and σ)
SBS1520					x	x		42[72], 27[46]	220[103]	
H1543-535			-	- (no data)			-	3.4[59], 3.4[98]	108[59], 116[98]	(probably S0 from mass and σ)
COMBO15422								63[77]	305[77]	S0-like [77]
MG1549+3047	-		- (disk? fit out-lier)					12[59]	188[103], 227[59]	E[60]
B1600+434	- (poor under)	-			- (interacting)			16[72], 12[58]		E, maybe S[60] S[58]
B1608+656	-	-		-	-	-		28[103], 42[72], 85[46], 52[58]	292[103], 247[72]	E, maybe S[60], may have a companion
MG1654+1346	x								206[103]	E, maybe S[60]
PKS1830-211										S[70]
B1933+503	-	-								S [96]
B1938+666		x						6[58]		E ? [62]
MG2016+112			-	x	-		-	110[59], 20.41[71], 52[72], 110[98]	304[59], 304[71], 299[103]	Giant E [72]
B2045		-			- (interacting?)			173[72] 86[58]	378[103]	Maybe Sa
B2114+022 G1		-						26 [58]		Post starburst elliptical. E+A. Dust makes M/L unreliable [26]
B2114+022 G2		x						52 [58]		E [26]

Name	Kee	Jack	J&K	Lei 09	Lei 11	Fer 05	Treu 04	M_{tot} ($10^{10} M_{\odot}$)	σ (km/s)	type/comment
HE2149					-	-		27[72],14[46]	203[103]	
Q2237	-			-	-			7[71],2.8[72], 2[46]	215[71], 168[103]	Sb or spiral bulge[72],[60]
COMBO34244								11[77]		May not be a lens[77]
COMBO40173								7[77]		
COMBO43242								12		Late type[77]
COMBO46446						-		8		

K Summary of the individual analyses

In the table below, we summarize the results of each individual analysis described from Section 4 to Section 9. Col(1): publication reference. Col(2): method used to compute the dark content. Col(3): best fit result (not yet normalized to $M/L(R_{min}/R_{max} = 0.7) = M_{tot}/M_*(R_{min}/R_{max} = 0.7) = 8$). Col(4) : number of elliptical galaxies that passed the selection criteria of Section 3.1. Col(5): reliability group, see Section 13, Col(6): weight factor wf, see Section 13. This a multiplicative factor to the uncertainties: the higher wf, the less impact the data set has on the global average. Col(7): specific notes regarding the analysis. Here, we give the best fit result in function of ellipticity ε rather than $R_{min}/R_{max} = 1 - \varepsilon$. “-” means that the data was not used in the global average.

Ref.	Method	Best fit	stat	rg	wf	Notes
[3]	Virial	$M/L_B = (13.08 \pm 2.97)\varepsilon_{ap} + (16.88 \pm 2.32)$	64	2	1.50	Added requirement that the galaxy characteristics listed in the 1985 Ref. [3] are compatible with recent characteristics given in NED [110]. Results using ellipticity corrections from σ^2 isotropic method.
[3]	Virial	$M/L_B = (5.91 \pm 4.67)\varepsilon_{ap} + (10.50 \pm 3.48)$	11	2	1.13	Same additional selection criterion as above. Results using ellipticity correction from μ^2 isotropic method.
[3]	Virial	$M/L_B = (6.19 \pm 3.59)\varepsilon_{ap} + (9.18 \pm 2.64)$	11	1	1.13	Same additional selection criterion as above. Results using ellipticity correction from μ^2 anisotropic method.
[6]	Virial	$M/L_B = (4.03 \pm 1.44)\varepsilon_{ap} + (6.20 \pm 1.07)$	35	3	2.37	
[61]	Virial	$M/L_V = (15.53 \pm 7.21)\varepsilon_{ap} + (20.52 \pm 5.95)$	5	4	1.00	Distant galaxies (cluster CL1358+62). Added $M_B \leq -20$ selection criterion to minimize contamination from boxy galaxies.
[69]	Virial	$M/L_B = (10.94 \pm 10.18)\varepsilon_{ap} + (23.83 \pm 7.80)$	10	4	6.09	M/L_B extracted for galactic cores. Same added selection criterion as [3].
[71]	Virial	$M_{vir}/L_I(R_{lense}) = (6.41 \pm 4.97)\varepsilon_{ap} + (6.30 \pm 3.95)$	8	2	1.00	Distant galaxies strongly lensing. Also analyzed with strong lensing method.
[84]	Virial	$M/L_B = (6.58 \pm 1.98)\varepsilon_{ap} + (8.99 \pm 1.68)$	102	2	1.32	
[86]	Virial	$M_{dyn}/M_* = (4.29 \pm 1.36)\varepsilon_{ap} + (5.04 \pm 1.25)$	16	3	1.35	Distant galaxies. M_* obtained with composite stellar population models using a Kroupa IMF [68].
[102]	Virial	$M/L_B = (5.36 \pm 1.24)\varepsilon_{ap} + (6.42 \pm 1.12)$	13	3	1.35	Distant galaxies.
[17]	Modeling	$M/L_{Jeans} = (1.47 \pm 1.56)\varepsilon_{true} + (3.84 \pm 1.10)$	6	1	1.38	Two estimates of M/L provided. One based on a 2-integral Jeans model and one on a 3-integral Schwartzchild model [92].
		$M/L_{Schw} = (1.09 \pm 1.68)\varepsilon_{true} + (3.48 \pm 1.17)$	6	1	1.38	
cap. 2013a	Modeling	$M/L = (2.02 \pm 1.47)\varepsilon_e + (3.51 \pm 0.42)$	31	1	1.86	
cap. 2013b	Modeling	$M/L = (4.72 \pm 2.18)\varepsilon_e + (3.33 \pm 0.59)$	31	1	1.86	
[67]	Modeling	$M/L_B _{in} = (4.58 \pm 7.04)\varepsilon_{ap} + (9.58 \pm 6.17)$	10	1	1.17	Kept LINERS, AGN and Seyfert galaxies because isothermal or virial equilibrium is not required.
		$M/L_B _{out} = (-6.53 \pm 14.48)\varepsilon_{ap} + (1.25 \pm 12.48)$	10	1	1.17	
[73]	Modeling	$M/L = (-0.69 \pm 4.95)\varepsilon_{ap} + (3.26 \pm 4.73)$	7	1	1.33	
[97] and [108]	Modeling	$M/L = (2.57 \pm 6.80)\varepsilon_{true} + (8.82 \pm 5.30)$	7	1	1.16	Distant galaxies (Coma cluster and Abell 262 cluster). $M/L _{sc}$ [97] was assumed to be independent of radius.
		$M/L _{sc} = (-0.57 \pm 7.02)\varepsilon_{true} + (6.67 \pm 5.57)$	7	2	1.63	
[104]	Modeling	$M/L_R = (3.43 \pm 0.92)\varepsilon_{ap} + (5.65 \pm 0.84)$	9	1	1.47	
[105]	Modeling	$M/L_B = (6.19 \pm 11.45)\varepsilon_{true} + (8.75 \pm 7.38)$	19	2	1.00	Distant galaxies.
[106]	Modeling	$M/L_B = (3.50 \pm 2.62)\varepsilon_{ap} + (9.59 \pm 2.08)$	17	1	2.04	Homogenized compilation of literature (local galaxies).
[16]	PNe/GC	$M/L_B = (19.43 \pm 7.85)\varepsilon_{ap} + (22.14 \pm 6.82)$	5		2.14	Relaxed selection: includes all galaxies except the disrupted ones, the ones showing possible interactions and the ones clearly non-elliptical.

Ref.	Method	Best fit	stat	rg	wf	Notes
[30]	PNe/GC	$M/L = (10.89 \pm 17.71)\varepsilon_{ap} + (21.45 \pm 12.73)$	7	1	1.24	Relaxed selection.
[74]	PNe/GC	$M/L = (2.45 \pm 8.60)\varepsilon_{ap} + (9.18 \pm 7.57)$	8	1	1.14	
[87]	PNe/GC	$M/L_B = (142.47 \pm 63.47)\varepsilon_{true} + (111.50 \pm 42.86)$	3	1	1.22	True axis ratios are from [17], [48] and [95].
[49]	X-ray	$M/L_B = (0.55 \pm 15.44)\varepsilon_{ap} + (5.29 \pm 11.74)$	7	2	1.17	
[78]	X-ray	$M/L_B(0.5R_{eff}) = (12.24 \pm 8.41)\varepsilon_{ap} + (20.94 \pm 6.01)$	3	2	1.17	
		$M/L_B(3R_{eff}) = (20.85 \pm 33.35)\varepsilon_{ap} + (38.32 \pm 23.74)$	3	2	1.17	
		$M/L_B(6R_{eff}) = (232.0 \pm 94.0)\varepsilon_{ap} + (182.5 \pm 59.9)$	2	2	1.17	
[9] and [8]	Gas disk	$M/L_B = (4.21 \pm 3.55)(1 - bc/a^2) + (5.83 \pm 2.09)$	4	1	1.15	Relaxed selection (kept LINERS and/or Sy types) a, b and c are the radii of the elliptical galaxy triaxial shape model.
[83]	Gas disk	$M/L_T = (1.39 \pm 13.13)(1 - q_0 p_0) + (4.83 \pm 6.80)$	4	1	1.15	Relaxed selection (kept LINERS and/or Sy types) q_0 and p_0 are the intrinsic axis ratios of the triaxial galaxy.
[2]	Lensing	$M_{tot}/M_* _{Chab} = (3.38 \pm 0.79)\varepsilon_{mass} + (4.92 \pm 0.66)$	34	1	-	S0 galaxies are already identified in [83]. Thus standard $\sigma \geq 225 \text{ km.s}^{-1}$ criterion is not applied in this analysis (and all other analyses using SLACS data). Mass ratios extracted using either a Chabrier [25] or a Salpeter IMF [89].
		$M_{tot}/M_* _{Sal} = (1.86 \pm 0.46)\varepsilon_{mass} + (2.76 \pm 0.38)$	34	1	-	
		$M_{tot}/M_* _{Chab} = (1.47 \pm 0.70)\varepsilon_{ap} + (3.30 \pm 0.57)$	34	1	2.04	
		$M_{tot}/M_* _{Sal} = (0.79 \pm 0.40)\varepsilon_{ap} + (1.84 \pm 0.32)$	34	1	-	
[5]	Lensing	$M/L _{Chab} = (33.1 \pm 16.7)\varepsilon_{true} + (37.2 \pm 13.9)$	10	1	2.05	M/L formed with DMf using either a Chabrier [25] or a Salpeter IMF [89].
		$M/L _{Sal} = (15.9 \pm 9.8)\varepsilon_{true} + (19.0 \pm 8.2)$	10	1	-	
[21]	Lensing	$M/L = (5.39 \pm 3.40)\varepsilon_{mass} + (9.32 \pm 2.85)$	13	1	-	
		$M/L = (1.94 \pm 3.52)\varepsilon_{ap} + (6.37 \pm 2.82)$	13	1	5.12	
[22]	Lensing	$M/L(R_{Ein}) = (4.57 \pm 2.79)\varepsilon_{mass} + (8.39 \pm 2.32)$	36	2	-	Use Secondary Infall Model and Salpeter IMF.
		$M/L(R_{Ein}) = (2.50 \pm 3.00)\varepsilon_{ap} + (6.59 \pm 2.40)$	36	2	4.92	
		$M/L(R_{eff}) = (8.17 \pm 1.60)\varepsilon_{mass} + (13.00 \pm 1.37)$	36	2	-	
		$M/L(R_{eff}) = (4.82 \pm 1.32)\varepsilon_{ap} + (10.00 \pm 1.09)$	36	2	1.00	
[44]	Lensing	$M_{tot}/M_* = (30.21 \pm 6.13)\varepsilon + (27.12 \pm 4.88)$	7	1	1.00	
[46]	Lensing	$M_{tot}/M_* _{V,Chab} = (1.83 \pm 5.78)\varepsilon_{ap} + (2.67 \pm 4.09)$	4	1	1.29	M_* determined with a Chabrier or a Salpeter IMF.
		$M_{tot}/M_* _{V,Sal} = (3.16 \pm 3.69)\varepsilon_{ap} + (2.61 \pm 3.40)$	4	1	-	
[47]	Lensing	$M_{tot}/M_* = (-0.47 \pm 2.63)\varepsilon_{ap} + (0.61 \pm 2.16)$ and	4	1	1.80	
		$M_{tot}/M_* = (-5.55 \pm 3.22)\varepsilon_{mass} + (-3.00 \pm 2.30)$	4	1	-	
[53]	Lensing	$M_{tot}/L_B _{Mar,Sal} = (1.65 \pm 0.97)\varepsilon_{ap} + (3.30 \pm 0.78)$	40	1	-	Stellar Composite Model used to obtain M_* with two different sets of metallicity template (Bruzual & Charlot [14] or Maraston [75]) and three different IMF (Salpeter [89], Kroupa [68] or Chabrier [25]).
		$M_{tot}/L_B _{BC,Sal} = (1.52 \pm 1.18)\varepsilon_{ap} + (3.27 \pm 0.94)$	40	1	-	
		$M_{tot}/L_B _{Mar,Krou} = (1.12 \pm 1.10)\varepsilon_{ap} + (2.95 \pm 0.87)$	40	1	-	
		$M_{tot}/L_B _{BC,Chab} = (1.75 \pm 1.06)\varepsilon_{ap} + (3.42 \pm 0.85)$	40	1	2.00	
[58]	Lensing	$M_{tot}/L_H = (0.80 \pm 1.67)\varepsilon_{ap} + (1.61 \pm 1.31)$	4	3	1.37	
[59]	Lensing	$M_{tot}/M_* = (1.24 \pm 0.92)\varepsilon_{ap} + (2.73 \pm 0.72)$	12	2	6.24	Use results with adiabatic compression (favored by the authors' analysis).
		$M_{tot}/M_* = (0.14 \pm 0.68)\varepsilon_{mass} + (1.87 \pm 0.50)$	12	2	-	
[60]	Lensing	$M/L_B = (36.22 \pm 15.14)\varepsilon_{mass} + (30.59 \pm 9.89)$	3	3	-	Due to the small number of galaxies, we relaxed the S0 rejection criterion and used $\sigma < 200 \text{ km.s}^{-1}$. Thus, this result is weighted out in the global average.
		$M/L_B = (0.00 \pm 10.27)\varepsilon_{ap} + (6.55 \pm 7.01)$	3	3	∞	
[65]	Lensing	$M_{tot}/M_* = (1.75 \pm 0.77)\varepsilon_{ap} + (2.67 \pm 0.64)$	9	1	2.52	
		$M_{tot}/M_* = (2.25 \pm 0.57)\varepsilon_{mass} + (3.20 \pm 0.49)$	9	1	-	
[71]	Lensing	$M/L_I = (5.51 \pm 3.27)\varepsilon_{ap} + (5.72 \pm 2.62)$	8	1	4.98	
[72]	Lensing	$M/L_V = (37.2 \pm 36.6)\varepsilon_{ap} + (-13.2 \pm 26.3)$	3	2	2.83	
[88]	Lensing	$M/M_* = (-0.49 \pm 2.90)\varepsilon_{ap} + (0.22 \pm 2.17)$	7	2	1.00	The M_* determined with a Chabrier or a Salpeter IMF are for M/L at R_{eff} . M/L at R_{Ein} does not need IMF input.
		$M/M_* = (-0.53 \pm 2.47)\varepsilon_{mass} + (0.18 \pm 1.88)$	7	2	-	
		$M_{tot}/M_* _{Sal} = (-3.62 \pm 8.81)\varepsilon_{ap} + (0.50 \pm 6.33)$	7	2	-	
		$M_{tot}/M_* _{Sal} = (4.66 \pm 1.43)\varepsilon_{mass} + (5.84 \pm 0.85)$	7	2	-	
		$M_{tot}/M_* _{Chab} = (6.17 \pm 14.65)\varepsilon_{ap} + (9.62 \pm 10.70)$	7	2	1.00	
		$M_{tot}/M_* _{Chab} = (9.89 \pm 4.85)\varepsilon_{mass} + (11.65 \pm 3.25)$	7	2	-	
[98]	Lensing	$M/L_B = (2.04 \pm 3.20)\varepsilon_{ap} + (6.63 \pm 2.45)$	3	1	1.23	

L Detailed analysis of the Bacon *et al.* data

This section provides the details of the analysis done using the Bacon *et al.* data. The results reported here are slightly different from the results given in Section 4.1 Since additional corrections, mostly addressing possible correlations, are applied. In addition, some of the NED data used may have become obsolete as they are from the 2008 database. The purpose of this section is to define the analysis method, identification requirement and most importantly, correlation investigations. The slight difference with Section 4.1 is thus irrelevant.

L.1 Data quality and galaxy selection

We apply our usual selection criteria. In addition, we reject the 8 last galaxies of [3] for lack of reference. Since the data [3] are old, we verified that they agree with data also available from NED (as of 2008). We exclude¹² from our sample galaxies for which their distance to Earth (redshift based) disagree by more than 20% between NED and [3]. We apply the same criterion for the apparent axis ratio R_{min}/R_{max} . The apparent magnitude from NED and [3] always agree within 10%, so no galaxy is excluded on the basis of an apparent magnitude discrepancy. We note that some of the uncertainties quoted in [3] may be underestimated since some of the sets are incompatible (assuming that the NED data are more accurate). Comparing the analysis done using the galactic characteristics from [3] and the analysis done using that of NED is useful for studying if the correlations seen between the galactic characteristics are due to measurement bias rather than a physical relation or an observational bias. When no uncertainty was available from NED, we used the uncertainty reported in [3]. To check for possible biases, we fit the Ref. [3] vs NED data for R_{min}/R_{max} , distance moduli DM , and apparent magnitudes using a linear function, see Figs. 63, 64, 65 and 66.¹³ No significant biases are found, except for the non-redshift based DM . Using the NED data, particularly its non-redshift based DM , significantly strengthen the M/L vs R_{min}/R_{max} correlation.

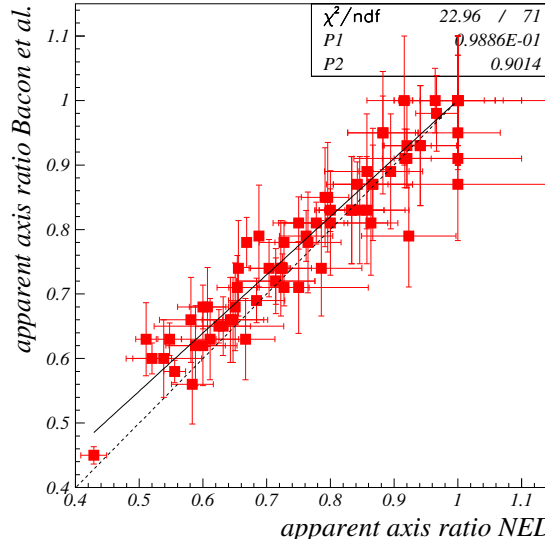


Figure 63: Apparent axis ratio R_{min}/R_{max} for NED vs [3]. The plain line is the best fit to the data and the dashed one indicates $y = x$. The best fit is $y = (0.901 \pm 0.048)x + (0.099 \pm 0.034)$. It reveals a slight bias: Ref. [3] tends to overestimate R_{min}/R_{max} , perhaps because older data have poorer resolution which tends to round ellipses.

All in all, we kept 73 galaxies in the sample. The list is: NGC57, 83, 97, 430, 584, 636, 720, 741, 990, 1008, 1016, 1199, 1209, 1426, 1439, 1521, 1573, 2675, 2693, 2778, 2800, 2810, 2954, 3070, 3562, 3640, 3710, 3812, 3818, 3837, 3853, 3904, 3940, 4070, 4187, 4213, 4239, 4365, 4473, 4478, 4489, 4510, 4551, 4564, 4648, 4660, 4860, 4869, 5029, 5223, 5329, 5546, 5642, 5710, 5845, 5966, 6020, 6137, 6411, 6487, 6623, 7391, 7454, 7458, 7507, 7619, 7660, 7778, 7785, and IC179, 948, 1152 and 1211. Among this sample, 12 galaxies have M/L available using two additional virial formulae presumably less sensitive to unknown true flattening [3]. They are: NGC584, 720, 2778, 3818, 3904, 4365, 4473, 4478, 4551, 5845, 7619 and 7785.

¹²We exclude the data rather than correct, with the NED value, M/L and other quantities: we prefer to assume that the discrepancy reflects a difficult measurement and hence a suspicious datum, rather than assuming that NED is correct and Ref. [3] wrong.

¹³We will account here for the horizontal uncertainty in a recursive way: we first fit the distribution without accounting for the horizontal error bars. We then use this first fit result to transform the horizontal errors in vertical ones and add the sum in quadrature. This procedure assumes that all errors are gaussian.

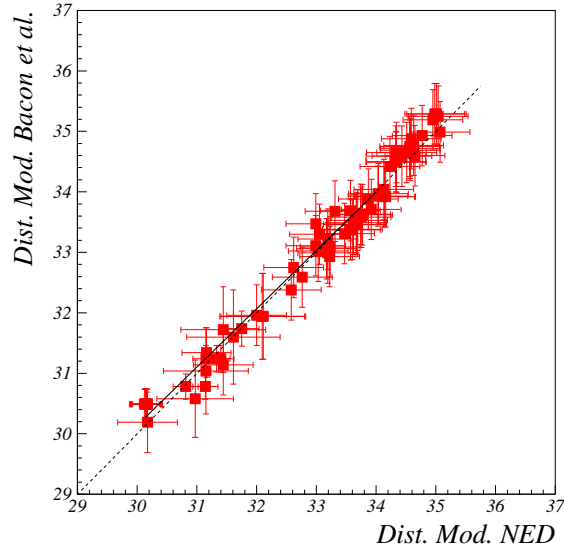


Figure 64: Distance Moduli from NED vs [3]. The plain line is the best fit to the data and the dashed one indicates $y = x$. The best fit is $y = (0.964 \pm 0.035)x + (1.235 \pm 1.126)$, with no indication of discrepancy.

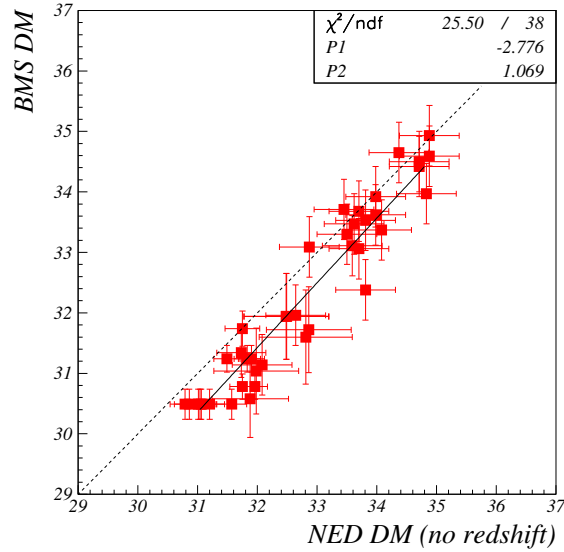


Figure 65: Distance Moduli from NED, determined without redshift information when available, vs [3]. The plain line is the best fit to the data and the dashed one indicates $y = x$. The best fit is $y = (1.067 \pm 0.054)x - (2.776 \pm 1.744)$, indicating that the non-redshift based NED's DM indicate larger distances from galaxies to Earth.

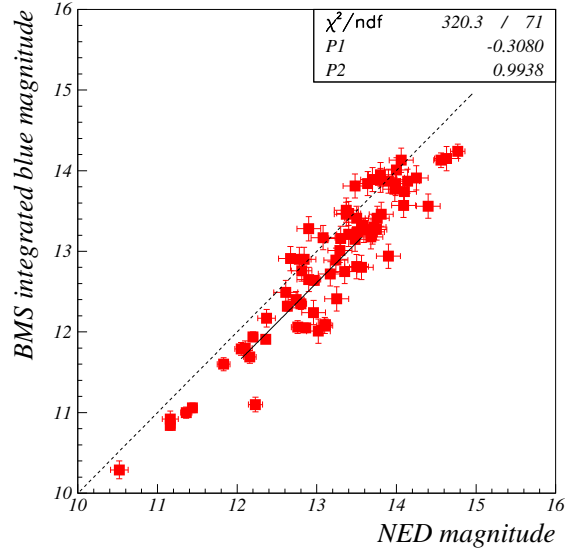


Figure 66: Apparent magnitude from NED vs integrated blue magnitude [3]. The plain line is the best fit to the data and the dashed one indicates $y = x$. The best fit is $y = (0.994 \pm 0.018)x - (0.308 \pm 0.229)$ with possibly a slight bias: the apparent magnitudes from [3] maybe slightly underestimated. Correcting for a larger apparent magnitude would lead to a smaller surface brightness (see Fig. 78) and thus a slightly larger M/L according the the virial formula in [3].

L.2 Data analysis

Selection is applied to the data sample. In addition, the ratio redshift distance from NED over distance from [3] is applied to M/L to correct these ratios on a galaxy per galaxy basis. We use R_{min}/R_{max} from [3] for consistency with the M/L calculations, as it is an important ingredient of the calculation. The results for the three M/L are shown in Figs. 67, 71 and 72. Correcting with the NED distance is not significant: not correcting yields similar

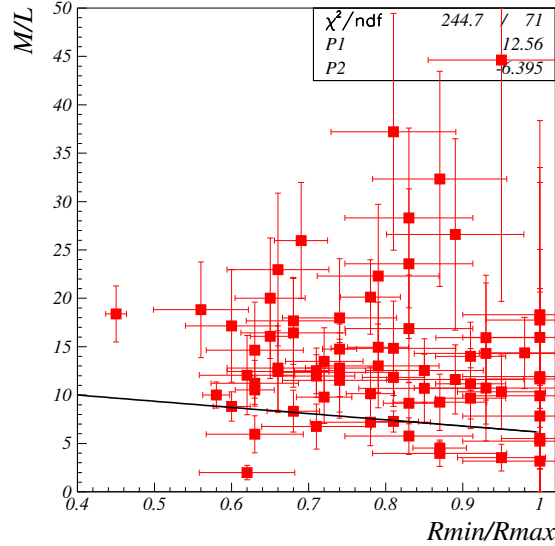


Figure 67: Correlation between M/L and the apparent R_{min}/R_{max} for 73 galaxies using the first virial formula of [3]. The best linear fit (plain line) is $y = (-6.40 \pm 2.32)x + (12.56 \pm 1.79)$, indicating a 2.8σ sigma effect. The large χ^2/ndf is mostly due to ellipsoid projection effect. A 2nd order polynomial fit yields a similar χ^2/ndf .

results (Fig. 68). Similarly, using NED's R_{min}/R_{max} does not change significantly the results (Fig. 69). All the fits give a slope of 6 ± 2 . The best linear fit for the data in Fig. 67 is $y = (-6.40 \pm 2.32)x + (12.56 \pm 1.79)$. A non-zero slope indicates a correlation, so the fit yields a significantly negative slope with a 2.8σ sigma confidence¹⁴, but

¹⁴The point at $R_{min}/R_{max} = 0.45$ stands outside the distribution. Although there is no reason to remove it since it passes the selection criteria, we checked that this datum is not solely responsible for the observed correlation. After removing the datum, the best fit slope becomes 4.01 ± 2.35 , a 1.7 sigma effect. Anticipating upcoming corrections, the final result (Fig. 95) becomes 10.69 ± 2.28 after removing the datum, that is a 4.7 sigma effect.

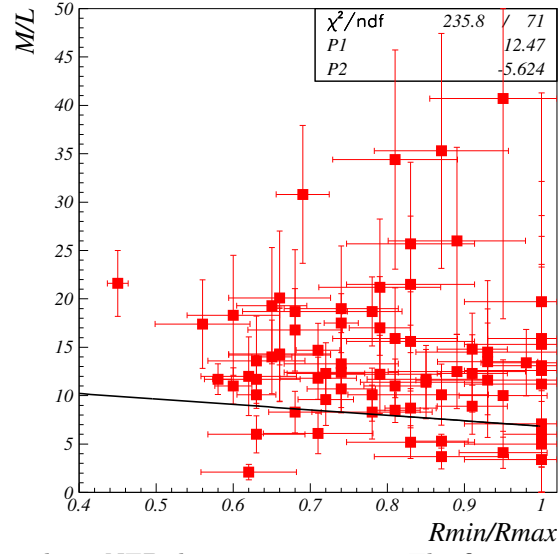


Figure 68: Same as Fig. 67 but without NED distance correction. The fit is $y = (-5.62 \pm 2.48)x + (12.47 \pm 1.91)$.

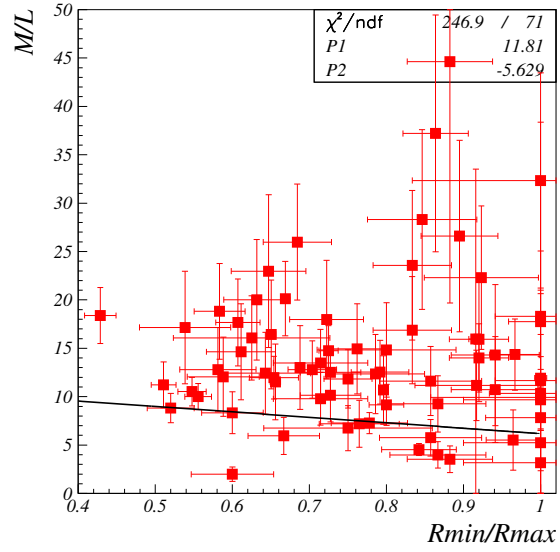


Figure 69: Same as Fig. 67 but with NED R_{min}/R_{max} . The fit is $y = (-5.63 \pm 2.15)x + (11.81 \pm 1.60)$.

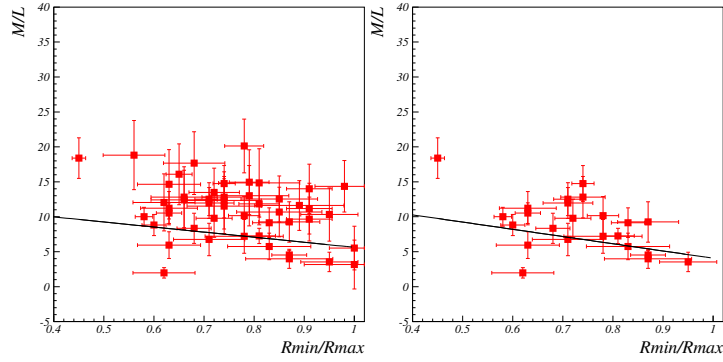


Figure 70: Same as Fig. 67 but using only data with uncertainties $\Delta M/L < 5$ (left panel) or $\Delta M/L < 3$ (right panel). These selections enhance the correlation. Since Ref. [3] gives *relative* uncertainties of similar magnitude for most data, the condition on the *absolute* uncertainty $\Delta M/L < 5$ or 3 removes mostly points at large M/L .

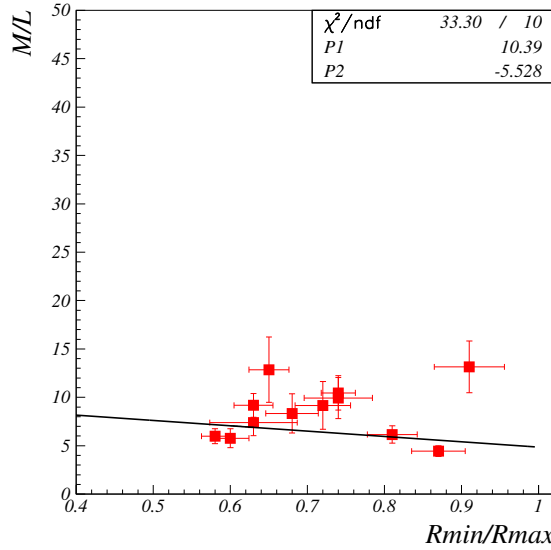


Figure 71: Correlation between M/L and the apparent axis ratio R_{min}/R_{max} for 12 galaxies using the 2nd virial formula of [3]. The best linear fit is $y = (-5.53 \pm 2.70)x + (2.00 \pm 3.71)$.

with a χ^2/ndf of 3.4. A 2nd order polynomial yields a similar χ^2/ndf . As we will show, the large χ^2/ndf of the *linear* fit comes mostly from the effect of the projection of the 3D elliptical galaxy shapes into flat ellipses on the observation plane. This transforms a, e.g., *linear* M/L dependence with *apparent* axis ratio R_{min}/R_{max} into a *non-linear* dependence with the *real* axis ratio.

Alternatively, to assess the correlation, one can compute the Pearson correlation coefficient r given by the covariance of R_{min}/R_{max} and M/L divided by their standard deviations: $r = \text{cov}(R_{min}/R_{max}, M/L) / \sigma_{R_{min}/R_{max}} \sigma_{M/L}$. We have $|r| \leq 1$ and larger values of $|r|$ indicates clearer (small dispersion) and/or stronger (steeper slope) correlations. However, since such statistical analysis does not account for statistical weights, contrarily to a fit, it is ill-suited for our sample that displays a large range in uncertainties. This problem can be partly circumvented by keeping data of a given absolute precision, see Fig. 70. Keeping data for which the uncertainty on M/L is smaller than 5 yields $r = -0.367$ (the sample is reduced to 48 galaxies. For this sample, the best linear fit is $y = (-7.26 \pm 2.39)x + (12.88 \pm 1.88)$, to be compared to the results in Fig. 67). Applying a tighter selection $\Delta M/L < 3$ reduces the sample to 23 galaxies and yields $r = -0.511$ (the best linear fit is $y = (-10.34 \pm 2.71)x + (14.41 \pm 2.06)$). Such values of r reveal a medium to large correlation between M/L and the axis ratio and confirm the conclusion from the fit method. Interestingly, selecting the highest precision data strengthen the M/L vs R_{min}/R_{max} correlation, both for the determination using of the Pearson criterion and for the determination from the linear fit.

Results using the two other determinations of M/L that employ an additional observable (maximum stellar rotation velocity) confirm in both cases (Figs. 71 and 72) the significant negative slope, with similar σ .

Although we assume in this appendix that the correct distances are given by the redshifts, we show in Fig. 73

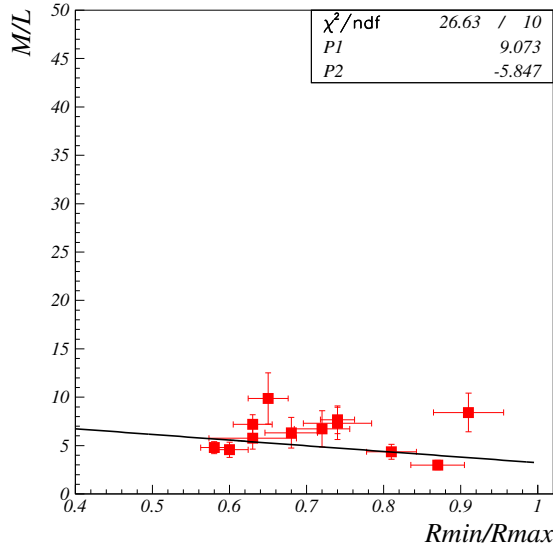


Figure 72: Correlation between M/L and the apparent axis ratio R_{min}/R_{max} for 12 galaxies using the 3^{rd} M/L results from [3]. The best linear fit is $y = (-5.847 \pm 2.32)x + (9.07 \pm 1.70)$.

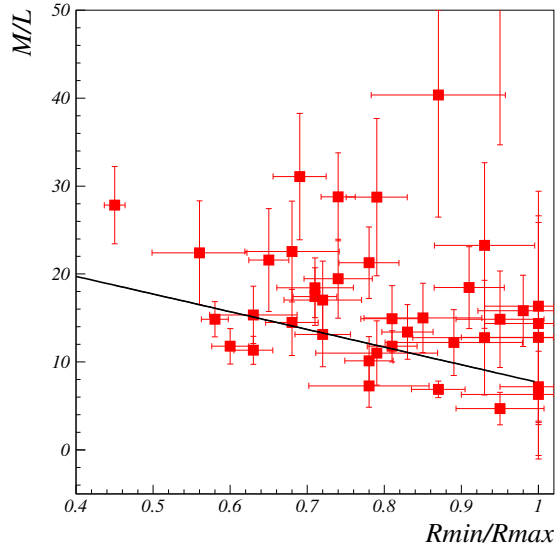


Figure 73: Correlation between M/L and the apparent axis ratio R_{min}/R_{max} for 40 galaxies for which NED distances not based on redshift are available. The linear correlation slope is -20.10 ± 4.14 .

the result using NED distances not based on redshifts. The vertical scale changes following $M/L \rightarrow M/L \times (\text{distance without redshift})/(\text{distance from redshift})$. In that case, since the no-redshift distances are systematically larger than the distances estimated from redshifts (see Fig. 65), the correlation is even stronger, with a slope of -20.10 ± 4.14 i.e, a 5σ effect. (We note that the 40 galaxies that have no-redshift distances available already had a larger correlation, even before the distance correction is applied to M/L .) The Pearson coefficient, after removing data with uncertainty of M/L greater than 5 (this reduces the sample to 25 galaxies), is $r = -0.440$.

L.3 Correlations

Studying correlations is critical since they can bias the studied correlation. Possible measurement or observation biases not directly related to M/L and R_{min}/R_{max} can propagate to them *via* correlations. Furthermore, a (not understood) correlation can be removed either by sample selection or be mathematically corrected for. However, this must be done carefully: if this correlation is actually a consequence of a M/L dependence with R_{min}/R_{max} propagating *via* other correlations, correcting or selecting it could wrongly suppresses the $M/L \longleftrightarrow R_{min}/R_{max}$ correlation. Thus, it is important to check the correlations between variables characterizing an elliptical galaxy and make sure they do not originate from measurement or observation biases. It should then be checked what is the effect of these correlation on M/L vs R_{min}/R_{max} .

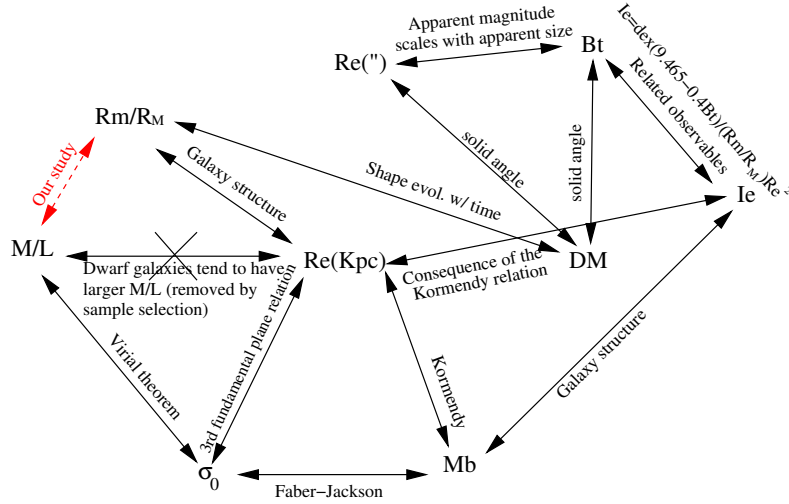


Figure 74: Expected correlations. The red dashed arrow is the possible correlation investigated in this study.

Except in one occasion, we do not investigate the possibility that characteristics other than the ones given in [3] are correlated to both M/L and R_{min}/R_{max} . This could certainly occur and it is a limitation of our analysis to keep in mind. (The exception mentionned above is the metallicity content of elliptical galaxies, see Section L.3.2.)

L.3.1 Expected correlations

- Effective radius Re (Kpc) vs velocity dispersion σ_0 ; effective radius Re (Kpc) vs absolute blue magnitude M_b ; central velocity dispersion σ_0 vs absolute blue magnitude M_b : those are the empirical fundamental plane relations [11], respectively the third fundamental plane relation; the Kormendy relation [66] and the Faber-Jackson relation [41].
- Distance Moduli DM vs effective radius Re'' and integrated blue magnitude B_t : they are trivial reductions of the apparent intensities of quantities with their distance to the observer¹⁵.
- Apparent blue magnitude B_t vs apparent radius Re'' : the larger the apparent radius is, the higher the apparent magnitude tends to be.
- Surface Brightness I_e vs absolute magnitude M_b . *Central* surface brightness vs absolute blue magnitude correlation has been observed [10].
- Integrated blue magnitude B_t vs surface brightness I_e : these two quantities describing the luminosity of a galaxy are related by the equation given in Fig. 74, where Re is in arcsec.
- Axis ratio R_{min}/R_{max} vs effective radius $Re(Kpc)$: this reflects the galaxy structure, with small galaxies tending to be more elongated.
- Mass to light ratio M/L vs effective radius $Re(Kpc)$: at both ends of the mass spectrum, dwarf and giant (e.g. BrClg) galaxies tend to have higher M/L . However, those are excluded from our sample. Consequently, we do not expect a strong correlation here.
- Mass to light ratio M/L vs velocity dispersion σ_0 . The virial theorem links potential and kinetic energy.

¹⁵If the DM span is large, i.e, we observe galaxies over a large time span over which they have time to evolve, we would also expect a correlation between DM and the galaxy characteristics, e.g. the absolute blue magnitude M_b , effective radius $Re(Kpc)$, axis ratio R_{min}/R_{max} or velocity dispersion σ_0 . Decrease of galaxy magnitudes (M_b) with time is established. Structure evolution with time (Re) has been observed by comparing high redshift galaxies to local ones [45]: older massive elliptical galaxies are more compact than younger ones. This would imply a DM -dependence of the axis ratio as well since the decrease of the galaxy size with time increases the rotation speed. Finally, it is known that relaxation with time reduces the central velocity dispersion. However, in our sample, DM varies between ~ 30 and ~ 35.5 , which corresponds to distances of 33 Megalight-years (Mly) and 411 Mly. The time span considered is thus 378 Myears. Since the galaxies were formed long before 411 Myears ago, and since we removed from our sample galaxies displaying signs of mergers or disturbances, galaxies had time to relax to their equilibrium. Consequently, we do not expect the sample galaxies to evolve significantly during the relatively short 378 Myears time span.

L.3.2 Correlation study

In this section we used arrow symbols with the following meanings:

- \Longleftrightarrow : strong correlation;
- \longleftrightarrow : clear correlation;
- \longleftrightarrow : clear but weaker correlation;
- $\leftarrow? \rightarrow$: unclear correlation. Weak if it exists.

The correlation strengths are summarized in Figs. 88 (summary table), 89 (clear correlations) and 90 (unclear weak correlations).

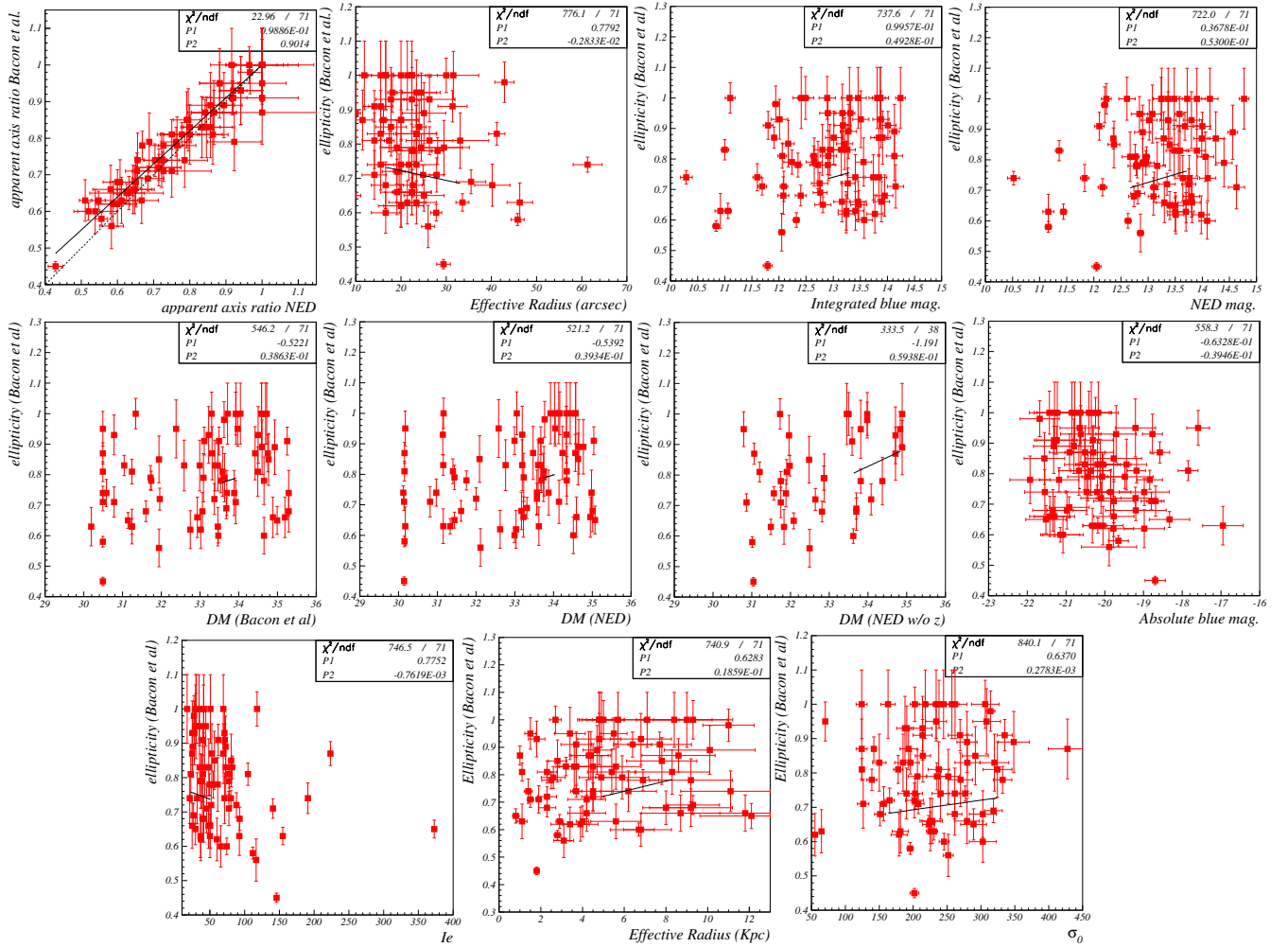


Figure 75: Correlations between apparent R_{min}/R_{max} from [3] and (from top left to bottom right): R_{min}/R_{max} from NED, apparent effective radius Re'' , integrated blue magnitude B_t , magnitude from NED, DM from [3], DM from NED using redshift information, DM from NED without redshift information, absolute blue magnitude, surface brightness I_e , effective radius (parsec) and velocity distribution σ_0 .

Correlations with apparent R_{min}/R_{max} from [3] The origins of the correlations are, from the top left plot to the bottom right one:

1. Apparent axis ratio from [3] vs NED apparent axis ratio: trivial correlation between different measurements of the same quantity. This is already discussed in Fig. 63.
2. Apparent axis ratio from [3] vs apparent effective radius Re'' : this possible weak correlation may be a measurement/observation bias. The more recent data from NED display a similar, even slightly stronger

correlation. It could be a consequence of the $R_{min}/R_{Max} \longleftrightarrow DM \Longleftrightarrow Re^{(“)}$ correlations. Using the fit results¹⁶ $(3.9 \pm 0.4)E^{-2}DM = R_{min}/R_{Max} + c$ and $(-2.1 \pm 0.2)DM = Re^{(“)} + c'$ yields $R_{min}/R_{Max} = (-1.9 \pm 1.6)E^{-2}Re^{(“)} + c''$, in agreement with the observed $R_{min}/R_{Max} = (-0.28 \pm 0.04)E^{-2}Re^{(“)} + C''$. Since $R_{min}/R_{Max} \longleftrightarrow DM$ is a measurement bias, $R_{min}/R_{Max} \longleftrightarrow Re^{(“)}$ is an indirect measurement bias.

3. Apparent axis ratio from [3] vs integrated blue magnitude B_t : this weak correlation may be a measurement/observation bias. The more recent data from NED, in particular the NED apparent axis ratio vs magnitude from NED in Fig. 76, display similar correlations. This correlation could be a consequence of the $R_{min}/R_{Max} \longleftrightarrow DM \Longleftrightarrow B_t$ correlations. Using the fit results $(3.9 \pm 0.4)E^{-2}DM = R_{min}/R_{Max} + c$ and $(1.2 \pm 0.0)B_t = DM + c'$ yields $R_{min}/R_{Max} = (4.7 \pm 0.5)E^{-2}B_t + c''$, in agreement with the observed $R_{min}/R_{Max} = (4.9 \pm 0.5)E^{-2}B_t + C''$. Thus, $R_{min}/R_{Max} \longleftrightarrow B_t$ is an indirect measurement bias.
4. Apparent axis ratio from [3] vs magnitude from NED: same as above.
5. Apparent axis ratio from [3] vs DM from [3]: this weak correlation could be a measurement bias: the further the galaxy, the harder it is to observe and so the rounder it tends to appear due to resolution. The more recent data from NED, in particular the NED apparent axis ratio vs magnitude from NED in Fig. 76, displays a somewhat smaller correlations, supporting that it is a measurement bias.
6. Apparent axis ratio from [3] vs DM from NED using redshift information: see above.
7. Apparent axis ratio from [3] vs DM from NED without redshift information: see above.
8. Apparent axis ratio from [3] vs absolute blue magnitude: the possible weak correlation could come from a measurement bias (the result from NED in Fig. 76 has somewhat smaller correlations). However, it seems to be a consequence of the $R_{min}/R_{Max} \longleftrightarrow DM \Longleftrightarrow M_b$ and $R_{min}/R_{Max} \longleftrightarrow M/L \longleftrightarrow M_b$ correlations: using the fit results $(3.9 \pm 0.4)E^{-2}DM = R_{min}/R_{Max} + c$ and $(-0.53 \pm 0.03)DM = M_b + c'$ yields $R_{min}/R_{Max} = (-7.4 \pm 1.2)E^{-2}M_b + c''$. Using the fit results $(-6 \pm 2)R_{min}/R_{Max} = M/L + c$ and $(-1.7 \pm 0.3)M_b = M/L + c'$ yields $R_{min}/R_{Max} = (0.28 \pm 0.14)M_b + c''$. Adding both results yields $R_{min}/R_{Max} = (0.20 \pm 0.16)M_b + c''$, in reasonable agreement with the observed $R_{min}/R_{Max} = (-3.9 \pm 0.6)E^{-2}M_b + c''$, suggesting that the correlation is an indirect measurement bias. Alternatively, we note that a correlation between axis ratio and mass is known: heavier (hence more luminous) galaxies tend to be rounder. Although we have rejected the heaviest elliptical galaxies, we may be seeing here the same correlation.
9. Apparent axis ratio from [3] vs surface brightness I_e : this clear correlation cannot be a (direct) measurement bias: it does not have the expected pattern (the dimmer, the more difficult the measurement so the larger R_{min}/R_{Max} would be). In addition, the newer NED data indicate a stronger correlation, see Fig. 76. This correlation could be a consequence of the $I_e \longleftrightarrow DM \longleftrightarrow R_{min}/R_{Max}$ correlations. Using the fit results $(-1.7 \pm 0.1)E^{-2}I_e = DM + c$ and $(3.9 \pm 0.4)E^{-2}DM = R_{min}/R_{Max} + c'$ yields $R_{min}/R_{Max} = (-6.6 \pm 1.1)E^{-4}I_e + c''$, in agreement with the observed $R_{min}/R_{Max} = (-7.6 \pm 0.7)E^{-4}I_e + C''$. This supports that the correlation is an indirect measurement bias.
10. Apparent axis ratio from [3] vs effective radius (parsec): this possible correlation would agree with the observation that smaller galaxies tend to be more elongated. However, this correlation appears to be a consequence of the $Re(Kpc) \longleftrightarrow DM \longleftrightarrow R_{min}/R_{Max}$ correlations. Using the fit results $(1.18 \pm 0.06)DM = Re + c$ and $(3.9 \pm 0.4)E^{-2}DM = R_{min}/R_{Max} + c'$ yields $R_{min}/R_{Max} = (3.3 \pm 0.5)E^{-2}Re + c''$, in agreement with the observed $R_{min}/R_{Max} = (1.9 \pm 0.2)E^{-2}I_e + C''$. This is an indirect measurement bias.
11. Apparent axis ratio from [3] vs velocity distribution σ_0 . No significant correlation is seen. The newer data from NED show no correlation. We expected that $R_{min}/R_{Max} \longleftrightarrow M/L \Longleftrightarrow \sigma_0$, $R_{min}/R_{Max} \longleftrightarrow DM \Longleftrightarrow \sigma_0$, $R_{min}/R_{Max} \longleftrightarrow Re(Kpc) \Longleftrightarrow \sigma_0$ and $R_{min}/R_{Max} \longleftrightarrow M_b \Longleftrightarrow \sigma_0$, would contribute to secondary correlations: using the fit results $(-6 \pm 2)R_{min}/R_{Max} = M/L + c$ and $(5.4 \pm 0.4)E^{-2}\sigma_0 = M/L + c'$ yields $R_{min}/R_{Max} = (-9.0 \pm 3.7)E^{-3}\sigma_0 + c''$. Using the fit results $(3.9 \pm 0.4)E^{-2}DM = R_{min}/R_{Max} + c$ and $(1.24 \pm 0.08)E^{-2}\sigma_0 = DM + c'$ yields $R_{min}/R_{Max} = (4.8 \pm 0.8)E^{-4}\sigma_0 + c''$. Using the fit results $(1.9 \pm 0.2)E^{-2}Re = R_{min}/R_{Max} + c$ and $(1.67 \pm 0.08)E^{-2}\sigma_0 = Re + c'$ yields $R_{min}/R_{Max} = (3.17 \pm 0.5)E^{-4}\sigma_0 + c''$. Using the fit results $(-4.0 \pm 0.6)E^{-2}M_b = R_{min}/R_{Max} + c$ and $(-1.29 \pm 0.08)E^{-2}\sigma_0 = M_b + c'$ yields $R_{min}/R_{Max} = (5.2 \pm 1.1)E^{-4}\sigma_0 + c''$. Naively adding linearly the four results yields $R_{min}/R_{Max} = (-7.7 \pm 4.0)E^{-3}\sigma_0 + c''$, a 2 sigma disagreement with the observed $R_{min}/R_{Max} = (0.3 \pm 0.1)E^{-3}\sigma_0 + c''$. However, these results cannot be simply added linearly because of the strong correlation between $Re(Kpc)$ & M_b . Also, M/L & M_b , DM & M_b and $Re(Kpc)$ & DM show significant correlations. We assume that overall the four results mostly cancel each other as suggested by the opposite signs of the correlations.

¹⁶This type of calculation is merely indicative, given the large χ^2/ndf of the fits.

Correlation with apparent R_{min}/R_{max} from NED The origins of the correlations are discussed in the previous section (Section L.3.2).

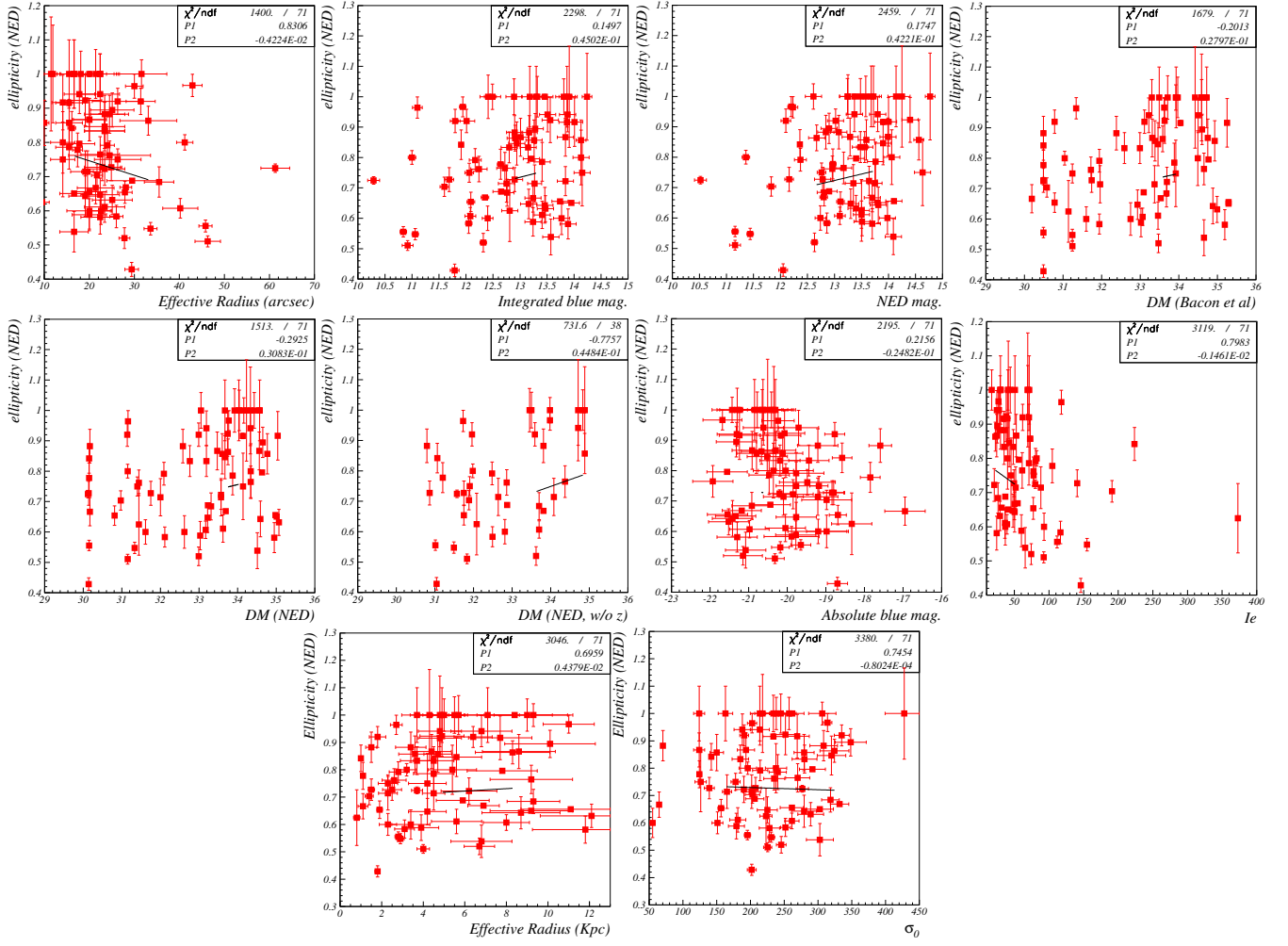


Figure 76: Correlations between the apparent R_{min}/R_{max} from NED and (from top left to bottom right): apparent effective radius Re'' , integrated blue magnitude B_t , magnitude from NED, DM from [3], DM from NED using redshift information, DM from NED without redshift information, absolute blue magnitude, surface brightness I_e , effective radius (parsec) and velocity distribution σ_0 .

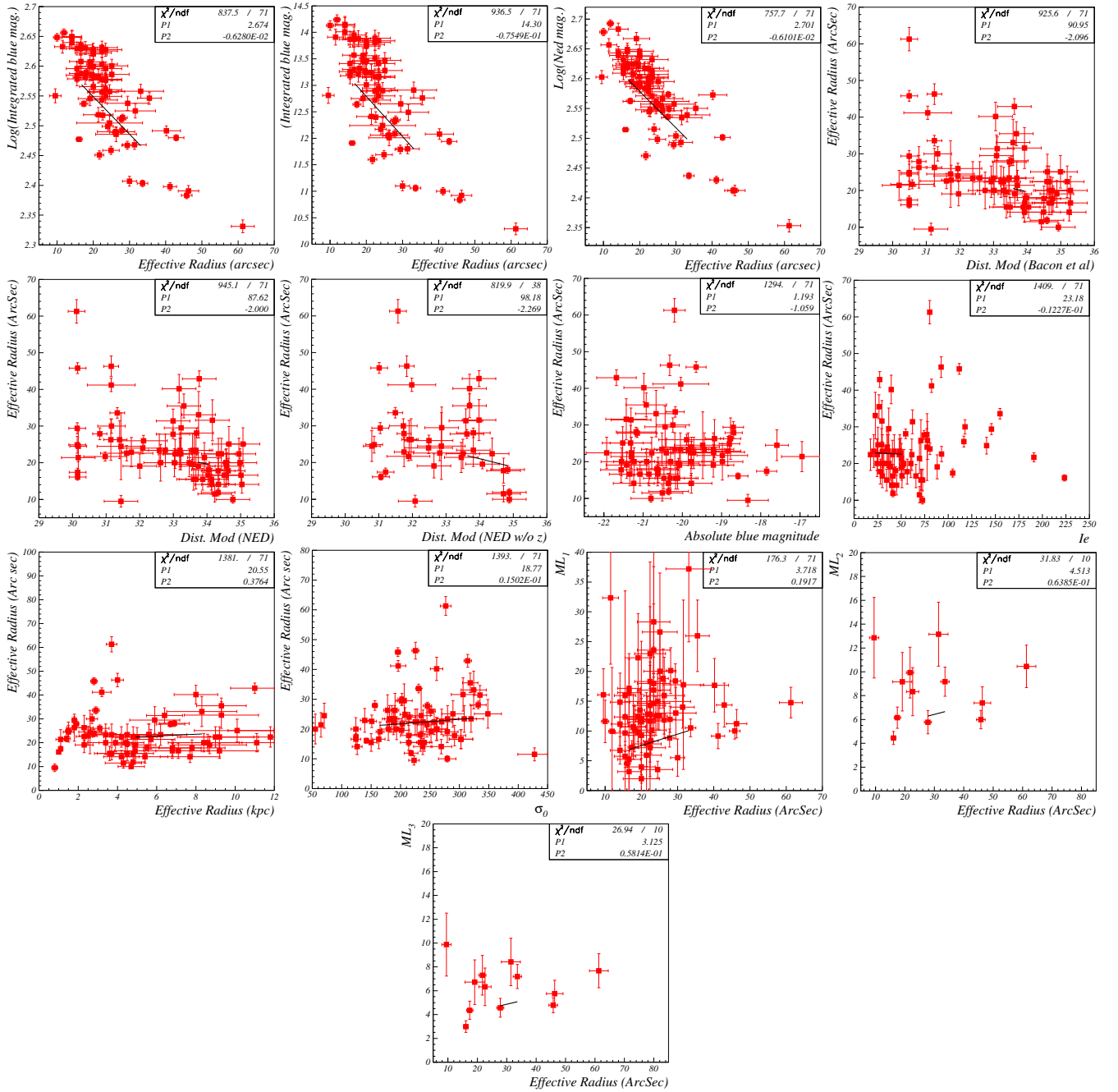


Figure 77: Correlations between the apparent effective radius $Re(“)$ and (from top left to bottom right): integrated blue magnitude B_t (with log and linear scales), magnitude from NED, DM from [3], DM from NED using redshift information, DM from NED without redshift information, absolute blue magnitude, surface brightness I_e , effective radius (parsec), velocity distribution σ_0 and M/L .

Apparent effective radius $Re(“)$ correlations The origins of the correlations are, from the top left plot to the bottom right one:

1. Effective radius $Re(“)$ vs integrated blue magnitude B_t : this strong correlation is expected from physics since the larger the apparent radius, the larger the apparent magnitude tends to be.
2. Same as above but with a linear vertical scale.
3. $Re(“)$ vs magnitude from NED: same as above.
4. $Re(“)$ vs DM from [3]: this is the trivial decrease of apparent size with distance to the observer.
5. $Re(“)$ vs DM from NED using redshift information: same as above.

6. Re'' vs DM from NED without redshift information: same as above.
7. Re'' vs absolute blue magnitude: no clear correlation is seen. A linear (or any functional) fit fails to account for the data distribution. We were expecting a clear secondary correlation of opposite sign from the $M_b \iff DM \iff Re''$ correlations. Using the fit results $(-0.53 \pm 0.03)DM = M_b + c$ and $(-2.1 \pm 0.2)DM = Re'' + c'$ yields $Re'' = (4.0 \pm 0.6)M_b + c''$. The other important contribution is from the $M_b \iff Re \text{ (Kpc)} \iff Re''$ correlations. Using the fit results $(-3.4 \pm 0.1)M_b = Re \text{ (Kpc)} + c$ and $(0.4 \pm 0.1)Re \text{ (Kpc)} = Re'' + c'$ yields $Re'' = (-1.4 \pm 0.4)M_b + c''$. Again, these two results cannot be added linearly because of correlations between DM & $Re \text{ (Kpc)}$, but the opposite signs of the two correlations suggest a cancellation.
8. Re'' vs surface brightness I_e : a weak possible correlation is seen. The correlations $Re'' \iff Bt \iff I_e$ and $Re'' \iff DM \iff I_e$ can both contribute to create it. Using the linear fit results $(-7.6 \pm 0.2)E^{-2}Re'' = Bt + c$ and $(-7.5 \pm 0.2)E^{-3}I_e = Bt + c'$ yields $Re'' = (9.8 \pm 0.1)E^{-1}I_e + c''$. Using the linear fit results $(-2.1 \pm 0.2)DM = Re'' + c$ and $(-1.7 \pm 0.1)E^{-2}I_e = DM + c'$ yields $Re'' = (3.6 \pm 0.1)E^{-2}I_e + c''$. As Bt & DM are strongly correlated, we cannot simply add these results, but their same sign suggests a strong correlation, in disagreement with the sign of the observed possible correlation. However, this disagreement may stem from the unreliable fit. The correlation itself, if it exists, is weak.
9. Re'' vs effective radius (parsec): because a distance in Kpc is given by $10^{0.2DM-2}$, then $Re'' = Re \text{ (Kpc)} / 10^{0.2DM-2} / 4.85E^{-6}$ ($4.85E^{-6}$ converts rad in arcsec).
10. Re'' vs velocity distribution σ_0 : no, or unclear, weak correlation.
11. Re'' vs M/L : this weak correlation may arise from the correlations $Re'' \iff R_{min}/R_{max} \iff M/L$, $Re'' \iff \sigma_0 \iff M/L$, $Re'' \iff DM \iff M/L$ and $Re'' \iff Bt \iff M/L$. Using the linear fit results $(-4.2 \pm 0.3)E^{-3}Re'' = R_{min}/R_{max} + c$ and $(-6 \pm 2)R_{min}/R_{max} = M/L + c'$ yields $M/L = (2.5 \pm 1.0)E^{-2}Re'' + c''$. Using the linear fit results $(1.5 \pm 0.4)E^{-2}\sigma_0 = Re'' + c$ and $(5.4 \pm 0.4)E^{-2}\sigma_0 = M/L + c'$ yields $M/L = (3.6 \pm 1.2)Re'' + c''$. Using the linear fit results $(-2.0 \pm 0.2)DM = Re'' + c$ and $(0.5 \pm 0.2)DM = M/L + c'$ yields $M/L = (-2.5 \pm 1.3)E^{-1}Re'' + c''$. Using the linear fit results $(-7.6 \pm 0.2)E^{-2}Re'' = Bt + c$ and $(-1.3 \pm 0.3)Bt = M/L + c'$ yields $M/L = (9.9 \pm 2.5)E^{-2}Re'' + c''$. R_{min}/R_{max} & DM , R_{min}/R_{max} & Bt , σ_0 & DM and DM & Bt are correlated. However, adding the contributions, we obtain $M/L = (3.47 \pm 1.4)Re'' + C''$, just 2.3σ away from the observed $M/L = (0.19 \pm 0.03)Re'' + C''$. This suggests that this weak correlation may originate from the four correlations $Re'' \iff R_{min}/R_{max} \iff M/L$, $Re'' \iff \sigma_0 \iff M/L$, $Re'' \iff DM \iff M/L$ and $Re'' \iff Bt \iff M/L$.

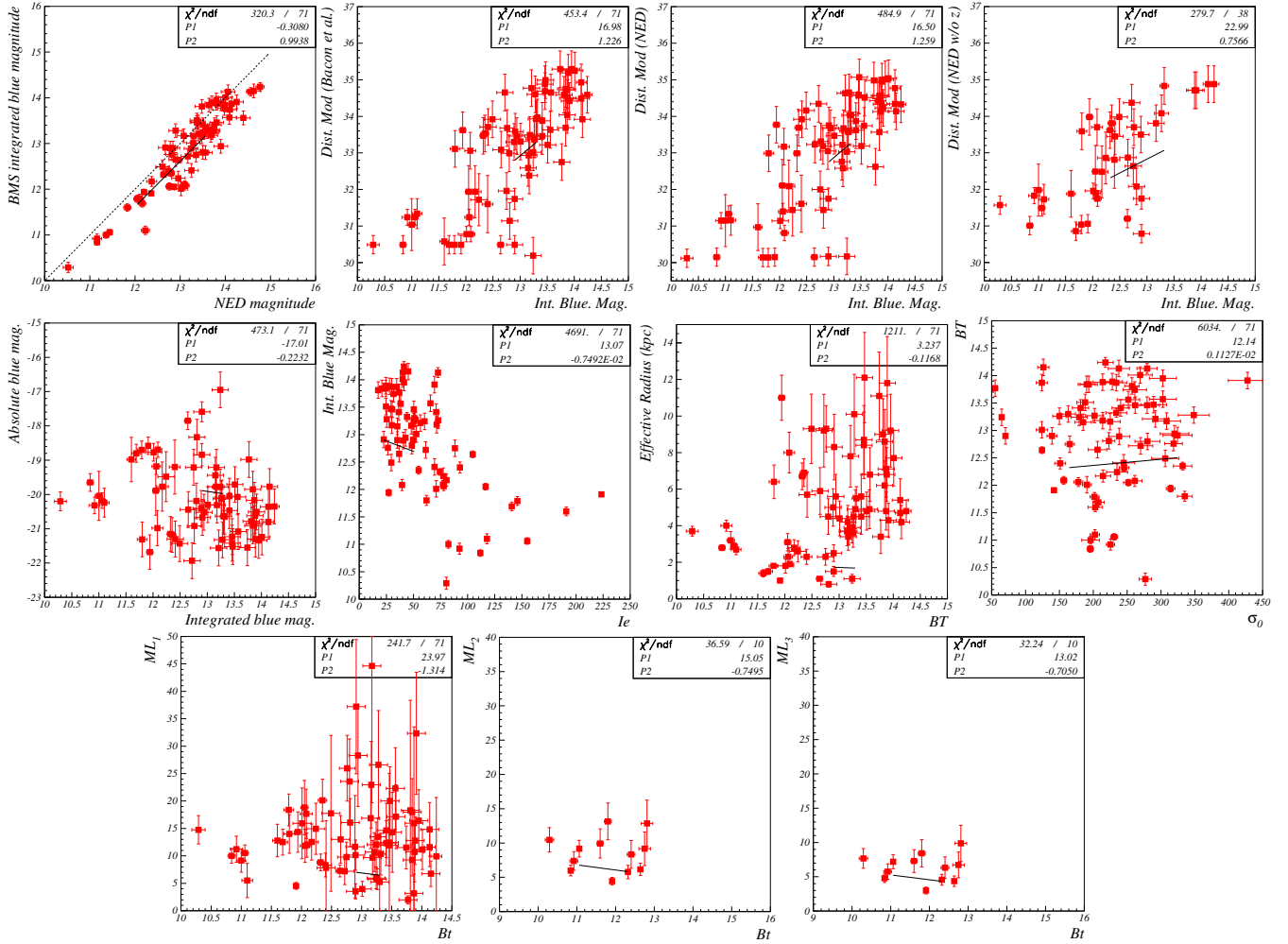


Figure 78: Correlations between the integrated blue magnitude B_t and (from top left to bottom right): magnitude from NED, DM from [3], DM from NED using redshift information, DM from NED without redshift information, absolute blue magnitude, surface brightness I_e , effective radius (parsec), velocity distribution σ_0 and M/L .

Integrated blue magnitude correlations The origins of the correlations are, from the top left plot to the bottom right one:

1. Integrated blue magnitude B_t vs magnitude from NED: this was already discussed (see Fig. 66).
2. B_t vs DM from [3]: this clear strong correlation is due to the trivial decrease of apparent brightness with distance to the observer.
3. B_t vs DM from NED using redshift information: same as above.
4. B_t vs DM from NED without redshift information: same as above.
5. B_t vs absolute blue magnitude: no or little correlation is observed. However we expect 3 strong secondary correlations to contribute: $B_t \iff DM \iff M_b$, $B_t \iff I_e \iff M_b$ and $B_t \iff Re(Kpc) \iff M_b$. Using the linear fit results $(1.23 \pm 0.04)B_t = DM + c$ and $(-0.53 \pm 0.03)DM = M_b + c'$ yields $M_b = (-0.65 \pm 0.06)B_t + c''$. Using the linear fit results $(-7.5 \pm 0.2)E^{-3}I_e = B_t + c$ and $(8.1 \pm 0.9)E^{-3}I_e = M_b + c'$ yields a contribution $M_b = (-1.08 \pm 0.15)B_t + c''$. Using the linear fit results $(-0.12 \pm 0.05)B_t = Re(Kpc) + c$ and $(-1.56 \pm 0.09)M_b = Re(Kpc) + c'$ yields a contribution $M_b = (0.08 \pm 0.04)B_t + c''$. These contributions cannot be linearly added since DM & I_e , DM & M_b , DM & $Re(Kpc)$ and I_e & $Re(Kpc)$ display significant correlations.
6. B_t vs surface brightness I_e : these observables are related by $I_e = dex(9.465 - 0.4B_t)/(R_{min}/R_{max})Re''^2$.
7. B_t vs effective radius (parsec): we expect a positive correlation from $Re(Kpc) \iff DM \iff B_t$. This is observed. However, we cannot verify it numerically due to the failure of the $Re(Kpc)$ vs B_t fit.

8. B_t vs velocity distribution σ_0 : no correlation is seen. We expected some contribution from $\sigma_0 \longleftrightarrow DM \longleftrightarrow B_t$, $\sigma_0 \longleftrightarrow Re(Kpc) \longleftrightarrow B_t$ and σ_0 . Using the linear fit results $(1.23 \pm 0.04)B_t = DM + c$ and $(1.24 \pm 0.08)E^{-2}\sigma_0 = DM + c'$ yields a contribution $B_t = (1.01 \pm 0.10)E^{-2}\sigma_0 + c''$. The second correlation cannot be computed due to the failure of the $Re(Kpc)$ vs B_t fit. However, we can estimate that it yields a contribution $B_t \sim 6E^{-3}\sigma_0 + c''$. Overall, the two small contributions agree with the observed absence of correlation (the smaller $B_t = (1.1 \pm 0.2)E^{-3}\sigma_0 + C''$ is unreliable due to the large χ^2/ndf of the fit).
9. B_t vs M/L . No correlation is expected (all secondary correlations involve a weak/unclear correlation). This is what is observed.

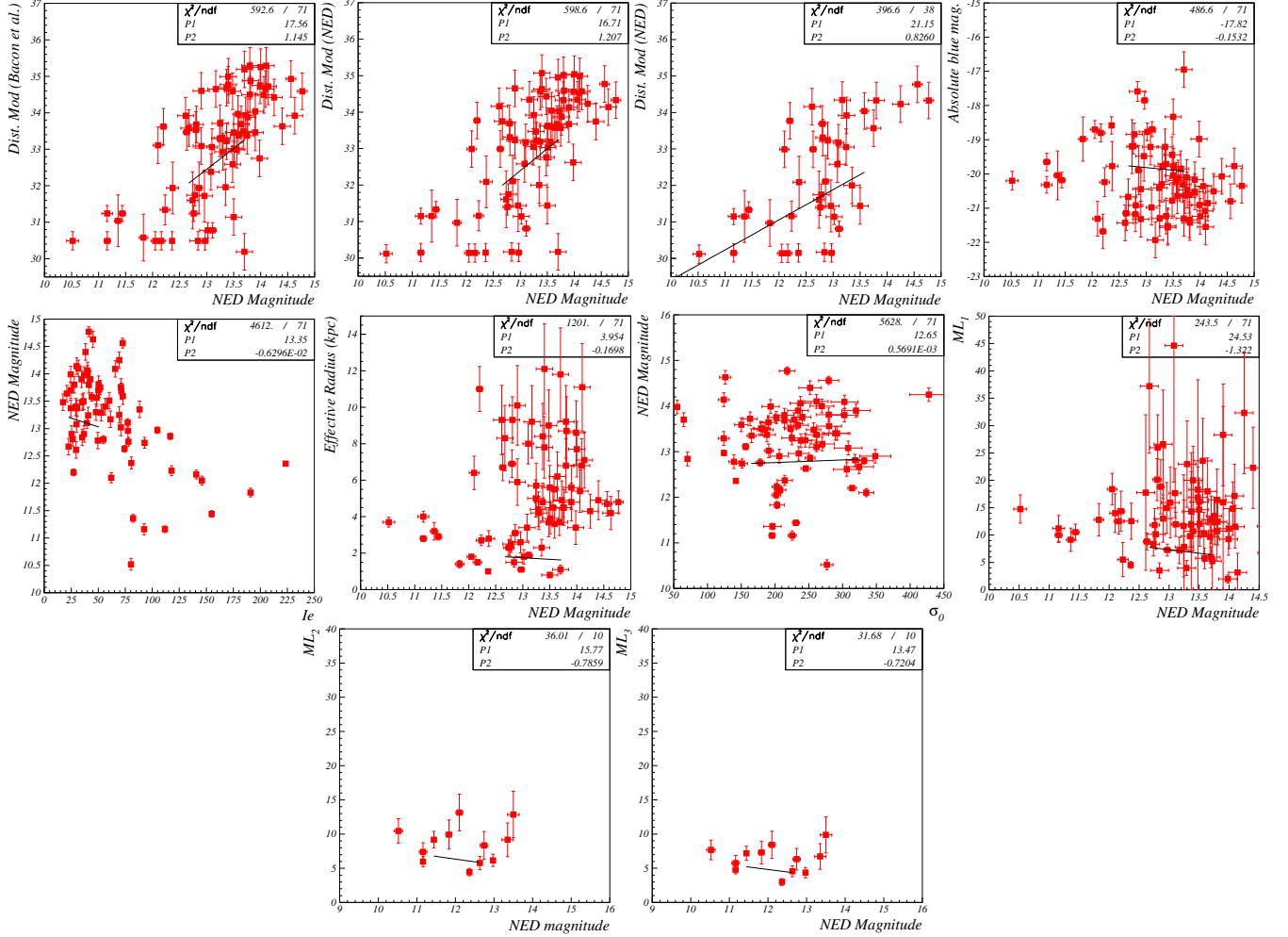


Figure 79: Correlations between the NED apparent magnitude and (from top left to bottom right): DM from [3], DM from NED using redshift information, DM from NED without redshift information, absolute blue magnitude, surface brightness I_e , effective radius (parsec), velocity distribution σ_0 and M/L .

Magnitude from NED correlations The origins of the correlations are similar to the ones discussed in Section L.3.2.

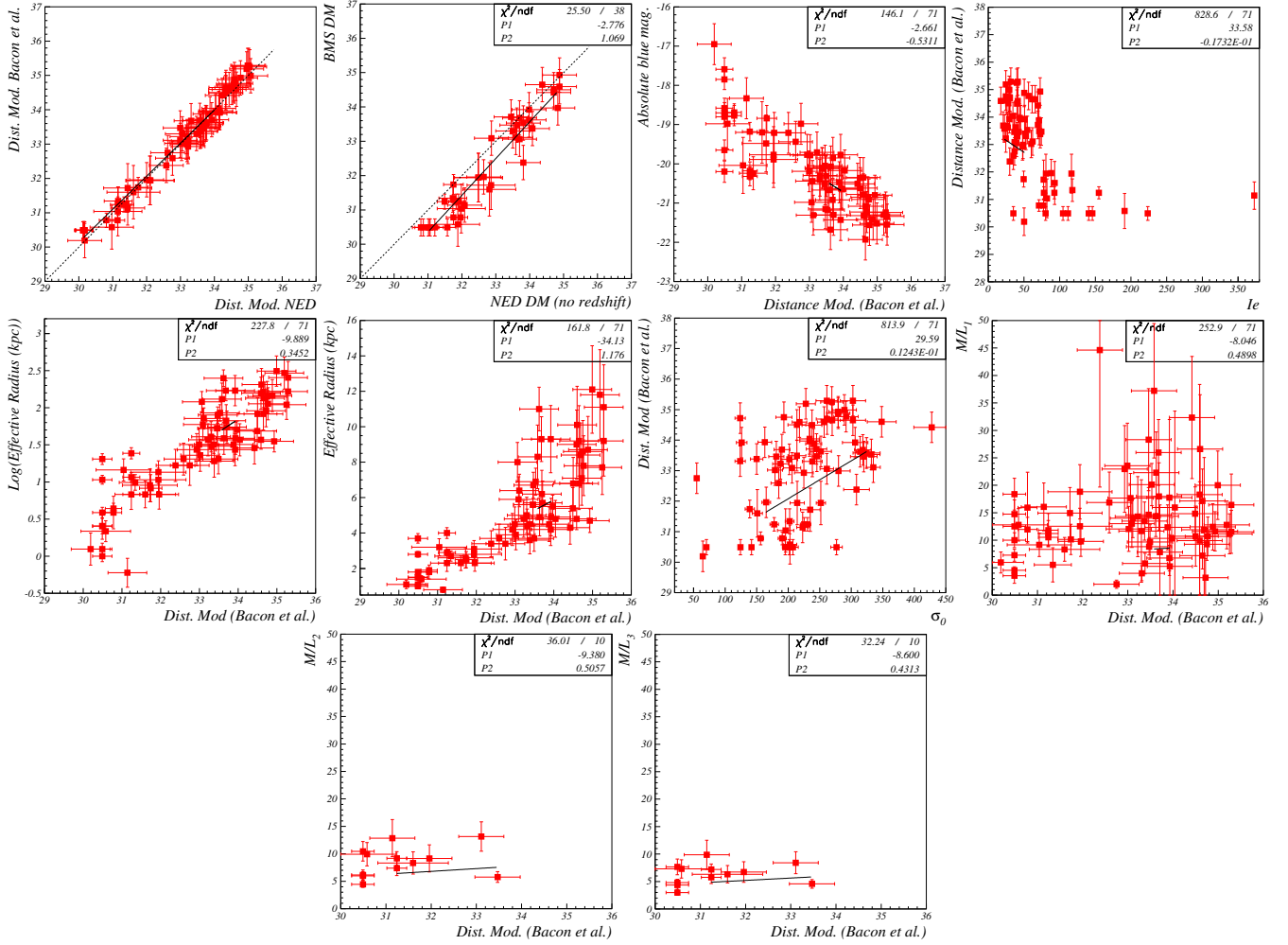


Figure 80: Correlations between the distance modulus DM from [3] and (from top left to bottom right): DM from NED using redshift information, DM from NED without redshift information, absolute blue magnitude, surface brightness I_e , $\log(\text{effective radius (parsec)})$, effective radius (parsec), velocity distribution σ_0 and M/L .

Distance Moduli ([3]) correlations The origins of the correlations are, from the top left plot to the bottom right one:

1. Distance modulus DM from [3] vs DM from NED using redshift information: this expected strict correlation was already discussed, see Fig. 64.
2. DM from [3] vs DM from NED without redshift information: this expected strict correlation was already discussed, see Fig. 65.
3. DM from [3] vs absolute blue magnitude: we observe a strong correlation. Since we do not expect significant time evolution, this must be an observational bias: at large DM , more luminous galaxies are easier to observe. At smaller DM , both luminous and dimmer galaxies can be seen, but the presence probability of luminous elliptical galaxies is smaller since the corresponding volume is smaller and luminous galaxies are rarer than dimmer ones. In all, luminous galaxies tend to be seen at large distances while dimmer ones are seen at shorter distances. That this is a measurement bias and not a physical characteristic is confirmed by the absence of DM vs M/L correlation, see point 8. below.
4. DM from [3] vs surface brightness I_e : surface brightness is independent of distances. The correlation seen is expected from the fact that $Re(Kpc)$ and DM are almost linearly related (see the two next plots) and that I_e and $Re(Kpc)$ are also correlated (consequence of the Kormendy relation [66]). Indeed, the pattern of I_e vs DM strongly resembles the one of I_e vs $Re(Kpc)$. This is an indirect consequence of the $M_b \iff DM$ observation bias.
5. DM from [3] vs effective radius (parsec): a significant secondary (indirect) correlation is expected from the Kormendy correlation $Re(Kpc) \iff M_b$ and $M_b \iff DM$ correlation. Using the linear fit results

$(-1.58 \pm 0.09)M_b = Re + c$ and $(-0.53 \pm 0.03)DM = M_b + c'$ yields $Re = (0.84 \pm 0.1)DM + c''$. Another indirect correlation is expected from the 3^{rd} fundamental plan correlation $Re(Kpc) \iff \sigma_0$ and the $\sigma_0 \iff DM$ correlation. Using the fit results $(1.67 \pm 0.08)E^{-2}\sigma_0 = Re + c$ and $(1.24 \pm 0.08)E^{-2}\sigma_0 = DM + c'$ yields $Re = (1.35 \pm 0.15)DM + c''$. These secondary correlations are similar to the observed $Re = (1.18 \pm 0.06)DM + c''$ (linear fit). In addition, we expect the same type of observational bias as for the DM vs M_b correlation. All in all, this is a consequence of the $M_b \iff DM$ observation bias.

6. Same as above but with a linear vertical scale.
7. DM from [3] vs velocity distribution σ_0 : we observe a significant correction of σ_0 with DM . We expect strong secondary correlations due to the Kormendy relation, the DM vs M_b observational bias, the Faber-Jackson and the 3^{rd} fundamental plane relations. This is again an indirect consequence of the $M_b \iff DM$ and $Re(Kpc) \iff DM$ observation biases.
8. DM from [3] vs M/L : we observe little correlation. This confirms that the DM vs absolute blue magnitude correlation is an unphysical bias: if the blue magnitude truly depended on DM , then, the M/L would display a similar dependence since we do not expect the mass of an undisturbed galaxy to evolve with time.

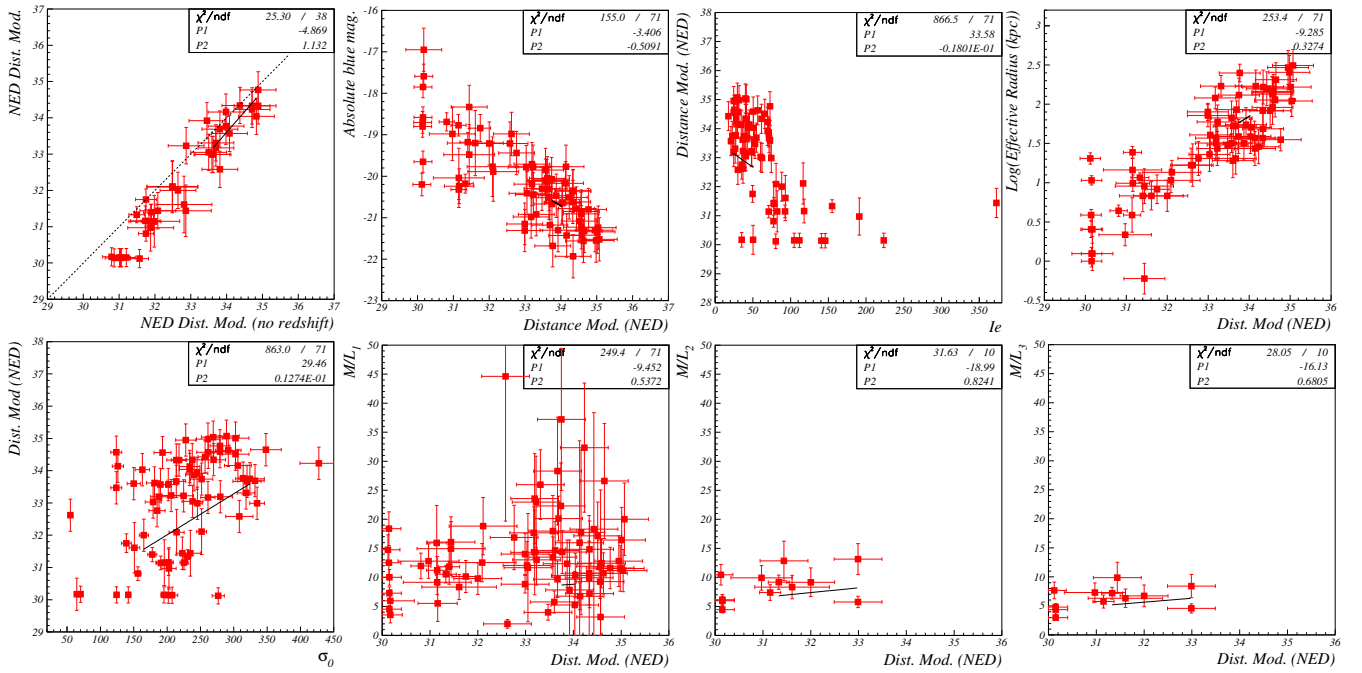


Figure 81: Correlations between the distance modulus from NED using redshift information and (from top left to bottom right): distance modulus from NED without redshift information, absolute blue magnitude, surface brightness I_e , effective radius (parsec), velocity distribution σ_0 and M/L .

Distance Moduli (NED with redshift information) correlations The origins of the correlations are the same as the ones discussed in Section L.3.2.

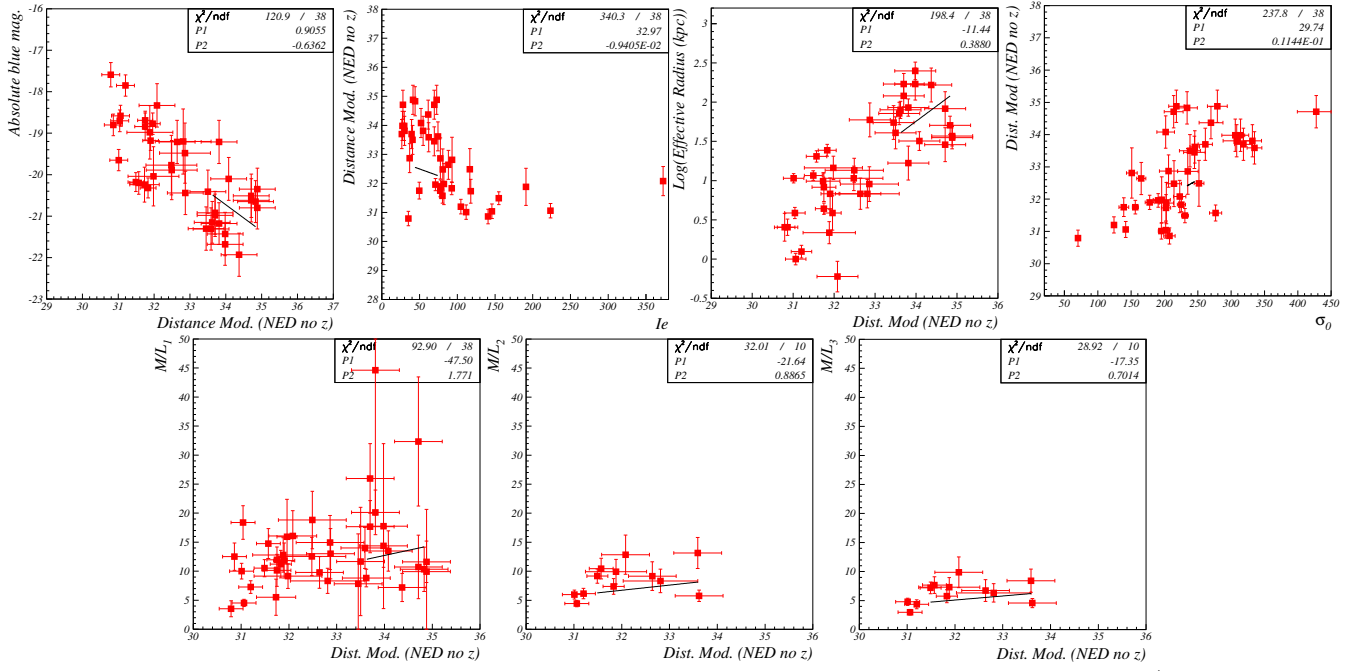


Figure 82: Correlations between the distance modulus from NED without redshift information and (from top left to bottom right): absolute blue magnitude, surface brightness I_e , effective radius (parsec), velocity distribution σ_0 and M/L .

Distance Moduli (NED without redshift information) correlations The origins of the correlations are the same as the ones discussed in Section L.3.2.

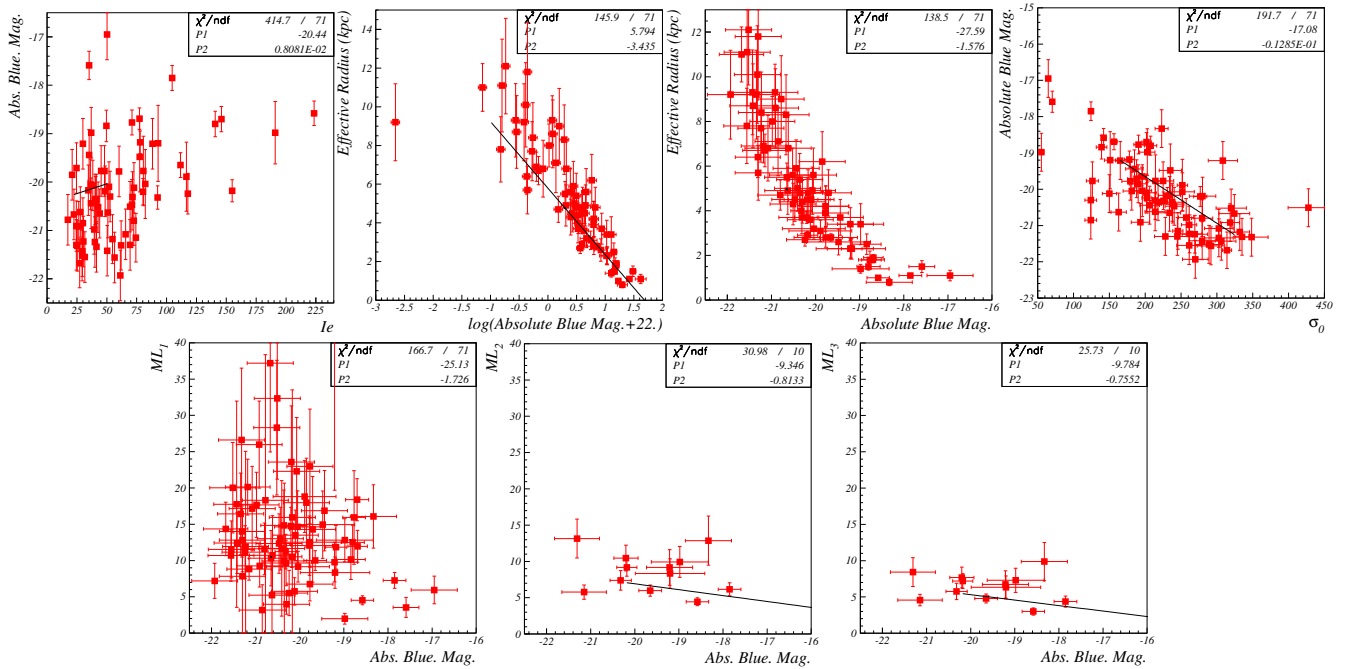


Figure 83: Correlations between the absolute blue magnitude and (from top left to bottom right): surface brightness I_e , effective radius (parsec), velocity distribution σ_0 and M/L .

Absolute magnitude M_b correlations The origins of the correlations are, from top left to bottom right:

1. Absolute blue magnitude M_b vs surface brightness I_e : this pattern agrees with the observed central surface brightness vs M_b relation [10]. However, it could also arise from two secondary correlations: $M_b \iff DM \iff I_e$ and possibly $M_b \iff Re(\text{kpc}) \iff I_e$. Using the linear fit results $(-0.53 \pm 0.03)DM =$

$M_b + c$ and $(-1.73 \pm 0.09)E^{-2}I_e = DM + c'$ yields $M_b = (0.92 \pm 0.10)E^{-2}I_e + c''$. Using the linear fit results $(-8.1 \pm 0.5)E^{-3}I_e = Re + c$ and $(-1.58 \pm 0.09)M_b = Re + c'$ yields a negligible contribution $M_b = (-5.1 \pm 0.6)E^{-3}I_e + c''$. This agrees with the observed $M_b = (0.81 \pm 0.09)I_e + C''$. This plot, however, suggests to reject the two lowest M_b points since they are close to the dwarf elliptical locus [10].

2. M_b vs effective radius (parsec): this is the well known Kormendy relation [66].
3. M_b vs velocity distribution σ_0 : this is the well known Faber-Jackson relation [41].
4. M_b vs M/L : a clear weak correlation is seen. It seems to be due to the virial theorem and the Kormendy relation: $M/L \iff \sigma_0 \iff M_b$. Using the linear fit results $(5.4 \pm 0.4)E^{-2}\sigma_0 = M/L + c$ and $(-1.3 \pm 0.1)E^{-2}\sigma_0 = M_b + c'$ yields $M/L = (-4.2 \pm 0.6)M_b + c''$. This is in qualitative agreement with the observed correlation. The value from the fit: $M/L = (-1.7 \pm 0.3)M_b + C''$ is underestimated since a linear form is not adapted for the fit. Another contribution could result from the fact that luminous/large elliptical galaxies tend to have stars that are more metal-rich than less luminous elliptical galaxies [94]. This tends to increase the M/L with increasing absolute luminosity M_b . In principle, this possibility has to be ruled out in order to cleanly interpret a dependence of M/L with R_{min}/R_{max} . In practice, there is only an uncertain weak correlation between R_{min}/R_{max} and M_b so it would have little influence on the M/L vs R_{min}/R_{max} dependence. Furthermore, as explained in the Section L.1, the most luminous galaxies are excluded from our data set. All in all, we can ignore the consequence that large elliptical galaxies are more metal rich.

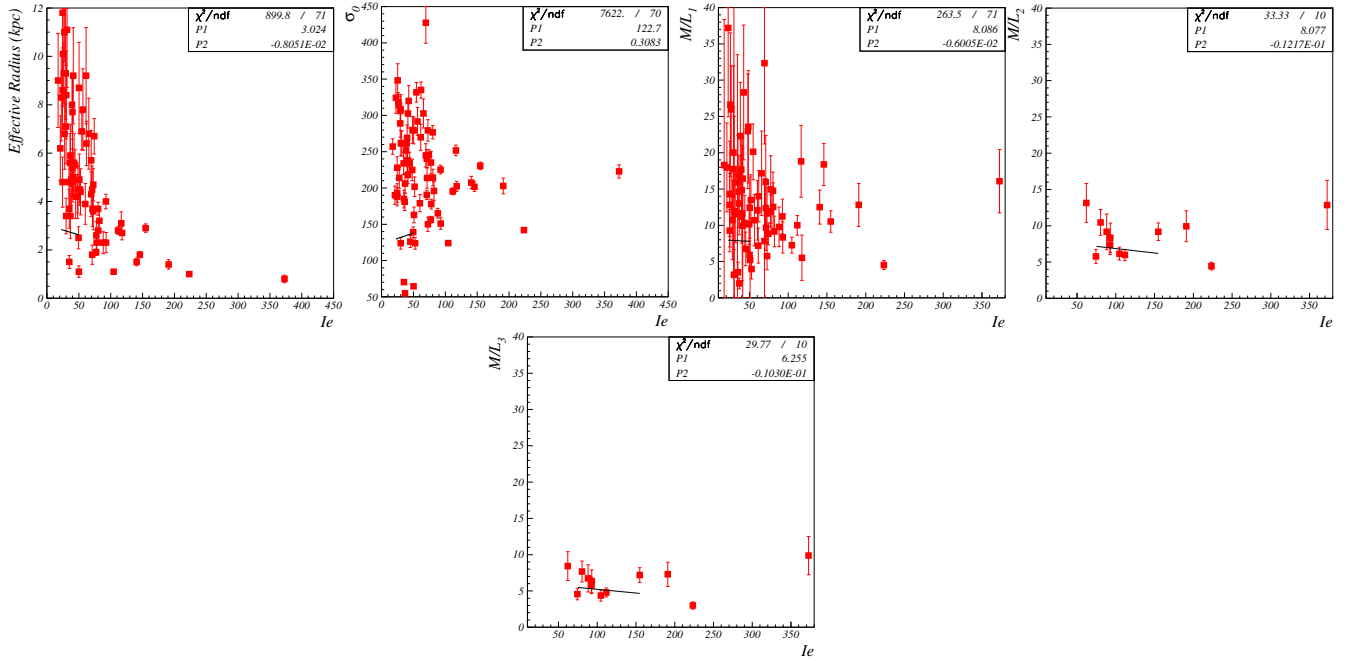


Figure 84: Correlations between the surface brightness I_e and (from top left to bottom right): effective radius (parsec), velocity distribution σ_0 and M/L .

Surface Brightness I_e correlations. The origins of the correlations are, from top left to bottom right:

1. Surface brightness I_e vs effective radius (parsec): this is expected from the Kormendy relation: it implies that the larger the galaxy, the lower its surface brightness (see e.g. [11] page 24), as seen on the plot.
2. I_e vs velocity distribution σ_0 : this is expected from the $Re(Kpc) \iff \sigma_0 \iff I_e$ distributions.
3. I_e vs M/L : this is similar to the just discussed I_e vs σ_0 distribution due to the strong $\sigma_0 \iff M/L$ correlation.

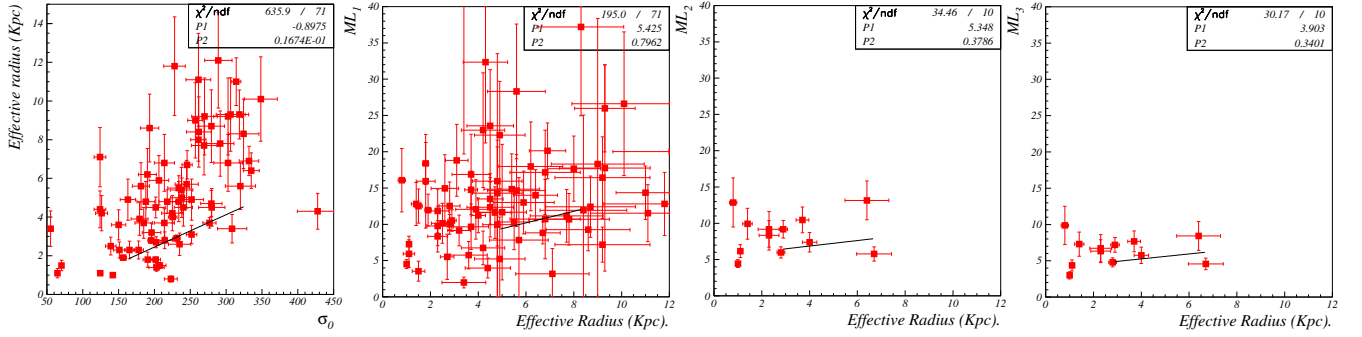


Figure 85: Correlations between the absolute effective radius and (from left to right): velocity distribution σ_0 and M/L .

Absolute effective radius Re correlations The origins of the correlations are, from left to right:

1. Effective radius (parsec) vs velocity distribution σ_0 : this correlation is the well known 3rd plane relation.
2. Effective radius (parsec) vs M/L : there is no or little correlation. This is opposite to what would have been expected if our sample had included dwarf elliptical galaxies, since they tend to have larger M/L . This validates our choice of selection criteria.

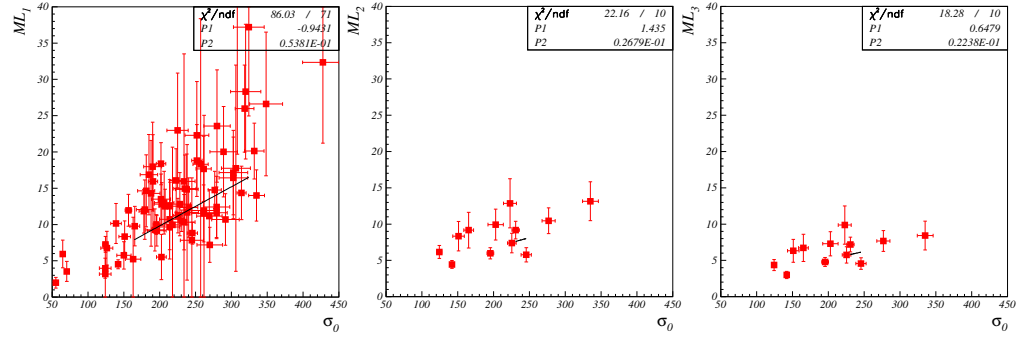


Figure 86: Correlations between the velocity distribution σ_0 and M/L .

Central velocity distribution σ_0 correlations The origin of the velocity distribution σ_0 vs M/L ratios correlation is the virial theorem.

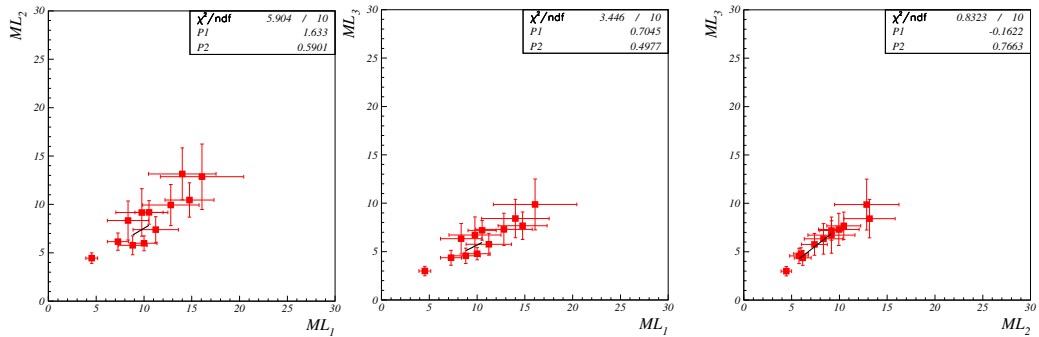


Figure 87: Correlations between the three methods used to obtain the M/L .

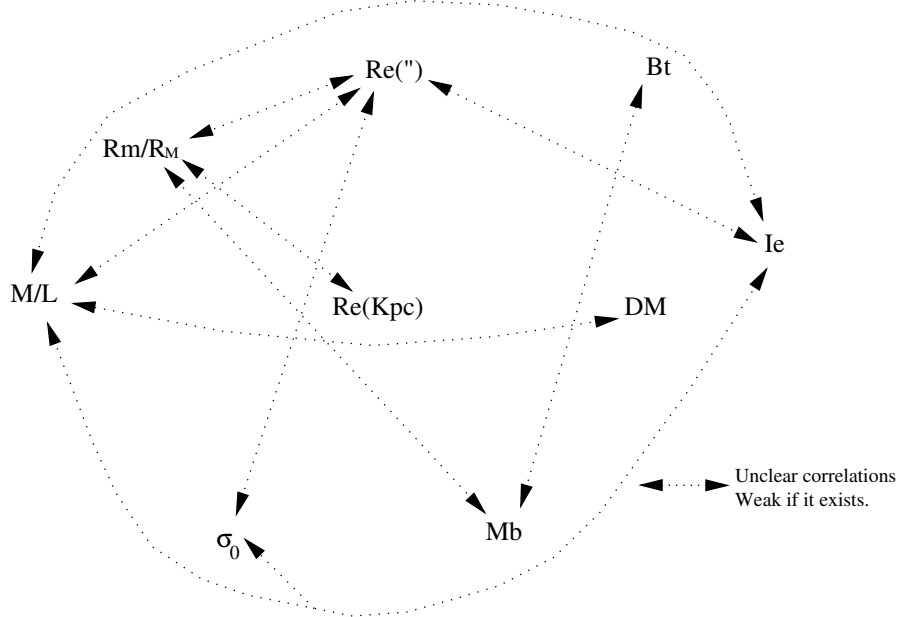
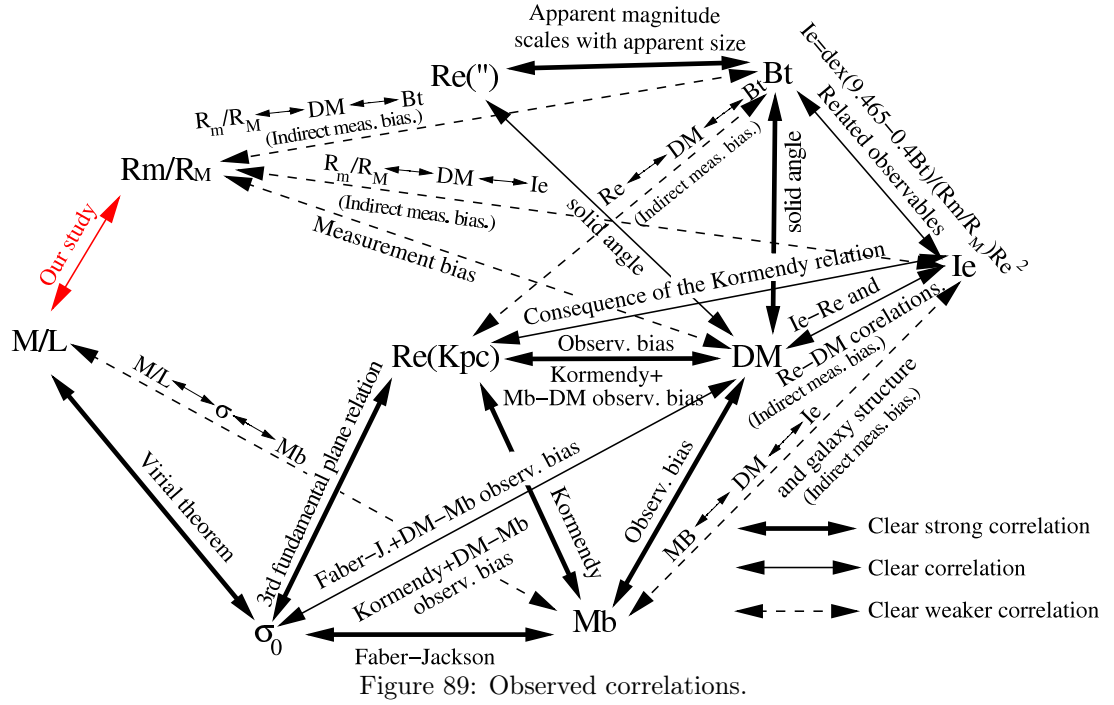
Mass to light ratio M/L correlations The too low χ^2/ndf , especially for the M/L_2 vs M/L_3 plot reveal that the three methods are not independent.

L.3.3 Discussion

A correlation summary is given in the table on page 111. The observed clear correlations are shown in Fig. 89. Possible weak correlations are shown in Fig. 90.

	Rmin/Rmax (BMS)	Rmin/Rmax (NED)	Re (")	Int. Blue mag. Bt (BMS)	NED mag.	Dist. Mod. (BMS)	Dist. Mod. (NED w/ z)	Dist. Mod. (NED w/o z)	Mb	Surf. Bright. le	Re (Kpc)	σ_0	M/L(1)	M/L(2)
Rmin/Rmax (NED)	strict correl. P1=0.099±0.034 P2=0.901±0.048 (Outliers cut)													
Re (")	Correl. P2=-(2.83 ±0.44) E-3	Correl. P2=-(4.22 ±0.33) E-3												
Int. Blue mag. Bt (BMS)	Correl. P2=(4.93 ±0.53) E-2	Log(Bt) Correl. P2=(-6.28± 0.19) E-3 Bt correl. P2= (-7.6±0.2) E-2												
NED mag.	Correl. P2=(6.30 ±0.54) E-2	Correl. P2=(4.22 ±0.29) E-2	Log(Bt) Correl. P2=(-6.10± 0.18) E-3	Correl. P2=0.994±0.018										
Dist. Mod. (BMS)	Correl. P2=(3.86 ±0.37) E-2	Correl. P2=(2.80±0.19) E-2	Correl. P2=-2.10±0.176	Correl. P2=1.226±0.044	Correl. P2=1.145±0.051									
Dist. Mod. (NED w/ z)	Correl. P2=(3.93 ±0.37) E-2	Correl. P2=(3.08±0.20) E-2	Correl. P2=-2.00±0.17	Correl. P2=1.259±0.049	Correl. P2=1.207±0.048	strict correl. P2=0.964±0.035 (Outliers cut)								
Dist. Mod. (NED w/o z)	Correl. P2=(6.94 ±0.64) E-2	Correl. P2=(4.48±2.2) E-2	Correl. P2=-2.27±0.244	Correl. P2=0.757±0.061	Correl. P2=0.826±0.061	strict correl. P2=1.067±0.054 (Outliers cut)	strict correl. P2=1.132±0.035 (Outliers cut)	Correl. P2=-0.509±0.032						
Mb	Correl. P2=(-3.95±0.57) E-2	Correl. P2=(-2.48±0.34) E-2	Correl. P2=-1.06±0.25	Correl. P2=-0.223±0.049	Correl. P2=-0.153±0.051	Correl. P2=-0.531±0.034	Correl. P2=-0.509±0.032	Correl. P2=-0.636±0.057						
Surf. Bright. le	Correl. P2=(-7.62±0.72) E-4	Correl. P2=(-1.46±0.08) E-3	Correl. P2=(-1.22±0.35) E-2	Correl. P2=(-7.49±0.19) E-3	Correl. P2=(-6.30±0.19) E-3	Correl. P2=(-1.73±0.09) E-2	Correl. P2=(-1.80±0.09) E-2	Correl. P2=(-0.94±0.10) E-2	Correl. P2=(8.08±0.89) E-3					
Re (Kpc)	Correl. P2=0.019±0.002	Correl. P2=(4.38 ±0.95) E-3	correl. P2=0.376±0.103	Correl. P2=-0.117±0.051	Correl. P2=-0.170±0.049	Correl. log(Re) P2=(-3.45±0.15) E-1 Re: P2=1.18±0.06	Correl. log(Re) P2=(-3.27±0.13) E-1	Correl. log(Mb) P2=-3.44±0.13 Mb P2=-1.58±0.09	Correl. P2=log(Mb) P2=-3.44±0.13 Mb P2=-1.58±0.09	Correl. P2=(-8.05±0.45) E-3				
σ_0	Correl. P2=(2.78 ±0.92) E-4	Correl. P2=(-8.02±4.08) E-5	Correl. P2=(1.50±0.41) E-2	Correl. P2=(1.12±0.19) E-3	Correl. P2=(0.57±0.19) E-3	Correl. P2=(1.24±0.08) E-2	Correl. P2=(1.24±0.08) E-2	Correl. P2=(1.14±0.09) E-2	Correl. P2=(-1.29± 0.08) E-2	Correl. P2=(-3.08±0.14) E-1	Correl. P2=(1.67±0.08) E-2			
M/L(1) (by default computed with NED DM)			Correl. P2=0.192±0.031	Correl. P2=-1.31±0.30	Correl. P2=-1.32±0.31	Correl. P2=0.50±0.19	Correl. P2=0.54±0.18	Correl. P2=1.77±0.19	Correl. P2=-1.73±0.27	Correl. P2=(-6.00±3.89) E-3	Correl. P2=(7.96±1.27) E-1	Correl. P2=(5.38±0.41) E-2		
M/L(2) (by default computed with NED DM)			Correl. P2=(6.39±2.40) E-2	Correl. P2=-0.75±0.47	Correl. P2=-0.79±0.47	Correl. P2=0.51±0.17	Correl. P2=0.82±0.17	Correl. P2=0.88±0.17	Correl. P2=-0.81±0.33	Correl. P2=(-1.22±0.50) E-2	Correl. P2=(3.79±1.78) E-1	Correl. P2=(2.68±0.66) E-2	Strict. correl. P2=0.59±0.13	
M/L(3) (by default computed with NED DM)			Correl. P2=(5.81±2.01) E-2	Correl. P2=-0.71±0.39	Correl. P2=-0.72±0.36	Correl. P2=0.43±0.14	Correl. P2=0.68±0.14	Correl. P2=0.70±0.14	Correl. P2=-0.76±0.28	Correl. P2=(-1.03±0.42) E-2	Correl. P2=(3.40±1.47) E-1	Correl. P2=(2.24±0.55) E-2	Strict. correl. P2=0.50±0.11	Strict. correl. P2=0.77±0.18

Figure 88: Correlation summary.



In most cases the χ^2/ndf are larger than 1. This is mostly because a linear fit is ill-suited to fit the data, and because two correlated variables can depend on other variables, which adds an additional non-gaussian dispersion. For example we already mentioned that the M/L vs R_{min}/R_{max} correlation has an additional variable, the (unknown) projection angle of the ellipsoid to the observed ellipse, which creates an additional dispersion.

All in all, the clear correlations seen in this section can all be classified as:

- Physical correlations;
- Observational biases;
- Unexplained but known correlations related to galaxy structure (e.g. Kormendy, Faber-Jackson relations...).

This is satisfactory since this clarifies how to account, if necessary, for the important correlations.

L.4 Corrections

L.4.1 Corrections for measurement biases

We will ignore the weak uncertain correlations shown in Fig. 90. Measurement biases seem to be *directly* at the origin of the $M_b \iff DM$ and $R_{min}/R_{max} \dashrightarrow DM$ correlations. Measurement biases seem to be *indirectly* at the origin of the $R_{min}/R_{max} \dashrightarrow B_t$, $R_{min}/R_{max} \longleftrightarrow Re(Kpc)$ and $R_{min}/R_{max} \dashrightarrow I_e$ correlations. Finally, measurement biases seem to be *indirectly* contributing *partly* to the $Re(Kpc) \iff DM$, $Re(Kpc) \dashrightarrow B_t$, $M_b \dashrightarrow I_e$, $I_e \longleftrightarrow DM$, and $DM \longleftrightarrow \sigma_0$ correlations. Unsurprisingly, DM is involved in all the measurement biases.

In order to study the effect of DM on the M/L dependence with R_{min}/R_{max} , we bin DM and plot M/L in function of R_{min}/R_{max} for each of the DM bins. The results for the linear fits $M/L = P_1 + P_2(R_{min}/R_{max})$ made for each DM bin are shown in Fig. 91. We choose DM bins of size 1, or smaller if the statistics is large. We use R_{min}/R_{max} and DM values from [3]. The values of $a = P_1$ and $b = P_2$ in function of the DM bins can be seen on the left panel of Fig. 92. Within the approximation of a linear dependence of M/L in function of R_{min}/R_{max} , then $b = \partial(M/L)/\partial(R_{min}/R_{max})$. Thus, b is our quantity of interest. Except for one outlying point, there is no strong dependence of a and b with DM : we find $b = (3.42 \pm 2.00)DM - 123.5 \pm 63.59$ for a reduced $\chi^2/ndf = 1.8$. This would suggest that the correction for the DM bias would increase the significance of our quantity of interest $b = \partial(M/L)/\partial(R_{min}/R_{max})$. Figs. 91 and 92 also suggest that there is something wrong with bin $32 \leq DM < 33$ (possibly because of the lowest point (galaxy NGC 4510) that has very small error¹⁷). The right panel of Fig. 92 shows the fit result with bin $32 \leq DM < 33$ excluded. We find similar fit values: $b = (3.25 \pm 2.00)DM - 118.7 \pm 62.94$ for a reduced $\chi^2/ndf = 0.8$. The value of the reduced χ^2/ndf , closer to the expected 1, supports excluding bin $32 \leq DM < 33$.

The correction for the DM bias would increase b by a factor $(-118.65 \pm 62.94)/(-13.00) = 9.13 \pm 4.84$ (here, -13.00 is the value of b at $< DM > = 32.5$). However, this assumes the reliability of a linear extrapolation over 31 units of DM , based on a fit performed over a DM range of 4.5 units. Such a procedure would yield average values of $M/L \simeq 80$ (P_1 coefficient of the top plots of Fig. 92), a value 6 times larger than the average $\langle M/L \rangle = 13.3$ for our data sample. Assuming similar effect, the DM bias correction would be reduced to $\sim 9.13/6 = 1.6$. This is still a large correction and given the uncertainties attached to it and the fact that ignoring it would reduce the signature of the correlation we are investigating, we choose to not apply the correction. However, we do retain the fact that bin $32 \leq DM < 33$ should be excluded from our analysis. The resulting linear fit of M/L vs R_{min}/R_{max} is $M/L = (-14.92 \pm 2.81)R_{min}/R_{max} + 20.63 \pm 2.19$ (Fig. 93), to be compared to the result shown in Fig. 67 ($M/L = (-6.40 \pm 2.32)R_{min}/R_{max} + 12.56 \pm 1.79$). The Pearson coefficient calculated when keeping data with uncertainties $\Delta M/L < 5$ is -0.44 (the linear fit becomes $M/L = (-15.69 \pm 2.92)R_{min}/R_{max} + 20.86 \pm 2.27$). When keeping data with $\Delta M/L < 3$ the Pearson coefficient becomes -0.64 (the linear fit becomes $M/L = (-19.56 \pm 3.46)R_{min}/R_{max} + 22.73 \pm 2.62$). Those indicate a large correlation.

¹⁷This small error is partly an artifact: Ref. [3] gives relative errors, hence small M/L values have small absolute errors, which might not reflect fully the uncertainty. Apart from re-performing a full error analysis, there is no easy way to correct this effect. We also refrain from removing this particular galaxy (NGC 4510) after close-up study: most of galaxies would have a particularity after close examination that one could use to justify excluding it from our sample. It would be thus possible to bias the result of our study in any arbitrary way. Obeying our general criteria and basic statistics rules protects us from such bias.

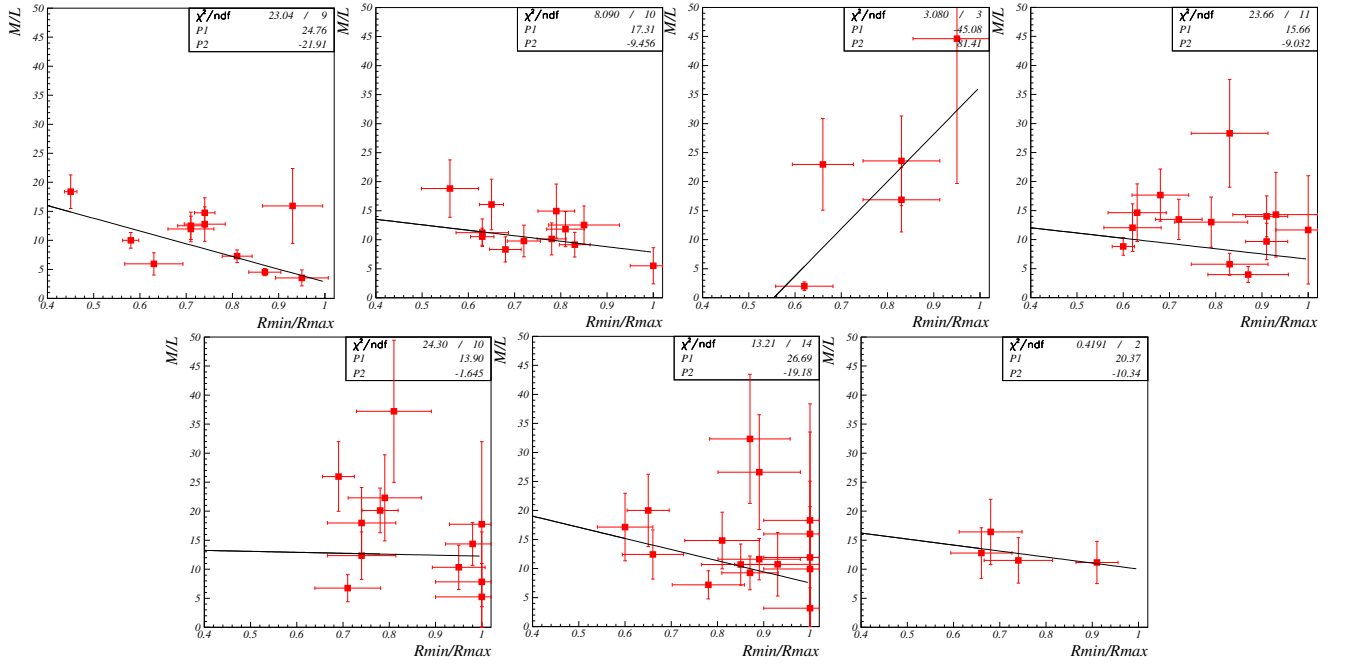


Figure 91: Linear fits for M/L vs R_{min}/R_{max} for various distance modulus DM bins. Those are, from top left to bottom right: $30 \leq DM < 31$, $31 \leq DM < 32$, $32 \leq DM < 33$, $33 \leq DM < 33.5$, $33.5 \leq DM < 34$, $34 \leq DM < 35$ and $35 \leq DM < 35.5$.

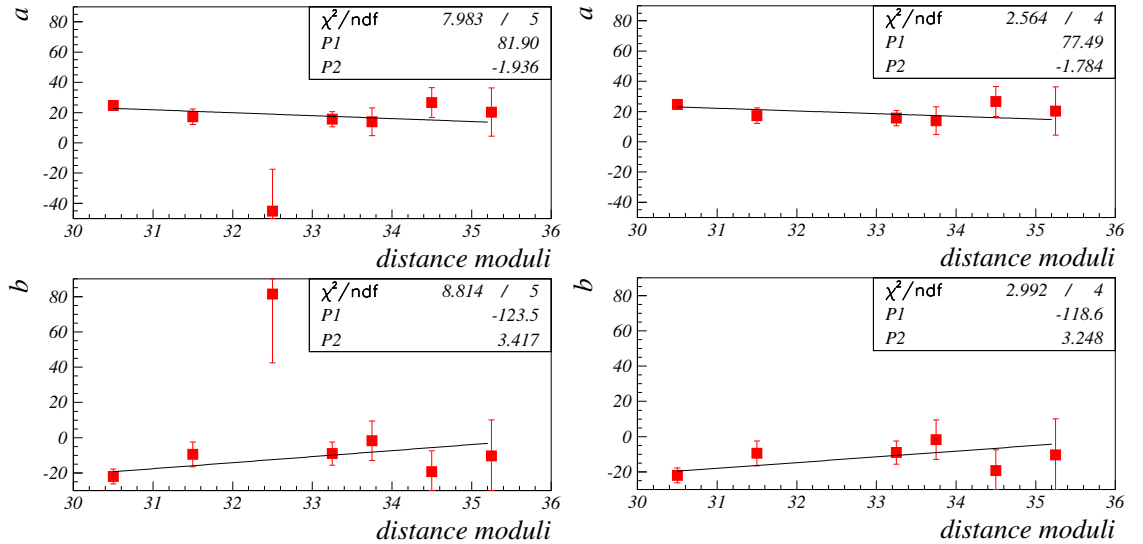


Figure 92: Left panel: fit coefficients a (top) and b (bottom) from Fig. 91 in function of DM . The P_1 and P_2 are the results of fits $a = P_1 + P_2 \times DM$ (top) and $b = P_1 + P_2 \times DM$ (bottom). Right panel: same but with bin $32 \leq DM < 33$ excluded.

L.4.2 Surface brightness vs absolute blue magnitude

We exclude from the sample the two galaxies that are close to the dwarf elliptical locus, see Section L.3.2 (we apply a selection at $M_b > -17.8$). This has no significant consequence on the M/L vs R_{min}/R_{max} relation: compare Fig. 94 to Fig. 93. The linear fit result is $M/L = (-14.48 \pm 3.00)(R_{min}/R_{max}) + 20.58 \pm 2.325$. Because this correction has little effect, we do not apply it in the rest of the analysis.

L.4.3 Hubble parameter correction

We must scale the slope of our assumed relation between M/L and R_{min}/R_{max} to account for the fact that [3] uses a large value of the Hubble parameter H_0 . This should be corrected for since redshift distances scale inversely to H_0

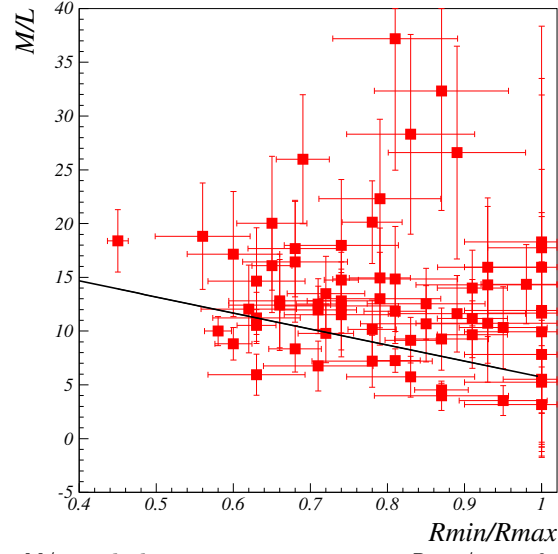


Figure 93: Correlation between M/L and the apparent axis ratio R_{min}/R_{max} for 68 galaxies (after removing bin $32 \leq DM < 33$). The computed Pearson coefficient reveals a large correlation (Pearson coefficient > 0.5).

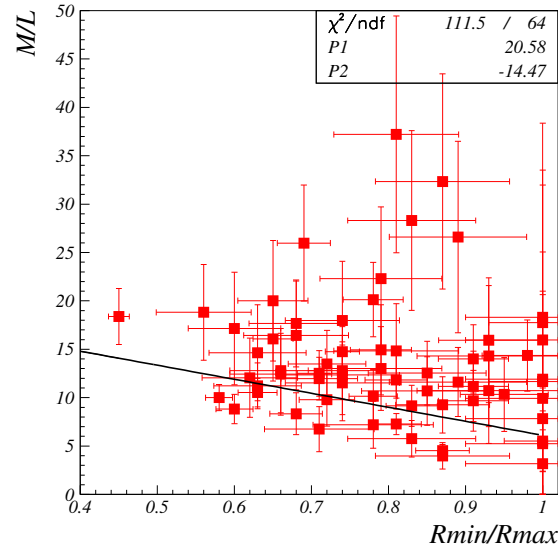


Figure 94: Correlation between M/L and the apparent axis ratio R_{min}/R_{max} for 66 galaxies (after removing bin $32 \leq DM < 33$ and two possible compact elliptical galaxies).

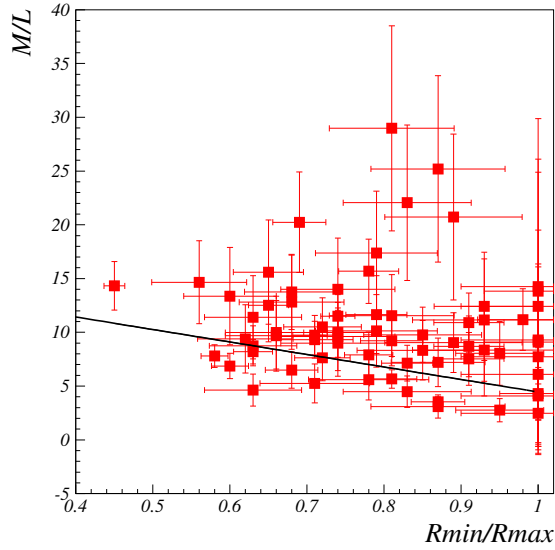


Figure 95: Same as Fig. 93 but after Hubble coefficient correction.

and M/L scales inversely with distances. Using $H_0=70 \text{ km s}^{-1} \text{ Mpc}^{-1}$ instead of the $95 \text{ km s}^{-1} \text{ Mpc}^{-1}$ used in [3] yields a M/L correction of $70/95 = 0.74$. The linear fit becomes $M/L = (-11.00 \pm 2.07)R_{min}/R_{max} + 15.20 \pm 1.61$.

L.4.4 Projection correction

This correction is discussed in detail for the Bacon *et al.* data [3] in Section 10.2.

L.5 Final result

The final result including the projection correction, the Hubble parameter correction and the exclusion of bin $32 \leq DM < 33$ but without applying the distance modulus bias correction (that would enhance further the M/L dependence with R_{min}/R_{max}) is shown in Fig. 96. Also excluded are the possible corrections discussed in Figs. 65, 66 and 73 (this is a conservative choice since this would enhance further the M/L dependence with R_{min}/R_{max}). Fig. 96 can be compared to Figs. 67, 93 and 95 that show the different stages of the analysis. The best linear fit yields $M/L = -(43.5 \pm 3.2)(R_{min}/R_{max}) + 46.7 \pm 2.4$, with a $\chi^2/ndf = 0.9$. This is a strong positive signature with a 13σ signal. The Pearson correlation coefficient is 0.87, or 0.91 after removing the galaxies with (uncorrected) uncertainty above $\Delta M/L = 5$ or $\Delta M/L = 3$ respectively, see Fig. L.5. In all cases, it indicates a strong correlation. Again, it is interesting to notice that if we select the highest precision data, then the M/L vs R_{min}/R_{max} correlation is enhanced, both for the determination using of the Pearson criterion and for the determination from the linear fit parameter p_2 .

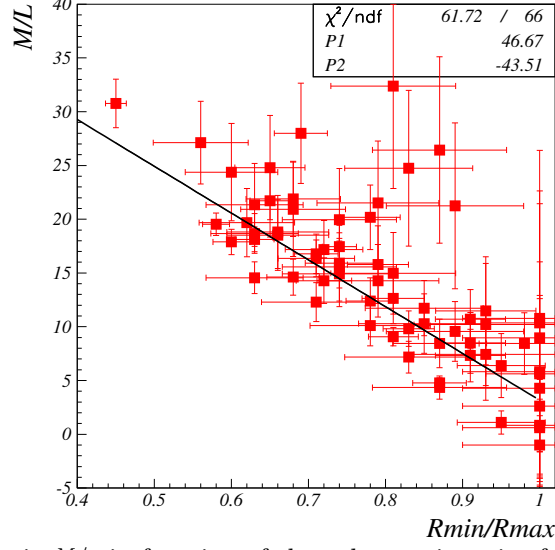


Figure 96: The mass to light ratio M/L in function of the galaxy axis ratios from our 68 galaxies sample, after correction for ellipticity projection and the Hubble parameter. The Pearson correlation coefficient is -0.64.

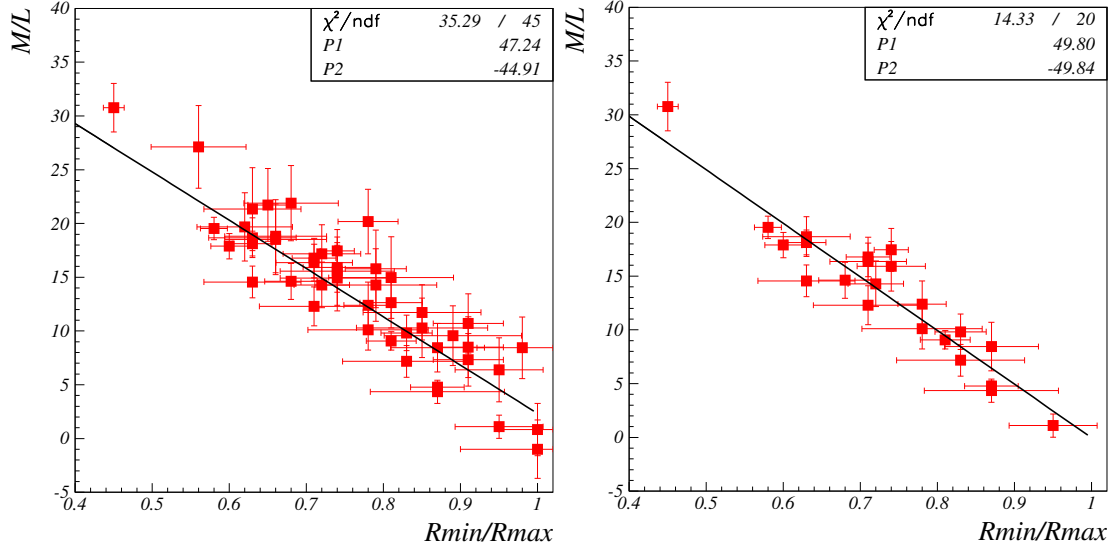


Figure 97: Left plot: Mass to light ratio M/L in function of the galaxy axis ratios after removing the galaxies with uncertainties $\Delta M/L > 5$. The Pearson correlation coefficient is -0.87. Right plot: same as left but after removing the galaxies with uncertainties $\Delta M/L > 3$. The Pearson correlation coefficient is -0.91. (Here, the values for $\Delta M/L$ refer to before applying the correction for the ellipticity projection.)